



**HAL**  
open science

# Development of polybenzimidazole and ionic liquid based membranes for high temperature proton exchange membranes (PEMs) and gas separation applications

Parashuram Kallem

► **To cite this version:**

Parashuram Kallem. Development of polybenzimidazole and ionic liquid based membranes for high temperature proton exchange membranes (PEMs) and gas separation applications. Other. Université Montpellier; Universidad de Zaragoza (Espagne), 2017. English. NNT: 2017MONTT196 . tel-01871369

**HAL Id: tel-01871369**

**<https://theses.hal.science/tel-01871369v1>**

Submitted on 10 Sep 2018

**HAL** is a multi-disciplinary open access archive for the deposit and dissemination of scientific research documents, whether they are published or not. The documents may come from teaching and research institutions in France or abroad, or from public or private research centers.

L'archive ouverte pluridisciplinaire **HAL**, est destinée au dépôt et à la diffusion de documents scientifiques de niveau recherche, publiés ou non, émanant des établissements d'enseignement et de recherche français ou étrangers, des laboratoires publics ou privés.

# THÈSE

Pour obtenir le grade de  
**Docteur**

Délivré par **l'Université de Montpellier (France)**  
**l'Universidad de Zaragoza (Espagne)**

Préparée au sein de l'Ecole Doctorale  
**Sciences Chimiques Balard (ED 459)**

Et de l'unité de recherche  
**Institut Européen des Membranes IEM (UMR 5635)**

Spécialité : **Chimie et Physicochimie des  
Matériaux**

Présentée par  
**Parashuram KALLEM**

**Développement de membranes à base de  
polybenzimidazole et de liquides ioniques pour  
applications à haute température comme  
membranes échangeuses de protons (PEMs) et  
pour la séparation de gaz**

**Soutenue le 15 Juin 2017  
devant le jury composé de**

Prof. Joao G. CRESPO, Universidade Nova de Lisboa (Portugal)

Rapporteur  
et Président du jury

Dr. Martin DROBEK, CR CNRS, Université de Montpellier (France)

Invité

Dr. Anne JULBE, DR CNRS, Université de Montpellier (France)

Directrice de thèse

A/Prof. Reyes MALLADA, Universidad de Zaragoza (Espagne)

Co-Directrice de thèse

Prof. Richard D. NOBLE, University of Colorado, Boulder (USA)

Rapporteur

Dr. Alfredo ORTIZ, Universidad de Cantabria (Espagne)

Examinateur

A/Prof. Maria Pilar PINA, Universidad de Zaragoza (Espagne)

Invitée



**Universidad  
Zaragoza**

1542



**UNIVERSITÉ  
DE MONTPELLIER**





**Universidad  
Zaragoza**



**UNIVERSITÉ  
DE MONTPELLIER**

**“Development of Polybenzimidazole and Ionic Liquid based Membranes for  
High temperature Proton Exchange Membranes (PEMs) and Gas Separation  
Applications”**

**A thesis submitted to obtain the degree of doctor, presented by**

**Parashuram KALLEM**

**Zaragoza, 19<sup>th</sup> March 2017**





**Development of Polybenzimidazole and Ionic Liquid based Membranes for  
High temperature Proton Exchange Membranes (PEMs) and Gas Separation  
Applications**

**A thesis**

Prepared in the framework of

Erasmus Mundus Doctorate in Membrane Engineering (EUDiME) to obtain  
multiple Doctorate degrees issued by

Universidad de Zaragoza, Departamento de Ingeniería Química y Tecnologías  
del Medio Ambiente



**Departamento de Ingeniería  
Química y Tecnologías  
del Medio Ambiente**  
**Universidad Zaragoza**

University of Montpellier (Sciences Chimiques Balard (ED 459), Institut  
Européen des Membranes IEM (UMR 5635))

**Supervisors:**

**Dr. Reyes Mallada**, Profesora Titular de Universidad, Departamento de Ingeniería Química y Tecnologías del Medio Ambiente. Instituto de Nanociencia de Aragón. Universidad de Zaragoza, Spain.

**Dr. Maria Pilar Pina**, Profesora Titular de Universidad, Departamento de Ingeniería Química y Tecnologías del Medio Ambiente. Instituto de Nanociencia de Aragón. Universidad de Zaragoza, Spain.

**Dr. Anne Julbe**, HDR, Directeur de Recherche CNRS, Institut Européen des Membranes, Université de Montpellier, France.



### **Supervisors:**

**Dr. Reyes Mallada**, Associate Professor, Institute of Nanoscience Aragon (INA), Department of Chemical and Environmental Engineering, University of Zaragoza, Spain

**Dr. Maria Pilar Pina Iritia**, Associate Professor, Institute of Nanoscience Aragon (INA), Department of Chemical and Environmental Engineering, University of Zaragoza, Spain

**Dr. Anne Julbe**, Directeur de Recherche CNRS, IEM (Institut Européen des Membranes), University of Montpellier, France

### **Jury members:**

**Dr. Joao Paulo Serejo Goulao Crespo**, Professor, Universidade Nova de Lisboa, Portugal

**Dr. Richard D. Noble**, Professor, University of Colorado Boulder, USA

**Dr. Alfredo Ortiz**, Department of Chemical and Biomolecular Engineering, Universidad de Cantabria, Spain.

**Dr. Reyes Mallada**, Associate Professor (INA), University of Zaragoza, Spain

**Dr. Anne Julbe**, Directeur de Recherche CNRS, IEM, University of Montpellier, France

### **Invited members:**

**Dr. Maria Pilar Pina**, Associate Professor (INA), University of Zaragoza, Spain

**Dr. Martin Drobek**, Chargé de Recherche CNRS, IEM, University of Montpellier, France





## **DEDICATION**

***To my GOD and LORD, JESUS CHRIST***

***My lovely wife, Krishnaveni***

***My daughter, Ariana Jessilyn***

***My beloved parents, Somaiah and Ramulamma***

***My siblings: Narasimha, Swami and Renu***



## Table of Contents

<b>Chapter 1:</b> Literature review.....	<b>1</b>
<b>Chapter 2:</b> Objectives and thesis outline.....	<b>43</b>
<b>Chapter 3:</b> On the incorporation of crosslinked Poly imidazolium based Ionic liquid on well-defined straight porous Polybenzimidazole microsieves: A new generation of phosphoric free proton Exchange Membranes for high temperature applications.....	<b>51</b>
<b>Chapter 4:</b> Hierarchical porous Polybenzimidazole microsieves fabrication by Liquid induced phase separation micromolding (LIPS $\mu$ M): An efficient architecture for anhydrous proton transport via Poly-ionic Liquids .....	<b>99</b>
<b>Chapter 5:</b> Supported Ionic liquid membranes (SILMs) based on PBI and protic Ionic liquids for methane upgrading.....	<b>137</b>
<b>Chapter 6:</b> Summary, Conclusions and Future Work .....	<b>165</b>



## ACKNOWLEDGEMENTS

All praise, honour, and glory to my Lord Jesus Christ for HIS richest grace and mercy for the accomplishment of this thesis. Throughout this entire study, HE took care of everything that would have stopped me in my tracks and strengthened me even through my most difficult times.

Time flies so fast. I started my PhD as part of Erasmus Mundus Doctorate in Membrane Engineering (EUDIME) at Institute of Nanoscience Aragon (INA), University of Zaragoza (UNIZAR) on March 9<sup>th</sup>, 2013. During my PhD, I got the chance to work in several countries (Spain, Netherlands and France) and learnt from the finest experts in the area of membrane science. During EUDIME PhD, I stayed 2.5 yr. in UNIZAR and six months each in 'Membrane Science and Technology (MST) - University of Twente (Utwente)' and 'Institute of European Membranes (IEM)-University of Montpellier (UM)', which taught me noticeable and lifelong lessons about work ethics, work management and decision making.

This thesis appears in its present form due to the assistance and guidance of **several people** from Spain, Netherlands and France. I would therefore like to express my deep appreciation and gratitude to all of them.

First of all I would like to thank **Prof. Reyes Mallada**, the supervisor of my thesis work. Reyes, thank you for your comprehensive knowledge and incisive insight on membrane science as well as your uncompromising and prudent attitude towards research and insistence on quality works have deeply influenced me and will certainly benefit my future study. I would equally like to thank **Prof. Maria Pilar Pina**, the second supervisor of my thesis work, whose contribution and constructive criticism has pushed me to pay the kind of efforts I have utilized to make this work as original as it can be. Thank you Pili, for your immense background and experience in electrochemical knowledge of fuel cell technology enabled me to work through many scientific and technical difficulties smoothly. Thank you both, I have experienced true research and my knowledge on the subject matter has been broadened. I will never forget you Reyes and Pili.

I would like to extend my deepest thanks to my exchange supervisor **Dr. Anne Julbe** (IEM-UM) for all the discussions we had and her valuable input on my work. Anne, thank you also for your positive thoughts when I received criticism on my work. I count myself lucky that I got the chance to work with you.

I would like to express my great appreciation to **Prof. Dorothea Catharina Nijmeijer**. Kitty, thank you for your endless motivation and support during my research in MST-Utwente.

My special thanks go to **Dr. Adela Eguizabal** (INA-UNIZAR) who was helpful to me in finding solutions to unexpected problems I face. Adela, this study would be much more challenging without your explanations, experiences and also friendship.

I would like to thank **Dr. Martin Drobek** (IEM, UM) whose guidance, suggestions and support helped me to develop a more deep understanding of the subject. Many thanks to **Dr. Christophe CHARMETTE** (IEM-UM) for providing his assistance, expertise and worthy contribution to one of the important parts of my thesis work. I would like to thank **Dr. Celine Pochat-Bohatier and Sakthivel Nagarajan** (IEM-UM) for their help in the mechanical characterization.

I also appreciate the efforts of **Magdalena Malankowska** (INA-UNIZAR) who assisted me with the solubility experiments. Magda, it was always a pleasure to talk to you and above all I could talk about the general problems of EUDIME PhD. I am grateful to **Dr. Nuria Navascues** (INA-UNIZAR) for the help in handling many instruments utilized during my thesis work. I also appreciate the assistance in providing structured molds by **Dr. Erik J Vriezolk** (MST-Utwente).

I would like to thank my jury for evaluating my thesis and allowing me to defend it. **Prof. João Paulo Serejo Goulão Crespo, Prof. Alfredo Ortiz Sainz de Aja** and **Prof. Richard D. Noble**, thank you for accepting the invitation to take part in my committee.

I would like to thank the financial support from the Government of Aragon and the Education, Audio visual and Culture Executive Agency (**EU-EACEA**) within the **EUDIME** – “Erasmus Mundus Doctorate in Membrane Engineering” program (FPA 2011-0014, SGA 2012-1719, <http://eudime.unical.it>). I am also indebted to the INA-UNIZAR for the research infrastructure support. I would also thank the LMA-INA for offering access to their instruments and expertise.

**My friends and colleagues at INA-UNIZAR** have contributed immensely to my personal and professional time at Zaragoza, Spain. The group has been a source of friendships in addition to good advice and collaboration, thanks for all the good memories. Many thanks also to the **INA staff members** who helped me with all kinds of experiments in the lab. Thank you **Pilar Borrajo** for helping me out with all the difficult procedures and bureaucracies in the (academic) world. I am grateful to all my **colleagues at MST-Utwente and IEM-UM** for providing me with moral support, cheerful environment as well as relaxing discussions. My sincere thanks also go to the entire **staff of the both MST-Utwente and IEM-UM**.

My special thanks to Indian friends and families in Zaragoza: Vaibhav, Naveen, Dev, Jayant, Mukesh, Swati, deepa and Chikarmane family, who made my time very refreshing, thanks to their cordial attitude that made me feel very comfortable in their company.

I am highly indebted to **my parents, Mr. Somaiah Kallem and Mrs. Ramulamma Kallem** who painstakingly laid the foundation for my education giving it all it takes. I especially want to thank my **grandma Buchamma**, for the childhood memories. I am thankful to my **brothers, Dr.Narasima, Swamy** and **sister, Renu** for their love and best wishes, which despite of their physical absence has helped me in the successful completion of my PhD in Europe. My sincere thanks for all years love and care.

I am and will forever be grateful to my loving wife **Krishnaveni** and **2.5 yr. old daughter Ariana Jessilyn** who have given everything possible and even given up important things to make sure I achieve this feat. I can't find the words that express my gratitude. Thank you so much for your incredible support and resilience during all this period of time. I love you!





# **Chapter- 1**

## **Literature review**



**Thesis title: Development of Polybenzimidazole and Ionic Liquid based Membranes for High temperature Proton Exchange Membranes (PEMs) and Gas Separation Applications**

**1. High temperature Proton Exchange Membranes (HTPEMs) for Fuel Cell Applications**

**1.1. Introduction to fuel cells**

Greenhouse gas emissions (GHG) are endlessly growing in an era where hydrocarbon (gas, oil, and coal) centered power generators govern. This is mainly a concern when taking into attention that our remaining supplies of oil and natural gas are hastily diminishing as world population grows. At present humanity is encountering a future of diminishing reserves of fossil fuels, growing energy demand as well as a greater understanding of the environmental influence by the use of fossil fuels. It is now of worldwide importance that GHG emissions related with energy production are significantly decreased in order to control the consequences of climate change and environmental pollution. The 1997 Kyoto Protocol agreements have been formed in order to attempt and moderate the results of climate change by decreasing the amounts of GHGs discharged into the atmosphere.

The European Union (EU) has fixed the following two targets: First target is GHG should be reduced to 20% below their 1990 levels by 2020. The second headline target is a 20% penetration of renewable energy by 2020. Recently the United Kingdom (UK) set out in its 2007 Energy White Paper that it would commit to an 80% GHG emission reduction compared to 1990 levels by 2050. The targets of both the UK and EU are remarkable, though there is now a common trend among many nations concerning targets of a low carbon future<sup>1-2</sup>.

Fuel cells have recently been identified as a crucial technological alternative on path to an upcoming low carbon built environment owing to their high efficiencies and low emissions. A fuel cell is an electrochemical device that converts the chemical energy of a fuel directly into electrical energy. The one-step class of this process, in comparison to the multi-step (e.g. from chemical to thermal to mechanical to electrical energy) processes involved in combustion-based heat engines, provides some exceptional benefits. Such as, the current combustion-based energy generation technologies are very harmful to the environment and are mostly contributing several global concerns, e.g. climate change, ozone layer depletion, acidic rains, and thus, the consistent reduction in the vegetation cover. Moreover, these technologies rely on the finite and diminishing world supplies of fossil fuels. Fuel cells, conversely, offer an efficient and clean mechanism for energy conversion. Furthermore, fuel cells are compatible with renewable sources and modern energy carriers (i.e., hydrogen) for sustainable development and energy security. Thus, they are considered as the energy conversion devices of the future. In summary, fuel cells offer a cleaner, more efficient, and possibly

the most flexible chemical-to-electrical energy conversion<sup>2-4</sup>. The fuel cell technology has a miscellany of application varying from stationary power plants to portable energy consumption. Globally, several countries are focusing on fuel cell based energy sources and fuel cell technology is successfully launched in different countries like Sweden, UK, Japan and USA<sup>4</sup>. The fuel cells are beneficial for many systems; however, there are principally three regions which are being more focused at present for fuel cell applications. These uses are transportation (cars, buses, trucks, submarines, ships, spacecrafts etc.), stationary power (power for remote locations, back-up power, stand-alone power plants for towns and cities, distributed generation for buildings and co-generation) and portable power (cell phones, radios and laptops etc.)<sup>5</sup>.

### **1.1.1. Development and challenges**

The fuel cell industry had revenues of roughly \$2.2 billion in 2014, a growth of almost \$1 billion over revenues in 2013. The major markets for fuel cells currently are in stationary power, portable power, auxiliary power units, backup power, and material handling equipment. Nearly 155,000 fuel cells were circulated globally in the four-year period from 2010 through 2013, accounting for 510–583 MW of fuel cell capacity. In 2014 alone, above 50,000 fuel cells accounting for over 180 MW of capacity were shipped. In transportation applications, makers have started to commercialize fuel cell electric vehicles (FCEVs). Hyundai and Toyota have recently introduced their FCEVs in the marketplace, and Honda is set to launch its new FCEV in the market in 2016. Others, including Daimler, reportedly are set to begin commercialization in 2017<sup>6</sup>.

The worldwide fuel cell industry market is expected<sup>7</sup> to reach \$19.2 billion by the year 2020<sup>7</sup> with the United States, Japan, Germany, South Korea, and Canada acting as the flagship countries in the development and commercialization of fuel cells. In 2016 annual plane of The Fuel Cell and Hydrogen 2 Joint Undertaking (FCH 2 JU)<sup>8</sup>, there is a special attention on manufacturing technologies of proton exchange membrane fuel cells (PEMFC) for transport applications. And it is mention that regardless of the maturity level of the PEMFC technology, it still encountering some real tasks in many aspects such as manufacturability, production efficiency and production cost. FCH 2 JU has committed a full project that will examine the process development of critical steps of PEMFC stack manufacturing and production of component engineering samples. The anticipated target of the project is to expand the production of PEMFC stack from few 100 stacks/ year up to 50,000 stacks/year in 2020, for a total power range about 5 MW per year with a single line. One more attractive project of FCH 2 JU will focus on improving the design of high efficiency and low-cost Balance-of-Plant (BoP) PEMFC system components on the cathode side including a compressor, humidification, intercooler, valves, and turbine/expander. The predictable outcome of this project is

to reach a production cost of 100 V/kW at a production rate of 50,000 units/year of the FC system and similarly to stabilize the Maximum power degradation at 10% after 6000 h in the passenger cars<sup>8</sup>.

Successful application of fuel cell technology in the transport sector has taken place in Europe and USA. Nevertheless, the fuel cell industry is still facing a number of tasks to commercialization. Fuel cell cost is one main task, the durability of the unit and its performance is one more critical one. The challenge of hydrogen infrastructure and storage is necessity for the technology wide spread in transportation<sup>9</sup>.

According to the U.S. Department of Energy's (DOE's)<sup>10</sup>, today fuel cells can be manufactured at low volume for around \$280/kW. If fuel cells were manufactured at high volume with the latest advanced materials and components demonstrated in the lab, the cost would be around \$55/kW; still short of the 30 US \$/kW ultimate DoE target. According to Figure 1.1, it can be seen that the costs, from those initially estimated, are continually dropping.



**Figure 1.1:** Modeled cost of an 80-kW PEM fuel cell system based on projection to high-volume manufacturing (500,000 units/year)<sup>11</sup>.

Current targets and the main objectives for most researchers in the development of novel membrane materials deal with increasing the performance and durability and to reduce the overall cost of fuel cells. Table.1.1 lists the 2020 US DOE targets for HT-PEM materials<sup>12</sup>. The targets incorporate the most important characteristics for PEMs, i.e. high conductivity, good thermal, mechanical and chemical stability, acceptable durability, and compatibility with other fuel cell

components, materials that are easy to work with and that can be recycled in an environmentally friendly manner.

**Table 1.1:** Targets for proton exchange membranes for transport application according US DOE<sup>12</sup>

Characteristic	2015 Target	2020 Target
Maximum operating temperature	120 °C	120 °C
Minimum electrical resistance	>5600 ohm cm <sup>2</sup>	1000 ohm cm <sup>2</sup>
Conductivity	100 mS cm <sup>-1</sup>	100 mS cm <sup>-1</sup>
Area specific proton resistance	0.072 Ω cm <sup>2</sup>	0.02 Ω cm <sup>2</sup>
Hydrogen/oxygen crossover at 1 atm	2.4 mA cm <sup>-2</sup>	2 mA cm <sup>-2</sup>
Cost	20 USD/m <sup>2</sup>	20 USD/m <sup>2</sup>
Durability	2500 h	5000 h

Although the concept of a fuel cell was developed in England in the 1800s by Sir William Grove, the first workable fuel cells were not produced until much later, in the 1950s. In 1959, Francis Thomas Bacon, an English engineer, demonstrated the first fully-operational fuel cell. His work was impressive enough to get licensed and adopted by NASA<sup>13</sup>.

### 1.1.2. Types of Fuel Cells

Based on the type of electrolyte used and the temperature operation, fuel cells can be divided into six types: alkaline fuel cells (AFC), polymer electrolyte membrane or proton exchange membrane fuel cells (PEMFC); Direct Methanol Fuel Cell (DMFC); phosphoric acid fuel cells (PAFC), solid oxide fuel cells (SOFC); and molten carbonate fuel cells (MCFC). All of the fuel cells perform in the same principal method, i.e., a fuel is oxidized into electrons and protons; oxygen is reduced to oxide species; proton or oxide ions are transported through the ion conducting but electronically insulating electrolyte. However, vary in various other features such as operating temperature, electrolyte, catalyst, and system structure and hence have dissimilar applications. Table.1.2 shows the types of fuel cells and compares their features and applications<sup>2, 14</sup>.

**Table 1.2:** Features of different types of fuel cells<sup>2, 14</sup>.

Fuel cell Type	Electrolyte	Charge carrier	Operating temp ( °C)	Fuel	Electrical Efficiency (%)	Applications
<b>AFC</b>	Alkaline	OH <sup>-</sup>	90-100	H <sub>2</sub> Pure	60	Military, Space
<b>PEMFC</b>	Polymer	H <sup>+</sup>	50-90* & 120-200**	H <sub>2</sub> , fuel	60	Backup power,
				Reformed	(Transportation)	Portable power,
<b>DMFC<sup>15</sup></b>	Polymer	H <sup>+</sup>	60-130	CH <sub>3</sub> OH	20-25	Consumer goods,
<b>PAFC</b>	Phosphoric acid	H <sup>+</sup>	150-200	H <sub>2</sub> , fuel	>40	Distributed power
				Reformed		
<b>SOFC</b>	Solid oxide	O <sup>-2</sup>	600-1000	H <sub>2</sub> , fuel	35-45	Large distributed generation
				Reformed		
<b>MCFC</b>	Molten	CO <sub>3</sub> <sup>-2</sup>	600-700	H <sub>2</sub> , fuel	45-47	Large distributed generation
	Carbonate			Reformed		

\*Low temperature. \*\*High temperature.

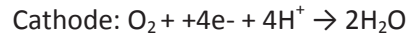
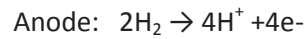
The principal focus of our efforts is on polymer electrolyte membrane fuel cells (PEMFC); therefore a more detailed discussion of PEM fuel cells and previously reported efforts on PEMs is given below.

### 1.1.3. Polymer electrolyte membrane fuel cells (PEMFCs)

Among the types of fuel cells, PEMFCs have the largest range of applications as they are extremely flexible. PEMFCs are the most promising candidates for transport applications due to their high power density, fast startup time, high efficiency, low operating temperature, and easy and safe handling. However, PEMFCs are still too expensive to be competitive or economically-feasible<sup>4</sup>.



The electrochemical processes in the fuel cell take place at the catalyst layers. In PEMFC, the processes at the anode and cathode, respectively, are:



Hydrogen fuel is provided to the anode (negative terminal) of the fuel cell where it gets oxidized to form electrons and protons together with the production of heat. Each takes a separate direction to the cathode. The protons migrate through the polymer electrolyte membrane and the electrons are transferred through an external circuit to generate electricity. At the cathode (positive terminal), oxygen reacts with the coming protons to form water. The only by-product of this electrochemical process is heat and water.

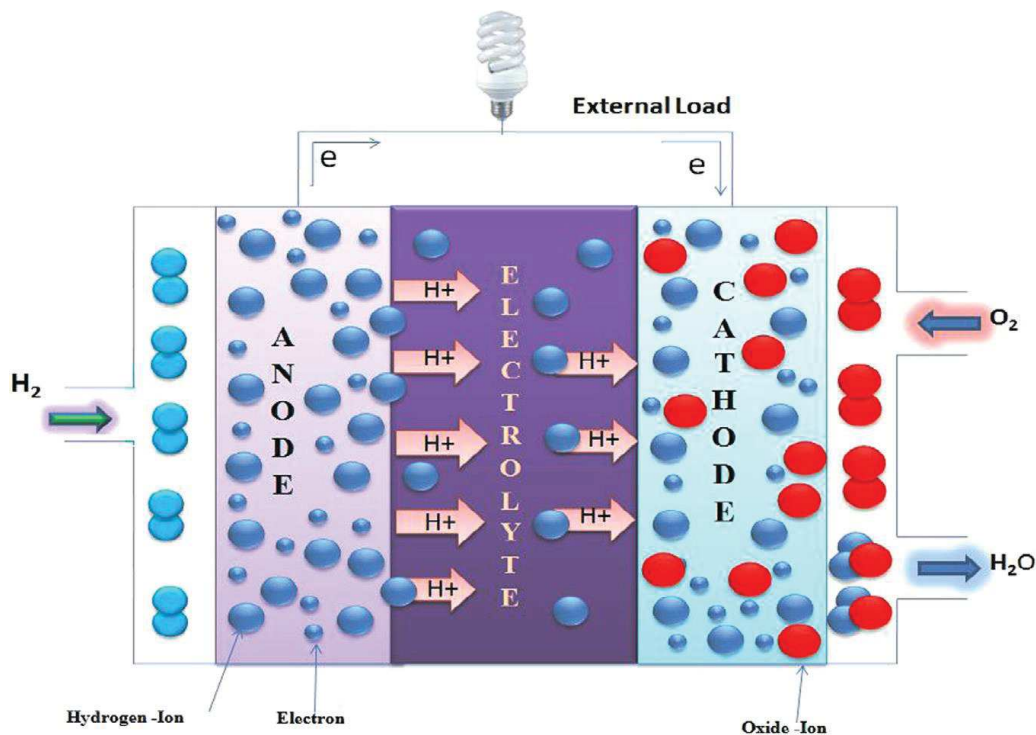


**Figure 1.2:** Schematic representation of a single fuel cell (PEMFC)<sup>14</sup>.

A fuel cell is composed of three active components: a fuel electrode (anode), an oxidant electrode (cathode), and an electrolyte sandwiched between them. The electrodes consist of a porous material that is covered with a layer of catalyst (often platinum in PEMFCs). Catalyst layers, normally 5-50  $\mu\text{m}$  thick, comprising platinum or platinum deposited on carbon, are merged onto each side of the PEM. Figure.1.2 is a schematic demonstration of a single PEMFC. The heart of the PEMFC is a polymer electrolyte membrane (PEM), which acts as a proton conductor as well as a fuel barrier besides a mechanical separator sandwiched between the anode and the cathode<sup>16</sup>. The gas diffusion layers

(GDL) made of carbon cloth or porous carbon paper, are in direct contact with the catalyzed membrane. These layers deliver efficient reactive gas supply to the catalyst layer and efficient water supply and eliminate in liquid or vapor form.

The electrodes need to be porous to facilitate sufficient space for the diffusion of gas to the active regions of the electrocatalyst. In addition, the cathode (where water is formed) is required to be hydrophobic so that the electrode does not turn into flooded with water resulting in additional mass transfer resistance. For real fuel cell operation, a three phase boundary is involved, where the electrocatalysts are in contact with PEM while access to reactant gas is provided. A complete cell contains current collector plates that mostly contain machined stream channels, as needed for successful distribution of reactant gasses near the surface of the electrodes. These plates become bipolar plates in the fuel cell stack, in which case they would have gas flow fields on both sides<sup>17</sup>.

## 1.2. High Temperature Operation of PEMFC

Although the PEMFC is considered one of the most promising alternative power sources especially for sub-megawatt scale applications, there are several technological and commercial reasons for operating PEM fuel cells at temperatures above 120 °C<sup>18-19</sup>.

i) The carbon monoxide concentration influences the performance of a PEM at low temperatures<sup>20</sup>. It is reported<sup>21-22</sup> that if the concentration of CO is excessive (~10 ppm), it will intensely adsorb to the platinum (Pt) surface then poison the platinum electro-catalyst (Figure. 1.3). It has been observed that the chemisorption of CO on Pt is related with high negative entropy, indicating that adsorption is elevated at low temperatures, and lowered at high temperatures. As a result, the CO tolerance will rise with rising temperature and is almost negligible at high temperatures (140 °C)<sup>20</sup>.

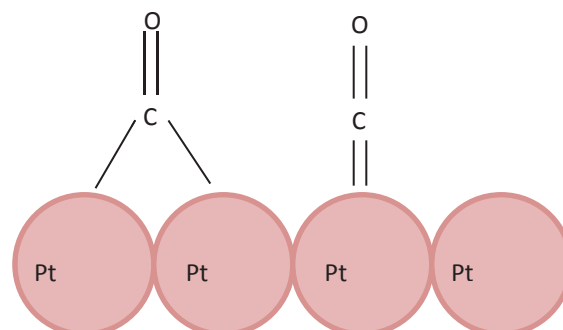


**Figure 1.3:** Adsorption of CO on Pt.

ii) By switching to higher temperatures would result in faster reaction kinetics at both electrodes particularly in Oxygen reduction reaction (ORR). Additionally, enhanced reaction kinetics at the

electrodes can significantly help in substituting platinum based catalysts with other non-platinum based catalysts which would help in overall cost reduction<sup>22-24</sup>.

iii) The major drawback of low- temperature PEMFCs (LT-PEMFCs) is the cooling of a system, during low temperature operation. A PEMFC functioning at 80 °C with an efficiency of 40–50% can produce a heavy amount of heat that must be removed from the PEMFC to sustain the working temperature. An increasing temperature of PEMFC will allow for existing cooling architectures present in transport vehicles to be used consequently increasing the weight and mass specific energy densities and the overall energy efficiency. The efficiency can be further increased when cogeneration and on-board reforming are considered<sup>3, 20</sup>.

iv) The diffusion coefficient of hydrogen is one order of magnitude greater than that of oxygen in the air at particular pressure and temperature. Thus, slower diffusion of oxygen is a controlling factor in the working of PEMFC in regard to reactant transport. It has been reported that oxygen transport is slower in liquid water than in water vapor<sup>25</sup>. Thus, by enhancing the operating temperature, the percentage of water vapor could be increased in the gas diffusion layer and catalyst layer of a cathode, so, improving oxygen transport and consequently, fuel cell performance<sup>3</sup>.

On the other hand, several researchers have also shown specific shortcomings with HTPEMFC which are following<sup>26</sup>. i) The durability of the PEMFC will diminish as a result of enhanced liability to structural plus chemical degradation. ii) The already remaining drawbacks of corrosion of carbon support can intensify with enhancing in working temperature of PEMFCs. It has been described that the corrosion rate of the carbon support intensifies with enhancing platinum loading and increasing temperature. Additionally accumulation of Pt nanoparticles (reduction of electrochemically active surface area), dissolution of Pt particles into acidic operating environment and re-deposition during long term operation aggravate with increasing temperature. iii) Membrane degradation is enhanced under low humidity and high temperature environments. iv) As the proton conductivity is highly relied on the water, dehydration of the PEM and resulting decline of proton conductivity is the main concern with HTPEMFC technology. v) If high relative humidity is required for high proton conductivity at high temperatures, an extremely elevated pressure is needed which is technically and commercially not attracting<sup>27</sup>.

### **1.3. Polymer Electrolyte Membranes (PEM)**

In this HTPEM scenario, the most important challenges are mainly related to the electrolyte performance and durability. The PEM can be considered in two parts: Firstly, the polymeric membrane material, including the backbone, the side chains and any fillers or support materials that

have been added to increase the material desirable properties. Secondly, the proton carrier, which is either water or an ionic medium such as phosphoric acid ( $\text{H}_3\text{PO}_4$ ) or an ionic liquid<sup>3</sup>.

Perfluorosulfonic acid -polymer and its derivative (PFSA) ionomers (e.g. Nafion, Figure. 1.4) have emerged as “state of the art” materials for low-temperature fuel cell applications. PFSA membranes are composed of carbon-fluorine backbone chains with perfluoro side chains containing sulfonic acid groups.

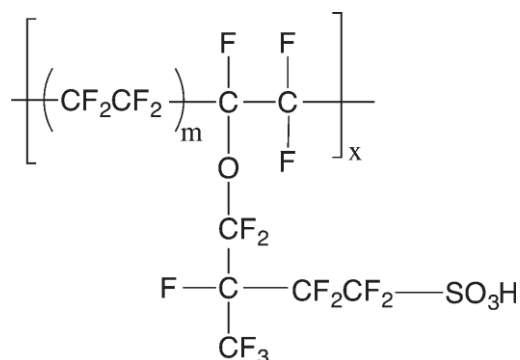


**Figure 1.4:** Nafion<sup>®</sup> chemical structures.

The Teflon-like molecular backbone provides these materials excellent long-term stability in both oxidative and reductive environments. The proton conductivity of Nafion<sup>®</sup> strongly rely on its water content as water is responsible for both the dissociation of the sulfonic acid protons which provides highly mobile hydrated protons and the proper percolation of these hydrophilic inclusions. Nafion shows high proton conductivity of up to  $100 \text{ mS cm}^{-1}$  under fully hydrated conditions<sup>28</sup>. The major shortcomings related with PFSA based membranes are listed briefly as follows: i) High cost ( $350\text{-}500 \text{ USD/m}^2$ ) ii) Decline in conductivity with decreasing relative humidity and inability to work at high temperatures iii) Poor mechanical strength at  $100 \text{ }^\circ\text{C}$ . iv) Shrinkage and cracking under dehydrated conditions accelerating gas-crossover v) Thermal and chemical degradation<sup>29</sup>.

### 1.3.1. Anhydrous Proton Conducting Membranes

The idea and possibility of acquiring high ionic conductivity in other dipolar solvent systems other than water opened the gate for many different approaches to HT-PEMFC technology.

Polymer based electrolyte membranes have been actively investigated over the last years for the development of new generation of proton exchange membranes (PEMs) adequate for high temperature (above  $100 \text{ }^\circ\text{C}$ ) applications<sup>20, 23, 30</sup>. Membranes under active development can be classified into the following groups and have been well reviewed in recent years: (i) modified perfluorosulphonic acid (PFSA) membranes<sup>25, 30</sup>; (ii) alternative membranes based on partially

fluorinated and aromatic hydrocarbon polymers<sup>3</sup>; (iii) inorganic–organic composites<sup>31</sup>; (iv) acid–base polymer membranes<sup>32</sup>, typically a basic polymer doped with a non-volatile inorganic acid or blended with a polymeric acid.

As the focus of this thesis, the discussion below is related to the acid–base type membranes. Acid–base complexation represents an effective approach to the development of proton conducting membranes. Polymers bearing basic sites like ether, alcohol, imine, amide, or imide groups react with strong or medium strong acids. The basic polymer acts as a proton acceptor like in a normal acid–base reaction, and an ion pair is formed. The polymers used in previous investigations include polyethyleneoxide (PEO), polyacrylamide (PAAM), poly(vinylpyrrolidone) (PVP), polyethyleneimine (PEI), and polybenzimidazole ((PBI)<sup>33</sup>. It is reported that high conductivity can only be obtained with amphoteric acids, especially phosphoric or phosphonic acids.

Among those, phosphoric acid doped PBI membranes have been recognized as promising PEM materials operating at high temperatures<sup>32-34</sup>.

### 1.3.2. Phosphoric acid doped Polybenzimidazole (PBI) membranes

PBI belongs to a big family of aromatic heterocyclic polymers containing benzimidazole units. PBI with different structures can be synthesized from hundreds of combinations of tetraamines and diacids. In a specific way, PBI refers to the commercial product under the trademark Celazole®, poly 2,2'-m-(phenylene)-,5,5'-bibenzimidazole(Figure 1.5). In the context of PBI with different structures, this specific PBI is also named as mPBI because the phenylene ring is meta-coordinated<sup>35</sup>.

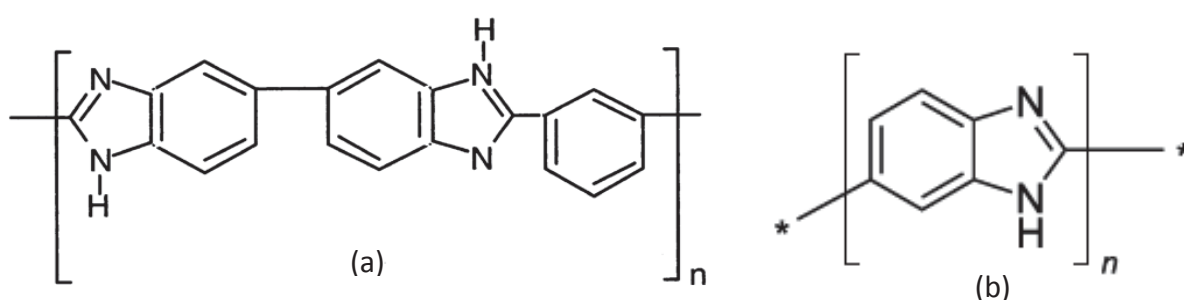


**Figure 1.5:** PBI backbone structures; (a) Poly(2,2'-(m-phenylene)-5,5'-bibenzimidazole); (b) Poly(2,5-benzimidazole) (AB-PBI).

Being as an amorphous thermoplastic polymer, the aromatic nuclei of PBI provide the polymer high thermal stability (glass transition temperature,  $T_g = 425\text{--}436\text{ }^\circ\text{C}$ ), excellent chemical resistance, retention of stiffness and toughness, however, with poor process ability, as reviewed previously<sup>36</sup>.

Primarily used in textile fibres, the selection of poly 2,2'-m-(phenylene)-5,5'-bibenzimidazole as the commercial product was made on the basis of its good fibre properties, availability of monomers and identification of suitable solvents for fibre extrusion<sup>35</sup>. The strong hydrogen bonding between =N and –NH–groups in PBI is the dominant molecular force, resulting in close chain packing and therefore good mechanical strength of membranes<sup>33, 35, 37</sup>. The pKa of benzimidazole group is about 5.5, which enables its absorption of acid as a plasticizer. In fact, PBI needs to be doped with acid to achieve adequate proton conductivity for fuel cell operation (more than 0.05 S·cm<sup>-1</sup>) due to its intrinsic conductivity is negligible i.e. 10<sup>-12</sup> S·cm<sup>-1</sup><sup>24</sup>. One of the most commonly used mineral acids is phosphoric acid (H<sub>3</sub>PO<sub>4</sub>). It is thermally stable at temperatures even above 100 °C. The proton conductivity of the fully doped PBI membrane 70 mS cm<sup>-1</sup> at 200 °C<sup>34</sup> which is almost as high as that of fully hydrated perfluorinated membranes (Nafion) and far less dependent on the relative humidity, thus allowing its use in HT-PEMFCs without humidifying the gas reactants.

Although phosphoric acid doped PBI membranes exhibits excellent properties needed for a good fuel cell performance, there are specific shortcomings which prevent the probability of its commercialization for HT- PEMFC application. At temperatures above 140 °C, the conductivity of phosphoric acid decreases under anhydrous conditions due to the formation of less conducting pyrophosphoric acid (H<sub>4</sub>P<sub>2</sub>O<sub>7</sub>), which is produced by condensing two phosphoric acid molecules and extracting a water molecule, as shown in the equation below.



The proton transfer in H<sub>3</sub>PO<sub>4</sub> doped PBI membranes mainly depends on the H<sub>3</sub>O<sup>+</sup> carrier motion. Though the rise in temperature could increase the ion motion and lower the membrane viscosity, the water evaporation at high temperature certainly affected the lack of proton carriers. So, the phenomenon of the fall on the conductivity of doped PBI membranes could be explained with temperature increasing<sup>38</sup>. These disadvantages include catalyst deactivation due to the adsorption of phosphate anions and carbon support corrosion remains as the main shortcomings<sup>39</sup>.

#### 1.4. Proton-Conducting Mechanisms

In the case of polymer electrolyte membrane, which is placed between the anode and cathode in PEMFCs, the complete knowledge of the proton transport mechanisms is extremely important because the generation of power by fuel cells is limited by proton conduction. In general, the proton transport mechanisms only can occur in the free spaces of membranes, such as surfaces and channels and pores connected to each other<sup>40</sup>.

There are two plausible proton-conducting mechanisms in PEMs: vehicle-type and Grotthuss-type mechanisms<sup>41</sup> as shown in figure 1.6: In the vehicle-type mechanism, protons migrate across the medium along with a “vehicle” or proton solvent such as  $\text{H}_3\text{O}$ ,  $\text{H}_5\text{O}_2^+$ , and  $\text{H}^9\text{O}_4^+$ . The overall proton conductivity is strongly relying on the vehicle diffusion rate. In the Grotthuss-type mechanism, protons are transferred from one site to another via the formation and breaking of hydrogen bonds (proton hopping), thus a vehicle or proton solvent is not required.

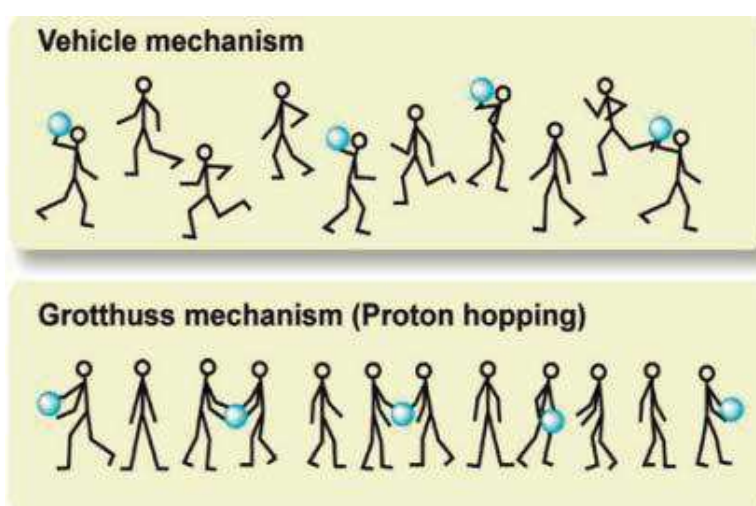


**Figure 1.6:** Types of conduction mechanisms<sup>41</sup>.

Generally, both of these mechanisms are not independent in PEMs and consistently could make joint involvements to proton conductivity. Mostly, in all the sulfonic acid attached PEMs, the vehicle-type mechanism is predominant in presence of water while the Grotthuss-type mechanism also contributes in the form of proton transfer via water molecules i.e., H-bond forming and breaking. In the N-heterocycle (e.g., imidazole) containing membranes at low temperatures, the vehicle-type mechanism is still dominant while the contribution of Grotthuss-type mechanism is significantly increased. For high temperature PEMFCs above 100 °C, it is difficult to maintain water in the membranes. High-temperature proton solvents like imidazole can be used to assist proton transfer, transforming vehicle-mechanism dominated PEMs to Grotthuss-mechanism dominated ones<sup>37, 41-42</sup>.

Figure 1.7 demonstrates the both mechanisms for phosphoric acid and an ionic liquid (1-butyl-3methylimidazolium bis (trifluoromethyl sulfonyl) imide)<sup>3, 43</sup>.

Because of water evaporation and mineral acids problems (i.e. phosphoric acid dehydration, corrosion and degradation issues) described above for PEMFC usage in elevated temperatures, a

more thermally stable, and the non-volatile dopant is required. In this work, we principally propose room temperature ionic liquids (RTIL) as ion conductor.

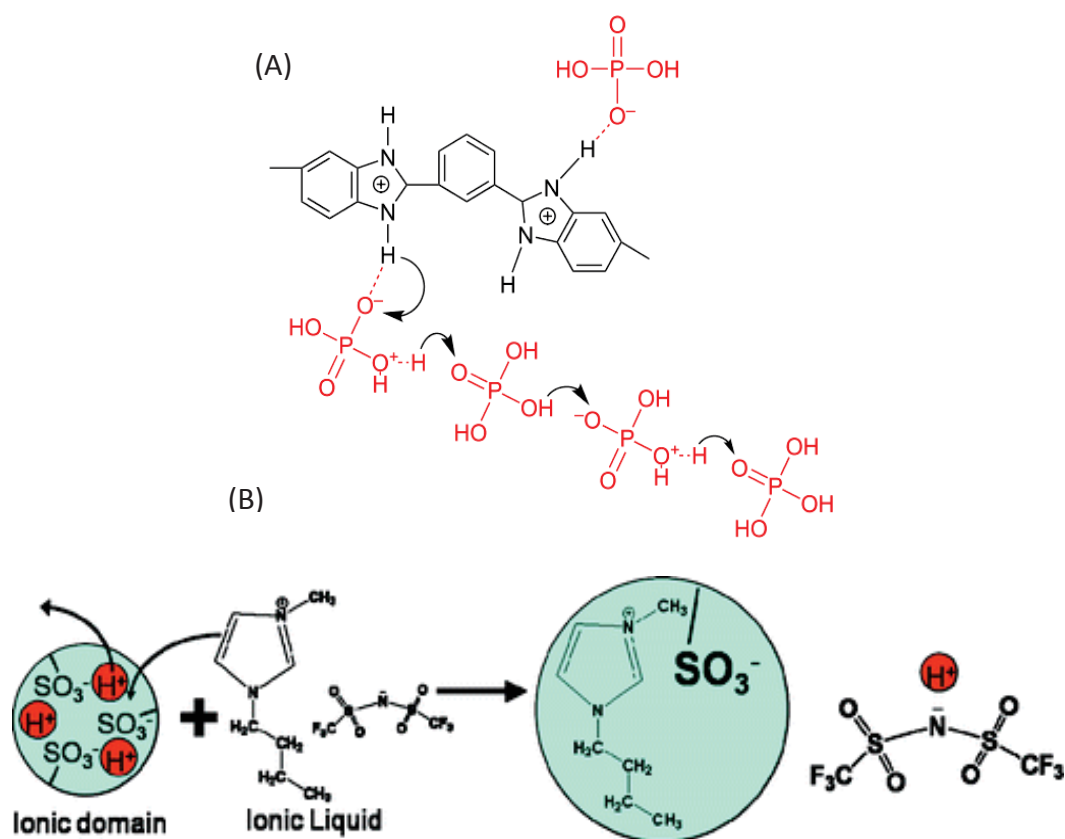


**Figure 1.7:** Proton conduction in (A) phosphoric acid<sup>43</sup> and (B) ionic liquids (1-butyl-3-methylimidazolium bis(trifluoromethyl sulfonyl) imide)<sup>3</sup>.

### 1.5. Ionic liquids as electrolytes in PEMFCs

Proton conducting room temperature Ionic Liquids (RTIL) have been considered as an alternative attractive electrolyte for high temperature application of PEMFCs. The first publication describing an IL by Paul Walden in 1914, who detected the special physical properties of ethylammoniumnitrate<sup>44</sup>.

Ionic liquids are salts completely composed of organic cations and either organic or inorganic anions, which have melting points below the typical temperature of 100 °C. This effect is from the low intermolecular interactions and weak packing efficiency of their asymmetrical ions and from the delocalization of their charges. They have attractive properties, such as negligible volatility, non-flammability, high thermal and electrochemical stability and outstanding ionic conductivity even under anhydrous conditions. They are formed entirely by ions and differ from ionic solutions in that



ionic liquids do not contain a solvent (Figure 1.8). Many ionic liquids are in liquid state at the room temperature and some of them even have a point of crystallization at very low temperatures<sup>45</sup>. The most commonly found cations and anions are presented in Figure 1.8.

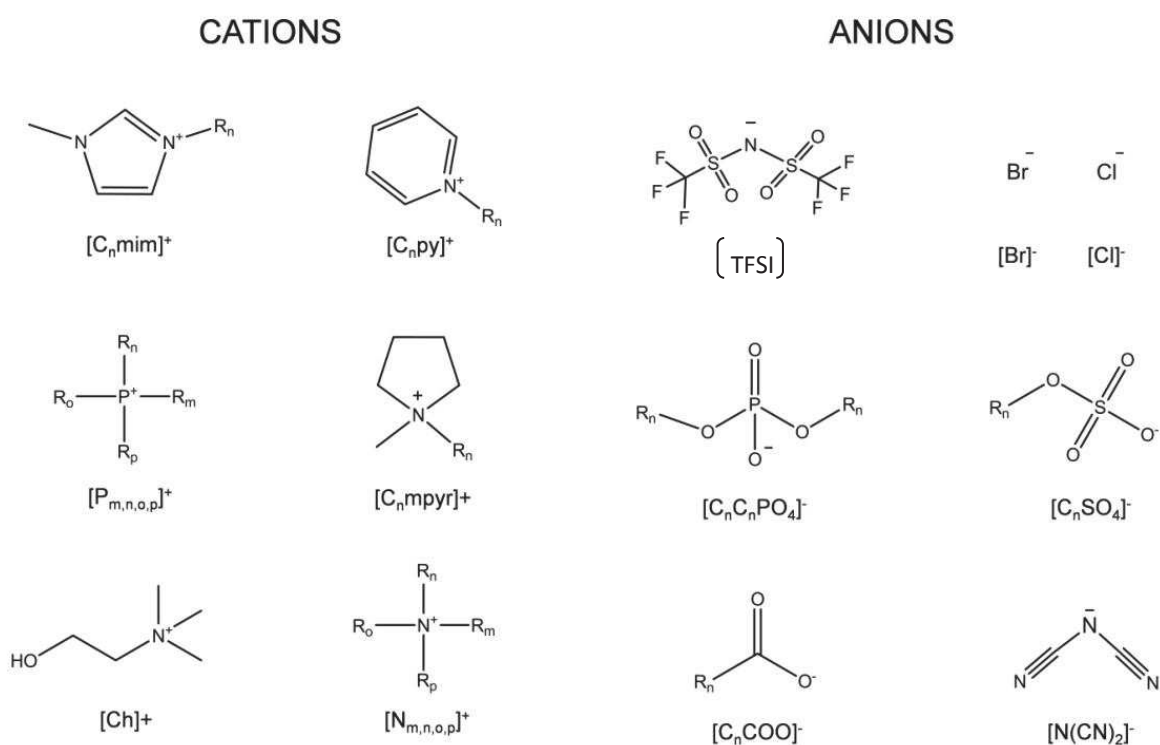


**Figure 1.8:** Cations and anions commonly used in ionic liquids.

Two general classes of ionic liquids exist: aprotic and protic. Aprotic ILs are categorized by a low melting point concerned to the difficulty of packing large asymmetrical cations with small anions. These ILs have a high mobility and ion concentration, making them appropriate electrolytes for lithium batteries. Protic ILs have a mobile proton positioned on the cation. The reactivity of this active proton makes them suitable for HTPEM applications<sup>45-46</sup>. A benefit of using protic IL is that system can be functioned at temperatures above 100 °C under anhydrous conditions since the proton transport is free of the water content.

The synthesis of protic ionic liquids is based on an acid-base neutralization reaction: a proton is transferred from a Brønsted acid to a Brønsted base



The most common cations available commercially and easier to synthesize are those based on imidazolium, so the selected ones for this work. There are so many efforts devoted to the characterization of different types of ILs for FC applications<sup>47</sup>.

Table 1.3 gives some typical physical properties viz. conductivity ( $\sigma$ ), density (d), and decomposition temperature ( $T_d$ ) of some common imidazolium based ionic liquids.

**Table 1.3:** Values of some physical parameters of few ionic liquids (adapted from Ref<sup>48</sup>).

Ionic liquids	Density, d (gm/cm <sup>3</sup> )	$\sigma$ (mS.cm <sup>-1</sup> ) at 30 °C <sup>49</sup>	$T_d$ ( °C)
	25 C°		
[MMIM][TFSI]	1.55	11.0	-
[EMIM][TFSI]	1.51	11.0	455
[BMIM][TFSI]	1.43	4.6	439
[HMIM][TFSI]	1.37	2.7	-
[OMIM][TFSI]	1.32	1.6	-
[BMIM][TfO]	1.29	3.6	392
[BMIM][PF <sub>6</sub> ]	1.37	1.9	349
[BMIM][BF <sub>4</sub> ]	1.14	4.5	403

The incorporation of ionic liquids in polymers has been widely reviewed for gas separation<sup>50</sup>, however, increasingly more research works are studying this approach for FC applications<sup>45</sup>.

The mixture Polymer/IL is attained normally by physical methods: i) blend of ILs in the polymer solution; ii) IL impregnation in the dense polymer film (polymer doped with IL) and iii) RTIL immobilization in the porous polymer film. In the first strategy, the membranes are prepared by a solution casting method, dissolving the polymer in a convenient solvent and concentration. Subsequently, suitable amounts of IL and mineral acid (if applicable) with different mole ratios is added to the polymer. The second strategy is the same concept of doping acid base polymers with mineral acids, but using a RTIL instead. However, the efficiency of this approach depends on the viscosity of RTIL used, and a large excess of IL remains on surface polymer. To overcome this

situation, the third strategy deals with porous polymer matrices to enhance RTIL immobilization into the membrane.

Very few works deal with the incorporation of ILs and mineral acid (if applicable) at different molar composition on the PBI casting solution<sup>51-55</sup>. Of course, the key point is the miscibility between the IL and the polymer.

The composite blend membranes based on  $H_3PO_4$ /1-methyl-3-propyl-methylimidazolium dihydrogen phosphate ( $PMIH_2PO_4$ )/PBI were developed by Ye and co-workers for HTPEMFCs<sup>51</sup>, exhibiting a proton conductivity of  $2 \text{ mS}\cdot\text{cm}^{-1}$  at  $150 \text{ }^\circ\text{C}$  under anhydrous conditions; the conductivity increases once the membranes absorb some water vapour.

Alternatively, composite membranes were prepared from an organosoluble, fluorine-containing PBI with the ionic liquid, 1-hexyl-3-methylimidazolium trifluoromethanesulfonate (HMI-Tf)<sup>52</sup>. In this study, PBI/HMI-Tf membranes with different HMI-Tf concentrations have been prepared, and maximum conductivity reached to  $16 \text{ mS}\cdot\text{cm}^{-1}$  at  $250 \text{ }^\circ\text{C}$  under anhydrous conditions. Our group<sup>56</sup> developed composite blend PEMs based on ionic liquids encapsulated in large pore zeolites and PBI for HTPEMFC applications. Adding 1-H-3-methylimidazolium bis(trifluoromethanesulphonyl)imide ([HMIM][TFSI]) in commercial zeolites to a PBI casting solution has been applied for HTPEMFC applications, and the achieved maximum proton conductivity was  $54 \text{ mS}\cdot\text{cm}^{-1}$  at  $200 \text{ }^\circ\text{C}$  with the best membrane composition. The development of PEMs from the incorporation of poly (2,5-benzimidazole) (ABPBI) in phosphoric acid ( $H_3PO_4$ ) and ionic liquid (IL) 1-butyl-3-ethylbenzimidazolium dihydrogen phosphate (BEBzIM-  $H_2PO_4$ ) was reported<sup>53</sup>. Maximum conductivity of  $0.1 \text{ mS}\cdot\text{cm}^{-1}$  at  $150 \text{ }^\circ\text{C}$  was achieved from 50% IL and 50% phosphoric acid impregnation. Mamlouk et al<sup>55</sup> developed PBI-Diethylamine bisulphate/sulphate ionic liquid HTPEMFC application. Composite hybrid membranes were fabricated at different composition ratios PBI/xDESH. The ionic conductivity of the hybrid membrane significantly increases with increased temperature and ionic liquid content and reaches a maximum value of  $40 \text{ mS}\cdot\text{cm}^{-1}$  at  $200 \text{ }^\circ\text{C}$  in the PBI/12DESH membrane.

Recently Hooshyari et al<sup>57</sup> prepared two types of innovative composite membranes based on polybenzimidazole (PBI) containing dicationic ionic liquid 1,3-di(3-methylimidazolium) propane bis (trifluoromethylsulfonyl) imide ( $PDC_3$ ) and monocationic ionic liquid 1-hexyl-3-methylimidazolium bis (trifluoromethanesulfonyl) imide ( $PMC_6$ ) as electrolyte for high temperature fuel cells applications under anhydrous conditions. The highest proton conductivity of  $81 \text{ mS}/\text{cm}$  is achieved for PA doped  $PDC_3$  composite membranes with PBI/IL mole ratio: 4 at  $180 \text{ }^\circ\text{C}$ . A power density of

0.44 W/cm<sup>2</sup> is obtained at 0.5 V and 180 °C for PA doped PDC composite membranes. From the same group<sup>58</sup>, the composite membranes based on polybenzimidazole (PBI) and dicationic ionic liquid 1,6-di(3-methylimidazolium) hexane bis (hexafluorophosphate) (PDC<sub>6</sub>) or monocationic ionic liquid 1-Butyl-3-methylimidazolium hexafluorophosphate (PMC<sub>4</sub>) were prepared with solution casting method. The maximum ionic conductivity of 78 mS cm<sup>-1</sup> and power density of 0.40 W cm<sup>-2</sup> (at 0.5 V) is achieved for PA doped PDC and composite membranes with PBI/ionic liquid mole ratio: 4 at 180 °C under anhydrous condition.

Table 1.4 reviews the current literature concerning the PBI-IL based blend/blend HT-PEMFC from similar materials proposed in this thesis.

**Table 1.4:** Summary of current progress concerning dense/blend PBI-IL based HT-PEMs

System	IL/PIL name	T ( °C)	$\sigma$ (mS.cm <sup>-1</sup> )
Blend of PBI+H <sub>3</sub> PO <sub>4</sub> +IL <sup>51</sup>	1-methyl-3-propylmethylimidazolium Dihydrogenphosphate [PMIMH <sub>2</sub> ][PO <sub>4</sub> ]	150	2
Dense PBI+ H <sub>3</sub> PO <sub>4</sub> + IL-NaY zeolite <sup>56</sup>	1-H-3-methylimidazolium bis(trifluoromethanesulphonyl)imide ([HMIM][TFSI])	200	54
Dense PBI+HCL+IL <sup>a</sup> <sup>54</sup>	Diethylmethylammonium trifluoromethanesulfonate [DEMA][TfO]	160	21
ABPBI + H <sub>3</sub> PO <sub>4</sub> +IL <sup>53</sup>	1-butyl-3-ethylbenzimidazolium dihydrogen phosphate (BEBzIm- H <sub>2</sub> PO <sub>4</sub> )	150	0.1
Blend of PBI+ IL <sup>52</sup>	1-hexyl-3-methylimidazolium trifluoromethanesulfonate (HMIM-TFSI)	250	16
Hybrid of PBI + IL <sup>55</sup>	Diethylamine bisulphate/sulphate ionic liquid	200	40
Blend of PBI+ IL-graphite-oxide <sup>59</sup>	1-(3-aminopropyl)-3-methylimidazolium bromide	175	35
Blend of PBI+PIL <sup>60</sup>	poly(diallyl dimethyl ammonium trifluoride methane sulphonate	150	70
Blend of PBI + H <sub>3</sub> PO <sub>4</sub> +IL <sup>57</sup>	1,3-di(3-methylimidazolium)propanebis (trifluoromethylsulfonyl)imide(PDC <sub>3</sub> )	180	81
Blend of PBI + H <sub>3</sub> PO <sub>4</sub> + IL <sup>58</sup>	1,6-di(3-methylimidazolium) hexane bis (hexafluorophosphate) (PDC <sub>6</sub> )	180	78

## 1.6. Polymeric ionic liquids (PILs) as PEMs

In PEMFCs, polymer membranes swelled with protic ionic liquids suffer from the hydro-dynamical solvation phenomenon which limits the lifetime of the cell<sup>61</sup>.

Since liquids, ILs could leach from polymer structure where they were originally incorporated, thus, immobilization into supports has not always been successful<sup>48</sup>. Consequently, the polymerization of ILs comes as a solution for their immobilization into polymers effectively or synthesizes pure IL dense membranes. Polymerization of ILs emerges as an attractive alternative in terms of safety, stability and mechanical properties. Polymeric ionic liquids (PILs) retain some of the unique properties of IL, such as thermal stability, tunable solution properties and chemical stability, which when combined with intrinsic polymer properties, are anticipated to offer more advantages than ILs<sup>62-63</sup>.

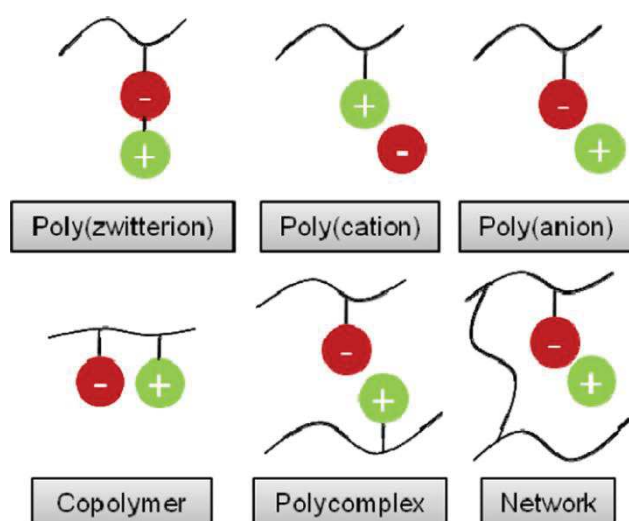


**Figure 1.9:** Polymeric ionic liquids<sup>64</sup>.

Polymeric ionic liquids also called Poly(ionicliquid)s, belong to a branch of polyelectrolytes that contain an ionic liquid (IL) species in each monomer repeating unit, connected through a polymeric backbone to form a macromolecular architecture<sup>62</sup>. Polymerised ionic liquids (PILs) include a wide variety of structures (Figure 1.9); they can be designed to form different systems, such as polycationic ILs, polyanionic ILs, poly-mer complexes, copolymers and poly(zwitterion)s, depending on the final application of the polyelectrolyte<sup>64</sup>.

The most innovative technique used to generate solid polymeric electrolytes from ionic liquids is the polymerisation of ionic liquids containing vinyl groups<sup>45</sup>.

PIL can be synthesized via two basic strategies: (1) direct polymerization of IL monomers, (2) chemical modification of existing polymers. In both approach, a couple of polymerization techniques are comprised, such as conventional and controlled radical polymerizations, ring opening metathesis polymerization, step-growth polymerization, and much more. From a synthetic perspective, each of these strategies as well as the polymerization techniques governs special structural factors of PILs and exhibits different benefits along with limits regarding the molecular design polymers<sup>44</sup>. The polymerization of IL monomers is a practically simple, intuitive, straightforward, and widely accepted approach to prepare PILs in many research groups. Figure 1.10 shows 5 major structures of IL monomers. In an IL monomer, a polymerizable unit can situate either on the cation (Figure 1.10A) or anion (Figure 1.10B), depending on the required polymeric design. IL monomers with two polymerizable units separated in the cation and anion (Figure 1.10C), or situated on the cations (Figure 1.10D and E) have also been reported to build up PIL networks.

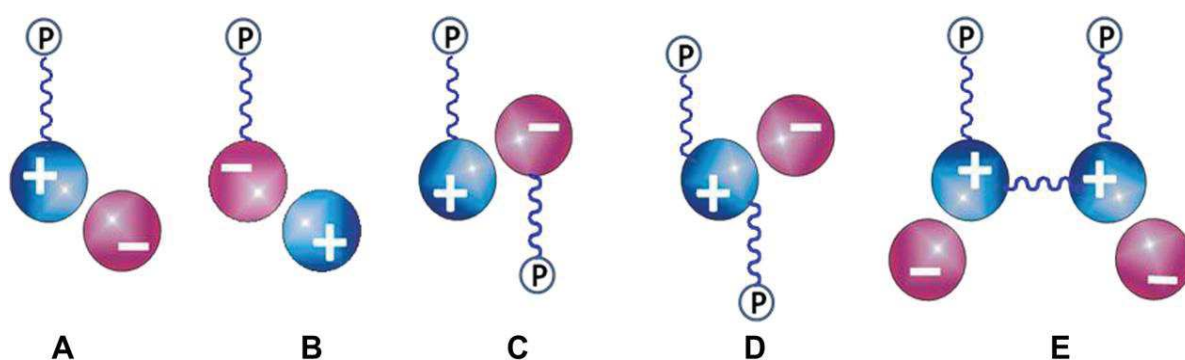


**Figure 1.10:** Basic IL monomers. “p” represents a polymerizing unit in an IL monomer<sup>44</sup>.

Several PIL structure designs have been driven by either curiosity or task-specific functions/properties reviewed by Yuan et al.<sup>62</sup>. They are collected and illustrated in figure 1.11.

Ionic liquid-containing polymers by direct bulk polymerization of N-vinyl imidazoliums were firstly reported by Ohno et al.<sup>65</sup> in 1998. Unfortunately, the ionic conductivity was about 1000 times lower after radical polymerization (from  $10 \text{ mS cm}^{-1}$  to  $10 \text{ }\mu\text{S cm}^{-1}$  at  $60^\circ\text{C}$  for the  $\text{EVIm}^+\text{TFSI}^-$  system) mainly due to a reduced number of mobile ions. Since then, conventional free-radical polymerization technique<sup>42, 44, 66-68</sup> has been widely used for the preparation of polymerized ionic liquids from mainly styrene derivatives, acrylic/methacrylic ester derivatives, vinyl ethers. In most of the cases, the polymerization process is induced by thermal initiators and usually needs relatively high temperatures ( $70\text{-}80^\circ\text{C}$ ) and long reaction times (2-24 h).

Lately, UV photo-polymerization at room temperature has gained significant importance<sup>69-70</sup>. This technique is versatile, easy to use, fast (minutes or seconds) and environmentally friendly, as energy consumption is low and there is no emission of volatile organic compounds, as the use of the solvent is almost avoided.

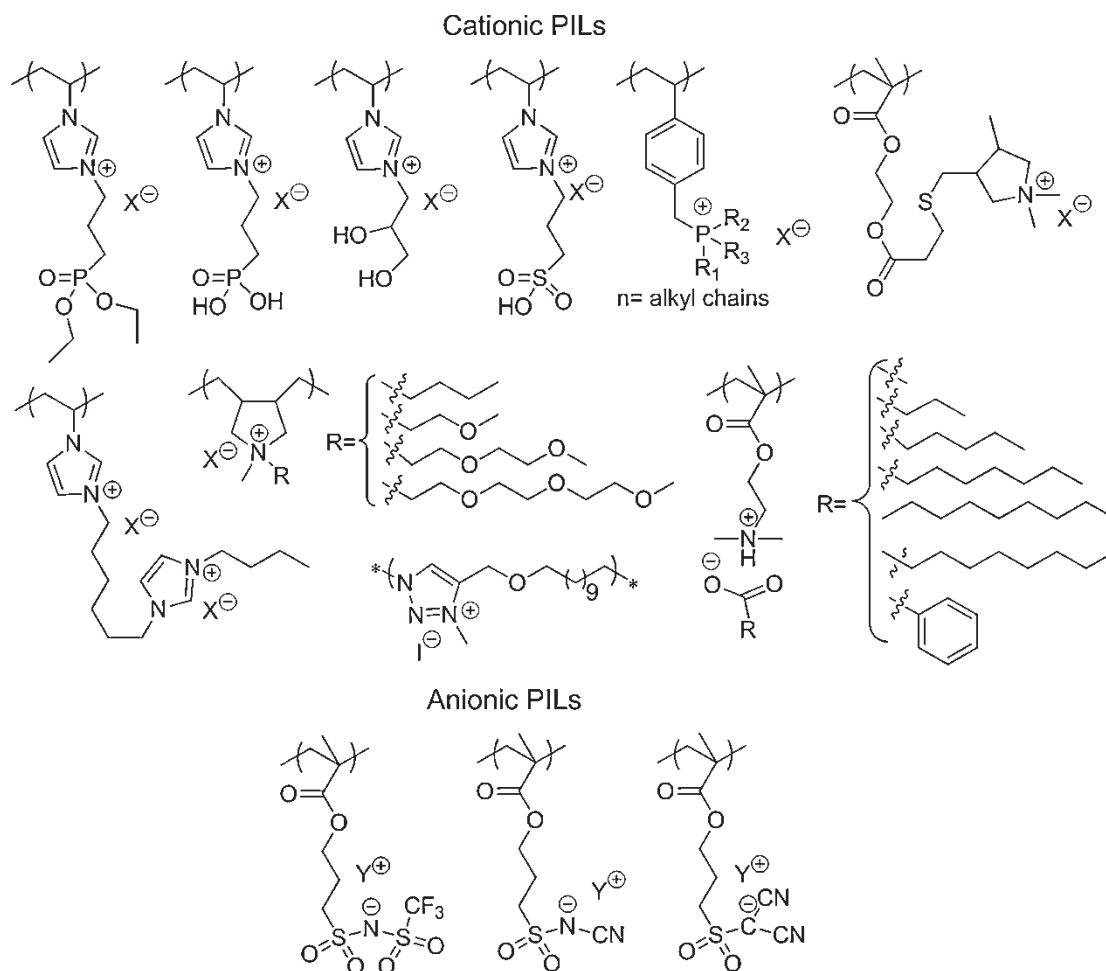


**Figure 1.11:** PIL chemical structures reported. References for cationic PILs , references for anionic PILs<sup>62</sup>.

Unlike other energy sources for polymerization synthesis, one of the main attractions of UV radiation is that it can be generated from a renewable source, i.e. by using solar ultraviolet lamps, which can be integrated into the future industrial production of polymer membranes from ILs. Moreover, it enables the full control of the process because the polymerization starts when the light is switched on and stops when the light is cut off. More specifically, the photopolymerization of ammonium and imidazolium RTIL monomers with either acrylate or styrene-based polymerizable groups have been already described for the preparation of dense films (20-200  $\mu\text{m}$  in thickness) after 300 s of irradiation time. However, the in situ polymerization may introduce some impurities into

the PILs such as unreacted monomer or initiator which may limit their electrochemical performance<sup>69, 71</sup>.

Following this approach, all solid state proton conductive films have been recently prepared in our group<sup>72</sup> by UV photo-assisted ( $\lambda=365$  nm for 15 min) polymerization of commercially available ammonium and imidazolium RTILs with vinyl-based reactive groups. Among the tested, the poly[1-(3H-imidazolium)ethylene] bis(trifluoromethanesulfonyl)imide with 2.5 mol.% of divinylbenzene as cross-linker represents the optimal tradeoff between conductivity and mechanical properties. Similarly, Ortiz et al<sup>69, 73</sup> have recently reported the fuel cell performance of PILs based on 1-(4-sulfobutyl)-3-vinylimidazolium trifluoromethanesulfonate] with divinylbenzene (10 mol.%) as a cross linker. Such electrolyte membrane showed a maximum power density of  $33 \text{ mW cm}^{-2}$  at  $25^\circ\text{C}$  under non-humidified conditions, but performance declined at temperatures above  $50^\circ\text{C}$  due to the membrane softening ( $T_g$  around  $10^\circ\text{C}$ ). PIL-PBI electrolyte blend membranes with adequate thermal and mechanical stability have been successfully prepared from poly(diallyl dimethyl ammonium trifluoride methane sulphonate)<sup>60</sup>. The maximum proton conductivity and power density values of blended membranes, upon phosphoric acid doping, were  $70 \text{ mS cm}^{-1}$  at  $150^\circ\text{C}$  and  $515 \text{ mW cm}^{-2}$  at  $160^\circ\text{C}$ , respectively. It is noteworthy to underline that the electrochemical performance of such blended PIL-PBI membranes is strongly dependent on the phosphoric acid uptake values.

### **1.7. PEMs based on porous membranes**

Yamaguchi's group<sup>74</sup> have focused on the concept of a conductive filler embedded into a porous, polymeric support (Figure 1.12 ). They have used poly(vinylsulfonic acid/acrylic acid) crosslinked conductive gel in a porous polytetrafluoroethylene (PTFE) open polymeric support, this synergistic concept combines the mechanical strength of the support with the conductivity of the conductive gel).



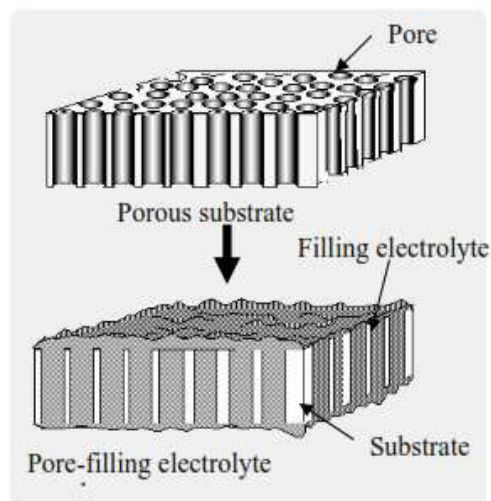


**Figure 1.12:** Schematic diagram of the concept of a pore-filling electrolyte membrane<sup>66, 74</sup>.

Table 1.5 reviews the literature concerning the porous polymer membranes embedded with different electrolytes (other than porous PBI+IL combination).

**Table 1.5:** Summary of some progress concerning porous polymer membrane-electrolyte based PEMs.

Porous support	electrolyte	Operation conditions	$\sigma$ (mS.cm <sup>-1</sup> )
Polytetrafluoroethylene (PTFE) <sup>74</sup>	Poly(vinylsulfonic acid/acrylic acid)	130 °C	70
Polybenzimidazole (PBI) <sup>75</sup>	Phosphoric acid (70 wt%)	140 °C	50
Matrimid <sup>76</sup>	Triethylammonium trifluoromethane sulphonate[TEA][TFSO <sub>3</sub> ]	130 °C	20
Poly(vinylidene fluoride) (PVDF) <sup>77</sup>	Tetrabutylammonium vinylbenzene sulfonate (TVS)- Cross-linked sulfonated polystyrene (CSPS)	4- 30% RH, 75 °C	7.8

The use of highly porous PBI membranes has been already described for PEMFC applications<sup>31, 70, 78-81</sup>. Owing to their higher specific surface area for acid doping or conducting phase embedding, the overall electrolyte performance is notably increased. Jheng et al<sup>80</sup>. proposed highly porous (83.1 vol.%) asymmetric PBI supports through a soft-templating method using 1-ethyl-3-methylimidazolium bis(trifluoromethanesulfonyl)imide, [EMIm][TFSI], as porogen agent. Proton conductivity values above 60 mS·cm<sup>-1</sup> at 160 °C were reported upon phosphoric acid doping (23.6 as

doping level). Van de ven et al<sup>78</sup>. reported macrovoid free random porous PBI membranes (65.6 % vol%) filled with ionic liquid 1-H-3-methylimidazolium bis(trifluoromethanesulfonyl) imide ([HMIM] TFSI). The obtained proton conductivity and power density of this PBI/IL membrane were 1.86 mS.cm<sup>-1</sup> at 190 °C and 0.039 W.cm<sup>-2</sup> at 150 °C respectively. Our group <sup>70</sup> has recently described the “in situ” UV polymerization 1-H-3-vinylimidazolium bis(trifluoromethanesulfonyl)imide on a highly porous PBI sponge-like matrix (above 75 vol%) achieving conductivity values above 300 mS cm<sup>-1</sup> at 200 °C under anhydrous conditions. While most of our attention was focused on the ion conductivity; their mechanical properties, of paramount importance for fuel cell application, revealed unsatisfactory: 0.2 GPa as Young Modulus and 1.3 MPa as tensile strength.

Table 1.6 reviews the current literature concerning the porous PBI-IL based HT-PEMs from similar approaches and materials proposed in this thesis.

**Table 1.6:** Summary of current progress concerning porous PBI-IL based HT-PEMs

System	IL/PIL name	T ( °C)	$\sigma$ (mS.cm <sup>-1</sup> )	Power density (mW.cm <sup>-2</sup> )
Porous PBI+IL <sup>78</sup>	1-H-3methylimidazoliumbis (trifluoromethanesulfonyl)imide [HMIM] [TFSI]	150	1.5	39
Porous PBI+IL+ H <sub>3</sub> PO <sub>4</sub> <sup>80</sup>	1-ethyl-3-methylimidazolium bis(trifluoromethanesulfonyl)imide [EMIM] [TFSI]	160	60	297
Porous PBI +PIL <sup>70</sup>	1-H-3-vinylimidazolium bis(trifluoromethanesulfonyl)imide [HVIM] [TFSI]	200	300	-

There is a challenging need for immobilizing ILs in solid devices for material applications while keeping their specific properties. Supported Ionic Liquid Membranes (SILM), widely used for gas separation, has been scarcely attempted for FC applications<sup>78-79, 82</sup>. This approach relies on RTILs immobilization in the pores of a porous support by capillary forces. Although the negligible protic ionic liquid vapor pressure alleviates one of the problems associated with traditional SILMs, namely liquid volatility; expulsion of the liquid from the membrane pores is a major concern. A proper design of the support, with sub-micron pores, combined with an ionic liquid having high surface tension leads to SLIMs with adequate physical stability for applications involving moderate to high trans-membrane pressures<sup>83</sup>. Fabricating a polymeric container with an optimized pore architecture is extremely essential<sup>84</sup> since the performance of PEM based on immersing a porous

support into ILs, mainly depends on the porous structure. Thus, the present thesis for HTPEM aims to improve both, the ion conductivity and the dimensional stability of the PIL supported membranes by a proper design of the porous architecture.

### 1.7.1. Microsieves

Microsieves are a special type of screen filters. Introduced in 1998 by Kuiper et al<sup>85</sup> microsieves have been growing steadily in application span. The main feature of a microsieve is the presence of well-defined, straight pores that go through the film. This porosity is characterized by a well-defined pitch, a narrow pore size distribution, and consistent pore shape<sup>86</sup>. we have recently fabricated PBI microsieves in our group by using microtransfer moulding<sup>87</sup>.

### 1.7.2. Microtransfer molding technique ( $\mu$ TM)- Photolithography:

Photolithography relies on the chemical change in a photoresist upon exposure to light, affecting, for example, the solubility of the resist. A schematic representation of photolithography is depicted in Figure 1.13.1-3. A thin layer of resist applied on substrate (Figure 1.13.1) is exposed to UV light through the pattern of a mask (Figure 1.13.2). When the resist is subsequently developed, the pattern on the mask is transferred to the resist (Figure 1.13.3). In microtransfer molding ( $\mu$ TM) the poly(dimethyl siloxane) (PDMS) mold is coated with a prepolymer will deposit on the master resist (Figure 1.13.4), and finally the fabricated PDMS mold is peel off the master after curing (Figure 1.13.4).

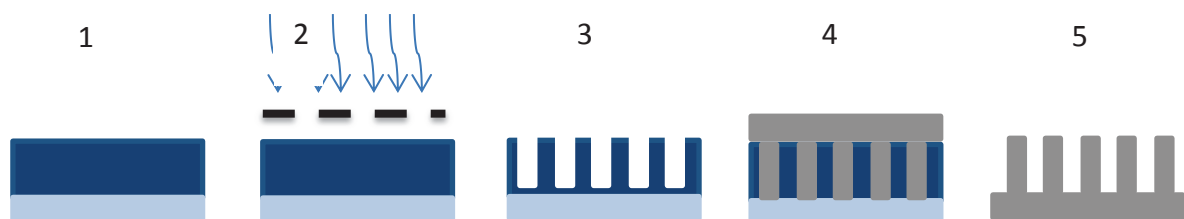


**Figure 1.13:** Schematic representation microtransfer molding ( $\mu$ TM) by photolithography

### 1.7.3. Phase Separation MicroFabrication (PS $\mu$ F)

Phase separation/inversion is a chemical phenomenon exploited in the fabrication of artificial membranes. It is performed by removing the solvent from a liquid-polymer solution, leaving a porous, solid membrane. Phase separation processes have been extensively used to produce

membranes for life support (water production, hemodialysis, controlled drug delivery) and for separation processes in chemical, pharmaceutical and food industry.

Phase separation MicroFabrication (PS $\mu$ F) is a versatile microfabrication technique, capable to structure a very broad range of polymers, including block copolymers, biodegradable and conductive polymers without the need for cleanroom facilities. PS $\mu$ F is a technique that is used to produce polymer films with patterned surfaces developed at University of Twente in 2003<sup>88</sup>. PS $\mu$ F combines the technique of phase inversion to fabricate membranes with the use of molds to fabricate negative replicates, i.e. microtransfer molding (Figure 1.14). The fabrication of microsieves is based on casting a polymer solution on a mold that contains uniform microstructures (Figure 1.14.A), for example, pillars or cones<sup>86</sup>.

In microsieve fabrication, phase separation occurs in two stages: vapor induced (VIPS) and liquid-induced phase separation (LIPS)<sup>89</sup>. 1. Vapor-induced phase separation (VIPS), also called "dry casting" or "air casting". Evaporation of the solvent will result in a dense or porous product depending on the polymer and the used solvent(s) mixtures; the vapor may contain water or organic solvent molecules that may be absorbed by the casted film and will influence the porosity of the product. 2. liquid-induced phase separation (LIPS, mostly referred to as "immersion casting" or "wet casting". During phase separation (Figure 1.14.B), the film solidifies, shrinks in both thickness and lateral directions<sup>90</sup>. Shrinkage of the polymer film in thickness allows the pillars to penetrate the entire film and leads to the formation of uniform pores<sup>86</sup>. Shrinkage in lateral directions leads to detachment of the film from the pillars, which makes it possible to (easily) peel off the film (Figure 1.14.C) from the mold<sup>91</sup>. Virtually every polymer/solvent combination that is suitable for phase inversion can be used for PS $\mu$ F, with the only requirement that shrinkage in both thickness and lateral direction must take place.

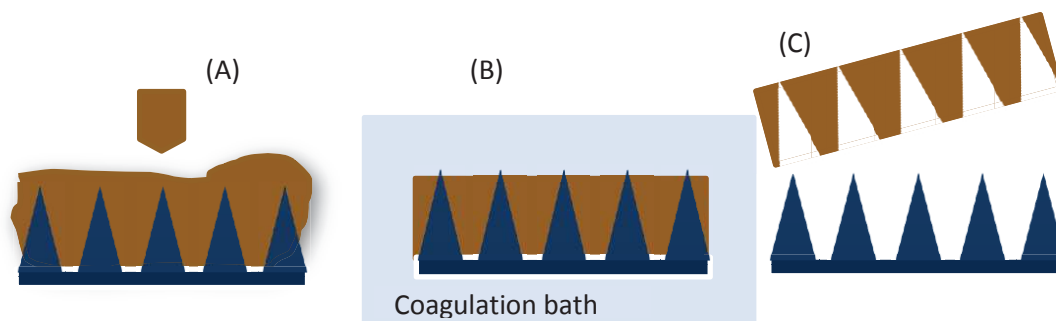


**Figure 1.14:** Principle of PS $\mu$ F. (A) Polymer solution is casted on a patterned surface (mold). (B) The polymer solidifies via phase separation and (C) a negative replica of the mold is obtained.

## 2. Supported Ionic liquid membranes (SILMs) for methane upgrading.

The necessity for natural gas (methane, CH<sub>4</sub>) is growing and that there is a rising need to develop the ability to upgrade subquality gas reserves, which manage to exist in relatively low quantities in remote zones. The global utilization is above 3.1 trillion cubic meters (110 trillion standard cubic feet) for every year, and is certainly the major industrial gas separation application. Fourteen percent of U.S. natural gas comprises additional N<sub>2</sub>, and cannot be shipped to the national pipeline without treatment. Upgrading this natural gas could allow access to an estimated 10 trillion scf (standard cubic feet per day) additional natural gas in the USA alone<sup>92-94</sup>.

Methane is produced from biodegradable waste anaerobic degradation in landfills and its major portion is comprised of CH<sub>4</sub> (30-65% in volume), CO<sub>2</sub> (25-50% in volume), N<sub>2</sub> (1-15% in volume) and with some trace gases<sup>95-97</sup>. As a landfill ages, gas generation decays, generating gas with lowered methane content and sometimes with discontinuous flow. Landfill gas (LFG) with high methane content is reasonably lead to burn and on current landfill sites is normally used to generate electricity. This prevents local pollution problems and significantly reduces the potential impact on global warming from the landfill site. Nevertheless, when the methane content of the landfill gas drops below a certain level (approximately 35-40% in volume) it cannot be used to generate electricity and the gas will require to be flared instead. Once the methane content drops again (approximately 20% in volume), there is absolutely not sufficient methane to keep a flare alight. Then the gas is classified as low calorific landfill gas and it is presently vented untreated into the atmosphere where it acts as a greenhouse gas above 20 times more powerful than carbon dioxide spot<sup>95, 97</sup>. Low methane content LFG is not appropriate for feeding engines and is usually flared. This type of landfill gas may be enhanced by recovering CH<sub>4</sub> from main stream<sup>97</sup>.

The inevitability and noticeable significance of separation technology in numerous areas of energy and chemical industries is fully recognized. Particularly, a major growth can be identified in development of technologies related to the separation of gaseous species. A separation mechanism based on molecular size works well in only if the differences between the kinetic diameters of the gas molecules are sufficiently high, but becomes less effective when the differences get smaller. As shown in table 1.7, methane and nitrogen are almost identical in size (methane d=3.8 Å, nitrogen d=3.64 Å), conventional separation technology cannot be worked to successfully separate N<sub>2</sub> from high-N<sub>2</sub> content natural gas.

**Table 1.7:** Kinetic diameter and critical temperature of various molecules

Gas	Kinetic diameter (Å)	Critical temperature (K)
H <sub>2</sub> O	2.65	647.3
H <sub>2</sub>	2.89	33.2
CO <sub>2</sub>	3.3	304.2
O <sub>2</sub>	3.46	154.6
N <sub>2</sub>	3.64	126.2
CH <sub>4</sub>	3.8	190.6

So far N<sub>2</sub> separation has been achieved via cryogenic distillation, nevertheless, cryogenic natural gas-nitrogen separation plants are capital intensive (table 1.8), and must be very large to take advantage of economy of scale. Membrane-based nitrogen separation has a promise market in smaller natural gas operations, where cryo-genic distillation is uneconomical. Low-cost methods are still needed for raising the quality of moderately small volumes of gas generated far from main processing centers. For these reasons, membrane-based natural gas processing has been pursued with particular focus on ionic liquid membranes, which differ from polymers in that they separate transport gases by sorption rate differences rather than by diffusion rates<sup>93</sup>.

**Table 1.8:** Cost comparison for removal of 8% nitrogen from subquality natural gas adapted from Scholes et al.<sup>93</sup>.

Technology	Total capital cost (US\$/ Mscfd)	Processing cost (US\$/ Mscf)
Cryogenic distillation	1184	1.30
Membranes	277	0.30

Membranes for natural gas processing were first commercialized in the 1980s, and have been the leading membrane gas separation process since then. Membrane technology is a powerful tool for gas separation processes because of their manufacturing and economical advantage and it can bring many advantages compared to other conventional separation technologies, namely the small scale of the equipment, reduced environmental impact, ease of incorporation into existing processes, low energy consumption, and operating costs. Membranes separate gasses based on the differences in physical and/or chemical interactions between the different gasses and the membrane material, which permit for some components to pass preferentially through the membrane. Depending upon

the material, membranes are normally categorized as inorganic (ceramic, metallic, carbon molecular sieves, silica, zeolites, metal organic supports), organic (polymeric membranes) and Mixed Matrix Membranes (inorganic-organic composite membranes)<sup>98</sup>.

The advantages of polymeric membranes specifically mechanical properties, low cost, synthetic feasibility, and large-scale fabrication chosen them more advantageous materials related to inorganic membranes for gas separation. Polymers are the simply processed material for membrane fabrication. They consist of excellent flexibility in their composition and modification is uncomplicated make them a better option<sup>99</sup>.

Membrane-based nitrogen separation has a potential market in smaller natural gas operations, for this separation, membranes can either be N<sub>2</sub> permeable or CH<sub>4</sub> permeable. In general glassy polymers are nitrogen permeable, while rubbery polymers are methane permeable<sup>93</sup>. For a 10% N<sub>2</sub> in CH<sub>4</sub> mixture, Baker<sup>94</sup> has shown that a membrane requires a CH<sub>4</sub>/N<sub>2</sub> selectivity of 6, however there are no membranes that can achieve this level of selectivity<sup>92-93</sup>. For a 10% N<sub>2</sub> in CH<sub>4</sub> mixture, membrane requires a N<sub>2</sub>/CH<sub>4</sub> selectivity of 17 to achieve the same level of separation in a single stage, but the best nitrogen-selective membrane currently known has a nitrogen selectivity of 2.5, which is far below the value required; this is why methane-permeable membranes are needed for this separation. The best methane-selective membrane (Polyamide-polyether copolymer- PEBAX 2533) currently known has a CH<sub>4</sub>/N<sub>2</sub> selectivity of 4.2 with 20 barrer permeability of CH<sub>4</sub>.

Polybenzimidazole (PBI) has received attention in the late 1960s as a membrane material; aliphatic polybenzimidazole was first invented by Brinker and Robeson. Soon after, Vogel and Marvel synthesized aromatic polybenzimidazole. Because of operability of PBI at extreme harsh conditions provided usage of this material in fire controlling for asbestos replacement, reverse osmosis, hydrogen purification, fuel cells<sup>35</sup>, electrolysis and electrochemical sensors<sup>100</sup>.

### **2.1. Ionic liquids for gas separation**

Not only Ionic liquids have been potentially used in chemical synthesis and catalysis, but also for gas separation processes, since their use as unique performing materials for vast different applications<sup>41, 101</sup>. From the literature, it has been recommended that ILs can be used as replacement solvents due to many advantages like lower energy demand for regeneration and negligible vapour pressure, which reduce the environmental issues concerning their use as solvents in gas absorption processes over traditional amine-based gas absorption<sup>102</sup>.

The anions of ILs have more influence on gas solubility<sup>103</sup> since gas molecules have a larger affinity for anion versus cation associations<sup>104</sup>. The anion effect on solubility was also examined through

molecular dynamics<sup>105</sup>, and the anion- gas molecule interactions were indicated to be the strongest solvation forces present. The bis(trifluoromethylsulfonyl)imide (TFSI) anion generally exhibits the best CH<sub>4</sub> selectivity<sup>106</sup> and have high overall CH<sub>4</sub> permeability<sup>103</sup>.

The effect of different functional groups, such as alkyl, ether, hydroxyl, nitrile, and fluorine, on the gas solubility properties of ILs has also been thoroughly studied<sup>107</sup>. It was found that increasing the gas solubility with increasing the cation alkyl side length, likely by increasing the existing volume for gas molecules thanks to a decrease in cation-anion interactions<sup>108</sup>.

## 2.2. Polymeric ionic liquid based membranes for gas separation

The performance of PILs as gas separation membranes was initially presented by Camper et al<sup>109</sup>. With CO<sub>2</sub>, CH<sub>4</sub> and N<sub>2</sub> solubility data and from the solution-diffusion mass transfer mechanism, permeabilities of immobilized ILs were calculated by decreasing the gas diffusion coefficients by following orders of magnitude, in a trial and error method.

Noble's group<sup>110</sup> investigated series of PIL membranes for gas separation applications. Five PILs containing alkyl-imidazolium cations bound to a polystyrene (Figure 1.15: PIL A 1-3) or polyacrylate backbone (Figure 1.15 PIL B 1-2) were synthesized by UV polymerization using a photo-initiator and a cross-linking agent.

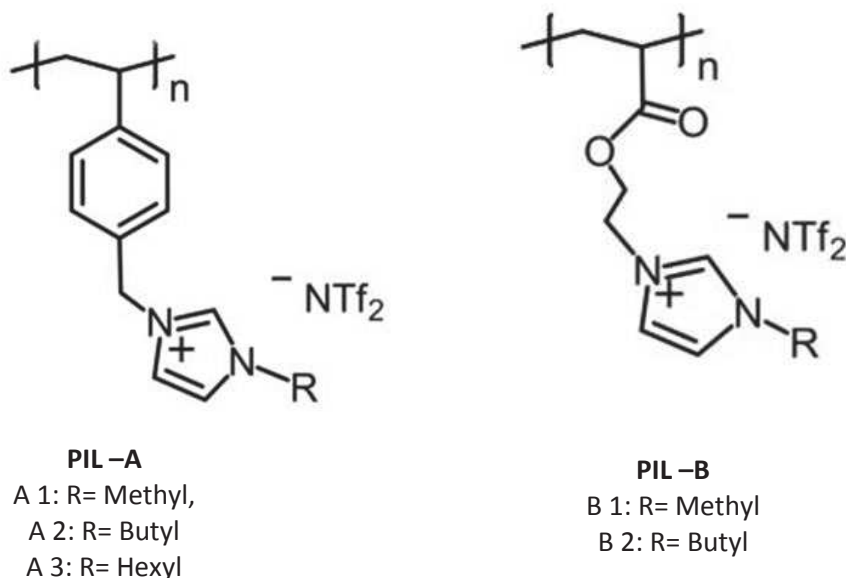


**Figure 1.15:** Chemical structures of cationic PILs with polystyrene and polyacrylate backbone that have been evaluated as gas separation membranes.



### 2.3. Supported ionic liquid membranes (SILMs)

The combination of ILs with membranes for gas separation is a relatively new concept developed in the last 15 years<sup>111</sup>. Many different types of membranes and membrane processes containing ILs have been reported, including supported IL membranes (SILMs), polymerized ionic liquid (PIL) membranes, polymer/IL gel membranes, as well as membrane absorption using membrane contactors (MCs) using ILs as absorbents.

A supported (or immobilized) liquid membrane (SLM) is a nondispersive-type liquid membrane, in which the liquid-phase selective material is immobilized in the pores of a porous support by capillary forces. If an IL is used in SLMs, the membranes are called Supported ionic liquid membranes (SILMs)<sup>50</sup>. Gas transport in an SLM involves three steps, as shown in Figure 1.16, gas molecules from feed side dissolve in the liquid phase of the SLM, diffuse through the SLM, and release to the permeate side of the SLM.

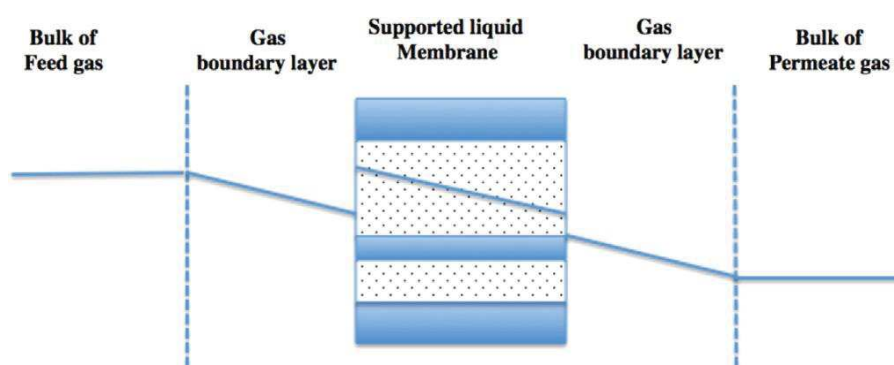


**Figure 1.16:** Gas transport in SLMs<sup>50</sup>.

The development of SILMs has received a recent boost mainly due to their easy preparation and versatility. Owing to the comparatively high viscosity of ILs compared to conventional solvents generally used in SILMs, the preparation method of SILMs plays a key role in liquid phase immobilization and thus in membrane stability. Three techniques have been mostly used to prepare SILMs, such as direct immersion/soaking, pressure method, and vacuum method. The main generally used method of preparing SILMs is soaking a porous support in the desired IL for few hours. Since ILs have relatively high viscosity and negligible vapor pressure, application of vacuum is normally applied to eliminate gas bubbles in resulting membranes. Toward the end of all these three procedures, excess IL is removed from the SILM surfaces either by leaving to drip overnight or by

wiping with a soft tissue paper. The amount of IL impregnated in the porous membrane support can be determined gravimetrically by weighing the membrane before and after immobilization<sup>98</sup>.

According to the Young–Laplace equation, smaller pore sizes ensure higher SILM stability, as higher pressure is needed to push the ILs out of the pores. As a higher porosity generally leads to a higher IL content in the SILM, pore size is also one of the significant concerns for membrane stability. Mostly, membranes with a pore sizes in the range 100–200 nm are used to prepare SILMs<sup>50</sup>.

Zhao et al.<sup>112</sup> systematically examined the liquid loss mechanism of SILMs, and they discovered that the liquid loss of SILMs could be attributed to two factors: membrane compression and IL extrusion from the large pores. Hence, by selecting an appropriate pore size for the porous support, the membrane system can bear a trans-membrane pressure up to 7.0 bar<sup>113</sup>. Several studies have examined the long-term stability of SILMs. For example, Scovazzo et al. reported SILMs without the loss of performance over more than 100 days<sup>114</sup>, and Hanioka et al. reported that their SILM showed 260 days of stable operation<sup>115</sup>. Most of the reported SILMs were prepared using microfiltration membranes as porous supports and operated under relatively low trans-membrane pressures. As reducing the pore size will enhance SILM pressure resistance, nanofiltration membranes have also been investigated as porous supports for SILMs. Experimental results showed that ILs do not discharge from the nanofiltration membrane structure even under a trans-membrane pressure up to 10 bar, suggesting that SILMs based on nanofiltration supports may be used for practical applications at relatively high pressures.

The effects of various operational parameters (e.g., moisture, temperature) on the separation performance of these SILMs have been thoroughly explored<sup>116-117</sup>. It has been noticed that overall, SILMs have long-term stability performance at low feed pressures but become unstable at high pressures. If the transmembrane pressure difference exceeds the capillary forces holding the IL in the porous material, the SILM membrane may crash as the ILs will be driven out of the porous support. Moreover, the permeability of gases normally increased with increasing temperature thanks to the strong temperature-dependency of the IL viscosity. Furthermore, reactive gas solubility usually decreases (Henry's Law constant increases) significantly with increasing temperature compared to other gases, leading to lower selectivity values at higher temperature. Wickramanayake et al.<sup>118</sup> prepared hollow-fiber SILMs using [C<sub>6</sub>mim][TFSI] and two commercially available polymers (Matrimid 5218, and Torlon 4000T)<sup>118</sup>. The results revealed that the drop in selectivity may be due to the fact that gas diffusion dominates at high temperatures. Moreover, the increasing temperature decreases the stability (i.e. by decreasing the surface tension) and the membranes may have formed pinholes.

The permeability of methane and other gases through some recently reported SILMs based on imidazolium cation, TFSI anion RTILs and the respective support materials are summarized in Table 1.9.

**Table 1.9:** Gas permeabilities and corresponding permselectivities of SILMs having imidazolium based cation and TFSI anion

IL	Support-temp	Gas permeability (Barrer)			Ideal selectivity
		H <sub>2</sub>	N <sub>2</sub>	CH <sub>4</sub>	CH <sub>4</sub> /N <sub>2</sub>
<b>IM cation with different anions</b>					
[C <sub>4</sub> MIM][BF <sub>4</sub> ]	Hydrophobic PVDF <sup>119</sup> - 30 °C	33.7	9.6	3.4	0.35
[C <sub>10</sub> MIM][BF <sub>4</sub> ]	-	77.1	22.3	7.2	0.32
[C <sub>2</sub> MIM][CF <sub>3</sub> SO <sub>3</sub> ]	Hydrophobic PVDF <sup>120</sup> - 30 °C	37.2	14.3	21.1	1.47
<b>[TFSI] anion with different cations</b>					
[C <sub>12</sub> mpyr][TFSI]	Hydrophobic PVDF <sup>121</sup> - 20 °C		12	24.2	2.0
[P <sub>(14)666</sub> ][TFSI]	Glass fiber <sup>106</sup> -30 °C		64	169	2.6
[N <sub>(4)111</sub> ][TFSI]	Glass fiber <sup>122</sup> -30 °C		41	63	1.53
<b>IM cation with [TFSI] Anion</b>					
[C <sub>2</sub> MIM][TFSI]	PES <sup>114</sup> -30 °C		73.6	139	1.88
[C <sub>n</sub> MIM][TFSI]	PES <sup>123</sup> -26 °C		12	16	1.33
[C <sub>2</sub> MIM][TFSI]	Hydrophilic PES <sup>124</sup> - 30 °C		51	94	1.84
[C <sub>4</sub> F <sub>5</sub> MIM][TFSI]	PES <sup>123</sup> - 23 °C		12	17	1.41

Among large diversity of ILs, those based on the TFSI anion with imidazolium cation typically present a higher permeability of CH<sub>4</sub>. So far, all these reported SILMs (based on IMIM cation and TFSI anion) were prepared with aprotic ILs.

## References:

1. Böhlinger, C.; Rutherford, T. F.; Tol, R. S. J., THE EU 20/20/2020 targets: An overview of the EMF22 assessment. *Energy Economics* **2009**, *31*, Supplement 2, S268-S273.
2. Elmer, T.; Worall, M.; Wu, S.; Riffat, S. B., Fuel cell technology for domestic built environment applications: State of-the-art review. *Renewable and Sustainable Energy Reviews* **2015**, *42*, 913-931.
3. Chandan, A.; Hattenberger, M.; El-kharouf, A.; Du, S.; Dhir, A.; Self, V.; Pollet, B. G.; Ingram, A.; Bujalski, W., High temperature (HT) polymer electrolyte membrane fuel cells (PEMFC) – A review. *Journal of Power Sources* **2013**, *231*, 264-278.
4. Sharaf, O. Z.; Orhan, M. F., An overview of fuel cell technology: Fundamentals and applications. *Renewable and Sustainable Energy Reviews* **2014**, *32*, 810-853.
5. National Fuel Cell Research Center at the University of California. <http://www.nfrcr.uci.edu/3/ABOUTUS/overview/default.aspx> (accessed October 15, 2016).
6. FUELCELLS SECTION. [http://www.energy.gov/sites/prod/files/2016/06/f32/fcto\\_myRDD\\_fuel\\_cells.pdf](http://www.energy.gov/sites/prod/files/2016/06/f32/fcto_myRDD_fuel_cells.pdf) (accessed October 15, 2016).
7. Tollefson, J., Tollefson J. US Congress revives hydrogen vehicle research. *Nature* **2009**, *460*:442–3.
8. Fuel cell and hydrogen joint undertaking <http://www.fch.europa.eu/> (accessed October 15, 2016).
9. Alaswad, A.; Baroutaji, A.; Achour, H.; Carton, J.; Al Makky, A.; Olabi, A. G., Developments in fuel cell technologies in the transport sector. *International Journal of Hydrogen Energy* **2016**, *41* (37), 16499-16508.
10. FUEL CELL TECHNOLOGIES OFFICE ACCOMPLISHMENTS AND PROGRESS. <https://energy.gov/eere/fuelcells/fuel-cell-technologies-office-accomplishments-and-progress> (accessed October 15, 2016).
11. Jacob Spendelow, J. M. Fuel Cell System Cost -2014 [https://energy.gov/sites/prod/files/2015/06/f22/14014\\_fuel\\_cell\\_system\\_cost\\_2014.pdf](https://energy.gov/sites/prod/files/2015/06/f22/14014_fuel_cell_system_cost_2014.pdf) (accessed October 15, 2016).
12. DOE TECHNICAL TARGETS FOR POLYMER ELECTROLYTE MEMBRANE FUEL CELL COMPONENTS. <https://energy.gov/eere/fuelcells/doe-technical-targets-polymer-electrolyte-membrane-fuel-cell-components> (accessed October 20, 2016).
13. Space applications of hydrogen and fuel cells. [http://www.nasa.gov/topics/technology/hydrogen/hydrogen\\_2009.html](http://www.nasa.gov/topics/technology/hydrogen/hydrogen_2009.html) (accessed October 15, 2016).
14. Raza, R.; Akram, N.; Javed, M. S.; Rafique, A.; Ullah, K.; Ali, A.; Saleem, M.; Ahmed, R., Fuel cell technology for sustainable development in Pakistan – An over-view. *Renewable and Sustainable Energy Reviews* **2016**, *53*, 450-461.
15. Li, X.; Faghri, A., Review and advances of direct methanol fuel cells (DMFCs) part I: Design, fabrication, and testing with high concentration methanol solutions. *Journal of Power Sources* **2013**, *226*, 223-240.
16. Rikukawa, M.; Sanui, K., Proton-conducting polymer electrolyte membranes based on hydrocarbon polymers. *Progress in Polymer Science* **2000**, *25* (10), 1463-1502.
17. Scott, K.; Shukla, A. K., Polymer electrolyte membrane fuel cells: Principles and advances. *Reviews in Environmental Science and Bio/Technology* **2004**, *3* (3), 273-280.

18. Thounthong, P.; Raël, S.; Davat, B., Energy management of fuel cell/battery/supercapacitor hybrid power source for vehicle applications. *Journal of Power Sources* **2009**, *193* (1), 376-385.
19. Liu, Y.; Lehnert, W.; Janßen, H.; Samsun, R. C.; Stolten, D., A review of high-temperature polymer electrolyte membrane fuel-cell (HT-PEMFC)-based auxiliary power units for diesel-powered road vehicles. *Journal of Power Sources* **2016**, *311*, 91-102.
20. Bose, S.; Kuila, T.; Nguyen, T. X. H.; Kim, N. H.; Lau, K.-t.; Lee, J. H., Polymer membranes for high temperature proton exchange membrane fuel cell: Recent advances and challenges. *Progress in Polymer Science* **2011**, *36* (6), 813-843.
21. Krishnan, P.; Park, J.-S.; Kim, C.-S., Performance of a poly(2,5-benzimidazole) membrane based high temperature PEM fuel cell in the presence of carbon monoxide. *Journal of Power Sources* **2006**, *159* (2), 817-823.
22. Kwon, K.; Yoo, D. Y.; Park, J. O., Experimental factors that influence carbon monoxide tolerance of high-temperature proton-exchange membrane fuel cells. *Journal of Power Sources* **2008**, *185* (1), 202-206.
23. Hogarth, W. H. J.; Diniz da Costa, J. C.; Lu, G. Q., Solid acid membranes for high temperature ( $\geq 140^\circ\text{C}$ ) proton exchange membrane fuel cells. *Journal of Power Sources* **2005**, *142* (1-2), 223-237.
24. Asensio, J. A.; Sanchez, E. M.; Gomez-Romero, P., Proton-conducting membranes based on benzimidazole polymers for high-temperature PEM fuel cells. A chemical quest. *Chemical Society reviews* **2010**, *39* (8), 3210-39.
25. Dupuis, A.-C., Proton exchange membranes for fuel cells operated at medium temperatures: Materials and experimental techniques. *Progress in Materials Science* **2011**, *56* (3), 289-327.
26. Shao, Y.; Yin, G.; Wang, Z.; Gao, Y., Proton exchange membrane fuel cell from low temperature to high temperature: Material challenges. *Journal of Power Sources* **2007**, *167* (2), 235-242.
27. Collier, A.; Wang, H.; Zi Yuan, X.; Zhang, J.; Wilkinson, D. P., Degradation of polymer electrolyte membranes. *International Journal of Hydrogen Energy* **2006**, *31* (13), 1838-1854.
28. Li, Q.; He, R.; Jensen, J. O.; Bjerrum, N. J., Approaches and Recent Development of Polymer Electrolyte Membranes for Fuel Cells Operating above  $100^\circ\text{C}$ . *Chemistry of Materials* **2003**, *15* (26), 4896-4915.
29. Mark F. Mathias, R. M., Hubert A. Gasteiger, Jason J. Conley,; Timothy J. Fuller, C. J. G., Shyam S. Kocha, Daniel P. Miller,; Corky K. Mittelsteadt, T. X., Susan G. Yan, Paul T. Yu, Two Fuel Cell Cars In  
Every Garage? *The Electrochemical Society Interface* **2005**, 24-35.
30. Li, H.-Y.; Liu, Y.-L., Nafion-functionalized electrospun poly(vinylidene fluoride) (PVDF) nanofibers for high performance proton exchange membranes in fuel cells. *Journal of Materials Chemistry A* **2014**, *2* (11), 3783.
31. Eguizábal, A.; Lemus, J.; Urbiztondo, M.; Garrido, O.; Soler, J.; Blazquez, J. A.; Pina, M. P., Novel hybrid membranes based on polybenzimidazole and ETS-10 titanosilicate type material for high temperature proton exchange membrane fuel cells: A comprehensive study on dense and porous systems. *Journal of Power Sources* **2011**, *196* (21), 8994-9007.
32. Ngamsantivongsa, P.; Lin, H.-L.; Yu, T. L., Crosslinked ethyl phosphoric acid grafted polybenzimidazole and polybenzimidazole blend membranes for high-temperature proton exchange membrane fuel cells. *Journal of Polymer Research* **2016**, *23* (2).
33. Li, Q.; He, R.; Jensen, J. O.; Bjerrum, N. J., PBI-Based Polymer Membranes for High Temperature Fuel Cells – Preparation, Characterization and Fuel Cell Demonstration. *Fuel Cells* **2004**, *4* (3), 147-159.
34. Lobato, J.; Cañizares, P.; Rodrigo, M. A.; Linares, J. J.; Aguilar, J. A., Improved polybenzimidazole films for H<sub>3</sub>PO<sub>4</sub>-doped PBI-based high temperature PEMFC. *Journal of Membrane Science* **2007**, *306* (1-2), 47-55.

35. Li, Q.; Jensen, J. O.; Savinell, R. F.; Bjerrum, N. J., High temperature proton exchange membranes based on polybenzimidazoles for fuel cells. *Progress in Polymer Science* **2009**, *34* (5), 449-477.
36. Chung, T.-S., A critical review of polybenzimidazoles: historical development and future R&D. *Journal of Macromolecular Science, Part C: Polymer Reviews* **1997**, *37* (2), 277-301.
37. Zuo, Z.; Fu, Y.; Manthiram, A., Novel Blend Membranes Based on Acid-Base Interactions for Fuel Cells. *Polymers* **2012**, *4* (4), 1627-1644.
38. Lobato, J.; Cañizares, P.; Rodrigo, M. A.; Linares, J. J., PBI-based polymer electrolyte membranes fuel cells: Temperature effects on cell performance and catalyst stability. *Electrochimica Acta* **2007**, *52* (12), 3910-3920.
39. Galbiati, S.; Baricci, A.; Casalegno, A.; Marchesi, R., Degradation in phosphoric acid doped polymer fuel cells: A 6000 h parametric investigation. *International Journal of Hydrogen Energy* **2013**, *38* (15), 6469-6480.
40. Sproll, V.; Nagy, G.; Gasser, U.; Balog, S.; Gustavsson, S.; Schmidt, T. J.; Gubler, L., Structure–property correlations of ion-containing polymers for fuel cell applications. *Radiation Physics and Chemistry* **2016**, *118*, 120-123.
41. Ueki, T.; Watanabe, M., Macromolecules in ionic liquids: progress, challenges, and opportunities. *Macromolecules* **2008**, *41* (11), 3739-3749.
42. Mecerreyes, D., Polymeric ionic liquids: Broadening the properties and applications of polyelectrolytes. *Progress in Polymer Science* **2011**, *36* (12), 1629-1648.
43. Ma, Y. L.; Wainright, J. S.; Litt, M. H.; Savinell, R. F., Conductivity of PBI Membranes for High-Temperature Polymer Electrolyte Fuel Cells. *Journal of The Electrochemical Society* **2004**, *151* (1), A8.
44. Yuan, J.; Antonietti, M., Poly(ionic liquid)s: Polymers expanding classical property profiles. *Polymer* **2011**, *52* (7), 1469-1482.
45. Díaz, M.; Ortiz, A.; Ortiz, I., Progress in the use of ionic liquids as electrolyte membranes in fuel cells. *Journal of Membrane Science* **2014**, *469*, 379-396.
46. Farnicola, A.; Scrosati, B.; Ohno, H., Potentialities of ionic liquids as new electrolyte media in advanced electrochemical devices. *Ionics* **2006**, *12* (2), 95-102.
47. Wang, X.; Chi, Y.; Mu, T., A review on the transport properties of ionic liquids. *Journal of Molecular Liquids* **2014**, *193*, 262-266.
48. Singh, M. P.; Singh, R. K.; Chandra, S., Ionic liquids confined in porous matrices: Physicochemical properties and applications. *Progress in Materials Science* **2014**, *64*, 73-120.
49. Tokuda, H.; Tsuzuki, S.; Susan, M. A. B. H.; Hayamizu, K.; Watanabe, M., How Ionic Are Room-Temperature Ionic Liquids? An Indicator of the Physicochemical Properties. *The Journal of Physical Chemistry B* **2006**, *110* (39), 19593-19600.
50. Dai, Z.; Noble, R. D.; Gin, D. L.; Zhang, X.; Deng, L., Combination of ionic liquids with membrane technology: A new approach for CO<sub>2</sub> separation. *Journal of Membrane Science* **2016**, *497*, 1-20.
51. Ye, H.; Huang, J.; Xu, J. J.; Kodiweera, N. K. A. C.; Jayakody, J. R. P.; Greenbaum, S. G., New membranes based on ionic liquids for PEM fuel cells at elevated temperatures. *Journal of Power Sources* **2008**, *178* (2), 651-660.
52. Wang, J. T.-W.; Hsu, S. L.-C., Enhanced high-temperature polymer electrolyte membrane for fuel cells based on polybenzimidazole and ionic liquids. *Electrochimica Acta* **2011**, *56* (7), 2842-2846.
53. Hernández Carrillo, R.; Suarez-Guevara, J.; Torres-González, L. C.; Gómez-Romero, P.; Sánchez, E. M., Incorporation of benzimidazolium ionic liquid in proton exchange membranes ABPBI-H<sub>3</sub>PO<sub>4</sub>. *Journal of Molecular Liquids* **2013**, *181*, 115-120.
54. Liu, S.; Zhou, L.; Wang, P.; Zhang, F.; Yu, S.; Shao, Z.; Yi, B., Ionic-liquid-based proton conducting membranes for anhydrous H<sub>2</sub>/Cl<sub>2</sub> fuel-cell applications. *ACS applied materials & interfaces* **2014**, *6* (5), 3195-200.

55. Mamlouk, M.; Ocon, P.; Scott, K., Preparation and characterization of polybenzimidazole/diethylamine hydrogen sulphate for medium temperature proton exchange membrane fuel cells. *Journal of Power Sources* **2014**, *245*, 915-926.
56. Eguizábal, A.; Lemus, J.; Pina, M. P., On the incorporation of protic ionic liquids imbibed in large pore zeolites to polybenzimidazole membranes for high temperature proton exchange membrane fuel cells. *Journal of Power Sources* **2013**, *222*, 483-492.
57. Hooshyari, K.; Javanbakht, M.; Adibi, M., Novel composite membranes based on PBI and dicationic ionic liquids for high temperature polymer electrolyte membrane fuel cells. *Electrochimica Acta* **2016**, *205*, 142-152.
58. Hooshyari, K.; Javanbakht, M.; Adibi, M., Novel composite membranes based on dicationic ionic liquid and polybenzimidazole mixtures as strategy for enhancing thermal and electrochemical properties of proton exchange membrane fuel cells applications at high temperature. *International Journal of Hydrogen Energy* **2016**, *41* (25), 10870-10883.
59. Xu, C.; Liu, X.; Cheng, J.; Scott, K., A polybenzimidazole/ionic-liquid-graphite-oxide composite membrane for high temperature polymer electrolyte membrane fuel cells. *Journal of Power Sources* **2015**, *274*, 922-927.
60. Rewar, A. S.; Chaudhari, H. D.; Illathvalappil, R.; Sreekumar, K.; Kharul, U. K., New approach of blending polymeric ionic liquid with polybenzimidazole (PBI) for enhancing physical and electrochemical properties. *Journal of Materials Chemistry A* **2014**, *2* (35), 14449-14458.
61. Martinelli, A.; Nordstierna, L., An investigation of the sol-gel process in ionic liquid-silica gels by time resolved Raman and <sup>1</sup>H NMR spectroscopy. *Physical chemistry chemical physics : PCCP* **2012**, *14* (38), 13216-23.
62. Yuan, J.; Mecerreyes, D.; Antonietti, M., Poly(ionic liquid)s: An update. *Progress in Polymer Science* **2013**, *38* (7), 1009-1036.
63. Li, M.; Yang, L.; Fang, S.; Dong, S., Novel polymeric ionic liquid membranes as solid polymer electrolytes with high ionic conductivity at moderate temperature. *Journal of Membrane Science* **2011**, *366* (1-2), 245-250.
64. Ohno, H., Design of Ion Conductive Polymers Based on Ionic Liquids. *Macromolecular Symposia* **2007**, *249-250* (1), 551-556.
65. Ohno, H.; Ito, K., Room-Temperature Molten Salt Polymers as a Matrix for Fast Ion Conduction. *Chemistry Letters* **1998**, *27* (8), 751-752.
66. Ohno, H., Molten salt type polymer electrolytes. *Electrochimica Acta* **2001**, *46* (10-11), 1407-1411.
67. Nishimura, N.; Ohno, H., 15th anniversary of polymerised ionic liquids. *Polymer* **2014**, *55* (16), 3289-3297.
68. Chen, H.; Elabd, Y. A., Polymerized Ionic Liquids: Solution Properties and Electrospinning. *Macromolecules* **2009**, *42* (9), 3368-3373.
69. Díaz, M.; Ortiz, A.; Vilas, M.; Tojo, E.; Ortiz, I., Performance of PEMFC with new polyvinyl-ionic liquids based membranes as electrolytes. *International Journal of Hydrogen Energy* **2014**, *39* (8), 3970-3977.
70. Lemus, J.; Eguizábal, A.; Pina, M. P., Endurance strategies for the preparation of high temperature polymer electrolyte membranes by UV polymerization of 1-H-3-vinylimidazolium bis(trifluoromethanesulfonyl)imide for fuel cell applications. *International Journal of Hydrogen Energy* **2016**, *41* (6), 3981-3993.
71. Díaz, M.; Ortiz, A.; Isik, M.; Mecerreyes, D.; Ortiz, I., Highly conductive electrolytes based on poly([HSO<sub>3</sub>-BVIm][TfO])/[HSO<sub>3</sub>-BMIm][TfO] mixtures for fuel cell applications. *International Journal of Hydrogen Energy* **2015**, *40* (34), 11294-11302.
72. Lemus, J.; Eguizábal, A.; Pina, M. P., UV polymerization of room temperature ionic liquids for high temperature PEMs: Study of ionic moieties and crosslinking effects. *International Journal of Hydrogen Energy* **2015**, *40* (15), 5416-5424.

73. Wojnarowska, Z.; Knapik, J.; Díaz, M.; Ortiz, A.; Ortiz, I.; Paluch, M., Conductivity Mechanism in Polymerized Imidazolium-Based Protic Ionic Liquid [HSO<sub>3</sub>-BVI<sub>m</sub>][OTf]: Dielectric Relaxation Studies. *Macromolecules* **2014**, *47* (12), 4056-4065.
74. Yamaguchi, T.; Miyata, F.; Nakao, S., Polymer Electrolyte Membranes with a Pore-Filling Structure for a Direct Methanol Fuel Cell. *Advanced Materials* **2003**, *15* (14), 1198-1201.
75. Mecerreyes, D.; Grande, H.; Miguel, O.; Ochoteco, E.; Marcilla, R.; Cantero, I., Porous Polybenzimidazole Membranes Doped with Phosphoric Acid: Highly Proton-Conducting Solid Electrolytes. *Chemistry of Materials* **2004**, *16* (4), 604-607.
76. Langevin, D.; Nguyen, Q. T.; Marais, S.; Karademir, S.; Sanchez, J.-Y.; Iojoiu, C.; Martinez, M.; Mercier, R.; Judeinstein, P.; Chappey, C., High-Temperature Ionic-Conducting Material: Advanced Structure and Improved Performance. *The Journal of Physical Chemistry C* **2013**, *117* (30), 15552-15561.
77. Kang, N.; Shin, J.; Hwang, T. S.; Lee, Y.-S., A facile method for the preparation of poly(vinylidene fluoride) membranes filled with cross-linked sulfonated polystyrene. *Reactive and Functional Polymers* **2016**, *99*, 42-48.
78. van de Ven, E.; Chairuna, A.; Merle, G.; Benito, S. P.; Borneman, Z.; Nijmeijer, K., Ionic liquid doped polybenzimidazole membranes for high temperature Proton Exchange Membrane fuel cell applications. *Journal of Power Sources* **2013**, *222*, 202-209.
79. Eguizábal, A.; J.lemus; Roda, V.; Urbiztondo, M.; Barreras, F.; Pina, M. P., Nanostructured electrolyte membranes based on zeotypes, protic ionic liquids and porous PBI membranes: Preparation, characterization and MEA testing. *International Journal of Hydrogen Energy* **2012**, *37* (8), 7221-7234.
80. Jheng, L.-C.; Hsu, S. L.-C.; Tsai, T.-Y.; Chang, W. J.-Y., A novel asymmetric polybenzimidazole membrane for high temperature proton exchange membrane fuel cells. *Journal of Materials Chemistry A* **2014**, *2* (12), 4225.
81. Eguizábal, A.; Sgroi, M.; Pullini, D.; Ferain, E.; Pina, M. P., Nanoporous PBI membranes by track etching for high temperature PEMs. *Journal of Membrane Science* **2014**, *454*, 243-252.
82. Eguizábal, A.; Pina, M. P., Protic Ionic Liquids Confinement in Macro, Meso and Microporous Materials for Proton Conduction. In *Encapsulation Nanotechnologies*, John Wiley & Sons, Inc.: **2013**, pp 347-389.
83. Hopkinson, D.; Zeh, M.; Luebke, D., The bubble point of supported ionic liquid membranes using flat sheet supports. *Journal of Membrane Science* **2014**, *468*, 155-162.
84. Liang, B.; Jiang, Q.; Tang, S.; Li, S.; Chen, X., Porous polymer electrolytes with high ionic conductivity and good mechanical property for rechargeable batteries. *Journal of Power Sources* **2016**, *307*, 320-328.
85. Kuiper, S.; van Rijn, C. J. M.; Nijdam, W.; Elwenspoek, M. C., Development and applications of very high flux microfiltration membranes. *Journal of Membrane Science* **1998**, *150* (1), 1-8.
86. Bikel, M.; Çulfaz, P. Z.; Bolhuis-Versteeg, L. A. M.; Pérez, J. G.; Lammertink, R. G. H.; Wessling, M., Polymeric microsieves via phase separation microfabrication: Process and design optimization. *Journal of Membrane Science* **2010**, *347* (1-2), 93-100.
87. Eguizábal, A.; Urbiztondo, M. A.; Pina, M. P., Pt based catalytic coatings on poly(benzimidazole) micromonoliths for indoor quality control. *Catalysis Today* **2015**, *241*, 114-124.
88. Vogelaar, L.; Barsema, J. N.; van Rijn, C. J. M.; Nijdam, W.; Wessling, M., Phase Separation Micromolding—PS $\mu$ M. *Advanced Materials* **2003**, *15* (16), 1385-1389.
89. Gironès, M.; Akbarsyah, I. J.; Nijdam, W.; van Rijn, C. J. M.; Jansen, H. V.; Lammertink, R. G. H.; Wessling, M., Polymeric microsieves produced by phase separation micromolding. *Journal of Membrane Science* **2006**, *283* (1-2), 411-424.
90. Bikel, M.; Pünt, I. G. M.; Lammertink, R. G. H.; Wessling, M., Shrinkage effects during polymer phase separation on microfabricated molds. *Journal of Membrane Science* **2010**, *347* (1-2), 141-149.



91. Vogelaar, L.; Lammertink, R. G.; Barsema, J. N.; Nijdam, W.; Bolhuis-Versteeg, L. A.; van Rijn, C. J.; Wessling, M., Phase separation micromolding: a new generic approach for microstructuring various materials. *Small* **2005**, *1* (6), 645-55.
92. Lokhandwala, K. A.; Pinnau, I.; He, Z.; Amo, K. D.; DaCosta, A. R.; Wijmans, J. G.; Baker, R. W., Membrane separation of nitrogen from natural gas: A case study from membrane synthesis to commercial deployment. *Journal of Membrane Science* **2010**, *346* (2), 270-279.
93. Scholes, C. A.; Stevens, G. W.; Kentish, S. E., Membrane gas separation applications in natural gas processing. *Fuel* **2012**, *96*, 15-28.
94. Baker, R. W.; Lokhandwala, K., Natural Gas Processing with Membranes: An Overview. *Industrial & Engineering Chemistry Research* **2008**, *47* (7), 2109-2121.
95. David Browell, M. G., Daniel Pawson, James Shaughnessy, Control of landfill gas containing low concentrations of methane *Environment Agency* [www.environment-agency.gov.uk](http://www.environment-agency.gov.uk)

**March 2009**, (Science Report – SC030305/SR2 ).

96. Yang, L.; Ge, X.; Wan, C.; Yu, F.; Li, Y., Progress and perspectives in converting biogas to transportation fuels. *Renewable and Sustainable Energy Reviews* **2014**, *40*, 1133-1152.
97. Lombardi, L.; Carnevale, E. A., Analysis of an innovative process for landfill gas quality improvement. *Energy* **2016**, *109*, 1107-1117.
98. Tome, L. C.; Marrucho, I. M., Ionic liquid-based materials: a platform to design engineered CO<sub>2</sub> separation membranes. *Chemical Society reviews* **2016**, *45* (10), 2785-2824.
99. Bernardo, P.; Drioli, E.; Golemme, G., Membrane Gas Separation: A Review/State of the Art. *Industrial & Engineering Chemistry Research* **2009**, *48* (10), 4638-4663.
100. Han, S. H.; Lee, J. E.; Lee, K.-J.; Park, H. B.; Lee, Y. M., Highly gas permeable and microporous polybenzimidazole membrane by thermal rearrangement. *Journal of Membrane Science* **2010**, *357* (1), 143-151.
101. Ho, T. D.; Zhang, C.; Hantao, L. W.; Anderson, J. L., Ionic liquids in analytical chemistry: fundamentals, advances, and perspectives. *Analytical chemistry* **2013**, *86* (1), 262-285.
102. Boot-Handford, M. E.; Abanades, J. C.; Anthony, E. J.; Blunt, M. J.; Brandani, S.; Mac Dowell, N.; Fernandez, J. R.; Ferrari, M.-C.; Gross, R.; Hallett, J. P.; Haszeldine, R. S.; Heptonstall, P.; Lyngfelt, A.; Makuch, Z.; Mangano, E.; Porter, R. T. J.; Pourkashanian, M.; Rochelle, G. T.; Shah, N.; Yao, J. G.; Fennell, P. S., Carbon capture and storage update. *Energy & Environmental Science* **2014**, *7* (1), 130-189.
103. Zhang, X.; Zhang, X.; Dong, H.; Zhao, Z.; Zhang, S.; Huang, Y., Carbon capture with ionic liquids: overview and progress. *Energy & Environmental Science* **2012**, *5* (5), 6668.
104. Jennifer L. Anthony; Jessica L. Anderson, E. J. M. a. J. F. B., Anion Effects on Gas Solubility in Ionic Liquids. *Journal of physical chemistry B* **2005**, *109* (13), 6366-6374.
105. Cadena, C.; Anthony, J. L.; Shah, J. K.; Morrow, T. I.; Brennecke, J. F.; Maginn, E. J., Why Is CO<sub>2</sub> So Soluble in Imidazolium-Based Ionic Liquids? *Journal of the American Chemical Society* **2004**, *126* (16), 5300-5308.
106. Ferguson, L.; Scovazzo, P., Solubility, Diffusivity, and Permeability of Gases in Phosphonium-Based Room Temperature Ionic Liquids: Data and Correlations. *Industrial & Engineering Chemistry Research* **2007**, *46* (4), 1369-1374.
107. Almantariotis, D.; Gefflaut, T.; Pádua, A. A. H.; Coxam, J. Y.; Costa Gomes, M. F., Effect of Fluorination and Size of the Alkyl Side-Chain on the Solubility of Carbon Dioxide in 1-Alkyl-3-methylimidazolium Bis(trifluoromethylsulfonyl)amide Ionic Liquids. *The Journal of Physical Chemistry B* **2010**, *114* (10), 3608-3617.
108. Shiflett, M. B.; Yokozeki, A., Solubilities and Diffusivities of Carbon Dioxide in Ionic Liquids: [bmim][PF<sub>6</sub>] and [bmim][BF<sub>4</sub>]. *Industrial & Engineering Chemistry Research* **2005**, *44* (12), 4453-4464.
109. Camper, D.; Bara, J.; Koval, C.; Noble, R., Bulk-Fluid Solubility and Membrane Feasibility of Rmim-Based Room-Temperature Ionic Liquids. *Industrial & Engineering Chemistry Research* **2006**, *45* (18), 6279-6283.

110. Bara, J. E.; Lessmann, S.; Gabriel, C. J.; Hatakeyama, E. S.; Noble, R. D.; Gin, D. L., Synthesis and Performance of Polymerizable Room-Temperature Ionic Liquids as Gas Separation Membranes. *Industrial & Engineering Chemistry Research* **2007**, *46* (16), 5397-5404.
111. Scovazzo, P.; Visser, A. E.; Davis, J. H.; Rogers, R. D.; Koval, C. A.; DuBois, D. L.; Noble, R. D., Supported Ionic Liquid Membranes and Facilitated Ionic Liquid Membranes. In *Ionic Liquids*, American Chemical Society: **2002**; Chapter 6, pp 69-87.
112. Zhao, W.; He, G.; Nie, F.; Zhang, L.; Feng, H.; Liu, H., Membrane liquid loss mechanism of supported ionic liquid membrane for gas separation. *Journal of Membrane Science* **2012**, *411-412*, 73-80.
113. Close, J. J.; Farmer, K.; Moganty, S. S.; Baltus, R. E., CO<sub>2</sub>/N<sub>2</sub> separations using nanoporous alumina-supported ionic liquid membranes: Effect of the support on separation performance. *Journal of Membrane Science* **2012**, *390-391*, 201-210.
114. Scovazzo, P.; Havard, D.; McShea, M.; Mixon, S.; Morgan, D., Long-term, continuous mixed-gas dry fed CO<sub>2</sub>/CH<sub>4</sub> and CO<sub>2</sub>/N<sub>2</sub> separation performance and selectivities for room temperature ionic liquid membranes. *Journal of Membrane Science* **2009**, *327* (1-2), 41-48.
115. Hanioka, S.; Maruyama, T.; Sotani, T.; Teramoto, M.; Matsuyama, H.; Nakashima, K.; Hanaki, M.; Kubota, F.; Goto, M., CO<sub>2</sub> separation facilitated by task-specific ionic liquids using a supported liquid membrane. *Journal of Membrane Science* **2008**, *314* (1-2), 1-4.
116. Tomé, L. C.; Patinha, D. J. S.; Freire, C. S. R.; Rebelo, L. P. N.; Marrucho, I. M., CO<sub>2</sub> separation applying ionic liquid mixtures: the effect of mixing different anions on gas permeation through supported ionic liquid membranes. *RSC Advances* **2013**, *3* (30), 12220.
117. Cichowska-Kopczyńska, I.; Joskowska, M.; Dębski, B.; Łuczak, J.; Aranowski, R., Influence of Ionic Liquid Structure on Supported Ionic Liquid Membranes Effectiveness in Carbon Dioxide/Methane Separation. *Journal of Chemistry* **2013**, *2013*, 1-10.
118. Wickramanayake, S.; Hopkinson, D.; Myers, C.; Hong, L.; Feng, J.; Seol, Y.; Plasynski, D.; Zeh, M.; Luebke, D., Mechanically robust hollow fiber supported ionic liquid membranes for CO<sub>2</sub> separation applications. *Journal of Membrane Science* **2014**, *470*, 52-59.
119. Neves, L. A.; Crespo, J. G.; Coelho, I. M., Gas permeation studies in supported ionic liquid membranes. *Journal of Membrane Science* **2010**, *357* (1-2), 160-170.
120. Cserjési, P.; Nemestóthy, N.; Bélafi-Bakó, K., Gas separation properties of supported liquid membranes prepared with unconventional ionic liquids. *Journal of Membrane Science* **2010**, *349* (1-2), 6-11.
121. Tomé, L. C.; Mecerreyes, D.; Freire, C. S. R.; Rebelo, L. P. N.; Marrucho, I. M., Pyrrolidinium-based polymeric ionic liquid materials: New perspectives for CO<sub>2</sub> separation membranes. *Journal of Membrane Science* **2013**, *428*, 260-266.
122. Condemarin, R.; Scovazzo, P., Gas permeabilities, solubilities, diffusivities, and diffusivity correlations for ammonium-based room temperature ionic liquids with comparison to imidazolium and phosphonium RTIL data. *Chemical Engineering Journal* **2009**, *147* (1), 51-57.
123. Bara, J. E.; Gabriel, C. J.; Carlisle, T. K.; Camper, D. E.; Finotello, A.; Gin, D. L.; Noble, R. D., Gas separations in fluoroalkyl-functionalized room-temperature ionic liquids using supported liquid membranes. *Chemical Engineering Journal* **2009**, *147* (1), 43-50.
124. Scovazzo, P.; Kieft, J.; Finan, D.; Koval, C.; Dubois, D.; Noble, R., Gas separations using non-hexafluorophosphate [PF<sub>6</sub>]<sup>-</sup> anion supported ionic liquid membranes. *Journal of Membrane Science* **2004**, *238* (1-2), 57-63.



## **Chapter- 2**

### **Objectives and thesis outline**



## Objectives:

This thesis aims to develop membranes suitable for high temperature applications, in particular two different applications:

1. Electrolyte membranes for High temperature Proton Exchange Membranes for fuel cells (HTPEMFCs).
2. Gas separation membranes for methane upgrading.

Special emphasis will be devoted to the study of membrane architecture (asymmetry, porosity, and connectivity), ionic liquid composition, casting solution formulation, membrane processing and post-treatments, and scalable manufacturing process.

In the case of electrolyte membranes for HTPEMFCs, It is of great importance to fabricate highly conductive electrolyte membranes capable to operate above 120°C under anhydrous conditions and in absence of mineral acids, without sacrificing the mechanical behavior. The main objective of this part is the consecution of high temperature proton exchange membranes (HTPEMs) with enhanced physicochemical, mainly thermal and mechanical, and electrochemical properties for applicability at temperatures above 120 °C under dry conditions. The consecution of a polymeric container with optimized pore architecture is extremely essential since the performance of PEM based on immersing a porous support into ILs, mainly depends on the porous structure. Therefore, the research efforts aims to improve both, the ion conductivity and the dimensional stability of the PIL supported membranes by a proper design of the porous architecture. For a proper consecution of the objectives, the experimentation has been systematically performed according to the following activities:

- i. Preparing different type of porous Polybenzimidazole(PBI) microsieves as supports.
- ii. Incorporation of the proton conductor by filling PBI supports with protic ionic liquids and in situ polymerization by UV radiation, also the addition of cross-linker agent is attempted.
- iii. Electrochemical and physico-chemical characterization of the PIL-PBI membranes.
- iv. Evaluation of the performance by intercomparison and discussion on the basis of the state of the art.

In the field of gas separation, the investigation has been merely focused on the study of single gas permeation properties of the PIL-PBI membranes, specifically designed for proton transport. Thus, the permeability of supported ionic liquids based membranes (SILMs) has been measured for

methane, hydrogen, carbon dioxide and nitrogen as a function of temperature. The CH<sub>4</sub>/N<sub>2</sub> separation performance of the prepared SILMS has been assessed by comparison with recent publications on separation technologies for landfill gas recovery and natural gas upgrading. For a proper consecution of the objectives, the experimentation has been systematically performed according to the following activities:

- v. Preparing random porous PBI supports
- vi. Incorporation of non polymerizable & polymerizable versions of ionic liquids that includes cross-linkers and functionalities active in the transport.
- vii. Measurement of the permeabilities of several single gases and physico-chemical characterization of the SILMS.

Therefore, the specific objectives (see Figure 2.1) refer to the synthesis and characterization of the different materials, PBI and PILs, with adequate properties for further assembly. These intermediate objectives (1 to 3) are required to accomplish the electrolyte membranes and gas selective membranes, defined as overall objectives (4 to 6).

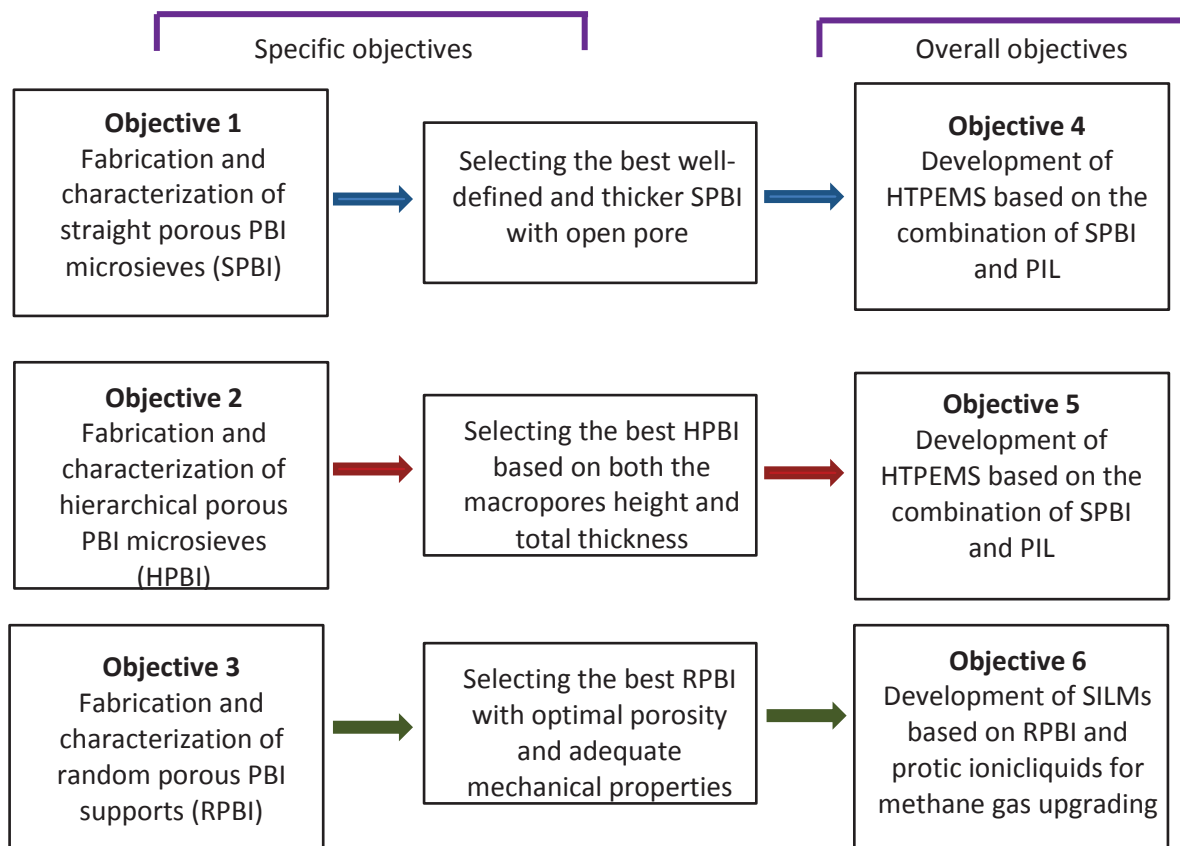


**Figure 2.1:** Specific and overall objectives of this thesis.

## Thesis outline:

To achieve the objectives outlined in Figure 2.1, many experimental methods, scientific and technological principles were used. All of these are explained and justified in chapters 3, 4 and 5, organized as follows:

- I. In **Chapter 3**, acid free high-temperature proton exchange membranes (HTPEMS) based on the combination of straight porous polybenzimidazole (SPBI) microsieves and imidazolium based polymeric ionic liquids (PIL) are developed. SPBI microsieves having straight pores on the micrometer scale and well defined porosity were fabricated by micro transfer moulding technique from a relief pattern of the poly (dimethylsiloxane) mould. The monomeric ionic liquid (MIL) 1-H-3-vinylimidazolium bis(trifluoromethanesulfonyl)imide (H-VIM TFSI) that fills the pores and polymerizes inside the pores of the PBI substrate (Figure 2.2). The comprehensive physico-chemical characterization of such novel ion conducting membranes, including the modification by crosslinking is accomplished and compared with published results for similar single components. **This work** has been published as **Parashuram Kallem, Adela Eguizabal, Reyes Mallada and Maria Pilar Pina**. *Constructing straight Poly-ionic liquid microchannels for fast anhydrous proton transport*. ACS Applied Materials & Interfaces, 2016, 8 (51), 35377–35389.



**Figure 2.2:** Schematic illustration of the pore filling of the SPBI

- II. In **Chapter 4**, HTPEMS were fabricated by infiltrating H-VIM TFSI into hierarchical structured polybenzimidazole (HPBI) support followed by UV light in-situ polymerization. In this chapter we proposed an innovative concept for the preparation of hierarchically structured PIL channels in HTPEMS, combining the advantageous features (fast infiltration process and high network connectivity) of both perforated straight pores and intrinsic porosity of HPBI supports (Figure 2.3). Liquid induce phase separation microfabrication (LIPS $\mu$ F) has been successfully used for manufacturing HPBI microsieves with specific pore



architecture (perforated macropores dispersed in nanoporous). Physicochemical properties such as proton conductivity, thermal, and mechanical stabilities have been studied for various membrane thicknesses and the influence of the cross-linker has been evidenced. In addition, the influences of skin layer thickness and the influence of PBI architecture on proton conductivity has been comprehensively examined. **This work** has been published as **Parashuram Kallem, Martin Drobek, Anne Julbe, Erik J. Vriezokolk, Reyes Mallada and Maria Pilar Pina.** *Hierarchical porous Polybenzimidazole microsieves: An efficient architecture for anhydrous proton transport via Poly-ionic Liquids* to *ACS Applied Materials & Interfaces*, 2017, 9(17):14844-14857.

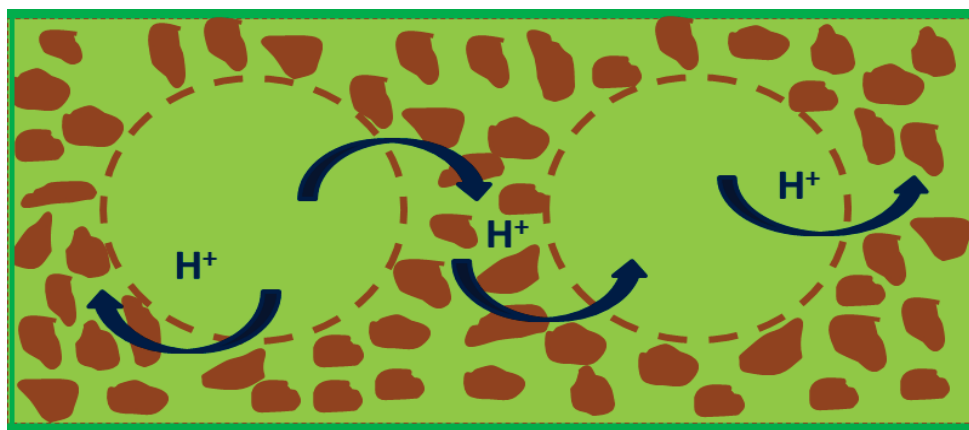


**Figure 2.3:** Schematic illustration of both the perforated straight and intrinsic channels of PIL-HPBI membranes.

- III. **Chapter 5** focuses on the usage of supported ionic liquid membranes (SILMs) based on randomly porous PBI and protic ionic liquids for methane gas upgrading. Three classes of SILMs (Figure 2.3), based on PBI with the protic 1-H-3-methylimidazolium bis(trifluoromethane sulfonyl)imide, the monomeric 1-H-3-vinylimidazolium bis(trifluoromethane sulfonyl)imide and the polymeric poly[1-(3H-imidazolium)ethylene]bis(trifluoromethanesulfonyl)imide were fully studied for single gas permeation. The methyl group substitution on the imidazolium cation has a great influence on the single gas permeances. Unexpectedly, PIL-PBI membranes shown promising values of ideal  $\text{CH}_4/\text{N}_2$  selectivities at lower temperatures. **This work**, entitled as “*Supported Ionic liquid membranes (SILMs) based on PBI and protic Ionic liquids for methane upgrading*” will be submitted to *Journal of Membrane Science* for publication.

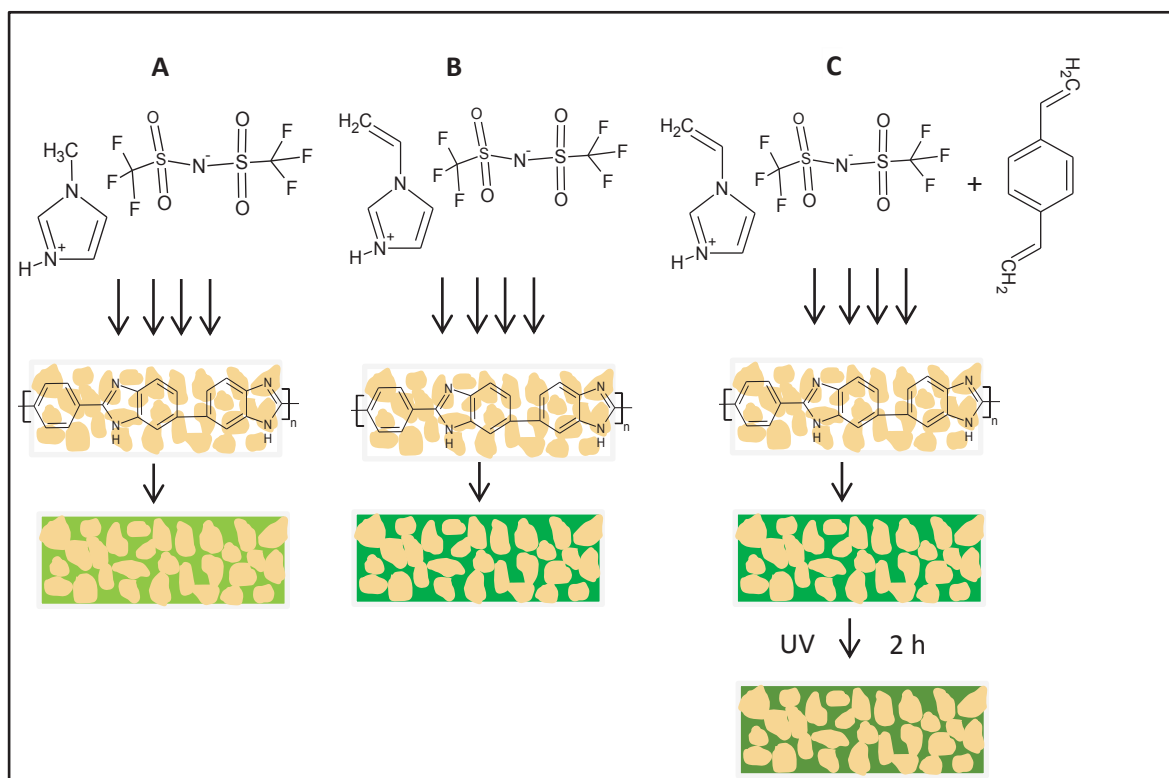


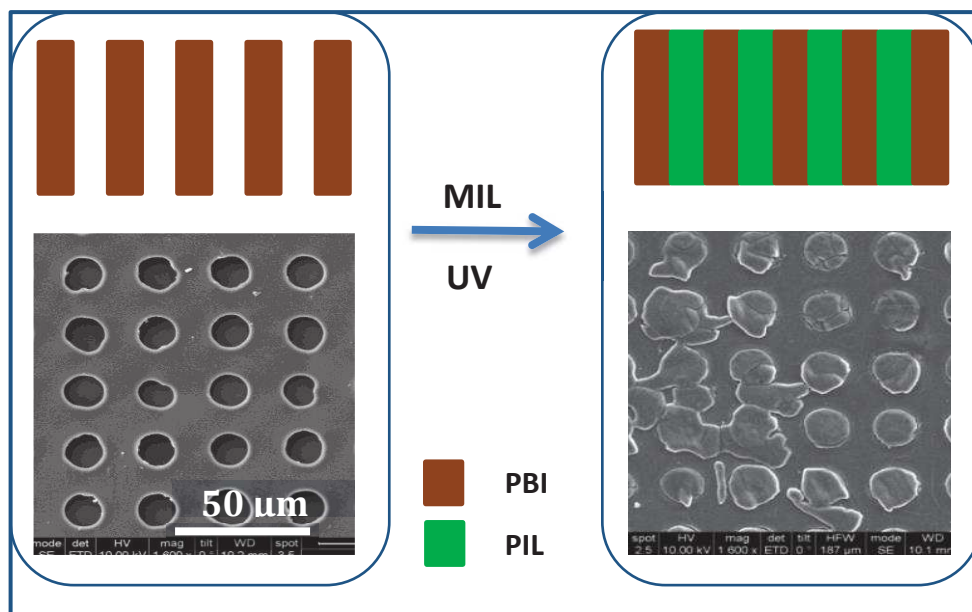
**Figure 2.3:** Schematic illustration of the preparation of three classes of SILMs for gas permeation.

Finally, **Chapter 6** summarizes and comprehensively compiles the conclusions of the different chapters and provides some guidance for future work.



## Chapter-3

On the incorporation of crosslinked Poly imidazolium based Ionic liquid on well-defined straight porous Polybenzimidazole microsieves: A new generation of phosphoric free proton Exchange Membranes for high temperature applications





## 1. Introduction

The current movement towards sustainable and more efficient power production has shifted the bias from the conventional fuels and internal combustion engines and increased the interest on alternative fuels and power sources<sup>1</sup>.

The Polymer Electrolyte Membrane Fuel Cell (PEMFC) is considered one of the most promising alternative power sources especially for sub-megawatt scale applications<sup>2</sup>. In particular, the fuel cell (FC) operation at high temperature is desirable since at temperatures over 120 °C overcome most of the functional problems currently associated with proton exchange membrane fuel cells (PEMFCs) such as catalyst CO poisoning, water management, efficiency (polarization effects and electrochemical reaction rates), and cogeneration possibilities are greatly improved. In this high temperature scenario, the most important challenges are mainly related to the electrolyte performance and durability. Polymer based electrolyte membranes have been actively investigated over the last years for the development of new generation of proton exchange membranes (PEMs) adequate for high temperature applications<sup>3-6</sup>. Among those, poly-benzimidazole (PBI) has received a lot of attention because of its excellent chemical and thermal stability. Generally, PBI is used in thermal protective clothing and fire blocking applications. In particular, acid doped PBI membranes have been recognized as promising PEM materials operating at high temperatures<sup>7-9</sup>. More specifically, phosphoric acid doped PBI membranes<sup>10-14</sup> exhibit excellent adequate proton conductivity, mechanical properties and fuel cross over behavior. However, pyrophosphoric acid formation<sup>12</sup>, catalyst deactivation due to the adsorption of phosphate anions<sup>15</sup> and carbon support corrosion<sup>16</sup> remains as the main shortcomings.

Ionic liquids (ILs) are becoming progressively in valuable materials for electrochemical applications<sup>17-20</sup> due to its unique properties such as negligible vapour pressure, thermal stability and non-flammability, combined with high ionic conductivity and wide electrochemical stability window. Room temperature ILs (RTILs) exhibits the melting point near or below room conditions and the ionicity higher than 99%. Accounting from the huge diversity of cation and anion combinations, they are recognized as multipurpose materials on the basis on their tunable physico-chemical properties (thermal and chemical stability, volatility, conductivity, polarity, melting point, viscosity, density etc.). In particular, thermal stability and non-volatile character of ILs outstands as the main advantages compared to mineral acid dopants.

Some previous works deal with the incorporation of ILs and mineral acid (if applicable) at different molar composition on the PBI casting solution<sup>21-25</sup>. Of course, the key point is the miscibility between

the IL and the polymer. Among those, the contribution from Liu et al.<sup>24</sup> on diethylmethylammonium trifluoromethanesulfonate - PBI blends outstand in terms of ionic conductivity; reaching values above  $20 \text{ mS cm}^{-1}$  at  $160 \text{ }^\circ\text{C}$ . So far, the attained results are revealed inadequate in terms of electrochemical and/or durability performance for practical fuel cell operation. At temperatures above  $100^\circ\text{C}$ , migration of IL towards the cathode by electro-osmotic drag was confirmed by Mamlouk et al<sup>25</sup> on composite diethylamine bisulphate/sulphate – PBI membranes under polarization conditions.

There is a challenging need for immobilizing ILs in solid devices for material applications, while keeping their specific properties. Supported Ionic Liquid Membranes (SILM), widely used for gas separation<sup>26</sup>, has been scarcely attempted for FC applications<sup>27-29</sup>. This approach relies on RTILs immobilization in the pores of a porous support by capillary forces. Although the negligible protic ionic liquid vapor pressure alleviates one of the problems associated with traditional SILMs, namely liquid volatility; expulsion of the liquid from the membrane pores is a major concern. A proper design of the support, with sub-micron pores, combined with an ionic liquid having high surface tension leads to SLIMs with adequate physical stability for applications involving moderate to high trans-membrane pressures<sup>30</sup>. In PEMFCs, polymer membranes swelled with protic ionic liquids suffer from the hydro-dynamical solvation phenomenon which limits the lifetime of the cell<sup>31</sup>.

Polymerization of RTILs emerges as an attractive alternative in terms of safety, stability and mechanical properties. Polymeric ionic liquids (PILs)<sup>32-39</sup> retain some of the unique properties of IL, such as thermal stability, tunable solution properties and chemical stability, which when combined with intrinsic polymer properties are anticipated to offer more advantages than ILs. Depending on the structure of the backbone of PILs, namely polycation or polyanion, the ionic conductivity will be associated with the transport of the counter-anions or counter-cations respectively. Free radical polymerization of RTILs monomers by photochemical initiation is very attractive due to the short reaction time and ambient working temperature. However, the in situ polymerization may introduce some impurities into the PILs such as unreacted monomer or initiator which may limit their electrochemical performance. Following this approach, all solid state proton conductive films have been recently prepared in our group<sup>37</sup> by UV photo-assisted ( $\lambda=365 \text{ nm}$  for 15 min) polymerization of commercial available ammonium and imidazolium RTILs with vinyl-based reactive groups. Among the tested, the poly[1-(3H-imidazolium)ethylene] bis(trifluoromethanesulfonyl)imide with 2.5 mol.% of divinylbenzene as cross-linker represents the optimal tradeoff between conductivity and mechanical properties. Similarly, Ortiz et al<sup>40-41</sup> have recently reported the fuel cell performance of PILs based on 1-(4-sulfobutyl)-3-vinylimidazolium trifluoromethanesulfonate] with divinylbenzene

(10 mol.%) as cross linker. Such electrolyte membrane showed a maximum power density of 33 mW cm<sup>-2</sup> at 25 °C under non-humidified conditions; but performance declined at temperatures above 50 °C due to the membrane softening.

Another popular strategy, named ion gels, consists in the formation of a three-dimensional network with percolates throughout the IL<sup>38, 42</sup>. The resulting gel type polymer electrolyte can be prepared from using not only PILs but different type of polymeric matrices leading to organic, inorganic or nanocomposite ionogels. Following this approach, composite electrolyte membranes based on the polymeric ionic liquid matrix from 1-(4-sulphobutyl)-3-vinylimidazolium trifluoromethanesulphonate and its analogue non-polymerizable ionic liquid 1-(4-sulphobutyl)-3-methylimidazolium trifluoromethanesulphonate, have been developed for PEMFC applications<sup>43</sup>. Stable electrolyte membranes containing 10 wt% of the ionic liquid showed the highest conductivity of 293 mS/cm, and the best FC performance, with a peak power density of 49 mW cm<sup>-2</sup> at 40 °C without external humidification. However, their mechanical and dimensional stability is not adequate for high temperature PEMFC application. PIL-PBI electrolyte membranes with adequate thermal and mechanical stability have been successfully prepared from poly(diallyl dimethyl ammonium trifluoromethane sulphonate)<sup>44</sup>. The maximum proton conductivity and power density values of blended membranes, upon phosphoric acid doping, were 70 mS cm<sup>-1</sup> at 150°C and 515 mW cm<sup>-2</sup> at 160 °C, respectively. It is noteworthy to underline that the electrochemical performance of such blended PIL-PBI membranes is strongly dependent on the phosphoric acid uptake values.

Unlike previously, our approach relies on the use of porous PBI matrix as poly-ionic liquid container. The underlying rationale is based on the pore-filling electrolyte membrane concept proposed by Yamaguchi for fuel cross-over suppression on direct methanol fuel cells<sup>45</sup>. Fabricating a polymeric container with an optimized pore architecture is extremely essential<sup>46</sup> since the performance of PEM based on immersing a porous support into ILs, mainly depends on the porous structure. Thus, the present work aims to improve both, the ion conductivity and the dimensional stability of the PIL supported membranes by a proper design of the porous architecture.

The wide spectra of porous polymers applications in membrane science have encouraged an intense research on reliable fabrication methods for preparation of porous polymer membranes with specific pore architecture. In particular, the fabrication of porous PBI membranes by phase inversion method, by leaching out a porogen and track-etching has been already described in the literature for FC applications<sup>27, 29, 39, 47-49</sup>. Recently, asymmetric porous PBI membranes prepared by soft-template method using 1-ethyl-3-methylimidazolium bis(trifluoromethanesulfonyl)imide as porogen has been described by Hsu et al.<sup>48</sup>. Maximum proton conductivities above 60 mS cm<sup>-1</sup> at 160 °C were attained



by highly porous PBI membranes (83.1 vol%) upon phosphoric acid doping (23.6 as doping level). However, high porosity usually leads to the decrease of tensile strength<sup>46, 48</sup>. In general, the mechanical properties are often sacrificed to obtain sufficient conductivity, which hinders the large scale commercialization of reliable PEMs for high temperature applications. Our group<sup>39</sup> has recently described the “in situ” UV polymerization 1-H-3-vinylimidazolium bis(trifluoromethanesulfonyl)imide on a highly porous PBI sponge-like matrix (above 75 vol%) achieving conductivity values above 300 mS cm<sup>-1</sup> at 200 °C under anhydrous conditions. While most of our attention was focused on the ion conductivity; their mechanical properties, of paramount importance for fuel cell application, revealed unsatisfactory: 0.2 GPa as Young Modulus and 1.3 MPa as tensile strength.

In this work, the developed electrolyte membranes are composed of two materials: an inert PBI microsieve having straight pores on the micrometer scale (20 µm, aspect ratio 1) and 36% in porosity; and 1-H-3-vinylimidazolium bis(trifluoromethanesulfonyl)imide ionic liquid that fills the pores and polymerizes inside the pores of the PBI substrate. The filling poly-ionic liquid exhibits proton conductivity and the PBI skeleton provides the mechanical reinforcement. During the past years, unconventional nanofabrication techniques, principally moulding, embossing and printing related techniques have cemented the route for 2D and 3D polymer structures with micrometer and nanometer sized topographies<sup>50</sup>. Among those, microtransfer moulding<sup>51</sup> has proved successful for the fabrication of the herein proposed PBI microsieves. Compared to sponge-like supports, the PBI microsieve would facilitate the electrolyte filling. Furthermore, enhanced conduction performance would be expected as the effective pathways become shorter<sup>28</sup>. To the best of our knowledge, the combination of PBI microsieves and PIL has not been attempted before for high temperature PEM applications. Thus, a comprehensive physico-chemical characterization of such novel ion conducting membranes, including the modification by crosslinking is accomplished and compared with published results for similar single components.

## **2. Experimental**

### **2.1 Materials**

All chemical reagents and solvents listed in the following were used as received: Poly[2,2'-(m-phenylene)-5,5'-bibenzimidazole] (PBI Fumion APH Ionomer, Mw 59,000-62,000, Fumatech), LiCl(99 wt%, Sigma-Aldrich), 1-H-3-vinylimidazolium bis(trifluoromethane sulfonyl)imide (98 wt%, SOLVIONIC), Divinylbenzene (80.0 wt%, Sigma-Aldrich), 2-hidroxy-2-methylpropiophenone (97.0 wt%, Sigma-Aldrich), N,N-dimethylacetamide (99.8 wt%, Aldrich).

## **2.2 PBI solution preparation**

2 g of PBI Fumion powder, 0.01 g of LiCl (as a stabilizer), and 9.3 g (40 mL) of N,N-dimethylacetamide (DMAc) were mixed in the autoclave then dissolved under autogenous pressure at 240 °C for 48 h to obtain the starting PBI solution of 5 wt% in DMAc.

## **2.3 Fabrication of PDMS molds**

PBI microsieves are prepared by microtransfer moulding technique from a reinforcement pattern of the poly (dimethylsiloxane) (PDMS) mold. The main processes to obtain the straight porous PBI membrane are: i) SU-8 master fabrication; ii) PDMS soft-mold fabrication; and iii) PBI membrane preparation (see Figure 3.1).

**Table 3.1:** Dimensions of circular shaped mask designs for SU-8 patterning

Name	Diameter ( $\mu\text{m}$ )	Pitch ( $\mu\text{m}$ )
S15	10	30
S20	15	30

The SU-8 master fabrication was prepared by photolithography following our previous work<sup>51</sup>. SU-8 2025 (MicroChem) was used to obtain layers 20  $\mu\text{m}$  thick at 4-in Si wafer level (step S1) by spin coating 3000 rpm for 15 s (step S2). Following a soft bake step at 95 °C for 6 min, the SU-8 layer was exposed to UV light (step S3) through specifically designed masks for 8 s (see geometrical parameters in Table 3.1 of the supporting information). A post exposure bake at 95 °C for 5 min was then carried out, before developing the SU-8 in propylene glycol methyl ether acetate (PGMEA), to obtain the SU-8 master (step S4). PDMS prepolymer solution was made by thoroughly mixing the silicon elastomer (Sylgard®184 supplied by Dow Corning) and the curing agent 184 in a 10:1 (v/v) ratio. The mixture was put under vacuum to remove air bubbles. Then, it was carefully poured onto the SU-8 master to cover its entire area, and finally cured at 80 °C for 30 min (step S5). The fabricated PDMS mold was peeled off the master (step S6) with the aid of tweezers and stored in a closed container under clean room conditions. Following this procedure, two different PDMS molds (see Table 3.2) containing uniform cylindrically shaped pillars with pitch value (center to center distance) of 30  $\mu\text{m}$  were prepared: mold P15 with pillars 15  $\mu\text{m}$  high and 20  $\mu\text{m}$  in diameter; and, mold P20 with pillars 20  $\mu\text{m}$  high and 18  $\mu\text{m}$  in diameter, respectively.

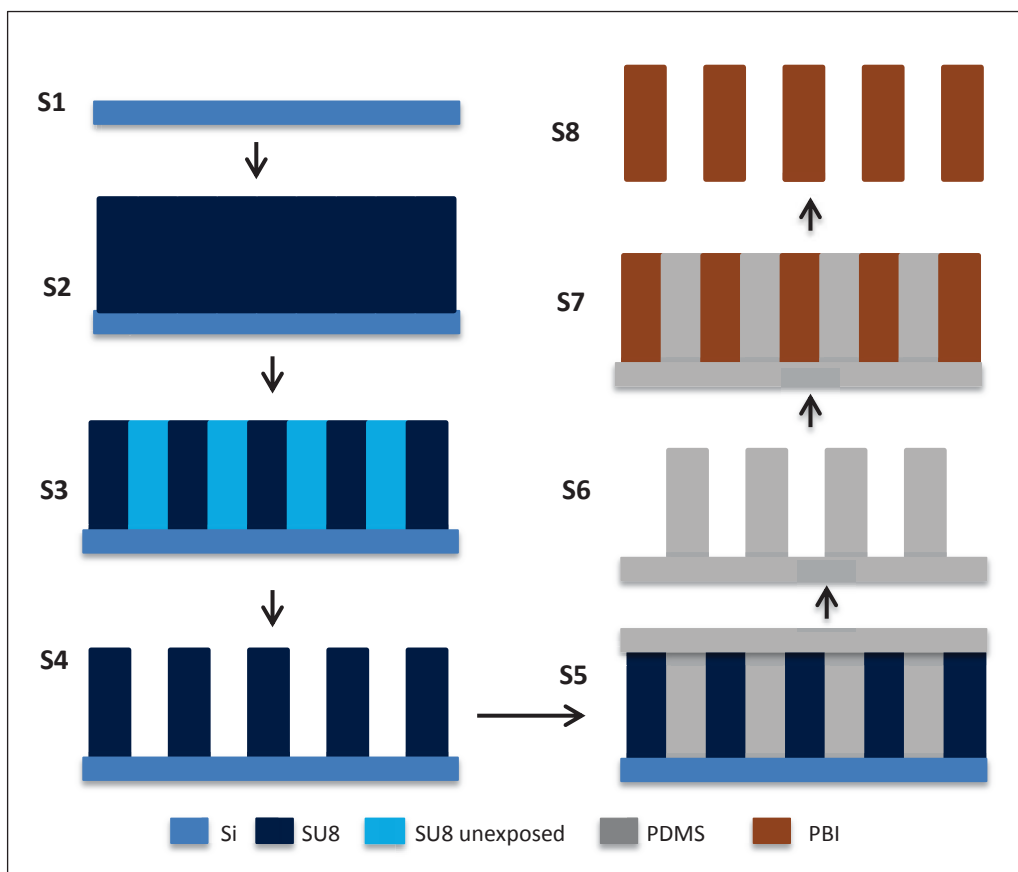


**Figure 3.1:** Schematic overview of micro transfer moulding technique process for the preparation of PBI microsieves: steps S1 to S8.

**Table 3.2:** Dimensions of PDMS molds used to fabricate straight porous PBI membranes

PDMS Mold	Pillar dimensions ( $\mu\text{m}$ )	
	Height	Diameter
P15	15	20
P25	20	18

#### **2.4 Fabrication of PBI microsieves by microtransfer moulding technique**

The PBI microsieves were prepared by transferring the pattern on the PDMS back into a replica of the original SU-8 master by the solution casting method. The starting PBI solution (5 wt%) was further diluted with DMAc to improve the conformational wetting and ensure the complete filling of the PDMS mold. The final PBI solution, once sonicated, was cast onto PDMS mold lying in the oven tray at 60 °C and perfectly aligned with the horizontal axis to ensure a homogeneous coverage (step

S7). After casting, DMAc was evaporated by natural convection from 60 to 90 °C at 5 °C/30 min. Finally, the system was kept at 90 °C for 12 h to ensure the solvent evaporation by forced convection and the fabricated PBI microsieve was spontaneously released from the elastomeric PDMS support (step S8).

The resulting microperforated PBI foil was immersed in boiling deionized water for 5 hours to remove LiCl and final drying is applied at 110 °C/50 mbar to remove all the traces of the solvent. The thickness of the as prepared samples was measured with Baxlo 4000/FILM precision micrometer with an accuracy of 1 micron.

## **2.5 Preparation of PEMS**

### *2.5.1 Fabrication of pure PIL and PIL-1%CL*

4.0 g of monomer was heated at 50°C, stirring constantly. Subsequently, 1 mol. % of crosslinker was added (i.e. 17.3 mg) and the contents were thoroughly mixed. Finally, 2 wt % of photo-initiator was added (i.e. 28.8 mg). Casting of pre-polymer solution was made on Teflon plates (see Figure 3.2), previously heated at 50°C. The plates were placed under a 365 nm UV lamp at the sample surface and exposed for 2h. Then, the plate was removed and then the solid film was carefully peeled off from the Teflon surface by inserting a clean blade and kept in a dry place. Pure PIL films were similarly prepared from a casting solution without CL agent.

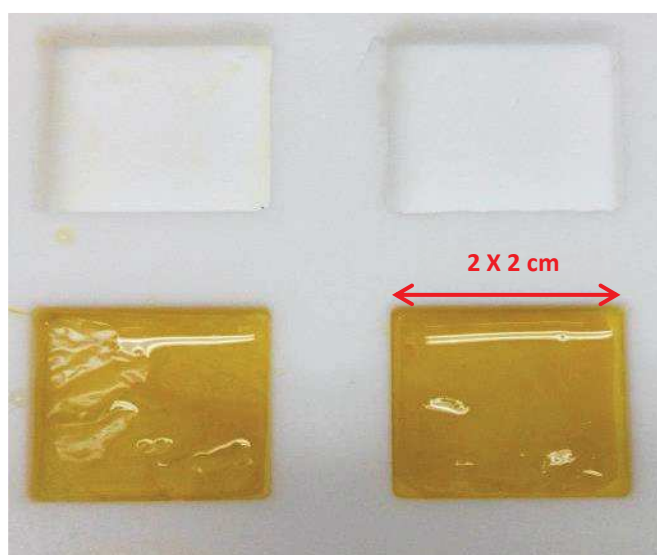


**Figure 3.2:** Home-made Teflon plates for the casting of pure PIL membranes

### 2.5.2 Preparation of reinforced PIL electrolytes on PBI microsieves

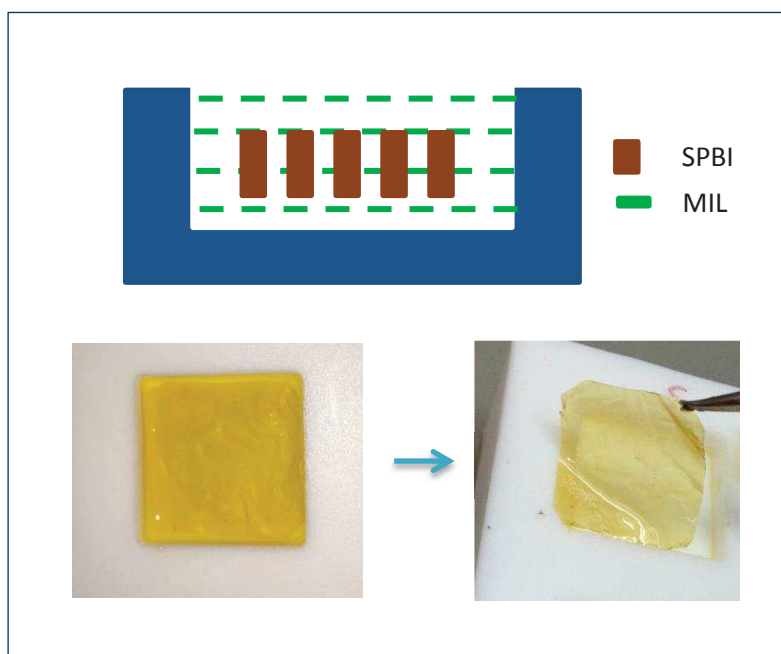


**Figure 3.3:** Schematic illustration of the pore filling membrane by 'Well method'.

In this 'Well method' (Fig 3.3), membrane placed on the Teflon's well (chamber) which is heated previously at 80° C with MIL and 2 wt% of photo-initiator was added. The plates were placed under a 365 nm UV lamp at the sample surface and exposed for 2h. Then, the plate was removed and then the PIL-SPBI membrane was carefully peeled off from the Teflon surface by inserting a clean blade and kept in a dry place. It was impossible to obtain homogeneous membranes with this method. Hence, in a next attempt INFILTRATION method has been carried out.

PBI microsieves were infiltrated with the monomeric ionic liquid (MIL) 1-H-3-vinylimidazolium bis(trifluoromethane sulfonyl)imide (see Figure 3.5) based on earlier efforts in our group<sup>28-29, 39</sup>. Considering the rheological similarities between MIL at 100 °C and the MIL: Acetone (1:10 v/v) solution, 8.6 mPa.s at ambient conditions; the latter has been extensively used in this work for the PBI pores filling for the sake of simplicity. Besides, the cross-linker agent and the photo initiator are soluble in acetone.

The pore-filling was performed in the Teflon home-made device shown in the Figure 3.4. Firstly, the acetone solution containing the 1-H-3-vinylimidazolium bis(trifluoromethane sulfonyl)imide ionic liquid, 2-hydroxy-2-metpropiophenone as

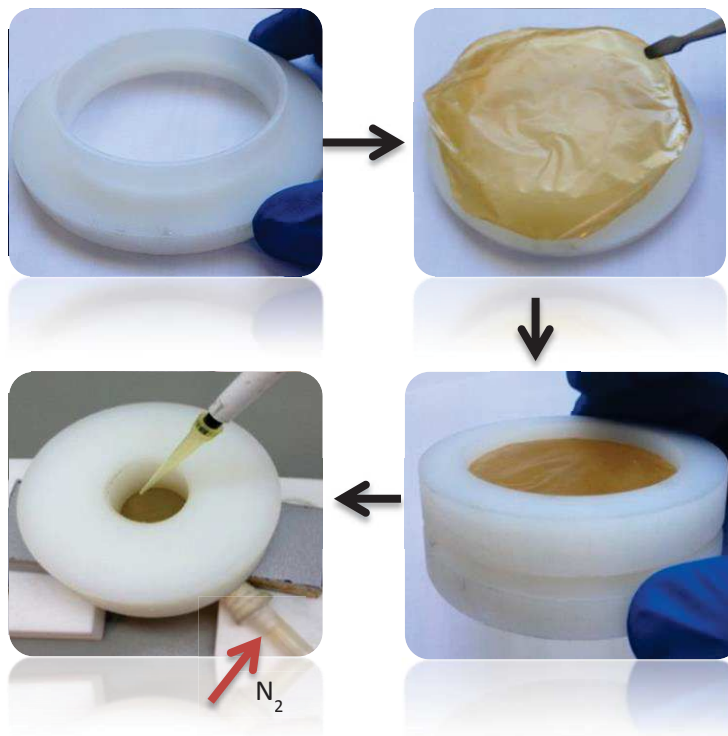


**Figure 3.4:** Home-made device for the MIL infiltration on the PBI microsieve.

photoinitiator (2 wt%, referred to the MIL), and divinylbenzene as crosslinker (from 0.2 mol.% up to 1 mol.% referred to the MIL), if applicable, was prepared. Afterwards, the solution to infiltrate was dropped on the membrane top surface at room temperature while dry N<sub>2</sub> was sweeping the bottom surface. Subsequently, the MIL and cross-linking agent (if applicable) reacted inside the pores of the porous PBI substrate by exposure to UV light (365 nm, Vilmer Lourmat lamp) with an intensity of 2.4 mW /cm<sup>2</sup> at the sample surface for 2 h on each side. After polymerization, the electrolyte membrane was gently wiped from any residuals with lab paper and removed from the device with the help of razor blade.

The amount of the electrolyte in the final PIL-SPBI membranes was experimentally determined by weight differences before and after introducing PIL and also by TGA analysis.

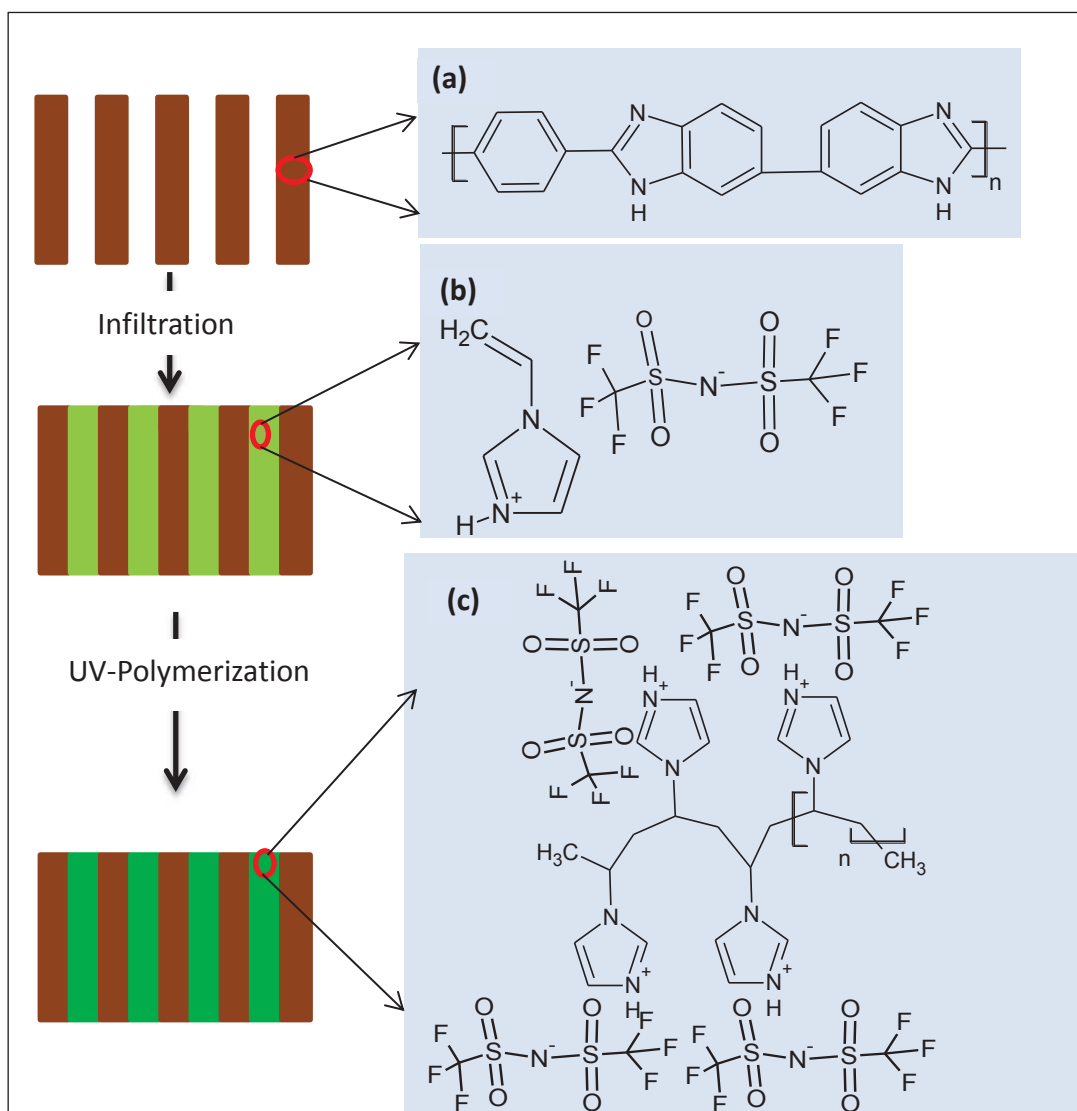


**Figure 3.5:** Schematic illustration of the pore filling membrane and chemical structures of: (a) repeating unit of Poly[2,2-(m-phenylene)-5,5-benzimidazole]; (b) monomeric ionic liquid 1-H-3-vinylimidazolium bis(trifluoromethanesulfonyl)imide; (c) homo poly[1-(3H-imidazolium)ethylene]bis(trifluoromethanesulfonyl)imide.

These values were compared with those theoretically calculated from the pore volume of the PBI container and the estimated PIL density values: 2.2, 2.3, 2.56 and 2.7 g/cm<sup>3</sup> for PIL-0%CL, PIL-0.2%CL, PIL-0.5%CL and PIL-1%CL respectively. Theoretical PIL (%) was calculated using following equation.

$$PIL (\%) = \frac{\rho_{PIL} X \phi}{(\rho_{PIL} X \phi) + \rho_{PBI} (1 - \phi)} X 100$$

### **2.5.3 Preparation of phosphoric acid doped PBI meicrosieve**

Piece of straight porous PBI membrane having thickness of 19  $\mu\text{m}$  was doped with phosphoric acid by immersion in 11M  $\text{H}_3\text{PO}_4$  for 24h. Removed the excess of acid by tissue and kept in the oven for 24h at 80° C. The phosphoric acid uptake values here reported have been calculated by weight difference between doped (W2) and undoped (W1) membrane respectively according to following Equation.

$$\text{H}_3\text{PO}_4 \text{ uptake } (\%) = \frac{W2 - W1}{W1} X 100$$

## **2.6 Characterization methods**

### **2.6.1 Porosity**

The porosity of the as prepared PBI microsieves was determined by a Helium displacement pycnometer (MicroMetrics AccuPyc 1330) equipped with 1  $\text{cm}^3$  sample module and reproducibility typically to within  $\pm 0.01\%$  of the nominal sample capacity. The herein reported porosity values were evaluated from PBI microsieves above 30  $\text{cm}^2$  in surface area (i.e. above 100 mg). Porosity calculated using following equation.

$$\text{Porosity } (\phi) = \frac{V_{\text{bulk}} - V_{\text{skeleton}}}{V_{\text{bulk}}} X 100$$

### **2.6.2 SEM characterization**

Morphology, thickness, pore size, and periodicity of the as prepared SPBI membranes and homogeneity of the SPBI-PIL membranes have been studied by scanning electron microscopy SEM (FEG INSPECT 50).



### 2.6.3 Contact angle measurements

Procedure: 6 uL MilliQ water/MIL as drop volumen for contact angles measuments on dense and straight porous PBI surfaces. The measurements are perfomed on 5 different positions on the polymeric surface according to sessile drop method using the CAS20 instrument.

### 2.6.4 Viscosity measurements

The rheological properties of mL at a different temperature, in addition, the mixture of IL: Acetone (1:10 v/v) at RT was measured using Rheometer- Physica UDS 200.

### 2.6.5 ATR-FTIR Spectra Measurements

ATR-FTIR analyses (VERTEX 70 equipment with microscope slide MKII Golden Gate ATR from 4000 to 600  $\text{cm}^{-1}$ , 256 scans and resolution of 0.05  $\text{cm}^{-1}$ ) were performed at room temperature to asses about the photopolymerization evolution and to investigate any possible changes on: i) the protonation site of the poly-cationic, i.e. poly[1-(3H-imidazolium)ethylene] backbone; ii) the vibrational spectrum of the trifluoromethane sulfonyl)imide anion due to ionic interactions; and, iii) the hydrogen bonding interactions between the benzimidazole from the PBI and the poly[1-(3H-imidazolium)ethylene]bis(trifluoromethanesulfonyl)imide. The degree of polymerization was evaluated by using the following expression, where I1662 / I1627 ratios before and after UV exposure are compared<sup>52</sup>

$$\% \text{ Polymerization} = \frac{\left[ \frac{I_{1662}}{I_{1627}} \right]_{\text{before}} - \left[ \frac{I_{1662}}{I_{1627}} \right]_{\text{after}}}{\left[ \frac{I_{1662}}{I_{1627}} \right]_{\text{before}}} \times 100$$

### 2.6.6 Thermal studies

Thermogravimetric analysis (TGA) was carried out using a Q500 IR TA instrument to evaluate the composition and thermal behavior of the as prepared PIL-SPBI membranes with and without cross linker. Studies were conducted using 4-5 mg samples, in the temperature range from room temperature to 900 °C at a controlled heating rate of 2°C /min under an inert atmosphere (N<sub>2</sub>).

### 2.6.7 Mechanical properties

The mechanical properties of the as prepared membranes were analyzed by extensional rheology to specify the mechanical behavior, i.e. Young modulus and tensile stress, as a function of the cross-linker content. This analysis was carried out using a rheometer MCR 301 (Anton Paar) equipped with the Universal Extensional Fixture UXF12. The temperature was controlled at 25 °C with a CTD180 Peltier system. The samples tested were 4x1cm<sup>2</sup> rectangles cut in different parts of the membranes. For a given membrane composition, the mechanical properties result from the average of at least 3 different samples.

### 2.6.8 Proton conductivity

Electrochemical properties of all the samples with and without cross linker were studied by Impedance Spectroscopy (EIS) using an Agilent 4294A Precision Impedance Analyzer from 40 Hz to 110 MHz with 500 mV test signal.

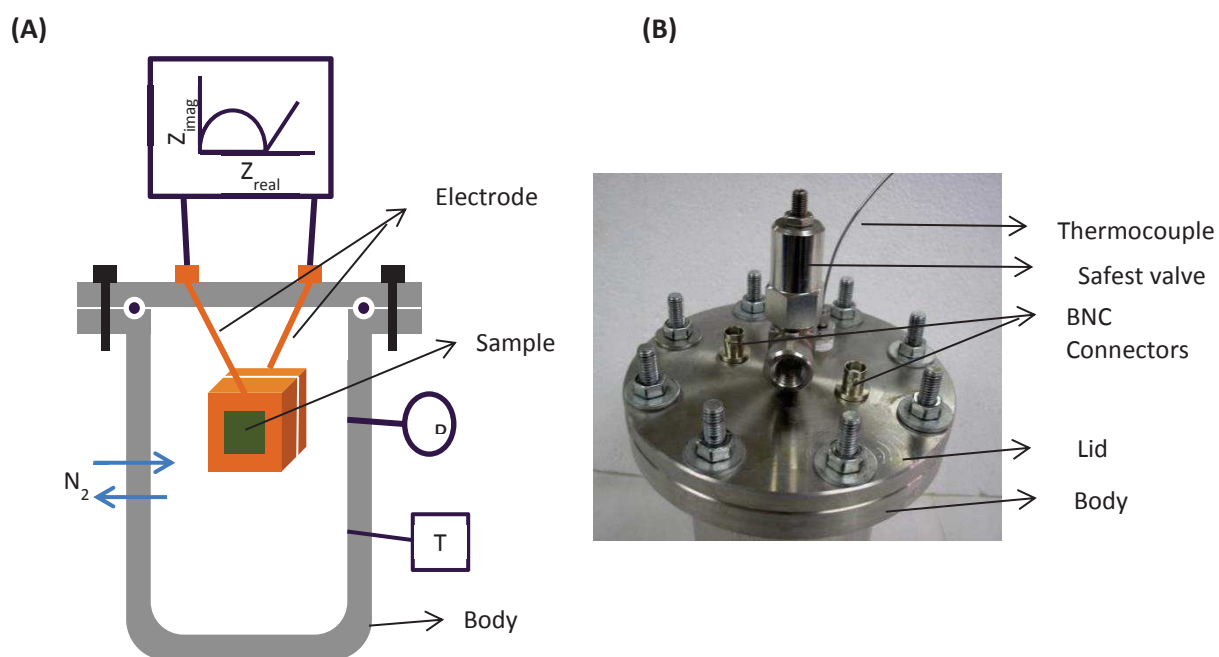


**Figure 3.6 :** A)Conductivity cell scheme; B) Upper part of the electrochemical cell: lid and body

Basically, through-plane conductivity measurements at anhydrous conditions, i.e. by sweeping with 100 cm<sup>3</sup> N<sub>2</sub> STP/min (from certified high purity gas cylinder > 99.998%), have been performed up to 200 °C in a closed home-made stainless-steel conductivity cell PTFE lined (Figure 3.6) inside provided

with annular gold electrodes (11 mm outlet diameter and 6.5 mm inlet diameter). The membrane resistance ( $R$ ) was determined from the real impedance-axis intercept of the Nyquist plot (see Figure 3.7 and Table 3.3).

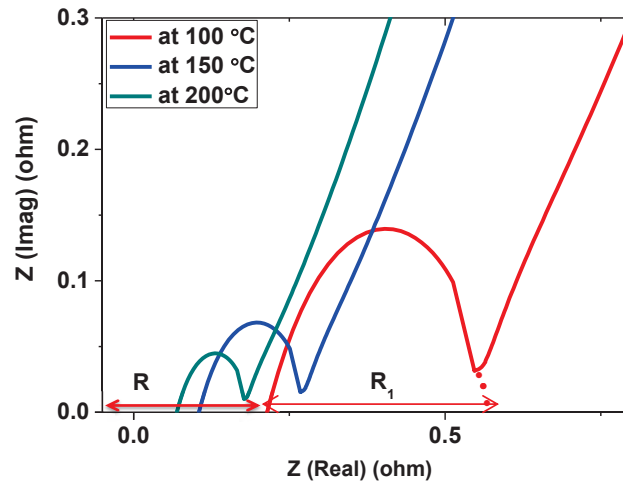


**Figure 3.7:** Nyquist plot of P20-1.5-1%CL with the function of temperature.  $R$ : Electrolyte resistance and  $R_1$ : Polarization resistance.

Thus, the proton conductivity was accordingly calculated following the procedure already described in our previous works<sup>29, 37, 39, 47</sup>.

**Table 3.3:** Resistance values obtained from Nyquist plot

Temp (°C)	$R_2$ ( $\Omega$ )	$R_1$ ( $\Omega$ )
100	0.221	0.332
150	0.108	0.162
200	0.071	0.113

For every membrane code, 3 different samples were measured and the average value was considered. From conductivity performance, the apparent activation energy was evaluated assuming an Arrhenius type dependence<sup>25, 39</sup>. The proton conductivity was calculated according to the following equation.

$$\text{Conductivity } (\sigma) = \frac{z}{RA}$$

Where  $\sigma$  is the proton conductivity in  $\text{mS} \cdot \text{cm}^{-1}$ ,  $z$  is the membrane thickness (the distance between the electrodes) in  $\text{cm}$ , and  $R$  and  $A$  are the obtained resistance in  $\text{Ohm}$  and electrodes surface area  $\text{cm}^2$  (0.618), respectively.

The apparent activation energy ( $E_a$ ) for all samples was estimated from conductivity measurements using the following equation.

$$\ln \sigma = \frac{-E_a}{RT} + \ln \sigma_0$$

Where  $\sigma$  is the proton conductivity in  $\text{mS} \cdot \text{cm}^{-1}$ ,  $R$  is the universal gas constant ( $8.314 \text{J mol}^{-1} \text{K}^{-1}$ ) and  $T$  is the absolute temperature in  $\text{K}$ .

### 3. Results and discussion

#### 3.1 Fabrication of PBI microsieves by micro transfer moulding technique

##### **3.1.1 Using P20 Mold**

The successful preparation of PBI microsieves mainly relies on the wetting properties of the PDMS mold with the casting solution. Thus, the effect of PBI concentration in the final DMAc solution was firstly investigated on the P20 mold wetting. Accordingly, the original PBI solution of 5 wt% was further diluted up to 0.75 wt%, by adding respective amounts of DMAc to identify the maximum PBI concentration for conformational pore filling of the P20 mold. At least, for preparing homogeneous PBI microsieves with pores connecting both sides, the total amount of PBI should not exceed the nominal value, i.e. 120 mg, corresponding to a microsieve thickness equal to the height of the PDMS pillars (i.e. 20  $\mu\text{m}$  for P20 mold).

**Table 3.4:** Optimization Conditions for the Casting of P20 and P15 PDMS molds.

PBI microsieve	Mold	PBI solution* (5 wt%) (g)	PBI Concentration in the casting solution (wt%)	PBI in the casting solution* (mg)	Open pores	Average thickness** ( $\mu\text{m}$ )
P20-2	P20	2	1.13	100	No	21.8 $\pm$ 0.6
P20-1.8	P20	1.8	1.06	90	No	19.9 $\pm$ 0.3
P20-1.5	P20	1.5	0.88	75	Yes	16.5 $\pm$ 0.9
P20-1.3	P20	1.3	0.77	66	Yes	12.4 $\pm$ 0.8
P15-2	P15	2	1.17	100	No	10.8 $\pm$ 0.2
P15-1.6	P15	1.6	0.97	83	No	9.9 $\pm$ 0.1
P15-1.3	P15	1.3	0.77	66	Yes	8.2 $\pm$ 0.8
P15-1	P15	1	0.59	50	Yes	7.3 $\pm$ 0.1
P15-0.75	P15	0.75	0.44	37	Yes	4.9 $\pm$ 0.2

\* For the casting of P20 and P15 mold at wafer level, i.e. filling of 0.11  $\text{cm}^3$  and 0.07  $\text{cm}^3$  respectively;

\*\*evaluated by SEM

After several attempts (see Table 3.4), it was found that the formation of the desired microperforated PBI membranes starts when then PBI concentration in the casting solution was 0.85 wt%. The attained thickness for the PBI microsieve foil (4 inch in diameter) by using 75 mg of PBI in the casting solution; namely, 8.9 g of the casting PBI-DMAc solution 0.84 wt% was 16.5 $\pm$ 0.9  $\mu\text{m}$ .

Among the tested, the best well-defined and thicker SPBI membranes were obtained using P20-1.5 casting solution conditions. A digital picture of the so obtained microsieve PBI foil is shown in Figure 3.8, where cross section and top surface SEM analyses after release from the P20 mold are also included. As it can be observed, homogeneous and continuous PBI microsieves have been fabricated without any deformation in the replicated features (see Figure 3.8A). The SEM analysis of P20-open pore surface, cross section images of P20-1.3 and P20-1.5 is shown in Figure 3.9a, 9b and 9c respectively. The SEM images confirm that the SPBI membrane adopts the cylindrical shape of the soft P20 mold pillars and the pillars perforate through the entire membrane thickness. The replicated pattern on PBI reveals homogeneous periodicity and pore size (Figure 3.9a).

The measured porosity by means of He picnometry, i.e.  $36 \pm 0.46 \%$ , agrees with the calculated from the SEM images. Obtained average pore diameter for mold side is  $18.4\mu\text{m}$  and for airside the observed pore diameter is slightly lower than mold side i.e.  $16.8\mu\text{m}$ , since the solvent evaporation and peeling process takes place at airside.

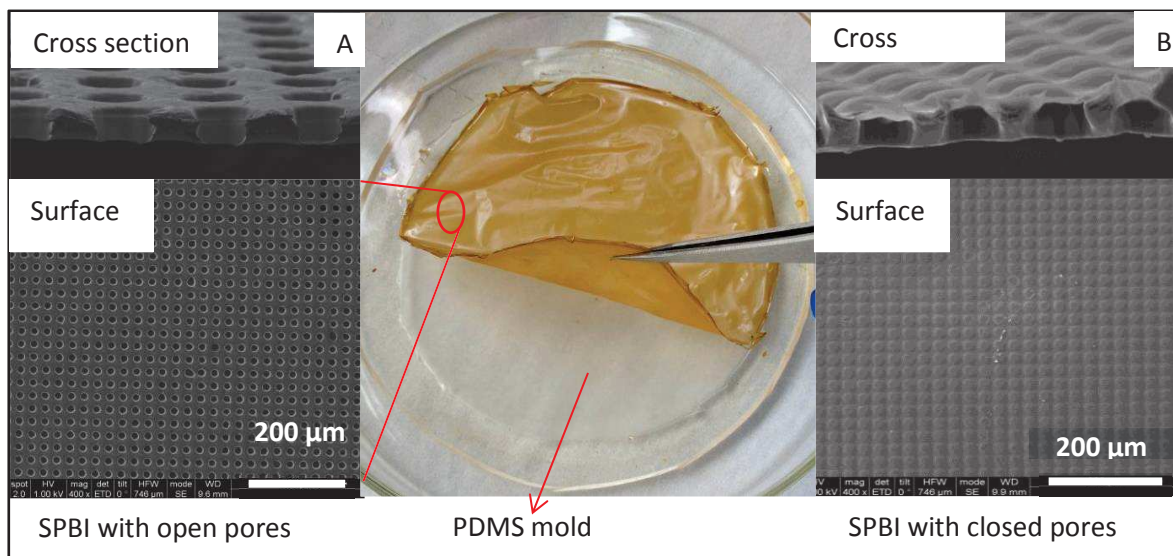


**Figure 3.8:** P20 PDMS mold used for the fabrication of SPBI by microtransfer moulding. SEM images of SPBI membranes with: A) open pores (P20-1.3 type samples); and, B) closed pores (P20-1.8 type samples).

Unlike the above, Figure 3.8B displays the morphology of P20-1.8 type samples where a thin dense layer on top responsible for the pore clogging is clearly distinguished. This effect is attributed to a minor excess in the amount of PBI solution used for the mold casting. On the contrary, the incomplete pore filling of the P20 mold is illustrated in Fig 3.9d where the SEM cross section view of

P20-2 sample is shown. The attained asymmetric structure, with a dense PBI layer 10  $\mu\text{m}$  thick, arises from wettability issues due to the concentration of the casting solution (1.08 %wt).

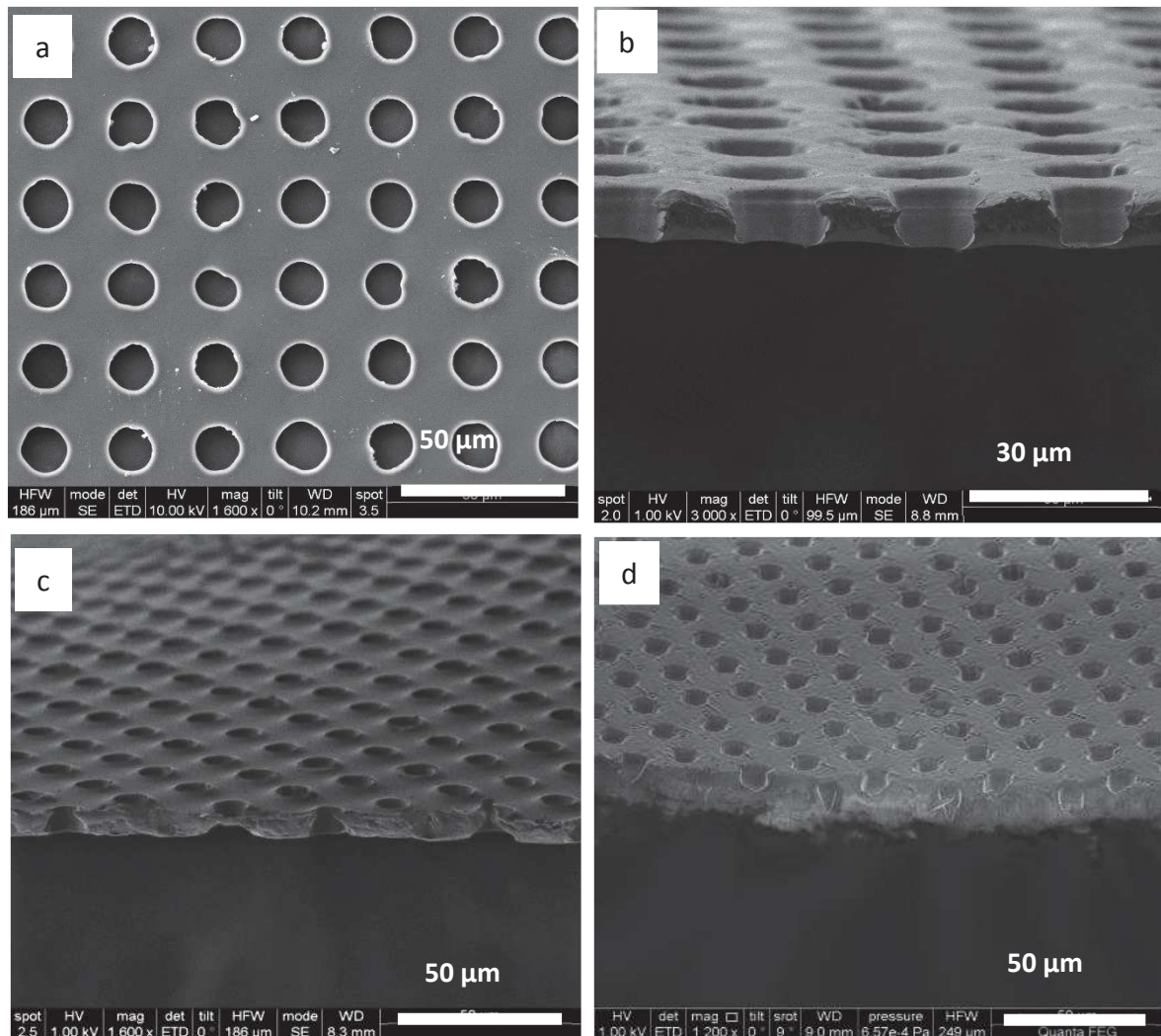


**Figure 3.9:** SEM images of SPBI microsieves obtained from P20 mold: a) P20 open pore surface; b-d) Cross section images of P20-1.3, P20-1.5, and P20-2.

### 3.1.1 Using P15 Mold

Following a similar approach, thinner PBI microsieves were also fabricated by replication from P15 mold. Table 3.4 summarizes the specific conditions for the consecution of well-defined SPBI membranes with open pores

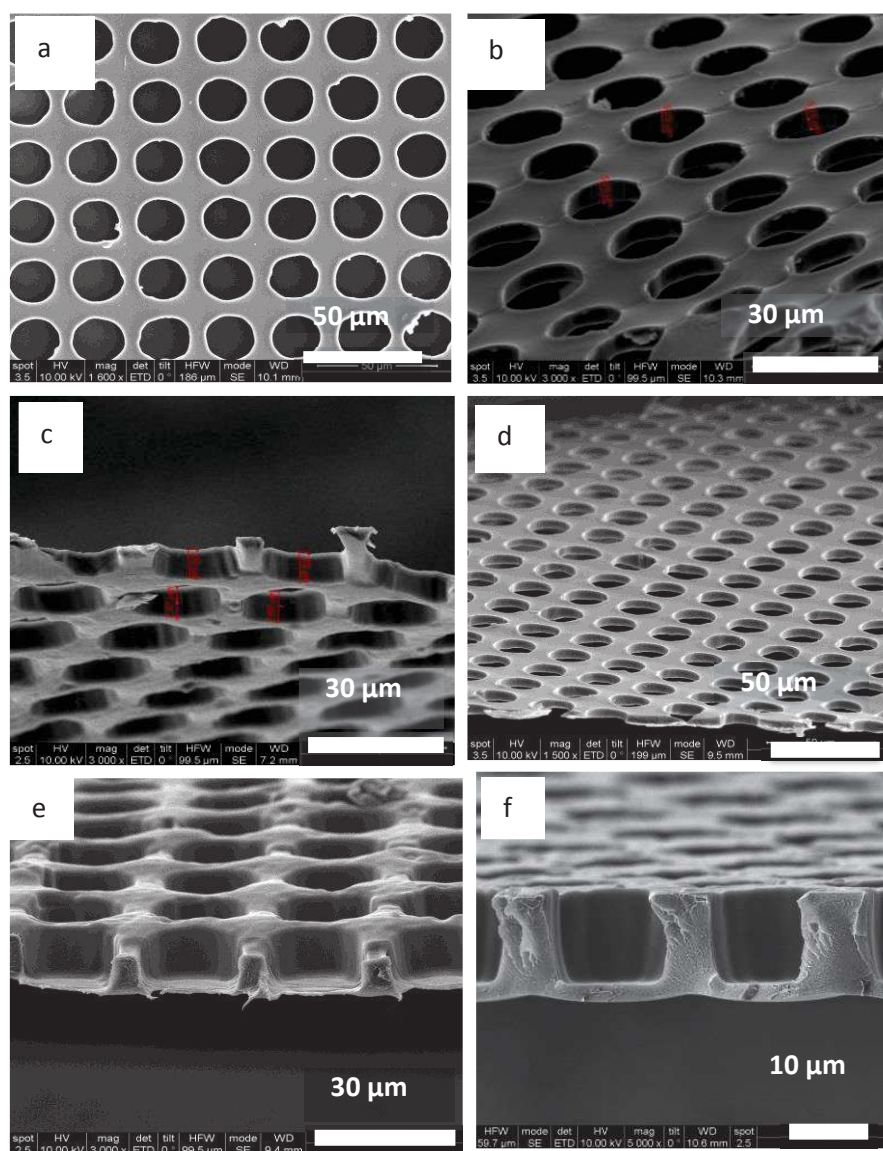


**Figure 3.10:** SEM images of SPBI microsieves obtained from P15 mold : a) P15 open pore surface; b-f) cross section images of P15-0.75, P15-1, P15-1.3, P15-1.6, P15-2 respectively.

In the same way, the original PBI solution of 5wt% was further diluted up to 0.44 wt%, by adding respective amounts of DMAc to recognize the limit PBI concentration for conformational pore filling of the P15 mold and for preparing homogeneous PBI microsieves with pores connecting both sides. It was found that the microperforated PBI membranes start when then PBI concentration in the casting solution was 0.77 wt%. The best well –defined and thicker SPBI membranes were obtained using P15-1.3 casting solution conditions. The obtained maximum thickness for the P15-1.3 was  $8.2 \pm 0.8 \mu\text{m}$ . The SEM images (see Figure 3.10b-d) confirm that the SPBI membrane adopts the cylindrical shape of the soft P15 mold pillars and the pillars perforate through the entire membrane thickness. The replicated pattern on PBI reveals homogeneous periodicity and pore size (Figure



3.10a). Cross section SEM images of P15-1.6 and P15-2 (Figure 3.10e-f) shows a thin dense layer on top responsible for the pore clogging, due to the excess in the amount of PBI casting solution.

These samples have not been further considered for the purposes of this work due to handling constraints.

### **3.2 Pore filling of PBI microsieves**

The protic 1-H-3-vinylimidazolium bis(trifluoromethanesulfonyl)imide monomeric ionic liquid (MIL) has been chosen for the preparation of PIL-SPBI electrolyte membranes accounting from its proton conductivity and based on its high conductivity, low water uptake values as well as thermal stability<sup>37</sup>.

Generally, ILs has a higher viscosity than regular solvents. Viscosity was firstly investigated prior to the infiltration of the monomeric Ionic lipid into SPBI homogeneously (Fig 3.11). Complex viscosity of MIL was decreased from 14.3 to 10.1 mPa.s from the temperature 50 to 100 °C respectively. Next, in the case of the mixture of MIL and acetone, the complex viscosity 8.6 Pa.s was observed at room temperature, thus the IL: Acetone (1:10 v/v) at RT was chosen for infiltration. During acetone evaporation, there was no any phase separation observed between MIL and cross-linker agent.

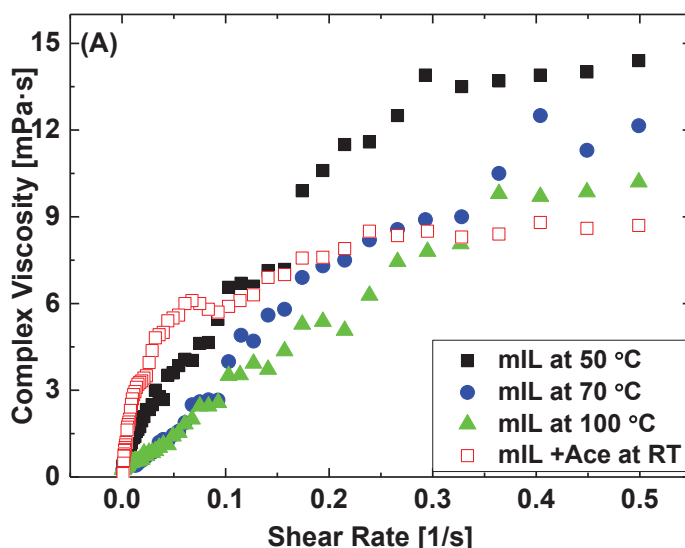


**Figure 3.11:** A) Viscosity vs. shear rate plot for monomeric Ionic liquid (MIL) at different temperatures and the mixture of MIL: Acetone (1:10 v/v) at RT

Additionally, the contact angle (CA) of 1-H-3-vinylimidazoliumbis(trifluoromethane sulfonyl)imide liquid on dense PBI and SPBI membranes was measured. Obtained CA (°) values for MIL were  $26.04 \pm 0.13$  and  $23.02 \pm 0.11$  for dense PBI and SPBI membranes, respectively (see Table 3.5); thus, relatively small compared to water as already reported<sup>30</sup>. These properties make MIL a useful wetting liquid for pore filling.

**Table 3.5:** Contact angle measurements of wetting liquids on PBI surfaces

Solvent	Water	MIL
Sample	Contact angle	
Dense PBI	$83.2 \pm 0.32$	$26.04 \pm 0.13$
SPBI	$73.1 \pm 0.21$	$23.02 \pm 0.11$

The prepared composite PIL-SPBI electrolyte membranes with and without cross-linker are listed in Table 3.6. Membrane P20-1.5-0%CL was fabricated based on the introduction of MIL into SPBI without any cross linker whereas P20-1.5-0.2%CL, P20-1.5-0.5%CL, and P20-1.5-1%CL membranes were based on MIL with 0.2, 0.5 and 1mol.% CL content referred to the MIL) respectively. In order to assess about the conduction performance of PIL-SPBI samples, pure PIL membranes<sup>37, 39</sup> without and with 1 mol.% CL, denoted as PIL and PIL-1% respectively; and, phosphoric acid (PA) doped SPBI membrane, denoted as P20-1.5-PA, prepared by SPBI immersion in 11 M acid solution for 24h at 80 °C<sup>47</sup> were also fully studied.

As shown in Table 3.6, the experimental PIL loadings increase with the CL content: from 46.1 % on P20-1.5-0%CL sample in which no CL is present up to 58.5% for P20-1.5-1%CL. This observation is mainly attributed to the PIL values varying from 2.2 to 2.7 g/cm<sup>3</sup> for PIL-0%CL and PIL-1%CL, respectively. In general, the theoretical electrolyte loadings reasonably match with those calculated from gravimetry and TGA measurements.

For non-crosslinked samples, the PIL/PBI wt% ratio derived from TGA experiment, i.e. 0.84 for 36% porosity, also agrees with the previously reported value<sup>39</sup> for PIL supported on randomly porous PBI supports, i.e. 1.95 for 80% porosity. This observation supports the complete pore filling of the PBI microsieve as illustrated on Figure 3.13e.

**Table 3.6.** Main characteristics of the PIL-SPBI electrolyte membranes prepared for this work.

PEM code	Thickness*	CL (mol.%)	PIL content (wt%)*			Conductivity* (mS·cm <sup>-1</sup> ) at 150 °C		
			Theoretical <sup>1</sup>	Exp <sup>2</sup>	TGA	5 h	24 h	50 h
PIL	95± 1 μm		-	-		330.8	-	-
PIL-1%CL	85± 1 μm		-	-		309.2	-	-
P20-1.5-PA	22± 1 μm	-	-	302 <sup>3</sup>		9.5	8.4	7.0
P20-1.5-0%CL	23± 1 μm	0	51.9	46.1	45.8	48.1	46.5	43.5
P20-1.5-0.2%CL	23± 1 μm	0.2	52.9	48.6	46.6	42.2	38.8	38.4
P20-1.5-0.5%CL	23± 1 μm	0.5	54.3	53.7	53.5	38.5	36.6	36.3
P20-1.5-1%CL	24± 1 μm	1	55.4	58.5	59.3	35.5	35.1	35.0

\*Average from 3 different samples; <sup>1</sup> based on density of PIL; <sup>2</sup> based on gravimetry; <sup>3</sup>PA content in wt% of PA: equivalent to 9.5 doping level in molar ratio.

### 3.2.1 Morphological study

Morphological analysis of the PBI microsives after electrolyte pore filling is shown in Figure 3.11 and 3.12. The relative high viscosity values of the MIL, i.e 14.3 mPa.s at 50 °C, led to heterogeneous and incomplete pore filling of the PBI substrate by WELL method (see SEM image in Fig 3.12). This method has not been further considered for the purposes of the pore filling of PBI microsieves.

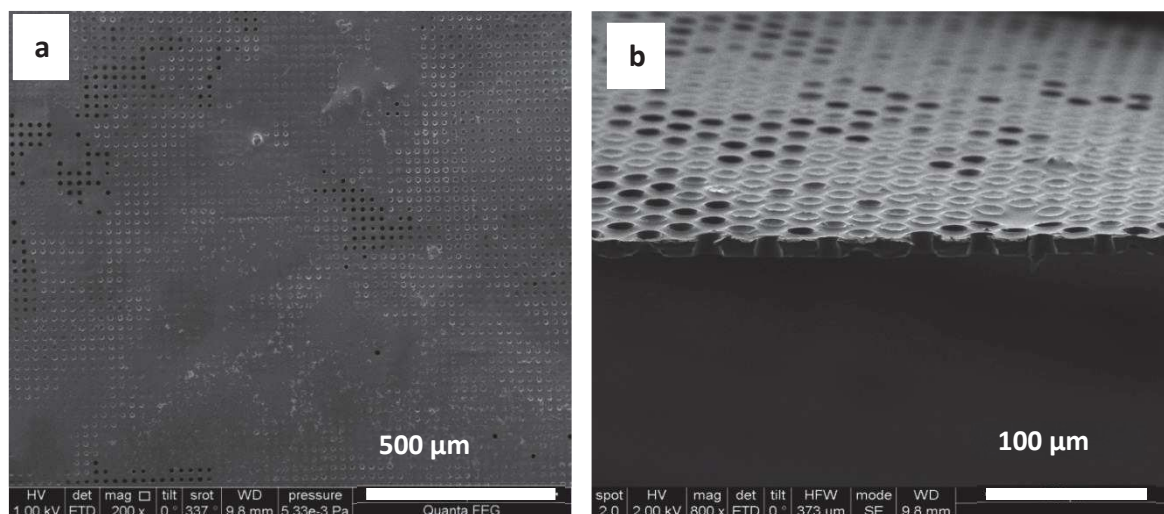


**Figure 3.12** :SEM image of heterogeneous PIL-PBI membranes resulting from WELL : a) surface, b) cross section

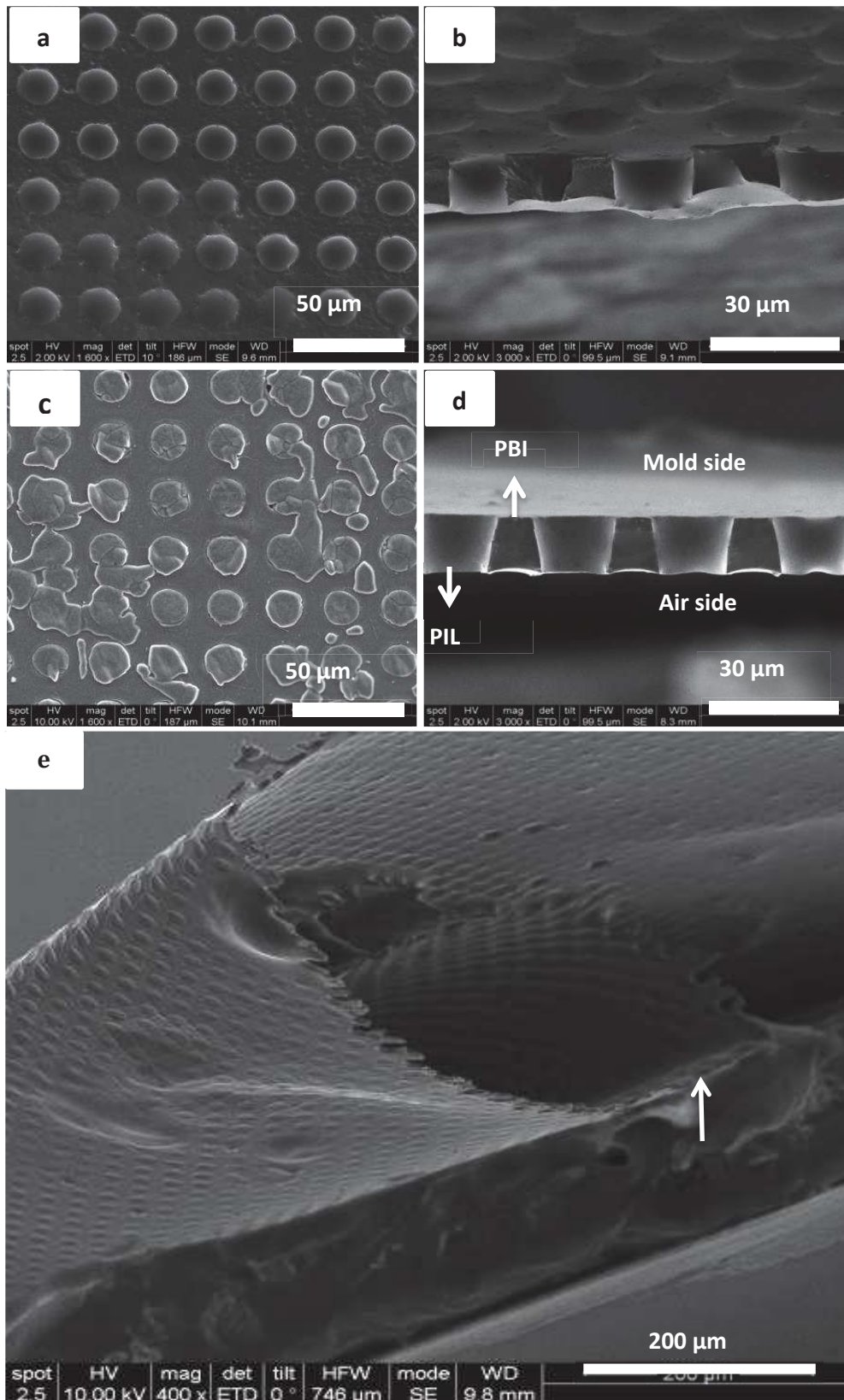


**Figure 3.13:** SEM images of homogeneous PIL-SPBI membranes after pore filling: a) P20-1.5-0%CL surface; b) P20-1.5-0%CL cross section; c) P20-1.5-1 %CL surface; d) P20-1.5-1 %CL cross section; e) P20-1.5-0% CL at low magnification (400X).

The uniform and complete filling (by infiltration method) of SPBI pores with PIL is the key factor of PEM performances. Thus, surface and cross-sectional images of PIL-SPBI membranes with and without cross linker are displayed in Figure 3.13a to 3.13d. In general, the boundary layer between the PIL and the wall surface of the microporous PBI container is almost indistinguishable, in agreement with the chemical compatibility among both components. However, excess of the electrolyte is appreciated on the top surface P20-1.5-1%CL sample (see Figure 3.13c). This behavior correlates with the electrolyte loadings compiled in Table 3.6, and it is related to the density and solubility of the PIL-1%CL electrolyte that hinders the wiping with acetone after the UV curing.

Finally, the complete and uniform filling of SPBI pores with PIL in absence of cracks and defects is clearly shown in Figure 3.13e, with the SEM image of the curly PIL-SPBI foil at lower magnification (x400).

### **3.2.2 Spectral analysis**

The success in the photo-polymerization of vinyl-polymerizable groups from the ionic liquid has been corroborated by FTIR analysis. Thus, ATR-FTIR spectra of the composite membranes before, denoted as MIL-SPBI, and after UV radiation exposure for 2 h (PIL-SPBI) are provided in Figure 3.15.A. The intense absorption bands in the 1400-1000  $\text{cm}^{-1}$  spectral region, observed in both MIL-SPBI and PIL-SPBI samples, are characteristics of the SO<sub>2</sub> and SNS vibrational modes of the bis(trifluoromethanesulfonyl)imide [TFSI] anion<sup>52</sup>. The characteristic infrared absorbance bands adopted to monitor the disappearance of the vinyl-monomer were 1665-1630  $\text{cm}^{-1}$  (stretching vibration in -CH=CH<sub>2</sub>) and 995-920  $\text{cm}^{-1}$  (out of plane bending of -CH=CH<sub>2</sub> groups). Separate spectral analysis on pure PIL samples; see Figure 3.14 as a function of UV exposure time (from 40 min up to 2 h) was performed in advance.

The changes upon polymerization were slight broadening of the characteristic band at 1662  $\text{cm}^{-1}$  arising from the -C=C- vibration of the ionic liquid monomer and relative decreases, due to the conversion of MIL to PIL with UV curing time. The degree of conversion of monomeric ionic liquid to PIL was estimated by the intensity ratio  $I_{1662}$  and  $I_{1700}$  (used as reference band). Among the tested conditions, the polymerization reactions always succeed due to the MIL conversion was above 89% in all cases. Particularly, a maximum polymerization yield of 97% upon 2 h UV exposure time was registered (Table 3.7), in agreement with previous results<sup>37</sup>.

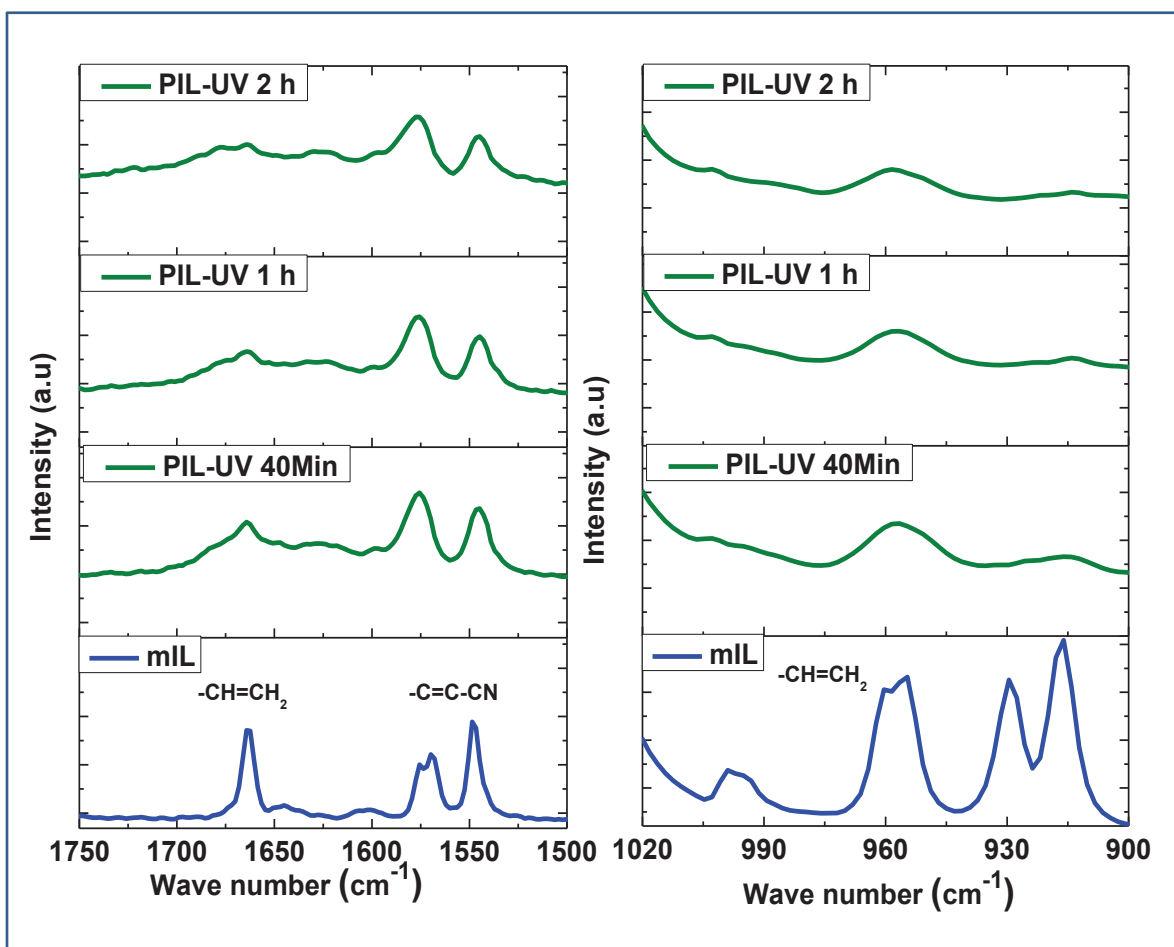


**Figure 3.14:** ATR-FTIR analysis of ionic liquid based films as a function of UV exposure time.

**Table 3.7:** Degree of pure PIL polymerization

UV Time (Min)	FTIR I1662/1700 After UV exposure	% of Polymerization for pure PILs
0	0.87	0
40	0.09	89.2
60	0.06	93.4
120	0.02	97.2

In order to assess PBI interactions with the PIL, FTIR spectra of the pure PBI microsieve and the composite PIL-SPBI are shown in Figure 3.15.B. For SPBI, the very broad peak located between 3700 and 2400  $\text{cm}^{-1}$  corresponds to the free N-H stretching,  $\text{N-H}\cdots\text{H}$  and  $\text{H}_2\text{O}\cdots\text{H}$  hydrogen bond

interactions. On the contrary, the PIL-SPBI spectrum in the region 3700-2400  $\text{cm}^{-1}$  is composed of less intense bands at 3565  $\text{cm}^{-1}$  attributed to stretching vibration of isolated non hydrogen bonds N-H group and 3270  $\text{cm}^{-1}$  attributed to the stretching vibration of physisorbed  $\text{H}_2\text{O}\cdots\text{H}$  hydrogen bonds. The relatively narrow peak centered at 3155  $\text{cm}^{-1}$  is assigned to the self-associated hydrogen bonded N-H groups and the shoulder at 3059  $\text{cm}^{-1}$  is due to the stretching modes of aromatics CH groups.

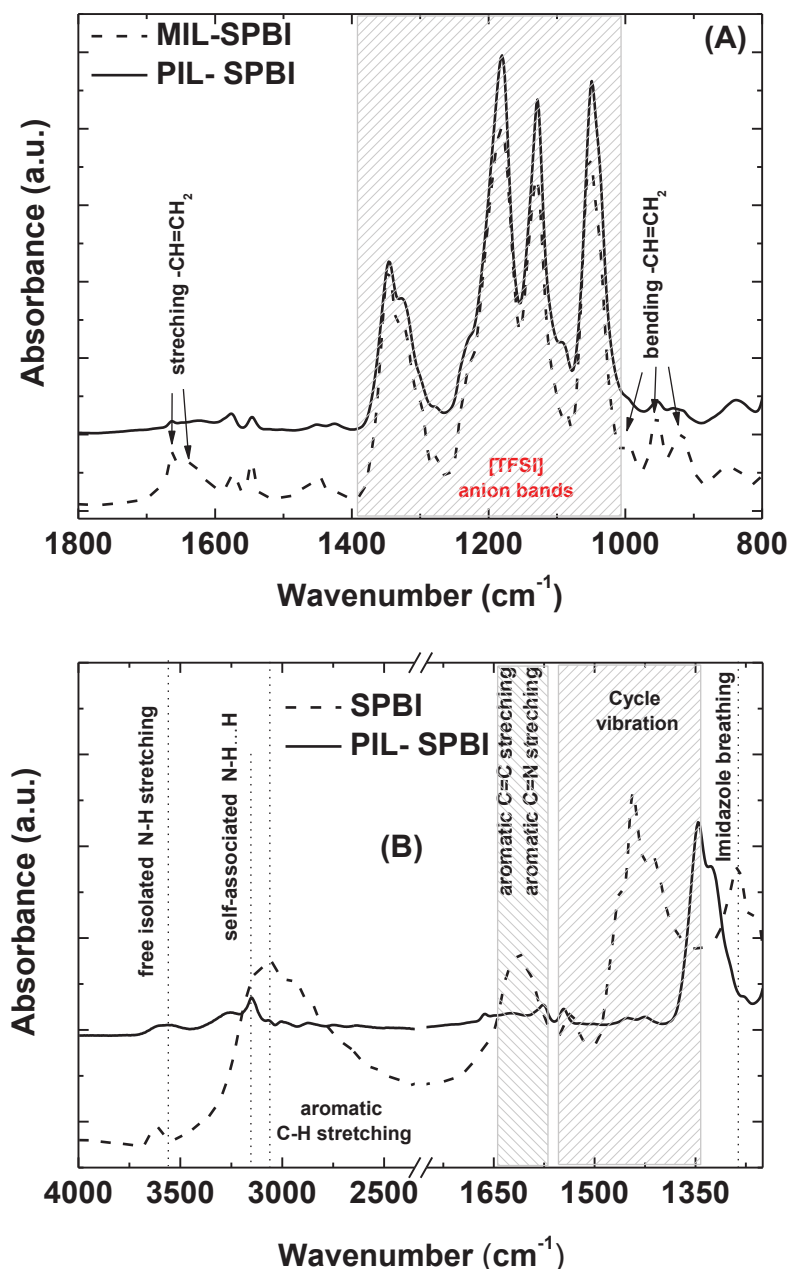


**Figure 3.15:** ATR-FTIR of: A) composite membranes before and after UV exposure; B) PBI microsieve with and without PIL electrolyte.

In the 1800 and 1400  $\text{cm}^{-1}$  region, The very broad band derived from aromatic C=C and C=N stretching modes is approximately centred at 1608  $\text{cm}^{-1}$  for SPBI sample. Besides, the peaks corresponding to the in plane ring vibrations of substituted benzimidazole and imidazole ring breathing are clearly located at 1532, 1442 and 1280  $\text{cm}^{-1}$  respectively. If the imine groups at the imidazole ring of the PBI are protonated<sup>25</sup>, frequency and intensity of some of the ring vibrations could decrease as it is observed in the composite PIL-SPBI sample. These observations support the interactions between the imidazole ring of PBI and the protic PIL.

In summary, the infiltration and polymerization of 1-H-3-vinylimidazolium bis(trifluoromethanesulfonyl)imide are affecting the PBI structure mainly due to: i) the hydrogen bonded N-H groups increase vs. the free isolated ones; ii) the imine group from the imidazole ring is protonated; and iii) the benzimidazole vibration and imidazole breathing are notably suppressed.

### **3.3 Proton Conductivity of PIL-SPBI electrolyte membranes**

Figure 3.16.A and Figure 3.16.B comparatively illustrate the Nyquist plots of PIL (40 Hz to 1.4 MHz) and PIL-SPBI (40 Hz to 110 MHz) membranes at 80 °C and 150 °C, respectively.

PIL-SPBI spectra show a compressed arc in the high frequency region and an inclined straight line indicating that an ion diffusion process plays the major role. A similar behavior has been observed for supported PIL on commercial track-etched alumina membranes (see Figure 3.16.C) (Anodisc<sup>TM</sup> - high purity alumina matrix supplied by Whatman®, 60  $\mu\text{m}$  thick, 70% in porosity, 100-200 nm pore size diameter)

The small diameter of the semicircle indicates that the polarization resistance is negligible on PIL-SPBI membranes for the tested conditions. Therefore, the electrolyte resistance can be found by reading the real axis value at the intercept. As it was expected, the intersections shift to lower values as the temperature increases from 80 °C to 150 °C.

Proton conductivity is considered to be a key property of HT PEMs. The proton conductivity of the PIL-SPBI composite electrolyte membranes as a function of temperature, from 70 °C up to 150 °C without humidification is shown in Figure 3.17A, where the conduction properties of pure and 1% crosslinked PIL and phosphoric acid doped PBI microsieve (see Table 3.6) are also included for reference purposes. As it can be observed, all the conductivity values increase with temperature.



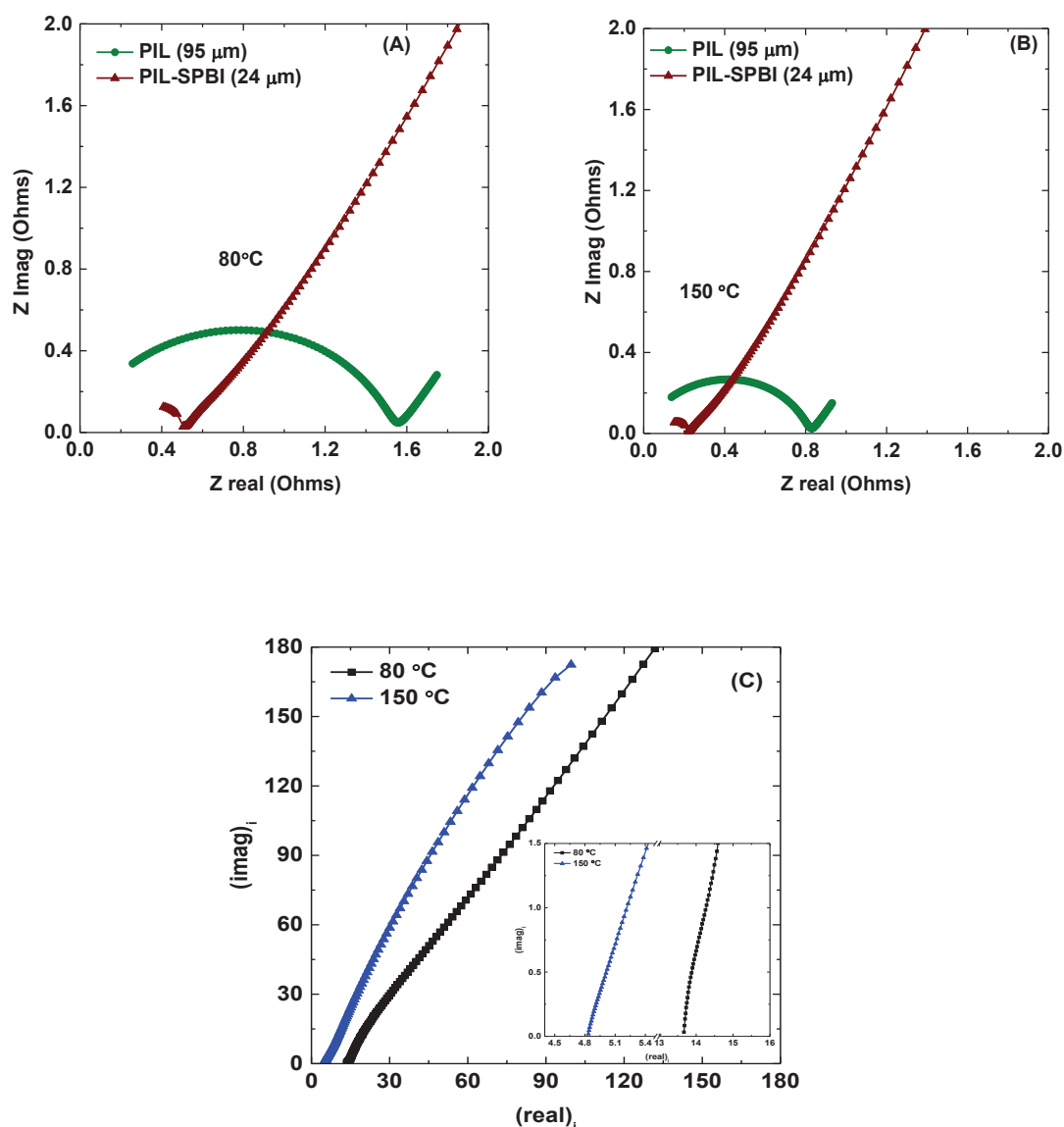


**Figure 3.16:** Nyquist Plot at (A) 80 °C and (B) 150 °C of pure PIL and P20-1.5-0%CL. (C) Nyquist plots of PIL supported on commercial track-etched Anodisc™ membranes

Pristine PBI microsieve has a negligible conductivity, i.e.  $0.73 \text{ mS}\cdot\text{cm}^{-1}$  at  $150^\circ\text{C}$ , and requires intrinsic conductors to facilitate proton transport. The “in situ” polymerization of MIL on SPBI yields to higher proton conductivity values compared to phosphoric acid doping of SPBI:  $16.8 \text{ mS}\cdot\text{cm}^{-1}$  for P20-1.5-0%CL at  $150^\circ\text{C}$  versus  $9.5 \text{ mS}\cdot\text{cm}^{-1}$  for P20-1.5-PA at  $150^\circ\text{C}$ . It is well-known that the mechanical strength of PBI diminishes upon phosphoric acid doping<sup>10-14</sup>. Thus, the pore filling followed by in-situ

polymerization of MIL onto PBI microsieve leads to conducting phosphoric acid-free electrolyte membrane able to operate at 150 °C under anhydrous conditions.

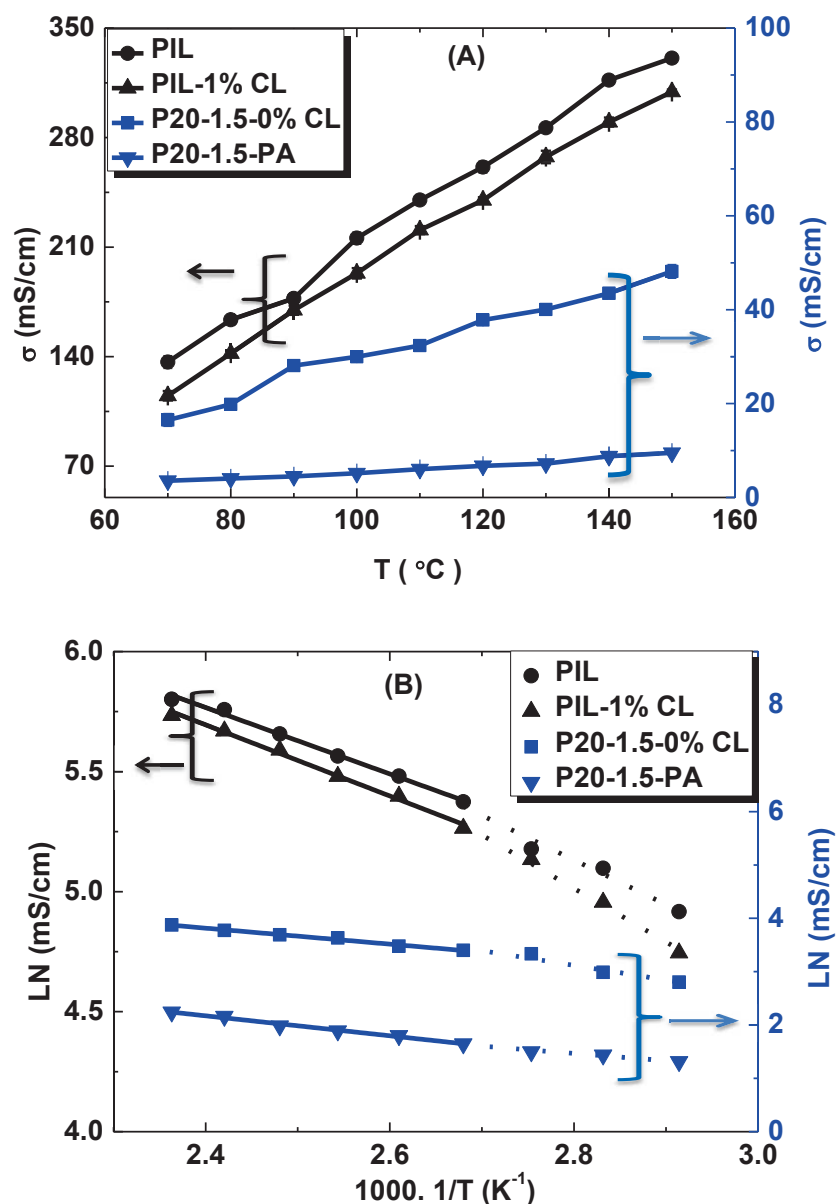


**Figure 3.17:** Conduction performance for pure PIL, PIL-1%CL, P20-1.5-0%CL and P20-1.5-0% PA (Phosphoric acid) as a function of temperature under anhydrous conditions: A) Conductivity values; B) Arrhenius type plot.

The values exhibited by pure PILs are one order of magnitude higher than the registered for the PIL-SPBI composite:  $330 \text{ mS}\cdot\text{cm}^{-1}$  and  $309 \text{ mS}\cdot\text{cm}^{-1}$  for PIL and PIL-1%CL vs.  $48.1 \text{ mS}\cdot\text{cm}^{-1}$  for P20-1.5-0%CL at 150 °C, respectively. Taking into account the porosity (36%) of SPBI membrane and the bulk

conductivity of PIL, conductivity value  $\sim 118 \text{ mS}\cdot\text{cm}^{-1}$  at  $150^\circ\text{C}$  would be expected. Similar tendency, but more exacerbated, is observed for PIL confined on APA supports 70% in porosity with 100-200 nm in pore size. The registered conductivity value  $\sim 11 \text{ mS}\cdot\text{cm}^{-1}$  at  $150^\circ$  (see Fig 3.16C) is significantly less than the expected ( $230 \text{ mS}\cdot\text{cm}^{-1}$  at  $150^\circ\text{C}$ ).

The proton transport inhibition in ionic<sup>25</sup> and poly-ionic<sup>44</sup> liquids on PBI blends has been already described in the literature. Specially, when the ionic liquid is confined to block copolymer domains<sup>54</sup>, the hydrogen-bond structure of the ionic liquid is clearly affected; and, consequently the proton transport via vehicle and proton-hopping mechanisms. According to our infrared studies, shown in the previous section, specific interactions between the PIL and the PBI negatively affect the dynamics of effective charge carriers and the amount of diffusion-enhancing proton hopping.

### **3.3.1 Activation energy of PIL, PIL-1%CL, Acid-doped SPBI and SPBI-PIL**

The activation energy “Ea” values for proton transport were calculated from the slope of the Arrhenius type plot (see Figure 3.17.B) in the intermediate range with temperature boundary conditions of 70 and  $100^\circ\text{C}$ ; and high temperature range from 100 to  $150^\circ\text{C}$ , respectively. In general, clear linear relationships in both temperature ranges are observed for all the tested membranes. Compared to the intermediate-temperature region, the estimated Ea values are lower when operating at 100 to  $150^\circ\text{C}$ , as expected for anhydrous conditions.

In particular for P20-1.5-PA, the obtained values:  $15.6 \text{ kJ}\cdot\text{mol}^{-1}$  ( $70\text{-}100^\circ\text{C}$ ) and  $11.3 \text{ kJ}\cdot\text{mol}^{-1}$  ( $100\text{-}150^\circ\text{C}$ ), are within the typical range for PBI membranes with similar doping levels.

PIL electrolytes seem quite attractive for HT PEMs applications. In agreement with the previous findings by our group<sup>37</sup>, the lowest Ea values, i.e.  $15.4 \text{ kJ}\cdot\text{mol}^{-1}$  ( $70\text{-}100^\circ\text{C}$ ) and  $11.5 \text{ kJ}\cdot\text{mol}^{-1}$  ( $100\text{-}150^\circ\text{C}$ ) correspond to PIL-0%CL due to the number of ion carriers and their mobility is the highest. For the PIL-1%CL, the Ea values increase as expected, i.e.  $18.5 \text{ kJ}\cdot\text{mol}^{-1}$  ( $70\text{-}100^\circ\text{C}$ ) and  $12.3 \text{ kJ}\cdot\text{mol}^{-1}$  ( $100\text{-}150^\circ\text{C}$ ), due to the loss in long-range segmental motion at the expense of better mechanical properties (see section below).

Finally, the calculated Ea ( $100\text{-}150^\circ\text{C}$ ) for PIL-SPBI composite, i.e.  $12.4 \text{ kJ}\cdot\text{mol}^{-1}$  is similar to the exhibited by PIL infiltrated on randomly porous PBI support described in our previous work<sup>39</sup>, i.e.  $13.6 \text{ kJ}\cdot\text{mol}^{-1}$ . This could imply that the proton transport would be dominated by the same mechanism. Furthermore, these values are also similar to the reported for ionic liquid and PBI blends<sup>22, 25, 44</sup>. On the basis of the Ea values for pure PIL membranes,  $15.4 \text{ kJ}\cdot\text{mol}^{-1}$  ( $70\text{-}100^\circ\text{C}$ ) and  $11.5 \text{ kJ}\cdot\text{mol}^{-1}$  ( $100\text{-}150^\circ\text{C}$ ), it can be concluded that the PIL-SPBI led to a higher Ea ( $22.8 \text{ kJ}\cdot\text{mol}^{-1}$  ( $70^\circ\text{-}100^\circ\text{C}$ ) due to the hopping transport and vehicular inhibition.

### 3.4 Thermal and Mechanical Properties of cross-linked PIL-SPBI electrolyte membranes

The final objective of this work is obtaining PEMs for improving physicochemical, mainly thermal and mechanical, and electrochemical properties for applicability at temperatures above 100°C under dry conditions.

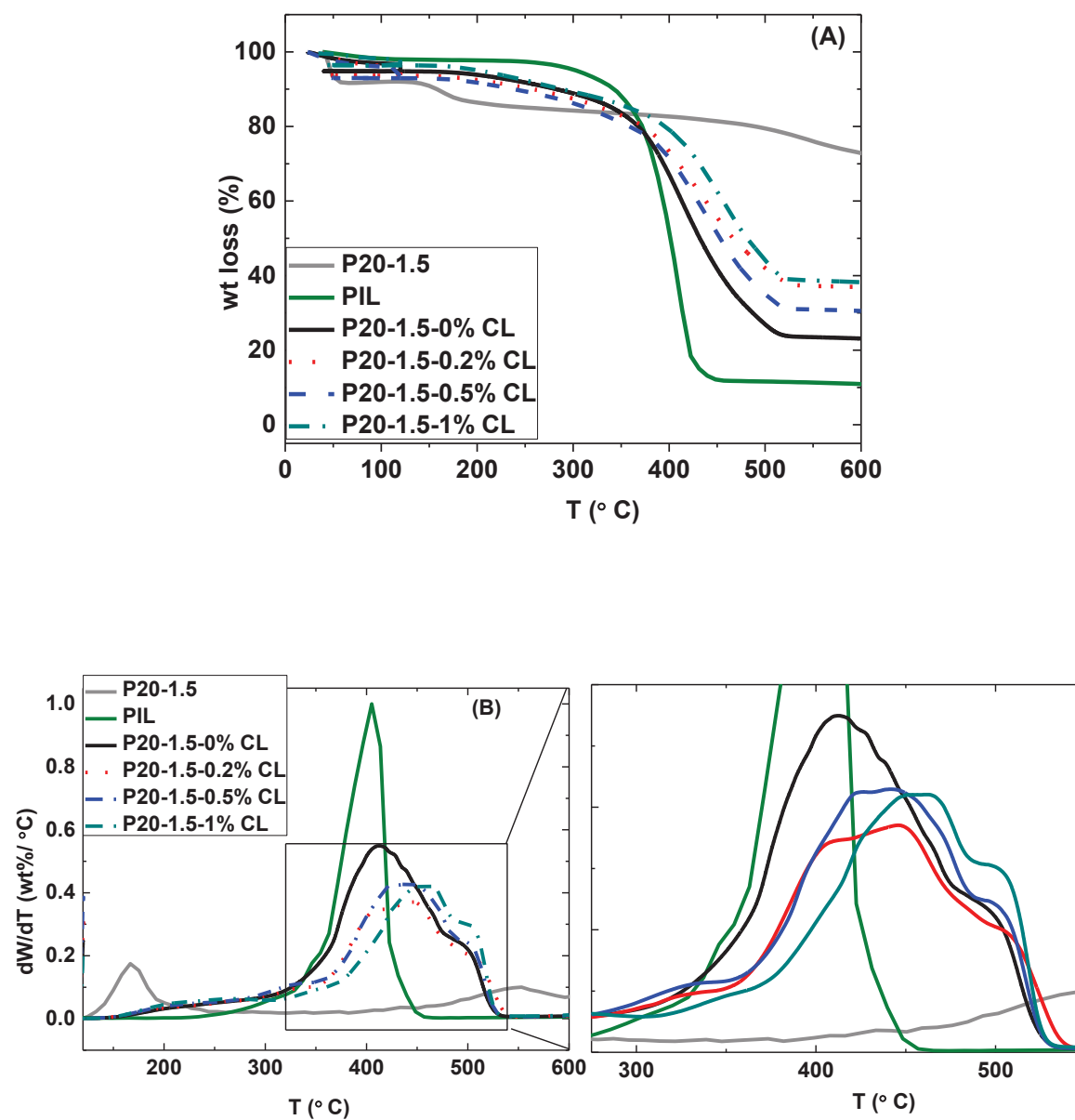


**Figure 3.18:** A) TGA and B) DTG thermograms of PIL based membranes (pure PIL and PBI microsieve also represented for comparison purposes).

For such purposes, the PIL electrolyte modification by crosslinking with divinylbenzene has been chosen to improve its fluidity behavior and mechanical strength. The cross linker content boundary conditions selected for this study, from 0.2 up to 1 mol.%, have been established on the results from our previous work<sup>37</sup> where molar percentages values up to 7.2 mol.% were investigated.

The TGA and DTG thermograms are shown in Figure 3.18.A and Figure 3.18.B respectively. The TGA curve of PIL-SPBI membranes indicates three main reaction stages. An initial weight loss over the temperature range of 50°-200°C (particularly noticeable for pristine PBI microsieve), a second one over 300°-540°C (particularly noticeable for pure PIL) and a third one beyond 600°C were noticed. The first weight loss is ascribed to the loss of absorbed water molecules and to the presence of traces of the photoinitiator (whose first onset temperature occurs at 200 °C).

Pure SPBI showed maximum weight loss (13.6%) in this region due to its hydrophilic nature (see Table 3.5). On PIL-SPBI samples, the % weight loss values are 6.1%, 7.3%, 8.2% and 4.7% for P20-1.5-0%CL, P20-1.5-0.2%CL, P20-1.5-0.5%CL and P20-1.5-1%CL respectively.

In particular, very low weight losses, 0.8%-1.5%) have been observed in all of the composite PIL-SPBI membranes within the 150°-200°C temperature range. The second and most noticeable weight loss was due to the decomposition of the PIL is centered at around 410°-450°C (vs. 405°C for pure PIL sample). The PIL degradation takes place within the range of 300°-540°C. Our study showed that the cross-linked samples started to decompose later due to the second peak become broader and shifted to higher temperature with divinylbenzene content. This effect is in agreement with an effective crosslinking.

Unlike pure PIL, a shoulder at around 490°-505°C was depicted on supported PIL membranes. The authors hypothesize that this event is related to the interactions between PIL and PBI support, already identified by FTIR (see Figure 3.15). Finally, the third weight loss, with an onset temperature above 600°C for the PIL-SPBI composites, was attributed to the decomposition of the PBI backbone.

Table 3.8 summarizes the mechanical properties of the electrolyte membranes prepared for this work. One of the vital requirements of PEM for practical operation relies on the mechanical stability.

Particularly, high storage modulus, and low swelling values are desirable<sup>55</sup>. In general, the mechanical properties of porous membranes depend on many factors e.g. the porosity, distribution, size and shape of the pores<sup>48</sup>. Although pure PILs electrochemically outperform PIL-SPBI composites; the mechanical properties reveal insufficient for FC applications, i.e the Young's modulus measured by incremental stretch relaxation tests is 215 MPa<sup>37</sup>. The strain-stress curves of the prepared PIL-SPBI membranes with and without cross linker are shown in Figure 3.19. As

predictable, the Young modulus values of the composite membranes are approximately one order of magnitude higher due to the structural support provided by the PBI microsieve 36% in porosity. It is noteworthy to underline that the mechanical properties of reinforced PIL on randomly porous PBI support 85% in porosity, described in our previous work<sup>39</sup>, is comparatively lesser: 0.2 GPa as Young Modulus and 1.3 MPa as tensile strength.

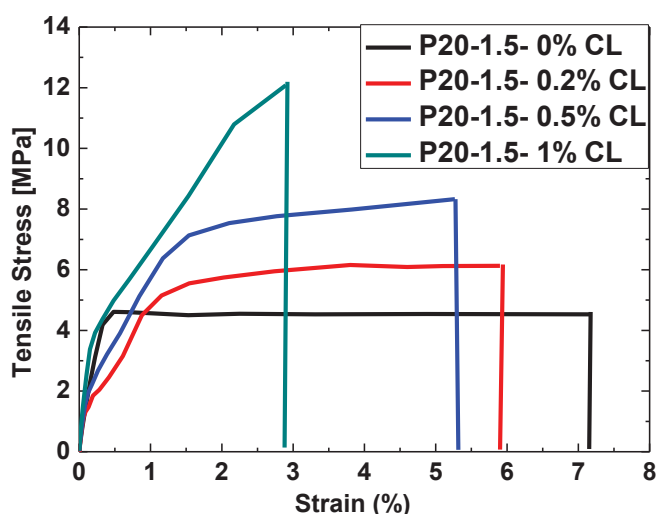


**Figure 3.19:** Stress–strain curve of PIL-SPBI membranes at room conditions.

**Table 3.8:** Mechanical properties of the electrolyte membranes prepared for this work at room conditions.

Membrane	Young Modulus (GPa)	Tensile Stress (MPa)	Tensile strain (%)
PIL*	0.21 ± 0.03	-	-
P20-1.5-0%CL	1.80 ± 0.327	4.63 ± 1.085	7.12 ± 0.281
P20-1.5-0.2%CL	2.20 ± 0.047	6.00 ± 0.374	5.80 ± 0.163
P20-1.5-0.5%CL	2.49 ± 0.071	8.40 ± 0.173	4.50 ± 1.212
P20-1.5-1%CL	2.60 ± 0.072	10.72 ± 2.161	2.57 ± 0.321
AsymPBI**	1.4±0.18	46.9±3.2	39.7±9.8

\* Data from<sup>37, 39</sup>; \*\* Data from Asymmetric PBI membrane 83% porosity<sup>48</sup>.

Concerning cross linked PIL-SPBI membranes, the moduli and strength increased with the increasing amount of CL agent <sup>44</sup>. The opposite behaviour is for the % elongation at break, due to the glassy nature may be increased with divinylbenzene due to a restriction of the polymer chain motion in the cross-linked network. Figure 3.5.c illustrates the suggested PIL structure for poly[1-(3H-imidazolium)ethylene]bis(trifluoromethanesulfonyl)imide. Furthermore, Figure 3.23.B describes the loss in long-range segmental motion as polymer chains become more restricted due to crosslinking effect between polycationic chains <sup>39</sup>.

In summary, a moderate enhancement in both thermal and mechanical stability is attained by crosslinking of the polycationic network.

### **3.5 Electrochemical Properties of cross-linked PIL-SPBI electrolyte membranes**

In order to investigate the tradeoff between thermal/mechanical and electrochemical properties of cross-linked samples, the influence of CL (divinylbenzene) on the proton conductivity was carefully studied. Thus, the conduction performance of PIL-SPBI membranes as a function of CL content, from 0% to 1% mol, was investigated up to 150°C under anhydrous conditions. As shown in Figure 3.20, the appearance of the as prepared membranes before and after the electrochemical characterization remains unaltered.

The temperature dependence of proton conductivity for the cross linked PIL-SPBI membranes is shown in Figure 3.21.A. As expected for all the membranes, the proton conductivity increased with temperature in the studied range. The maximum conductivity of P20-1.5-0.2%CL membrane is 42.2 mS·cm<sup>-1</sup> at 150 °C, lower than the membrane without CL (48.1 mS·cm<sup>-1</sup> at 150°C). The conductivity was dropped slightly as the CL amount was increasing from 0.2 to 0.5 mol.% which reflects the important role of the divinylbenzene in the chemical structure of the PIL-SPBI membrane. A further decrease in conductivity in PIL-SPBI membrane as the CL amount increased 0.5% to 1 mol. %. The maximum conductivity of P20-1.5-0.5%CL and P20-1.5-1%CL membranes is 38.8 and 35.5 mS·cm<sup>-1</sup> respectively at 150°C. The above results signify that the mobility of proton is somewhat affected by the cross linker amount. This indicates that minor amount of cross linker hinders (Figure 3.23.B) the proton mobility by reason of the loss in the long-range segmental movement of polymeric chains. Besides, the cross linker divinylbenzene is a weak electrochemical in nature. On the other hand, the thermal and mechanical properties decreases upon decreasing the cross linker amount (see Table 3.4).

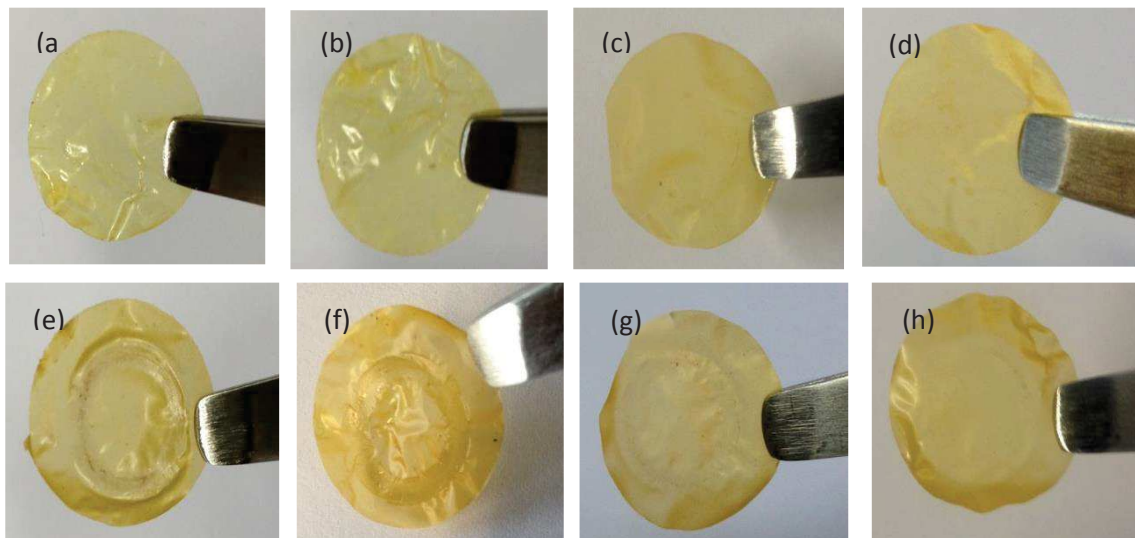


**Figure 3.20:** Appearance of PIL-SPBI based membranes. Top: Fresh membranes, (a) P20-1.5-0%CL; (b) P20-1.5-0.2%CL; (c) P20-1.5-0.5%CL; (d) P20-1.5-0%CL; Bottom: Used membranes at 150°C, (e) P20-1.5-0%CL; (f) P20-1.5-0.2%CL; (g) P20-1.5-0.5%CL; (h) P20-1.5-1%CL.

### 3.5.1 Stability

In addition, conductivity measurements were prolonged up to 50 h for durability purposes (see Table 3.6). Therefore, as soon as the membrane conductivity was firstly estimated according to Figure 3.21A protocole, it was kept for 50h at 150°C. The maximum decline in conductivity is 9.6%, 8.9%, 6.5% and 1.5% for P20-1.5-0%CL, P20-1.5-0.2%CL, P20-1.5-0.5%CL, and P20-1.5-1%CL respectively. Figure 3.20 shows the pictures of the prepared PIL-SPBI membranes before and after conductivity measurements. Before testing, see Figure 3.20: a-d, all membrane surfaces appeared relatively light yellow which indicates a successful polymerization. The level of shininess between the membrane's two sides was decreased with the cross linker amount. All the membranes were free standing films and handled without any difficulty; although the cross-linked PIL-SPBI membranes behave mechanically better than P20-1.5-0%CL. Upon durability test, see Figure 3.20: e-h, the membrane surface revealed unaffected in terms of cracks and defects. However, the membrane surface in contact with the measuring annular electrodes is clearly drawn on P20-1.5-0%CL and P20-1.5-0.2%CL samples in accordance to their comparatively lower Young modulus value (see Table 3.8).



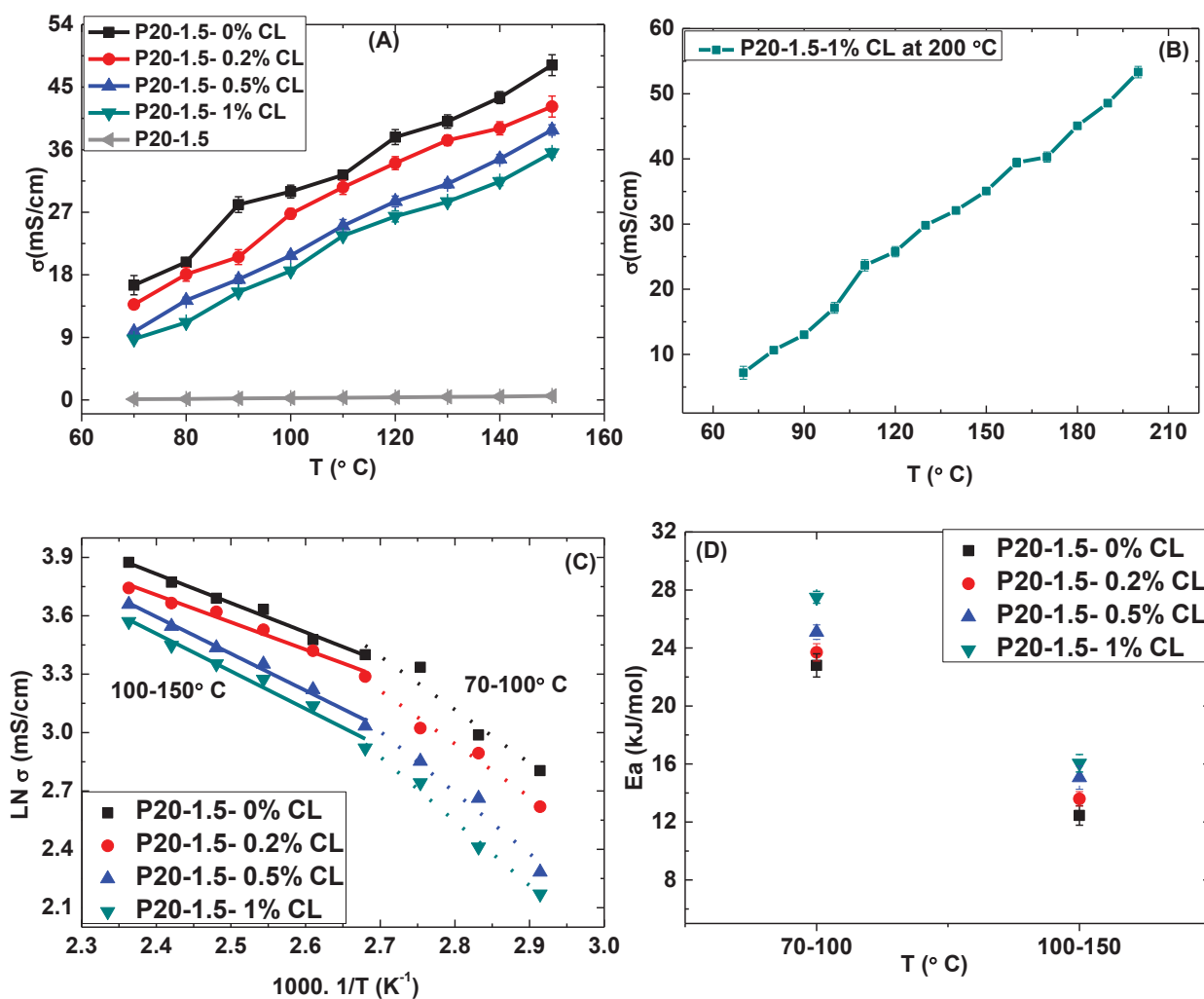


**Figure 3.21:** Conductivity measurement of PIL-SPBI membrane with the influence of Cross linker A) Conductivity performances; B) Conduction performance of P20-1.5-1%CL up to 200°C; C) Arrhenius type dependence; D) Variation of  $E_a$  of composite PIL-SPBI membranes at different temperature windows.

As a result, the optimal formulation as tradeoff between proton transport and mechanical properties corresponds to P20-1.5-1%CL (see Figure 3.22). Among the tested, the P20-1.5-1%CL membrane outstands as the optimal tradeoff between proton transport (53.3 mS·cm<sup>-1</sup> at 200°C) and mechanical properties (Young modulus and Tensile-stress values are 2.6 GPa and 10.7 MPa respectively).

Figure 3.21.B shows the conduction performance of P20-1.5-1%CL from 70°C up to 200 °C. The registered proton conductivity under anhydrous conditions was 53.3 mS·cm<sup>-1</sup> at 200°C.

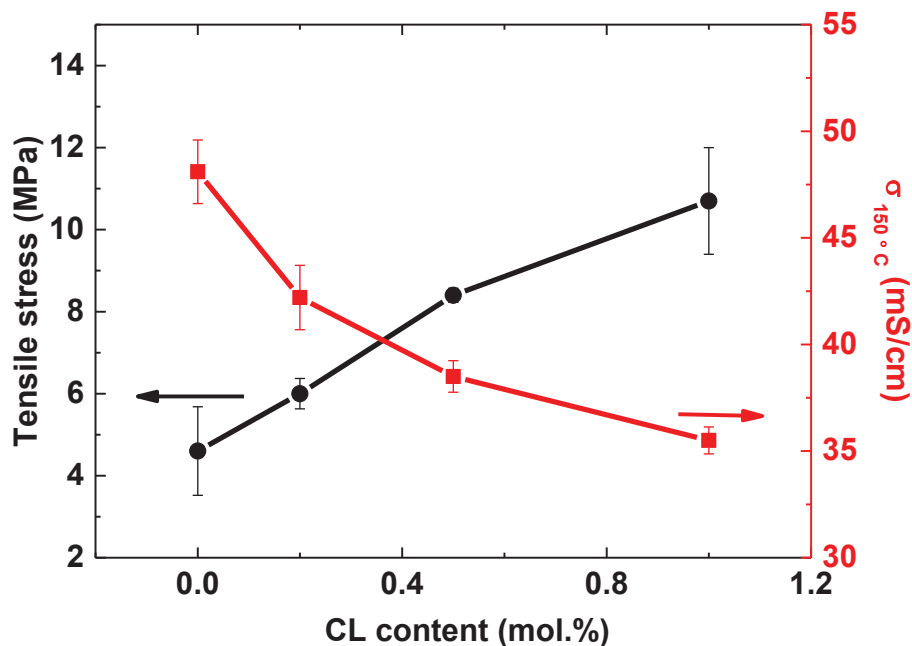


**Figure 3.22:** Tradeoff between proton transport and mechanical properties of PIL-SPBI membrane with the influence of Cross linker.

In order to elucidate the effects of PIL crosslinking in the PIL-SPBI membranes, the activation energy for proton transport was evaluated. The analysis of the apparent Arrhenius-type activation energies ( $E_a$ ) for proton transport in two different temperature windows are on the basis of temperature dependence presented in Figure 3.21.C and Table 3.9.

**Table 3.9.** Slope and  $R^2$  values of PIL-SPBI electrolyte membranes as a function of crosslinking.

Membrane	SLOPE (m)			
	70°C - 100°C	$R^2$	100°C - 150°C	$R^2$
P20-1.5-0%CL	2742	0.948	1498	0.988
P20-1.5-0.2%CL	2850	0.982	1635	0.982
P20-1.5-0.5%CL	3006	0.971	1804	0.990
P20-1.5-1%CL	3295	0.970	1924	0.990

### 3.5.2 Activation Energy

All the tested showed similar temperature dependent conductivity (see Figure 3.21.A); which indicates a similar proton transport mechanism. Figure 3.21.D shows the  $E_a$  values as a function of CL content for two different temperature windows: 70°-100°C and 100°-150°C.

The calculated  $E_a$  values of all cross linked membranes at 100°-150°C are relatively lower than the  $E_a$  values obtained at 70°-100°C due to the PIL's fluidity increases.

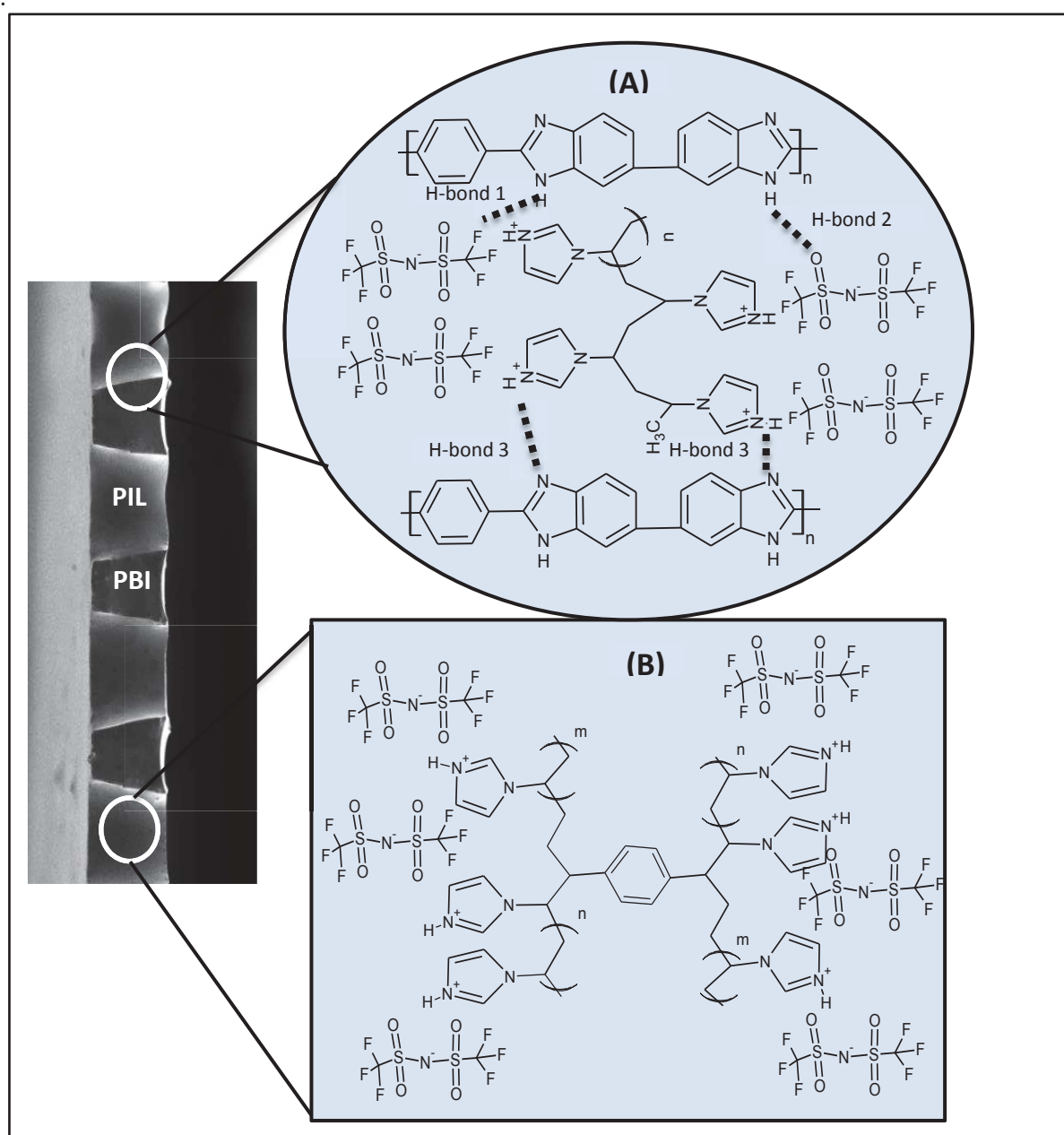


**Figure 3.23:** Postulated proton transport mechanism on PIL-SPBI membranes at: A) the surface layer near the pore-wall surface); B) the inner layer (far away from the pore-wall surface).

According to the Nyquist plot registered for all the composites, the conduction pattern is dominated by the fluidity of PIL chains confined in the macropores of the PBI microsieve. As it was expected, the  $E_a$  for proton transport increases with the % of cross-linker agent due to the loss in long-range segmental motion. The activation energy obtained ranges from 23.7, 25.0 and 27.4  $\text{kJ}\cdot\text{mol}^{-1}$  at 70°-100°C and 13.6, 15.0 and 16.0  $\text{kJ}\cdot\text{mol}^{-1}$  at 100°-150°C for P20-1.5-0.2%CL, P20-1.5-0.5%CL, and P20-1.5-1%CL respectively. These values are slightly higher than those exhibited by P20-1.5-0%CL, i.e. 22.8  $\text{kJ}\cdot\text{mol}^{-1}$  (70°-100°C) - 12.4  $\text{kJ}\cdot\text{mol}^{-1}$  (100°-150°C).

When comparing with  $E_a$  data from unsupported PIL membranes, the lowest value corresponds to pure PIL: 15.4  $\text{kJ}\cdot\text{mol}^{-1}$  at 70°-100°C and 11.5  $\text{kJ}\cdot\text{mol}^{-1}$  at 100°-150°C; followed by PIL-1%CL: 18.5  $\text{kJ}\cdot\text{mol}^{-1}$  at 70°-100°C and 12.3  $\text{kJ}\cdot\text{mol}^{-1}$  at 100°-150°C. Hence, our hypothesis for the proton transport inhibition relies on the hydrogen bonding interactions between the electrolyte and the confining PBI matrix (see Figure 3.23.A) at the pore-wall surface. The reactive 1H-benzimidazol group from PBI would interact with oxygen (H-bond 1) and fluorine (H-bond 2) atoms of free [TFSI] anions. In addition, hydrogen bonding interactions (H-bond3) could generate from the proton from the poly cation and the imine group from the PBI backbone. The FTIR and TGA analyses also support this postulation.

Indeed, Figure 3.24 presents comparative FTIR spectra obtained from the PIL-SPBI composites to distinguish significant differences due to crosslinking and PBI confinement. Comparison of spectra for PIL-SPBI composites reveals that they are almost indistinguishable. However, the appearance change in the peak centered at around  $762\text{ cm}^{-1}$ , assigned to the vibration of SNS from [TFSI], when compared to pure PIL, is likely due to the hydrogen-bond structure previously described. Similar interactions have been proposed for PBI with 1-hexyl-3-methylimidazolium trifluoromethanesulfonate<sup>22</sup> and with the poly(diallyl dimethyl ammonium trifluoride methane sulphate)<sup>44</sup>; and for doped polyaniline films with 1-ethyl-3-methylimidazolium trifluoromethanesulfonate ionic liquid<sup>56</sup>.

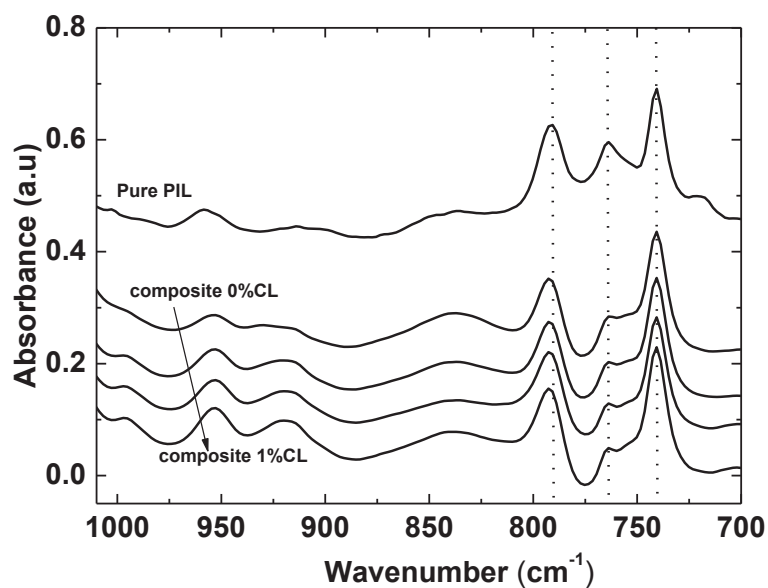


**Figure 3.24:** ATR-FTIR of PIL-SPBI composite membranes as a function of the CL content (pure PIL is also included for comparison).

Summarizing, the properties of poly [1-(3H-imidazolium)ethylene] bis(trifluoromethanesulfonyl)imide in the surface layer would be affected by the substrate wall-fluid interactions. These interactions slow down the proton transport dynamics and so the viscosity in the surface layer is expected to be high <sup>11</sup>.

On the contrary, the properties of molecules inside the inner layers would be only controlled by the interactions among the polycationic chains and the free anions (see Figure 3.23.B). As a consequence, the viscosity in this layer is expected to be lower; and correspondingly, higher proton conductivity. Such a description would be reasonably accepted for the macroporous support herein studied with 15-17  $\mu\text{m}$  as pore size. However, the PIL in the confined geometry experimentally behaves clearly different.

#### 4. Conclusions

In this work, highly conductive proton exchange electrolyte membranes capable to operate at temperatures up to 200 °C have been successfully prepared. The fabrication process involves the infiltration of 1-H-3-Vinyl imidazolium bis(trifluoromethanesulfonyl) Imide solution into straight porous PBI support (36% in porosity and 17 μm in pore size) obtained by microtransfer moulding technique followed by in situ UV polymerization of the ionic moieties. The developed flexible electrolyte membranes, less than 25 μm thick, are composed of straight poly-ionic liquid microchannel circa 15μm in diameter embedded in the polybenzimidazole skeleton. The hydrogen bonding interactions between the benzimidazole unit of the SPBI support and the protic PIL network impart thermal and mechanical stability to the electrolyte membrane at the expense of proton transport inhibition. Similarly, the addition of divinylbenzene cross linker to the imidazolium based polymeric ionic liquid improves the endurance behavior of the electrolytes above 120 °C. In general, all the composite PIL-SPBI membranes, with and without cross-linker, exhibit adequate thermal, mechanical, and electrochemical properties for PEM applications up to 150 °C under anhydrous conditions in absence of mineral acid molecules. Among the tested, the sample with 1 mol.% of cross linker content (referred to the PIL) outstands as the optimal tradeoff between proton transport ( $53.3 \text{ mS}\cdot\text{cm}^{-1}$  at 200°C) and mechanical properties (Young modulus and Tensile-stress values are 2.6 GPa and 10.7 MPa respectively). This novel fabrication approach is very promising for the development of high temperature flexible electrolytes with excellent proton conductivities for electrochemical devices.

## 5. References

1. Debe, M. K., Electrocatalyst approaches and challenges for automotive fuel cells. *Nature* **2012**, *486* (7401), 43-51.
2. Thounthong, P.; Raël, S.; Davat, B., Energy management of fuel cell/battery/supercapacitor hybrid power source for vehicle applications. *Journal of Power Sources* **2009**, *193* (1), 376-385.
3. Bose, S.; Kuila, T.; Nguyen, T. X. H.; Kim, N. H.; Lau, K.-t.; Lee, J. H., Polymer membranes for high temperature proton exchange membrane fuel cell: Recent advances and challenges. *Progress in Polymer Science* **2011**, *36* (6), 813-843.
4. Hogarth, W. H. J.; Diniz da Costa, J. C.; Lu, G. Q., Solid acid membranes for high temperature ( $\geq 140^\circ\text{C}$ ) proton exchange membrane fuel cells. *Journal of Power Sources* **2005**, *142* (1-2), 223-237.
5. Li, Q.; He, R.; Jensen, J. O.; Bjerrum, N. J., Approaches and Recent Development of Polymer Electrolyte Membranes for Fuel Cells Operating above  $100^\circ\text{C}$ . *Chemistry of Materials* **2003**, *15* (26), 4896-4915.
6. Shao, Y.; Yin, G.; Wang, Z.; Gao, Y., Proton exchange membrane fuel cell from low temperature to high temperature: Material challenges. *Journal of Power Sources* **2007**, *167* (2), 235-242.
7. Li, Q.; Jensen, J. O.; Savinell, R. F.; Bjerrum, N. J., High temperature proton exchange membranes based on polybenzimidazoles for fuel cells. *Progress in Polymer Science* **2009**, *34* (5), 449-477.
8. Asensio, J. A.; Sanchez, E. M.; Gomez-Romero, P., Proton-conducting membranes based on benzimidazole polymers for high-temperature PEM fuel cells. A chemical quest. *Chemical Society reviews* **2010**, *39* (8), 3210-39.
9. Chandan, A.; Hattenberger, M.; El-kharouf, A.; Du, S.; Dhir, A.; Self, V.; Pollet, B. G.; Ingram, A.; Bujalski, W., High temperature (HT) polymer electrolyte membrane fuel cells (PEMFC) – A review. *Journal of Power Sources* **2013**, *231*, 264-278.
10. Li, Q.; He, R.; Jensen, J. O.; Bjerrum, N. J., PBI-Based Polymer Membranes for High Temperature Fuel Cells – Preparation, Characterization and Fuel Cell Demonstration. *Fuel Cells* **2004**, *4* (3), 147-159.
11. Li, Q.; He, R.; Berg, R. W.; Hjuler, H. A.; Bjerrum, N. J., Water uptake and acid doping of polybenzimidazoles as electrolyte membranes for fuel cells. *Solid State Ionics* **2004**, *168* (1-2), 177-185.
12. Ma, Y. L.; Wainright, J. S.; Litt, M. H.; Savinell, R. F., Conductivity of PBI Membranes for High-Temperature Polymer Electrolyte Fuel Cells. *Journal of The Electrochemical Society* **2004**, *151* (1), A8.
13. He, R.; Li, Q.; Bach, A.; Jensen, J.; Bjerrum, N., Physicochemical properties of phosphoric acid doped polybenzimidazole membranes for fuel cells. *Journal of Membrane Science* **2006**, *277* (1-2), 38-45.
14. Lobato, J.; Cañizares, P.; Rodrigo, M. A.; Linares, J. J.; Aguilar, J. A., Improved polybenzimidazole films for  $\text{H}_3\text{PO}_4$ -doped PBI-based high temperature PEMFC. *Journal of Membrane Science* **2007**, *306* (1-2), 47-55.
15. Galbiati, S.; Baricci, A.; Casalegno, A.; Marchesi, R., Degradation in phosphoric acid doped polymer fuel cells: A 6000 h parametric investigation. *International Journal of Hydrogen Energy* **2013**, *38* (15), 6469-6480.
16. Qi, Z.; Buelte, S., Effect of open circuit voltage on performance and degradation of high temperature PBI- $\text{H}_3\text{PO}_4$  fuel cells. *Journal of Power Sources* **2006**, *161* (2), 1126-1132.
17. MacFarlane, D. R.; Forsyth, M.; Howlett, P. C.; Pringle, J. M.; Sun, J.; Annat, G.; Neil, W.; Izgorodina, E. I., Ionic Liquids in Electrochemical Devices and Processes: Managing Interfacial Electrochemistry. *Accounts of Chemical Research* **2007**, *40* (11), 1165-1173.
18. Armand, M.; Endres, F.; MacFarlane, D. R.; Ohno, H.; Scrosati, B., Ionic-liquid materials for the electrochemical challenges of the future. *Nat Mater* **2009**, *8* (8), 621-629.

19. Díaz, M.; Ortiz, A.; Ortiz, I., Progress in the use of ionic liquids as electrolyte membranes in fuel cells. *Journal of Membrane Science* **2014**, *469*, 379-396.
20. MacFarlane, D. R.; Tachikawa, N.; Forsyth, M.; Pringle, J. M.; Howlett, P. C.; Elliott, G. D.; Davis, J. H.; Watanabe, M.; Simon, P.; Angell, C. A., Energy applications of ionic liquids. *Energy & Environmental Science* **2014**, *7* (1), 232-250.
21. Ye, H.; Huang, J.; Xu, J. J.; Kodiweera, N. K. A. C.; Jayakody, J. R. P.; Greenbaum, S. G., New membranes based on ionic liquids for PEM fuel cells at elevated temperatures. *Journal of Power Sources* **2008**, *178* (2), 651-660.
22. Wang, J. T.-W.; Hsu, S. L.-C., Enhanced high-temperature polymer electrolyte membrane for fuel cells based on polybenzimidazole and ionic liquids. *Electrochimica Acta* **2011**, *56* (7), 2842-2846.
23. Hernández Carrillo, R.; Suarez-Guevara, J.; Torres-González, L. C.; Gómez-Romero, P.; Sánchez, E. M., Incorporation of benzimidazolium ionic liquid in proton exchange membranes ABPBI-H<sub>3</sub>PO<sub>4</sub>. *Journal of Molecular Liquids* **2013**, *181*, 115-120.
24. Liu, S.; Zhou, L.; Wang, P.; Zhang, F.; Yu, S.; Shao, Z.; Yi, B., Ionic-liquid-based proton conducting membranes for anhydrous H<sub>2</sub>/Cl<sub>2</sub> fuel-cell applications. *ACS applied materials & interfaces* **2014**, *6* (5), 3195-200.
25. Mamlouk, M.; Ocon, P.; Scott, K., Preparation and characterization of polybenzimidazole/diethylamine hydrogen sulphate for medium temperature proton exchange membrane fuel cells. *Journal of Power Sources* **2014**, *245*, 915-926.
26. Noble, R. D.; Gin, D. L., Perspective on ionic liquids and ionic liquid membranes. *Journal of Membrane Science* **2011**, *369* (1-2), 1-4.
27. van de Ven, E.; Chairuna, A.; Merle, G.; Benito, S. P.; Borneman, Z.; Nijmeijer, K., Ionic liquid doped polybenzimidazole membranes for high temperature Proton Exchange Membrane fuel cell applications. *Journal of Power Sources* **2013**, *222*, 202-209.
28. Eguizábal, A.; Pina, M. P., Protic Ionic Liquids Confinement in Macro, Meso and Microporous Materials for Proton Conduction. In *Encapsulation Nanotechnologies*, John Wiley & Sons, Inc.: **2013**, pp 347-389.
29. Eguizábal, A.; J.lemus; Roda, V.; Urbiztondo, M.; Barreras, F.; Pina, M. P., Nanostructured electrolyte membranes based on zeotypes, protic ionic liquids and porous PBI membranes: Preparation, characterization and MEA testing. *International Journal of Hydrogen Energy* **2012**, *37* (8), 7221-7234.
30. Hopkinson, D.; Zeh, M.; Luebke, D., The bubble point of supported ionic liquid membranes using flat sheet supports. *Journal of Membrane Science* **2014**, *468*, 155-162.
31. Martinelli, A.; Nordstierna, L., An investigation of the sol-gel process in ionic liquid-silica gels by time resolved Raman and 1H NMR spectroscopy. *Physical chemistry chemical physics : PCCP* **2012**, *14* (38), 13216-23.
32. Li, M.; Yang, L.; Fang, S.; Dong, S., Novel polymeric ionic liquid membranes as solid polymer electrolytes with high ionic conductivity at moderate temperature. *Journal of Membrane Science* **2011**, *366* (1-2), 245-250.
33. Mecerreyes, D., Polymeric ionic liquids: Broadening the properties and applications of polyelectrolytes. *Progress in Polymer Science* **2011**, *36* (12), 1629-1648.
34. Yuan, J.; Antonietti, M., Poly(ionic liquid)s: Polymers expanding classical property profiles. *Polymer* **2011**, *52* (7), 1469-1482.
35. Ye, Y.-S.; Rick, J.; Hwang, B.-J., Ionic liquid polymer electrolytes. *J. Mater. Chem. A* **2013**, *1* (8), 2719-2743.
36. Yuan, J.; Mecerreyes, D.; Antonietti, M., Poly(ionic liquid)s: An update. *Progress in Polymer Science* **2013**, *38* (7), 1009-1036.
37. Lemus, J.; Eguizábal, A.; Pina, M. P., UV polymerization of room temperature ionic liquids for high temperature PEMs: Study of ionic moieties and crosslinking effects. *International Journal of Hydrogen Energy* **2015**, *40* (15), 5416-5424.



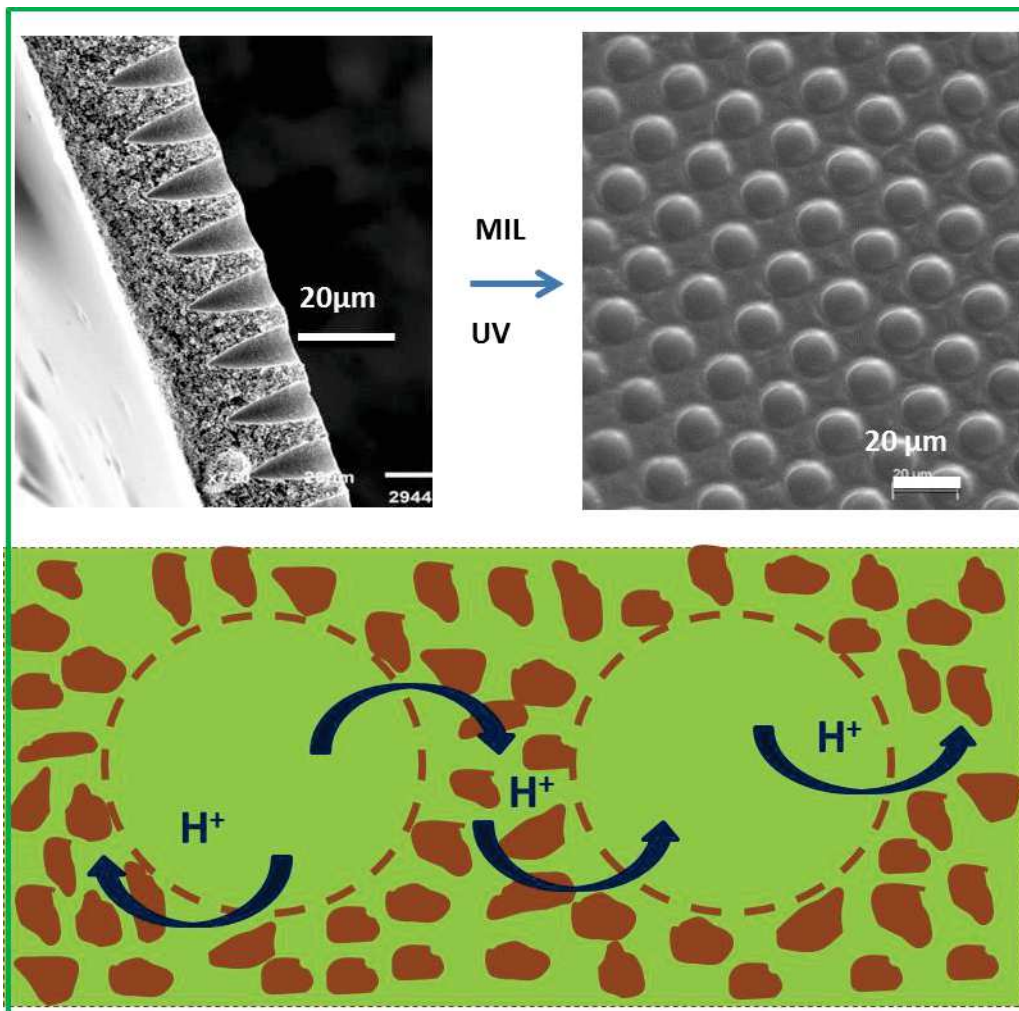
38. Shaplov, A. S.; Marcilla, R.; Mecerreyes, D., Recent Advances in Innovative Polymer Electrolytes based on Poly(ionic liquid)s. *Electrochimica Acta* **2015**, *175*, 18-34.
39. Lemus, J.; Eguizábal, A.; Pina, M. P., Endurance strategies for the preparation of high temperature polymer electrolyte membranes by UV polymerization of 1-H-3-vinylimidazolium bis(trifluoromethanesulfonyl)imide for fuel cell applications. *International Journal of Hydrogen Energy* **2016**, *41* (6), 3981-3993.
40. Díaz, M.; Ortiz, A.; Vilas, M.; Tojo, E.; Ortiz, I., Performance of PEMFC with new polyvinyl-ionic liquids based membranes as electrolytes. *International Journal of Hydrogen Energy* **2014**, *39* (8), 3970-3977.
41. Wojnarowska, Z.; Knapik, J.; Díaz, M.; Ortiz, A.; Ortiz, I.; Paluch, M., Conductivity Mechanism in Polymerized Imidazolium-Based Protic Ionic Liquid [HSO<sub>3</sub>-BVI<sub>m</sub>][OTf]: Dielectric Relaxation Studies. *Macromolecules* **2014**, *47* (12), 4056-4065.
42. Le Bideau, J.; Viau, L.; Vioux, A., Ionogels, ionic liquid based hybrid materials. *Chemical Society reviews* **2011**, *40* (2), 907-925.
43. Díaz, M.; Ortiz, A.; Isik, M.; Mecerreyes, D.; Ortiz, I., Highly conductive electrolytes based on poly([HSO<sub>3</sub>-BVI<sub>m</sub>][TfO])/[HSO<sub>3</sub>-BMIm][TfO] mixtures for fuel cell applications. *International Journal of Hydrogen Energy* **2015**, *40* (34), 11294-11302.
44. Rewar, A. S.; Chaudhari, H. D.; Illathvalappil, R.; Sreekumar, K.; Kharul, U. K., New approach of blending polymeric ionic liquid with polybenzimidazole (PBI) for enhancing physical and electrochemical properties. *Journal of Materials Chemistry A* **2014**, *2* (35), 14449-14458.
45. Yamaguchi, T.; Zhou, H.; Nakazawa, S.; Hara, N., An Extremely Low Methanol Crossover and Highly Durable Aromatic Pore-Filling Electrolyte Membrane for Direct Methanol Fuel Cells. *Advanced Materials* **2007**, *19* (4), 592-596.
46. Liang, B.; Jiang, Q.; Tang, S.; Li, S.; Chen, X., Porous polymer electrolytes with high ionic conductivity and good mechanical property for rechargeable batteries. *Journal of Power Sources* **2016**, *307*, 320-328.
47. Eguizábal, A.; Lemus, J.; Urbiztondo, M.; Garrido, O.; Soler, J.; Blazquez, J. A.; Pina, M. P., Novel hybrid membranes based on polybenzimidazole and ETS-10 titanasilicate type material for high temperature proton exchange membrane fuel cells: A comprehensive study on dense and porous systems. *Journal of Power Sources* **2011**, *196* (21), 8994-9007.
48. Jheng, L.-C.; Hsu, S. L.-C.; Tsai, T.-Y.; Chang, W. J.-Y., A novel asymmetric polybenzimidazole membrane for high temperature proton exchange membrane fuel cells. *Journal of Materials Chemistry A* **2014**, *2* (12), 4225.
49. Eguizábal, A.; Sgroi, M.; Pullini, D.; Ferain, E.; Pina, M. P., Nanoporous PBI membranes by track etching for high temperature PEMs. *Journal of Membrane Science* **2014**, *454*, 243-252.
50. Gates, B. D.; Xu, Q.; Stewart, M.; Ryan, D.; Willson, C. G.; Whitesides, G. M., New Approaches to Nanofabrication: Molding, Printing, and Other Techniques. *Chemical Reviews* **2005**, *105* (4), 1171-1196.
51. Eguizábal, A.; Urbiztondo, M. A.; Pina, M. P., Pt based catalytic coatings on poly(benzimidazole) micromonoliths for indoor quality control. *Catalysis Today* **2015**, *241*, 114-124.
52. Garcia, H.; Barros, A. S.; Gonçalves, C.; Gama, F. M.; Gil, A. M., Characterization of dextrin hydrogels by FTIR spectroscopy and solid state NMR spectroscopy. *European Polymer Journal* **2008**, *44* (7), 2318-2329.
53. Howlett, P. C.; Brack, N.; Hollenkamp, A. F.; Forsyth, M.; MacFarlane, D. R., Characterization of the lithium surface in N-methyl-N-alkylpyrrolidinium bis(trifluoromethanesulfonyl) amide room-temperature ionic liquid electrolytes. *Journal of the Electrochemical Society* **2006**, *153* (3), A595-A606.
54. Hoarfrost, M. L.; Tyagi, M. S.; Segalman, R. A.; Reimer, J. A., Effect of Confinement on Proton Transport Mechanisms in Block Copolymer/Ionic Liquid Membranes. *Macromolecules* **2012**, *45* (7), 3112-3120.

55. Bauer, F.; Denneler, S.; Willert-Porada, M., Influence of temperature and humidity on the mechanical properties of Nafion® 117 polymer electrolyte membrane. *Journal of Polymer Science Part B: Polymer Physics* **2005**, *43* (7), 786-795.
56. Trchova, M.; Sedenkova, I.; Moravkova, Z.; Stejskal, J., Conducting polymer and ionic liquid: Improved thermal stability of the material - A spectroscopic study. *Polymer Degradation and Stability* **2014**, *109*, 27-32.



## Chapter- 4

Hierarchical porous Polybenzimidazole microsieves fabrication by Liquid induced phase separation micromolding (LIPS $\mu$ M): An efficient architecture for anhydrous proton transport via Poly-ionic Liquids





## 1. Introduction

In this chapter, a novel asymmetric PBI matrix has been designed and used as a skeleton for the IL-based electrolyte membrane. The selected porous PBI architecture plays a key role to satisfy both mechanical and handling requirements and also to provide efficient proton transport through the heterogeneous media. The use of highly porous PBI membranes has been already described for PEMFC applications<sup>1-3</sup>. Owing to their high specific surface area for either acid doping or conducting phase embedding, the overall electrolyte performance was notably increased. Jheng et al<sup>3</sup>. proposed highly porous (83.1 vol.%) asymmetric PBI supports through a soft-templating method using 1-ethyl-3-methylimidazolium bis(trifluoromethanesulfonyl)imide, [EMIm][Tf<sub>2</sub>N], as porogen agent. Proton conductivity values above 60 mS·cm<sup>-1</sup> at 160 °C were reported upon phosphoric acid doping (23.6 as doping level). Van de Ven et al<sup>2</sup>. described the fabrication of macrovoid-free randomly porous PBI membranes (65.6 vol.%) impregnated with H-3-methylimidazolium bis(trifluoromethanesulfonyl) imide, [HMIm][Tf<sub>2</sub>N], ionic liquid. The proton conductivity and power density of such PBI/IL membranes were 1.86 mS·cm<sup>-1</sup> at 190 °C and 0.039 W·cm<sup>-2</sup> at 150 °C, respectively. However, ILs tend to drain out from the membranes after long-time operation<sup>4</sup>. In this respect, polymerization of ILs emerges as an attractive option for ILs based PEMs in terms of safety, stability and mechanical properties. Polymeric ionic liquids (PILs)<sup>5-10</sup> are likely to provide a continuous route with ionic character, and at the same time retain some of the unique properties of ILs. Among others, the thermo-chemical stability and tuneable solution properties combined with the intrinsic polymer properties, are expected to offer additional benefits compared to classical ILs. Free radical polymerization of ILs monomers by photochemical initiation is a very attractive option owing to the short reaction time and ambient working temperature.

Very recently, our group<sup>1</sup> has investigated the *in-situ* UV polymerization of 1-H-3-vinylimidazolium bis(trifluoromethanesulfonyl)imide [HVIm][Tf<sub>2</sub>N] onto a highly random porous PBI sponge-like support (above 75 vol%) achieving conductivity values above 300 mS cm<sup>-1</sup> at 200 °C under anhydrous conditions. Unfortunately, the excellent conduction performance was hampered by the brittleness of the membranes. This finding was in line with previously reported studies confirming that high porosity leads to a decrease of both storage modulus and tensile strength<sup>3, 11-12</sup>. Similar drawbacks are commonly alleviated by using supports with optimized pore architecture. In particular, better PIL filling and enhanced conduction would be expected with a pattern of perforated macropores having straight well defined geometries, as the effective pathways become shorter compared to porous supports with random pores shapes, sizes and locations. A feasible solution relies on the application of microsieves. This type of porous materials were introduced over a decade ago<sup>13</sup>, and since then, the span of their applications has been growing steadily, e.g. in micromechanics,

microelectromechanical systems, biochips, microreactors, and several types of sensors<sup>14-16</sup>. The main features of microsieves rely on the presence of straight-through, high density, uniform and well-ordered pores between 0.5 and 10  $\mu\text{m}$  in diameter<sup>17-18</sup>.

Over the last decade Wessling group<sup>19-21</sup> has extensively developed phase separation micromolding (PS $\mu\text{M}$ ) techniques for the preparation of microsieves based on polymethylmethacrylate, polycarbonate, polystyrene, polyvinylidene fluoride, polyimide, polylactic acid or polyaniline with tunable porosity, using either hard or soft structured molds. In PS $\mu\text{M}$ , the phase separation of a polymer solution is combined with replication of structures on a micro-to submicrometer scale. In this way, PS $\mu\text{M}$  not only expands the range of available materials applicable in microfabrication, but also offers the possibility to introduce intrinsic porosity in polymer films. Compared to the thermally induced PS $\mu\text{M}$  process progressed by Vogelaar et al<sup>22</sup>, in liquid induced phase separation micromolding (LIPS $\mu\text{M}$ ), the phase separation proceeds mainly through an exchange of solvent and non-solvent taking place between the polymer solution and the coagulation bath<sup>17, 22</sup>. In a step further, the manufacturing of membranes with a variety of pore sizes (down to only 0.2  $\mu\text{m}$ ) using just single mold has been fully investigated by using solvent-shrinkage approach<sup>23</sup>.

Herein, we propose an innovative HTPEM concept consisting of hierarchically structured PIL channels embedded in a HPBI microsieve. Although at first sight, the intrinsic porosity of the HPBI support may seem useless or even unwanted, the inner surface created by the intrinsic porosity enables for ionic liquid confinement and offers additional pathways for proton transport through the PIL network. Furthermore, such intrinsic porosity might offer a solution for problems derived from both the fluidity and poor mechanical strength of PILs. Our rationale is mostly based on the synergic combination of both PBI and PIL emerging materials together with sustainable and easy scaling-up of membrane technologies. Such PIL-HPBI electrolyte membranes are expected to retain the advantageous features (fast infiltration process and high network connectivity) of both perforated straight pores and intrinsic random of the HPBI microsieves. Compared to sponge-like supports or dense PBI microsieves, better performance is expected for such PIL-HPBI electrolytes since higher and well-connected PIL loadings are achievable without sacrificing the mechanical resistance. Thus, a comprehensive physicochemical and electrochemical characterization of these proton conducting membranes, before and after cross-linking has been accomplished up to 200 °C under anhydrous conditions. Particular emphasis is devoted to the analysis of the skin layer effect and to the influence of PBI pore architecture on the exhibited conduction performance.

## 2. Experimental Section

### 2.1 Materials

All chemical reagents and solvents listed hereafter were used as received: poly[2,2-(*m*-phenylene)-5,5-benzimidazole] (PBI Fumion APH Ionomer,  $M_w$  59,000-62,000, Fumatech), LiCl (99 wt%, Sigma-Aldrich), poly(vinylpyrrolidone) (PVP) K30 ( $M_w$  = 40000, Fluka), PVP K90 ( $M_w$  = 360000, Fluka), 1-*H*-3-vinylimidazoliumbis(trifluoromethane sulfonyl)imide (98 wt%, SOLVIONIC), divinylbenzene (80.0 wt%, Sigma-Aldrich), 2-hydroxy-2-methylpropiophenone (97.0 wt%, Sigma-Aldrich), *N*-methyl-2-pyrrolidone (NMP anhydrous, 99.5 wt%, Sigma-Aldrich).

### 2.2 Structured molds

The structured Si molds were prepared by photolithographic techniques and cryogenic deep reactive ion etching (DRIE) on the Si wafer according to method published elsewhere<sup>23</sup>. Three molds with different pillar dimensions were used as substrates in order to tune the membrane pore diameter and skin layer thickness to get suitable microsieves for PEMs preparation. The dimensions of used molds are described in Table 4.1.

**Table 4.1:** Dimensions of the molds used for LIPS $\mu$ M.

Mold	Pillar Shape	Pillar Height ( $\mu\text{m}$ )	Base diameter( $\mu\text{m}$ )	Periodicity ( $P_d$ ) ( $\mu\text{m}$ )
P	Pyramid	20	8	15
P1	Pyramid	18	10	15
C	Cylindrical	20	9	15

Mold P and P1 had uniform pyramid shaped pillars with base diameter of 8 $\mu\text{m}$  and 10 $\mu\text{m}$  with height of 20  $\mu\text{m}$  and 18  $\mu\text{m}$  respectively. Mold C had uniform cylindrical shaped pillars with base diameter of 8 $\mu\text{m}$  with height of 20  $\mu\text{m}$ . In all molds pillars were placed in every 15  $\mu\text{m}$ , center to center (periodicity).

### 2.3 PBI solution preparation

PBI was used as a polymer for membrane fabrication. Polymer solutions were prepared according to a protocol published in the literature<sup>1</sup>, by mixing 4.5 g of PBI powder, 1 g of LiCl, 1 g of PVP K30, 1 g of PVP K90 and 42.5 g of NMP at 175 °C for 24 h, to obtain polymer solutions with 15% wt. of solids.



Polymer solutions were then outgassed for 2 h in order to remove all air bubbles. Addition of PVP controls macrovoid formation upon phase separation process while LiCl stabilizes the PBI solution.

#### **2.4 PBI microsieves preparation**

The casting device with an adjustable casting knife is shown in Figure 4.1. Distances between the casting knife and the mold were adjusted within 1  $\mu\text{m}$  accuracy with the help of micrometric screws. Casting distances ( $cd$ ) were altered between 3 and 25  $\mu\text{m}$  above pillar level.

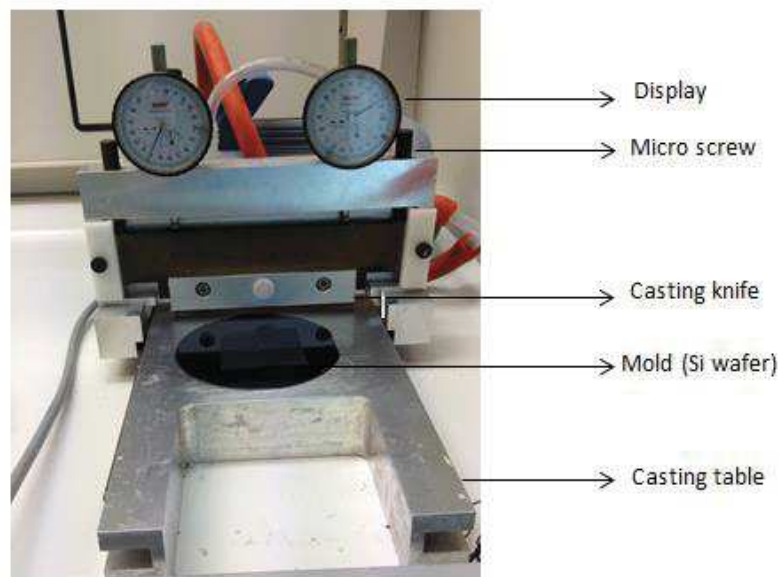


**Figure 4.1.** Photograph of the casting device used to fabricate Hierarchical structured membranes

PBI microsieves were prepared by liquid induced phase separation micromolding (LIPS $\mu\text{M}$ ) method, as schematically shown in Figure 4.2. Polymer solution composed of PBI, PVP, LiCl and NMP was poured onto the structured silicon mold (Figure. 4.2A) and cast with a custom-made casting device. After casting, the mold with polymer solution was immersed for 30 min at room temperature (RT) into the coagulation bath (Fig. 4.2B) containing a NMP/water solution (50/50 wt%). Then, it was transferred into a non-solvent bath (pure water) at RT for 30 minutes in order to wash out NMP traces (Fig. 4.2C). The solidified PBI membrane, peeled off from the mold, was first immersed in ethanol for 30 min (Fig. 4.2D), and then in hexane for another 30 min in order to ensure complete water removal. Finally, in order to remove all volatile compounds, the as-formed membranes were sandwiched between two glass plates and placed in an oven at 150  $^{\circ}\text{C}$ . After the casting procedure, molds were cleaned by NMP and rinsed with acetone.

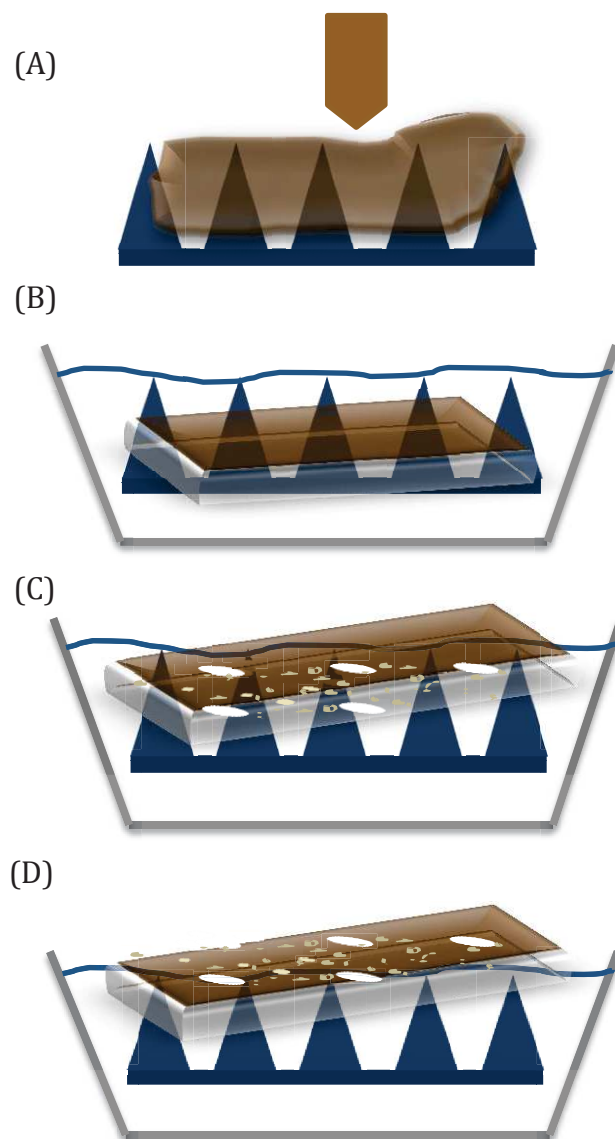


**Figure 4.2.** Schematic representation of liquid induced phase separation micromolding (LIP $\mu$ M): (A) solution casting on structured mold, (B) system immersion in NMP/H<sub>2</sub>O solution (50/50 wt.%), (C)&(D) system immersion in pure water and ethanol, respectively.

Different types of hierarchically structured PBI (HPBI) microsieve supports were fabricated by adjusting the casting distance (see Table 4.2). In fact, the nomenclature adopted for microsieve description includes the casting distance value.

**Table 4.2.** Casting parameters used for the fabrication of HPBI microsieve supports with a P-type mold

S.No.	HPBI microsieve code	Casting distance cd ( $\mu\text{m}$ )
1	P-3 $\mu\text{m}$	3 $\pm$ 1
2	P-5 $\mu\text{m}$	5 $\pm$ 1
3	P-15 $\mu\text{m}$	15 $\pm$ 1
4	P-25 $\mu\text{m}$	25 $\pm$ 1
5	P1-3 $\mu\text{m}$	3 $\pm$ 1
6	P1-5 $\mu\text{m}$	5 $\pm$ 1
7	P1-10 $\mu\text{m}$	10 $\pm$ 1
8	C-10 $\mu\text{m}$	10 $\pm$ 1

### **2.5 Polymer electrolyte membranes preparation**

Polymer electrolyte membranes (PEMs) were prepared by infiltration of PBI with monomeric ionic liquid (MIL) 1-H-3-vinylimidazolium bis(trifluoromethane sulfonyl)imide (H-VIM TFSI) as previously published by our research group<sup>1</sup> (see Figure 4.3).

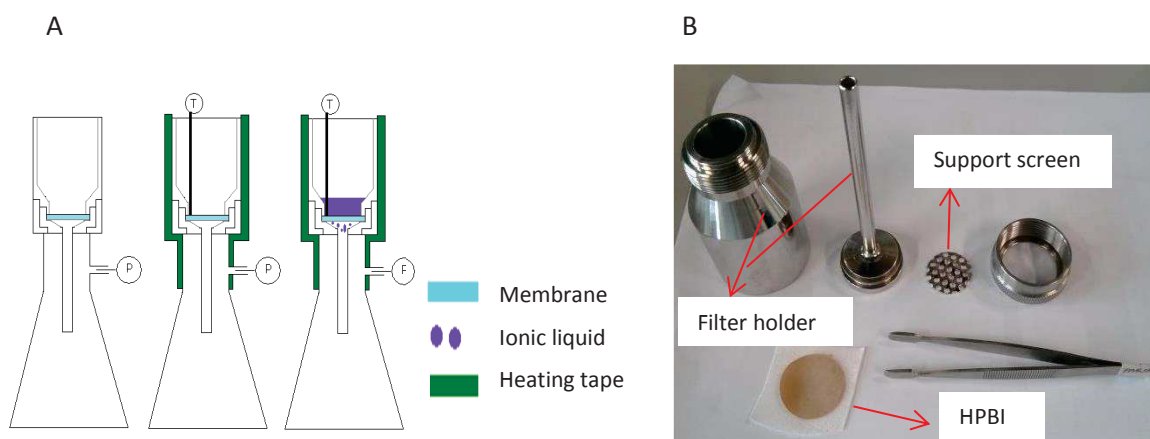


**Figure 4.3.** Scheme of general procedure to immobilize ionic liquids into porous membranes

The monomeric ionic liquid (MIL) was first melted at 50 °C and then placed in contact with the HPBI microsieve support previously dried under vacuum at 120 °C and 100 mbar. The infiltration process was conducted by pouring the MIL on the HPBI surface at 100 °C under vacuum (160 mbar). The

membrane was then removed out from the filter holder and the excess of ionic liquid on the membrane surface was wiped off with a tissue. Finally, 2-hydroxy-2-methylpropiophenone was added on the membrane top surface to initiate the photopolymerization process. For the polymerization, the composite membrane surface was exposed to UV lamp irradiation (Vilber Lourmat, with an intensity of  $2.4 \text{ mW cm}^{-2}$  and wavelength  $\sim 365 \text{ nm}$ ) for 2 hours on each side to get composite PIL-HPBI membrane. Three types of cross-linked PIL-HPBI membranes were prepared by varying the amount of cross-linking agent divinylbenzene: from 0.2 to 1.0 mol % (referred to the MIL). After polymerization, the composite membranes were gently wiped from any residuals with lab paper and acetone. The amount of PIL in the membranes was determined by weight measurements.

## **2.6 Characterization methods**

### **2.6.1 Porosity**

The porosity of the as-prepared HPBI microsieve supports was evaluated by immersion in n-butanol for 2h according to the protocol published elsewhere<sup>24</sup>. The porosity ( $\varepsilon$ ) was calculated using following equation:

$$\varepsilon (\%) = \frac{w_B/\rho_B}{w_M/\rho_M + w_B/\rho_B} \times 100$$

where  $w_B$  is the amount of absorbed n-butanol,  $\rho_B$  the density of n-butanol,  $w_M$  the weight of HPBI microsieve support and  $\rho_M$  its density.

### **2.6.2 Scanning Electron Microscopy (SEM)**

The morphology and thickness of as-prepared HPBI microsieves and derived PIL-HPBI membranes were investigated by Scanning Electron Microscopy (SEM, JSM 6010LA operating at 5kV). The tabulated values result from an average of at least 3 different samples. SEM samples were dried under vacuum at  $60 \text{ }^\circ\text{C}$  for 15 h and coated with a thin gold layer (Balzer Union SCD 040 sputtering at 210 V and 13 mA, during 180 s in 10 mbar Ar atmosphere). Both pore diameters and their periodicity were measured by using SemAfore software.

### **2.6.3 Atomic Force Microscopy (AFM)**

AFM measurements have been carried out in tapping mode using a NSG30 ND-MDT tip (Multimode 8 system, Veeco/Bruker) with force constant around 22-100 N/m.

#### **2.6.4 Transmission Electron Microscopy (TEM)**

Membranes were embedded in epoxy resin, and ultrathin slices (~ 50 nm thick) were cut with an ultramicrotome (Leica EM UC7) at room temperature. The as-prepared slices were placed on TEM copper grids with carbon film, and analysed by Transmission Electron Microscopy (Tecnai T20 - FEI Company) at a working voltage of 200kV. TEM Bright Field Images were acquired with a side-mounted Veleta CCD Camera.

#### **2.6.5 Infrared Spectroscopy (FTIR)**

ATR-FTIR analyses (Bruker VERTEX 70 with Golden Gate ATR from 4000 to 600  $\text{cm}^{-1}$ , 256 scans, and resolution of 4  $\text{cm}^{-1}$ ) were performed at room temperature to monitor the photo-polymerization reaction and to investigate any possible changes on: *i*) protonation site of the poly-cationic backbone, i.e. poly[1-(3H-imidazolium)ethylene]; *ii*) vibrational spectrum of trifluoromethane sulfonyl)imide anion originating from ionic interactions, and *iii*) hydrogen bonding interactions between the benzimidazole groups in PBI and the poly[1-(3H-imidazolium)ethylene]bis(trifluoromethanesulfonyl)imide.

#### **2.6.6 Thermogravimetric analyses (TGA)**

Thermogravimetric analyses (Q500 IR TA instrument) were used to evaluate the composition and thermal behaviour of PIL-HPBI membranes with or without any cross-linker. Studies were conducted with 4-5 mg samples, in the temperature range from 25° C to 900 °C with a heating rate of 2°C/min under N<sub>2</sub> atmosphere.

#### **2.6.7 Mechanical properties**

The Young's modulus and tensile strength of the PIL-HPBI (P1-9-25 $\mu\text{m}$ ) membranes were analyzed by extensional rheology (Anton Paar rheometer MCR 301 equipped with Universal Extensional Fixture UXF12). The temperature was controlled at 25 °C (CTD180 Peltier system). The tested samples (4x1  $\text{cm}^2$ ) were cut in different areas of the membranes. For a given membrane composition (cross-linker amount), the mechanical parameters values result from the average of at least 3 different samples.

#### **2.6.8 Impedance spectroscopy**

Proton conductivity of membranes prepared with and without any cross-linker was measured by electrochemical impedance spectroscopy (ESI- Agilent 4294A precision impedance analyzer in the range 40 Hz- 110 MHz). Membranes were sandwiched between two gold electrodes and resistance

through the plane was measured in anhydrous conditions, using high purity  $N_2$  (> 99.998%) as a sweep gas ( $100 \text{ cm}^3 \text{ STP/min}$ ). Measurements were performed every  $10^\circ\text{C}$  from  $70^\circ\text{C}$  to  $200^\circ\text{C}$  in a closed home-made stainless-steel conductivity cell PTFE lined inside provided with annular gold electrodes (11 mm outlet and 6.5 mm inlet diameter), as described in our previous works<sup>25-26</sup>. Proton conductivity ( $\sigma$  in  $\text{mS}\cdot\text{cm}^{-1}$ ) was calculated from measured resistance values ( $R$  in Ohms) using the equation  $\sigma = z/RA$  where  $z$  is the membrane thickness in cm, and  $A$  is the electrodes surface area in  $\text{cm}^2$ . Electrolyte resistance was derived from the real impedance-axis intercept of the Nyquist plot (Figure 4.4). The activation energy for ionic conduction was calculated assuming Arrhenius-type dependence.

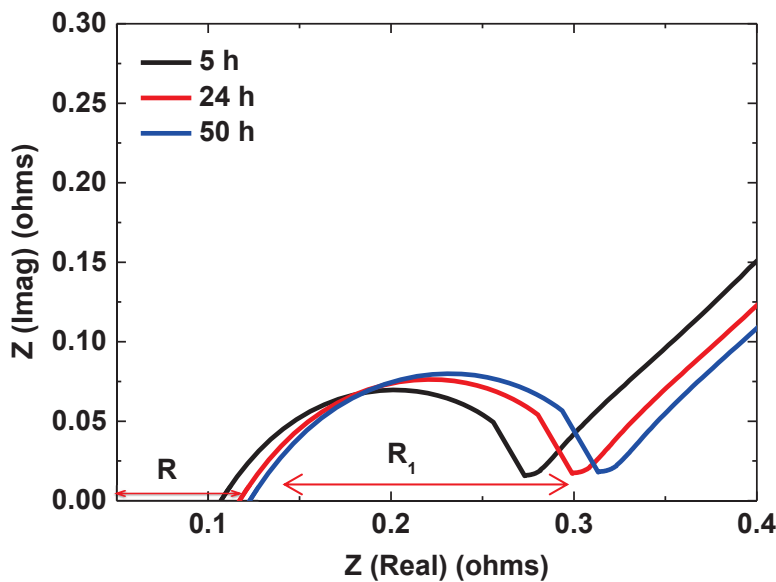


**Figure 4.4.** Nyquist plot of P-25 $\mu$ -0%CL at  $150^\circ\text{C}$  as a function of the operation time: R denotes electrolyte resistance and R1 denotes polarization resistance.

### 3. Results and Discussions

#### ***3.1 Fabrication of Hierarchical PBI microsieves (HPBI) by LIPS $\mu$ M***

The main characteristics of the prepared microsieves are presented in Table 4.3. Both the macropores height and total thickness of the asymmetric HPBI microsieve mainly depend on the casting distance (cd). Accordingly, the cd was altered between 3 and 25  $\mu\text{m}$  above pillar level. The skin layer thickness increases with increasing cd and the nominal macropore height ( $\sim 19.5 \mu\text{m}$ ) could be obtained when cd exceeds 15  $\mu\text{m}$ .

**Table 4.3.** Main characteristics of the HPBI microsieves fabricated by LIPS $\mu$ M.

Microsieve code	Macropore dimensions ( $\mu\text{m}$ )		Periodicity ( $\mu\text{m}$ )	Thickness z ( $\mu\text{m}$ )		Porosity $\epsilon$ (%)		
	Diameter*	Height		Total	Skin layer	Total	Intrinsic <sup>#</sup>	Intrinsic/Macro
P-3 $\mu\text{m}$	9.1 $\pm$ 0.1	12.1 $\pm$ 0.1	14.9 $\pm$ 0.1	12.4 $\pm$ 1	-	61.2	53.8	7.2
P-5 $\mu\text{m}$	8.7 $\pm$ 0.1	15.5 $\pm$ 0.1	15.4 $\pm$ 0.1	15.8 $\pm$ 1	0.3 $\pm$ 0.2	57.1	49.7	6.7
P-15 $\mu\text{m}$	8.9 $\pm$ 0.1	19.5 $\pm$ 0.1	15.5 $\pm$ 0.1	30.6 $\pm$ 1	11.1 $\pm$ 0.2	46.1	38.7	5.2
P-25 $\mu\text{m}$	8.9 $\pm$ 0.1	19.5 $\pm$ 0.1	15.5 $\pm$ 0.1	40.2 $\pm$ 1	21.1 $\pm$ 0.2	42.5	35.1	4.7
P1-5 $\mu\text{m}$	10.2 $\pm$ 0.1	16.7 $\pm$ 0.1	15.7 $\pm$ 0.1	20.5 $\pm$ 1	3.8 $\pm$ 0.1	-	-	-
P1-10 $\mu\text{m}$	10.5 $\pm$ 0.1	14.3 $\pm$ 0.1	15.4 $\pm$ 0.1	22.6 $\pm$ 0.3	8.3 $\pm$ 0.2	-	-	-
C-10 $\mu\text{m}$	8.6 $\pm$ 0.1	17.8 $\pm$ 0.1	14.7 $\pm$ 0.1	24.5 $\pm$ 0.3	6.7 $\pm$ 0.1	-	-	-

\*mold side; <sup>#</sup>evaluated by subtracting the nominal macro porosity, i.e.7.4%, from total  $\epsilon$ .

Moreover it has been found out that the obtained porosity depends on the skin layer thickness (Table 4.3) and it decreases for thicker skin layers. The highest porosity ( $\sim 60\%$ ) was obtained for membranes with almost no skin layer (P-3 $\mu\text{m}$  and P-5 $\mu\text{m}$ ). However, these membranes have not been used further due to handling constraints. In comparison, mechanically more stable membranes, i.e. P-15 $\mu\text{m}$  and P-25  $\mu\text{m}$ , exhibit a porosity of 46.1%, 42.5 %, respectively.

Pyramidal type pillar structured Si-mold and SEM images of the as-prepared HPBI microsieves (air side, mold side and cross-section with intrinsic pores of 50-100 nm are displayed in Figure 4.5. It must be noted that the straight-through macropores are generated by pillar perforation of the Si-mold, while the small (intrinsic) pores result from the phase inversion process<sup>21, 23</sup>.

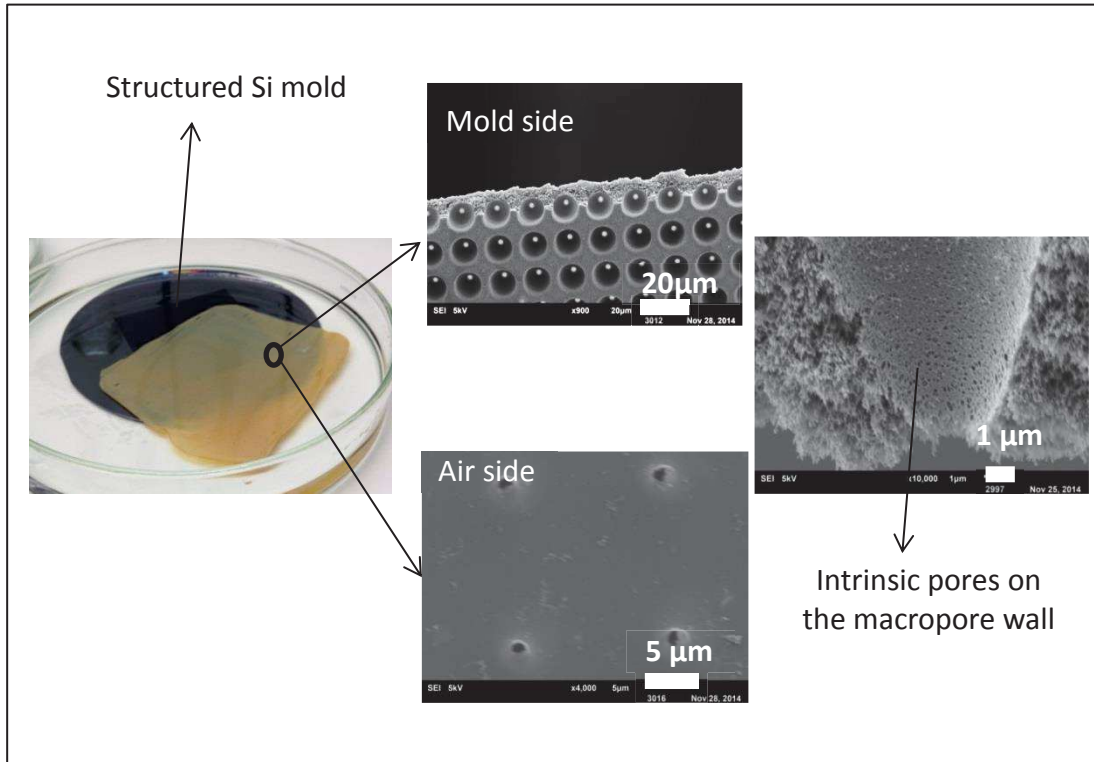


**Figure 4.5.** Pyramidal type pillar structured Si-mold used for the fabrication of HPBI. SEM images of P-5 $\mu$ m type microsieves: mold side, air side and cross-section.

SEM observations (see Figure 4.6) clearly confirm that cast polymer adapts the structure of the structured mold. As published in the literature on LIPS $\mu$ M<sup>17, 19, 23</sup>, two types of shrinkages have to be considered for the polymer film on the mold: in-plane/lateral and thickness/perpendicular shrinkages. Thickness shrinkage occurs at a greater level than lateral shrinkage. It permits film perforation and result in completely open microstructure. On the other hand, lateral shrinkage is responsible for film loosening from the mold, thus facilitating its release. These shrinkages yielded microsieves with perforated macropores of slightly different size than the diameter of the pillars of the mold<sup>20</sup>. Figure 4.5C-F reveal that skin layer thickness decreased with decreasing  $cd$  and the pillars did perforate through the whole film thickness (Figure 4.5C and 5D) at the minimum applied  $cd$ , i.e. 3 and 5  $\mu$ m, respectively. SEM observations of both P-15 $\mu$ m and P-25 $\mu$ m microsieves (Figure 4.5E and F) evidenced perforated macropores with similar dimensions (height  $\sim$ 19  $\mu$ m and periodicity  $\sim$ 15  $\mu$ m) for both samples with a skin layer thickness of  $\sim$ 11 and  $\sim$ 21  $\mu$ m, respectively.

In the same way, HPBI microsieves were prepared using P1 and C molds, dimensions of these membranes are displayed in Table 4.3. The Figure 4.7 presents the morphology of the HPBI fabricated from P1 and C molds.



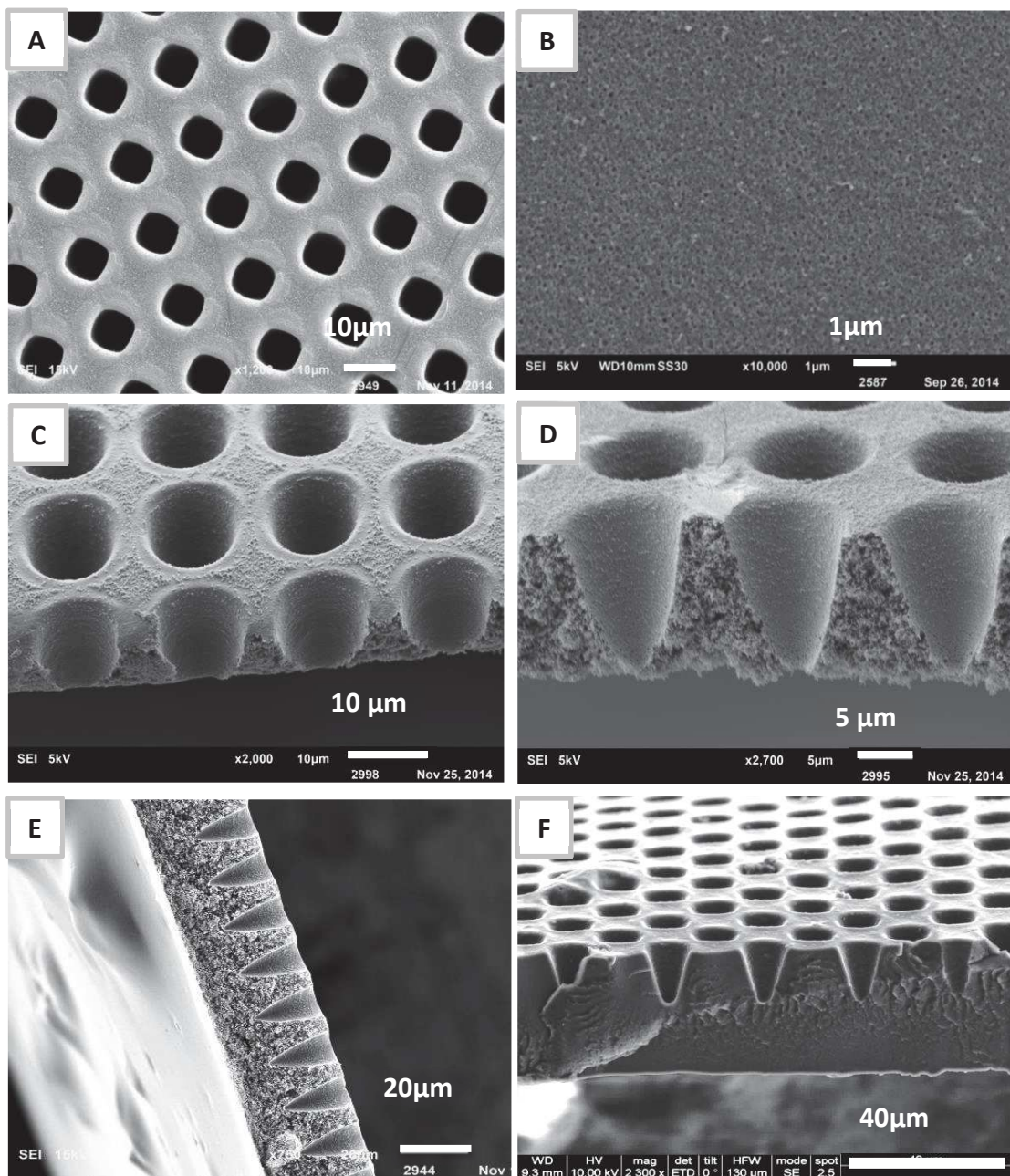


**Figure 4.6.** SEM images of HPBI microsieve with different skin layer thicknesses: A) P-25 $\mu$ m surface mold side; B) P-25 $\mu$ m surface air side; C) P-3 $\mu$ m cross -section; D) P-5 $\mu$ m cross section; E) P-15 $\mu$ m cross-section; F) P-25 $\mu$ m cross-section.

Prepared microsieves required to fulfill some criteria to be counted mechanically stable: easy peeling from mold without deformation of the replicated microstructure, flexibility, thickness and low brittleness during processing<sup>21</sup>. HPBI microsieves from C mold resulted in tearing at the edge of the filed. Since, the aspect ratios enhance in C, the molds turn into more fragile at the regions that undergo higher stress upon release and lower lateral shrinkage, as a result pyramidal pillars are

chosen to cylindrical pillars in order to endure the forces applied during microsieve peeling<sup>21</sup>. HPBI microsieves from P1 mold have not been used further studies for the purpose of this chapter due to handling and brittleness constrains.

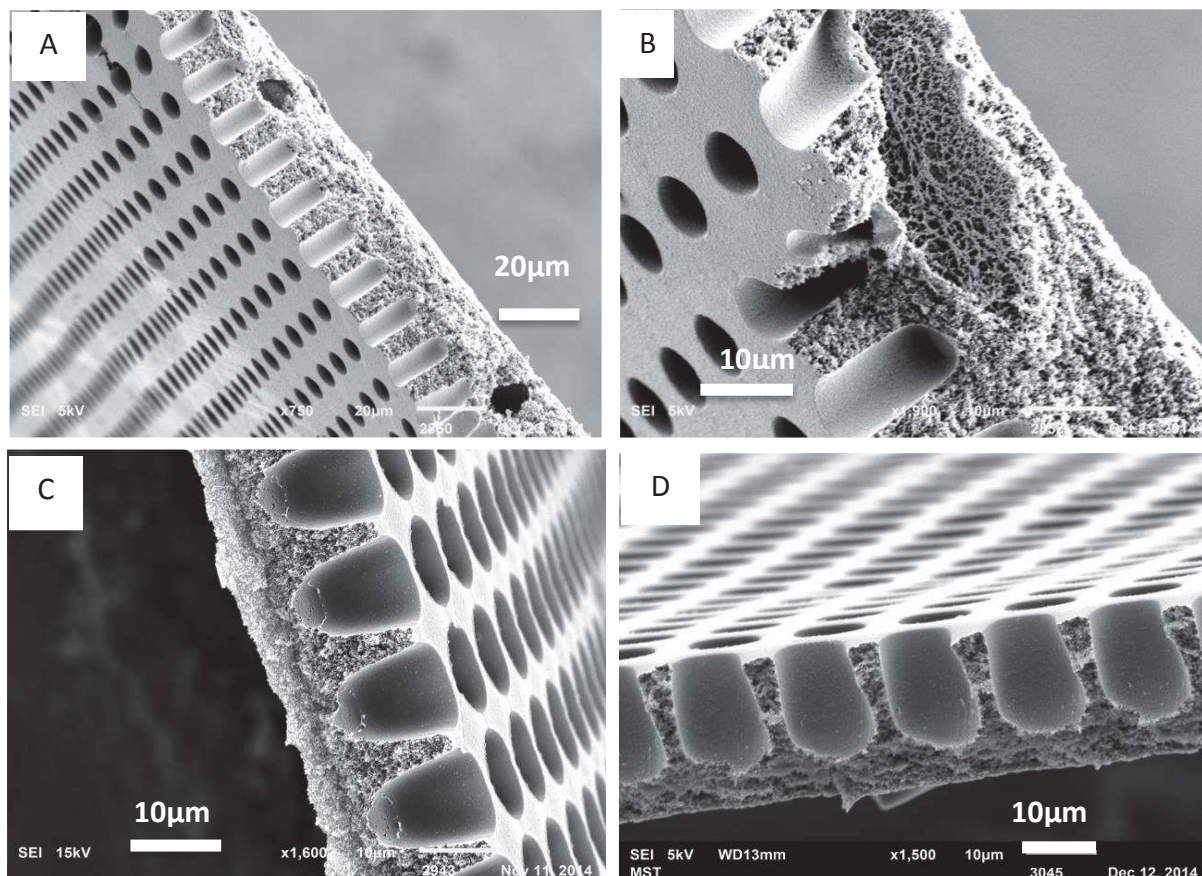


**Figure 4.7.** SEM images of HPBI microsieves obtained from C and P1 molds. : A) C-10µm cross section; B) C-10µm with tearing; C) P1-5µm cross section; D) P1-10µm cross section.

### **3.2 Pore filling –PIL uptake**

Due to its high proton conductivity, low water uptake values and high thermal stability<sup>1</sup>, the monomeric ionic liquid (MIL) 1-H-3-vinylimidazolium bis(trifluoromethanesulfonyl)imide has been selected as a precursor for the preparation of PIL-HPBI composite membranes. The reported contact angle value for PBI films<sup>27</sup> was ( $26^\circ \pm 0.13$ ) which makes the MIL an appropriate wetting liquid for efficient pore filling. The MIL viscosity was 14.3 mPa at 50 °C and 8.6 mPa at 100 °C<sup>27</sup>. Therefore, the infiltration process was conducted at 100 °C for ensuring complete pore filling.

Table 4.4 summarizes the list of prepared PIL-HPBI polymer electrolyte membranes (PEMs) with and without any cross-linker (CL).

**Table 4.4.** Main characteristics of the PEMS prepared for this chapter.

PEM code	Thickness z ( $\mu\text{m}$ )	CL content (mol %)	PIL content (wt %)		
			Theoretical <sup>1</sup>	Exp <sup>2</sup>	TGA
P-25 $\mu\text{m}$ -PA	45.1 $\pm$ 1	-	-	310 <sup>3</sup>	
P-25 $\mu\text{m}$ -0%CL	45.6 $\pm$ 1	0	42.7	63.3	65
P-25 $\mu\text{m}$ -0.2%CL	43.5 $\pm$ 1	0.2	45.0	59.4	65
P-25 $\mu\text{m}$ -0.5%CL	44.1 $\pm$ 1	0.5	45.2	54.6	46
P-25 $\mu\text{m}$ -1%CL	45.1 $\pm$ 1	1.0	47.5	49.5	43
P-15 $\mu\text{m}$ -0%CL	32.5 $\pm$ 1	0	43.8	67.4	-
P-15 $\mu\text{m}$ -0.2%CL	33.1 $\pm$ 1	0.2	43.4	59.6	-
P-15 $\mu\text{m}$ -0.5%CL	34.2 $\pm$ 1	0.5	47.5	49.7	-
P-15 $\mu\text{m}$ -1%CL	34.0 $\pm$ 1	1.0	47.2	46.2	-
PIL/SPBI-1%CL <sup>4</sup>	24.0 $\pm$ 1	1.0	55.4	58.5	59.3
PIL/RPBI-1%CL <sup>5</sup>	120.0 $\pm$ 3	1.0	82.5	86.5	78.6

<sup>1</sup>theoretical value based on PIL density and membrane porosity; <sup>2</sup>experimental value based on gravimetry measurements; <sup>3</sup>PA content in wt.% of PA, equivalent to a 9.5 doping level; <sup>4</sup>Data from <sup>27</sup>; <sup>5</sup>Data from <sup>1</sup>.

The nomenclature adopted for the electrolyte membrane description includes both the HPBI microsieve code and the CL percentage in the MIL solution. Thus, P-25 $\mu\text{m}$ -0%CL and P-15 $\mu\text{m}$ -0%CL membranes were prepared by the introduction of MIL into P-25 $\mu\text{m}$  and P-15 $\mu\text{m}$  microsieves respectively, without any cross-linker. On the other hand, P-25 $\mu\text{m}$ -0.2%CL, P-15 $\mu\text{m}$ -0.2%CL and P-25 $\mu\text{m}$ -0.5%CL, P-15 $\mu\text{m}$ -0.5%CL and P-25 $\mu\text{m}$ -1%CL, P-15 $\mu\text{m}$ -1%CL membranes were based on MIL with 0.2, 0.5 and 1.0 mol % CL respectively. In order to evaluate the influence of PBI pore architecture on PIL uptake and conduction properties, PIL samples supported either on randomly porous PBI (PIL/RPBI-1%CL) supports or on dense PBI microsieve (PIL/SPBI-1%CL) were separately prepared according to our previous works<sup>1, 27</sup>. Finally, in order to assess the electrochemical performance of PIL-PBI PEMs, phosphoric acid (PA) doped P-25 $\mu\text{m}$  membrane (denoted as P-25 $\mu\text{m}$ -PA) was prepared by HPBI immersion in 11 M phosphoric acid solution for 24h at 80 °C, and was also studied. Table 4.4 shows that the PIL uptake depends on the PBI support porosity and architecture in the range from 46 % to 87 %. When considering P-15 $\mu\text{m}$  and P-25 $\mu\text{m}$  microsieves, the experimental PIL content values (based on gravimetry and TGA measurements-if applicable) were always higher than theoretical values with the exception of 1%CL samples. This phenomenon was probably caused by difficulty in wiping the excess of viscous PIL from the membrane surface. It has been confirmed

that the amount of PIL uptake into the HPBI microsieves after the crosslinking procedure is lower than in the absence of any CL. This effect is mainly attributed to the restriction of relatively high viscous MIL+CL mixture which limits its infiltration into the intrinsic porosity of the HPBI supports. In fact, this intrinsic porosity of the support is 4.7-5.2 folds higher than its nominal macroporosity, i.e. 7.4 vol% (Table 4.3).

SEM analysis of PIL-HPBI PEMs is displayed in Figure 4.8. The key factor for PEMs performances relies on both uniform and complete filling of HPBI pores with PIL.

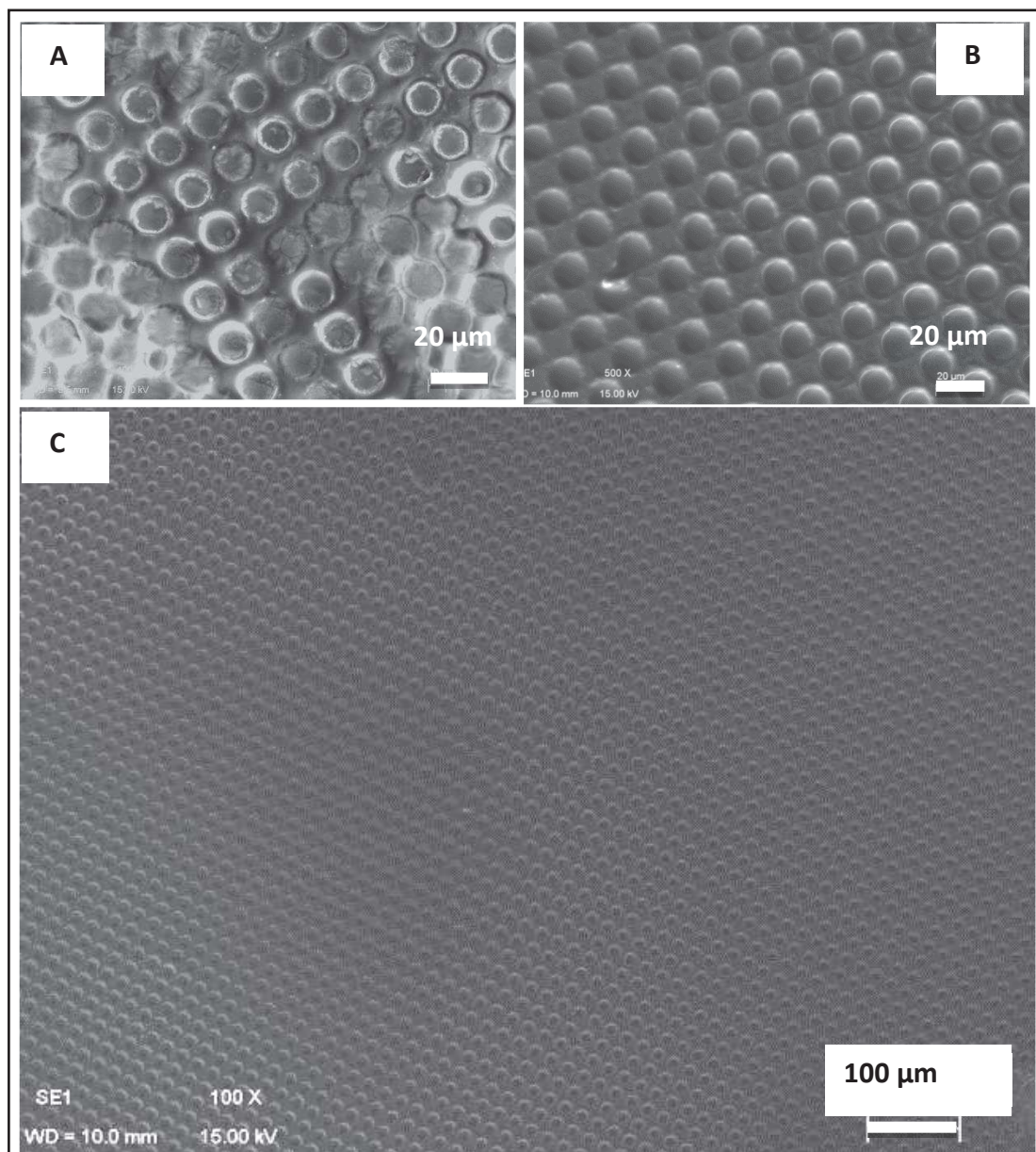


**Figure 4.8.** SEM images of HPBI microsieves after pore filling: A) P-25µm-0%CL; B) P-25µm-1%CL at high magnification (500x); and C) P-25µm-0%CL at low magnification (100x).

The SEM images of PIL-HPBI PEMs prepared with and without any CL are shown in Figures 4.8A and 8B, respectively. In particular, the boundary layer between the PIL and the walls of the perforated porous HPBI microsieve is indistinguishable. Although PIL excess can be noticed on the surface (P-25 $\mu$ m-0%CL, Figure 4.8A), it correlates well with PIL loadings listed in Table 4.4. The entire and uniform filling of HPBI pores with PIL without any detectable cracks or defects is clearly evidenced in Figure 4.8C.

ATR-FTIR spectra have been used to corroborate the successful polymerization of MIL into the support and to explore any possible interactions between the PIL and PBI microsieves. Accordingly, the spectra of pure MIL, PIL, HPBI, and PIL-HPBI have been recorded (Figure 4.9). The presence of vinyl group in the MIL was observed in the region 1665-1630  $\text{cm}^{-1}$  assigned to the stretching vibration of in-plane  $\text{CH}=\text{CH}_2$  bending (Figure 4.9A). The absence of the characteristic peaks of these vinyl monomers in PIL and PIL-HPBI confirms successful polymerization. The degree of MIL conversion to PIL was above 97% upon 2 h of UV light exposure in good agreement with our previous studies<sup>27</sup>. The intense peaks between 1400 and 1000  $\text{cm}^{-1}$  (Figure 4.9A), characteristics of O=S=O and S-N-S vibrational modes in the bis(trifluoromethanesulfonyl)imide [TFSI] anion<sup>27-28</sup>, remain unaltered for both PIL and PIL-HPBI samples. On the contrary, the broad band centred at 1608  $\text{cm}^{-1}$  corresponding to aromatic C=C and C=N stretching modes, and the peak at 1539  $\text{cm}^{-1}$ , resulting from in-plane ring vibrations of substituted benzimidazole (Figure 4.9A), are clearly diminished for the PIL-HPBI composite. The very broad band in the region 3700-2400  $\text{cm}^{-1}$  is attributed to the free N-H stretching and  $\text{N-H}\cdots\text{H}$ , and  $\text{H}_2\text{O}\cdots\text{H}$  hydrogen bonds interactions (see Figure 4.9B). These distinctive features, although notably less intense due to the hydrophobic nature of the PIL, are also observed on the PIL-HPBI spectrum. The peak centered at 3059  $\text{cm}^{-1}$ , assigned to the stretching modes of aromatics CH groups and clearly observed for HPBI sample, is notably suppressed for PIL-HPBI. These observations provide evidence on the interactions between the benzimidazole rings of PBI and the poly-cationic chains.

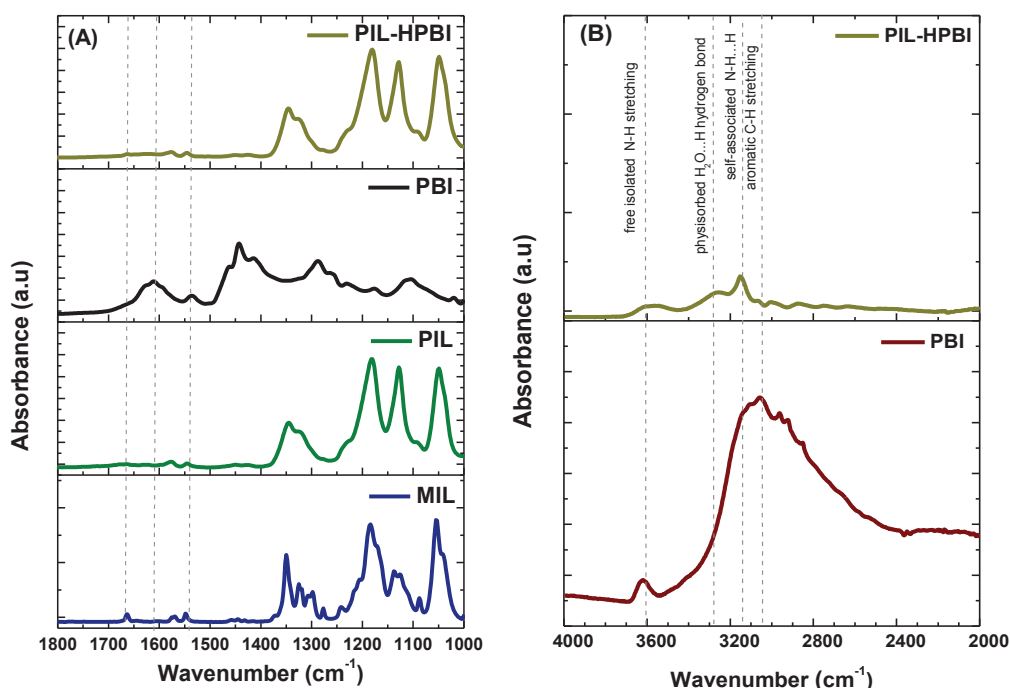


**Figure 4.9.** ATR-FTIR of PIL-HPBI composite membranes versus MIL, PIL and PBI counterparts: (A) 1800- 1000  $\text{cm}^{-1}$  region; (B) 4000 - 2000  $\text{cm}^{-1}$  region.

### **3.3 Thermal and mechanical stability of PIL-HPBI membranes**

An important design criterion for HT PEMs is their thermal stability. Figure 4.10 shows the TGA and DTG thermograms of both pure PIL and composite PIL-HPBI membranes. The first weight loss, registered at temperatures below 200 °C corresponds to both residual water and traces of the photoinitiator<sup>1</sup> (4.5 to 8.9 wt %). The pure PIL decomposition is centred at around 405 °C (weight loss between 315 to 450 °C). On the other hand, the decomposition of PIL inside the porous HPBI matrix takes place within a wider temperature range, i.e. 320 - 540 °C. It can be observed that the onset temperature for decomposition is also shifted to higher values for cross-linked membranes (particularly with 0.5 and 1%CL). In addition, a distinctive shoulder at temperatures above 440 °C, and up to 510 °C is observed for all composite samples, whatever the CL content. This behaviour is attributed to hydrogen bonding interactions between PIL and the confining PBI matrix, already evidenced by FTIR (Figure 4.9). In general, the obtained thermograms are in good agreement with those described in the literature for PEMs containing PBI and IL/PIL<sup>1-2, 29-30</sup>. All the composite PIL-HPBI membranes are stable up to 300 °C, which is far above the operating temperature for HT PEMFCs.

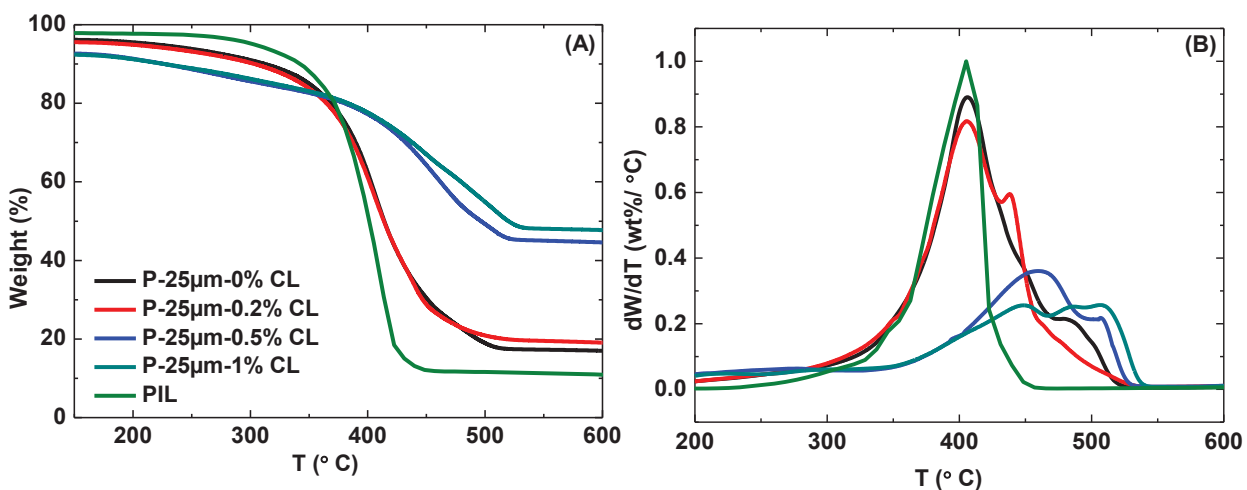


**Figure 4.10.** A) TGA and B) DTG thermograms for PIL based membranes (pure PIL behaviour is also represented for comparison purposes).

The mechanical properties of the composite PIL-HPBI membranes were measured at ambient RH and 25 °C (see Table 4.5). The strain-stress curves (see Figure 4.11), show that all the PIL-SPBI membranes exhibited a glassy nature.

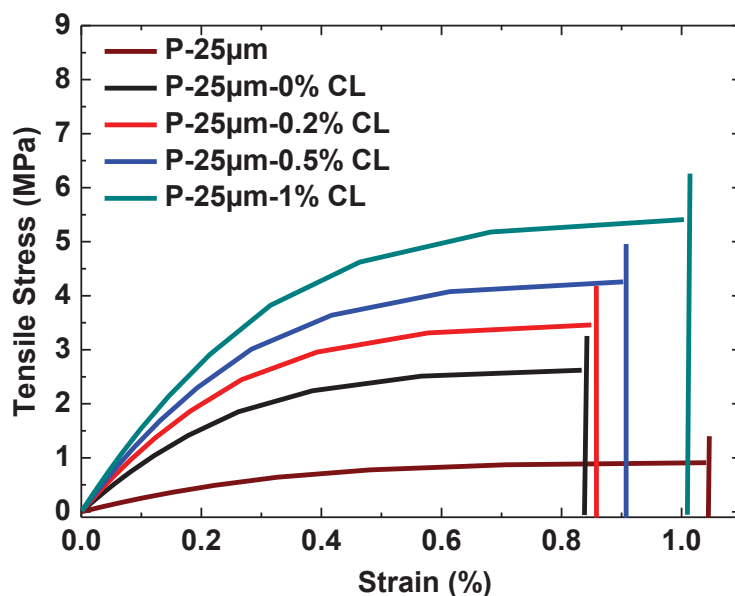


**Figure 4.11.** Stress–strain curve of PIL-HPBI membranes at room conditions.

As essential requirements for practical operation of PEMs rely on their mechanical stability, both high storage modulus and low swelling values are pursued<sup>31</sup>. Our aims is to improve the dimensional stability issues related to PIL- based membranes by using HPBI microsieves as structural supports. The pristine HPBI microsieve, i.e P-25µm sample, appears quite rigid with Young's modulus and

tensile stress about  $0.2 \pm 0.021$  GPa and  $0.9 \pm 0.7$  MPa, respectively. However, both parameters are notably improved upon in situ polymerization of ionic liquid moieties. Thus, the evaluated Young's modulus of P-25 $\mu$ m-0%CL was  $0.9 \pm 0.04$  GPa, which is more than 4 folds higher than the reported values for pure PIL<sup>1, 7</sup>. Furthermore, the mechanical strength of composite PIL-HPBI membranes increased moderately (77% in Young modulus and 112% in tensile stress) when cross-linking the polycationic network.

Among the tested samples, P-25 $\mu$ m-1%CL membrane presented the maximum Young modulus and tensile stress of  $1.6 \pm 0.02$  GPa and  $5.3 \pm 0.5$  MPa, respectively. These values are 8 times higher in Young modulus and more than 4 times higher in tensile stress than those for PIL supported on randomly porous PBI (85% in porosity)<sup>1</sup>, denoted as PIL/RPBI-1%CL. These values are also clearly superior to the characteristic values for acid-doped PBI<sup>30</sup> and Nafion115<sup>32</sup> membranes. Above all, the mechanical behaviour of P-25 $\mu$ m-1%CL sample was clearly outstanding during handling and assembly of the electrochemical cell.

**Table 4.5.** Mechanical properties of the PEMs prepared for this chapter

PEM code	Young Modulus (GPa)	Tensile Stress (MPa)
P-25 $\mu$ m-0%CL	$0.90 \pm 0.04$	$2.5 \pm 0.5$
P-25 $\mu$ m-0.2%CL	$1.20 \pm 0.01$	$3.4 \pm 0.3$
P-25 $\mu$ m-0.5%CL	$1.40 \pm 0.07$	$4.1 \pm 0.8$
P-25 $\mu$ m-1%CL	$1.60 \pm 0.02$	$5.3 \pm 0.5$
PIL/RPBI-1%CL	$0.19 \pm 0.09$	$1.2 \pm 0.03$
PIL <sup>*</sup>	$0.21 \pm 0.03$	-
Dense PBI <sup>**</sup>	0.08	9.4
P-25 $\mu$ m <sup>***</sup>	$0.20 \pm 0.02$	$0.9 \pm 0.7$

<sup>\*</sup> Data from<sup>1</sup>; <sup>\*\*</sup> Data from dense PBI membrane after H<sub>3</sub>PO<sub>4</sub> doping<sup>30</sup>;

<sup>\*\*\*</sup> Pristine HPBI microsieve as reference.

### **3.4 Electrochemical performance of PIL-HPBI electrolytes**

#### **3.4.1 Crosslinking effect**

The proton conductivity measured for all the composite PIL-HPBI membranes as a function of temperature is presented in Figure 4.12A. Measurements performed for the pristine HPBI microsieve under anhydrous conditions confirmed its negligible conductivity, i.e.  $0.73 \text{ mS}\cdot\text{cm}^{-1}$  at 150 °C. As can



be seen, the proton conductivity increases with temperature. This phenomenon is associated with the viscosity reduction of the poly cation (poly[1-(3H-imidazolium)ethylene])<sup>29, 33</sup>.

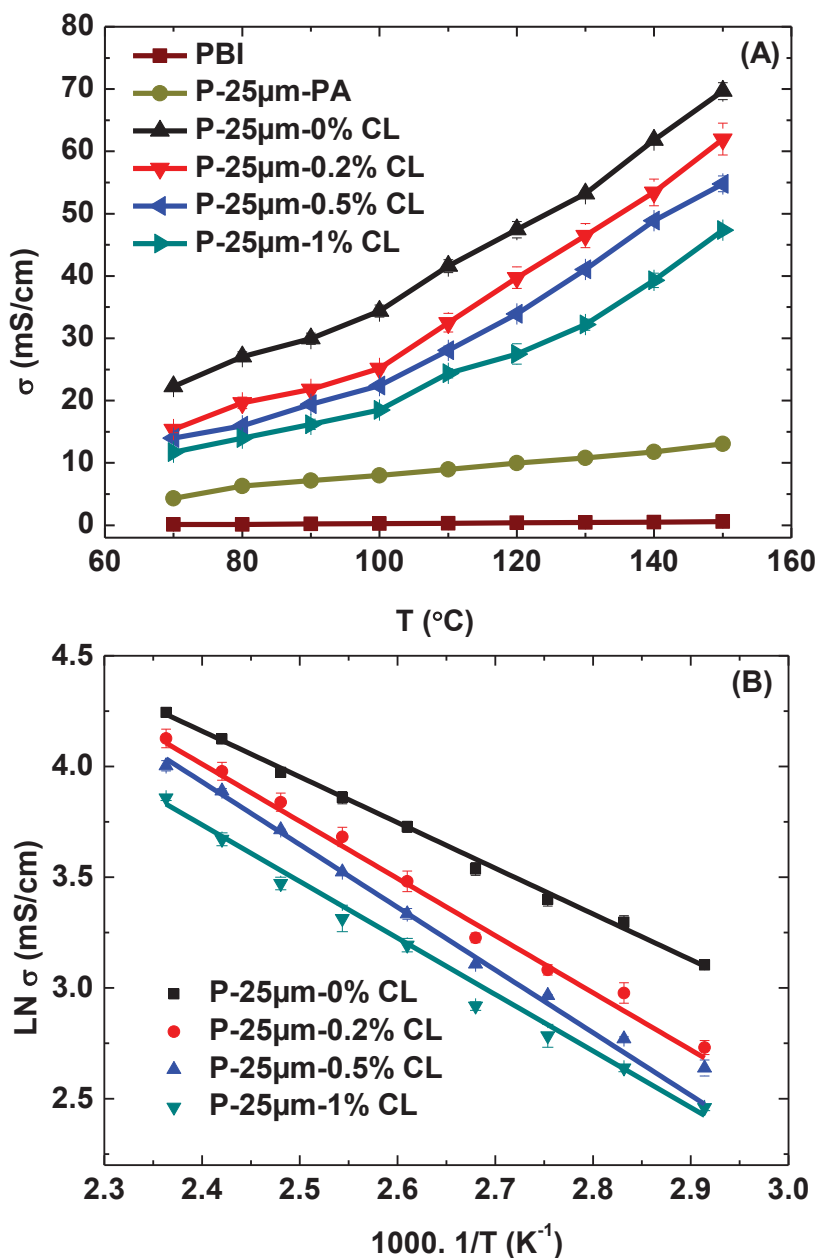


**Figure 4.12.** Conductivity measurements for PIL-HPBI membrane as a function of CL content (HPBI-PA and pure PBI are included for the comparison): A) conduction characteristics; B) Arrhenius type plot.

The proton conductivity of P-25 $\mu$ m-0%CL membranes increases from 22.2 mS·cm<sup>-1</sup> to 69.6 mS·cm<sup>-1</sup> when temperatures increases from 70 to 150 °C, respectively. These values are 5-6 times higher than those registered for phosphoric acid doped HPBI membrane ( $\sigma = 4.3$  mS·cm<sup>-1</sup> to 13.2 mS·cm<sup>-1</sup> in the

same temperature range). In addition, it has been reported that the phosphoric acid doping diminishes the mechanical strength of PBI<sup>34-37</sup>. Hence, prefilling HPBI supports with MIL followed by its *in-situ* polymerization enables the synthesis of proton conducting phosphoric acid-free electrolyte membrane operating at 150 °C under anhydrous conditions. An increased amount of CL generates a significant decrease in the proton conductivity. For the P-25µm-0.2%CL membrane, the maximum proton conductivity at 150 °C was 61.9 mS·cm<sup>-1</sup>; whereas at the same temperature, the P-25µm-0.5%CL and P-25µm-1%CL membranes exhibited proton conductivity values limited at 54.7 mS·cm<sup>-1</sup> and 47.3 mS·cm<sup>-1</sup>, respectively. These results could be explained by the effect of more a pronounced cross-linking resulting in restrict chain mobility and in the corresponding proton-conduction ability of the PEM<sup>1, 38-39</sup>. Moreover, the cross-linker itself, i.e. divinylbenzene, is weak electrochemical in nature.

For the sake of further investigation of the proton conduction properties, activation energy (Ea) for proton transport was evaluated by using Arrhenius type dependence (see Figure 4.12.B and Table 4.6). As expected, due to the loss in long-range segmental motion, Ea slightly increases with the percentage of cross-linker, ranging the values from 17.1 kJ·mol<sup>-1</sup> for P-25µm-0%CL up to 21.8 kJ·mol<sup>-1</sup> for P-25µm-1%CL. The values are also comparable with those reported for ionic liquid and PBI blends<sup>29-30, 40</sup>.

**Table 4.6.** Activation energy values of PIL-HPBI electrolyte membranes as a function of cross-linker content and skin layer thickness.

PEM	Slope (m)	Ea(kJ/mol)	R <sup>2</sup>
P-25µm-0%CL	2062	17.1	0.998
P-25µm-0.2%CL	2556	20.3	0.983
P-25µm-0.5%CL	2595	21.0	0.998
P-25µm-1%CL	2628	21.8	0.999
P-15µm-0%CL	2020	16.8	0.998
P-15µm-1%CL	2477	20.6	0.999

Some replica conductivity measurements were also performed for both heating (from 70 to 150 °C) and cooling (from 150 to 70 °C) cycles in order to clarify whether any water adsorption influenced the conductivity of the PEMs<sup>41</sup>. It has been confirmed (Figure 4.13) that conduction performance shows a thermal reversibility.

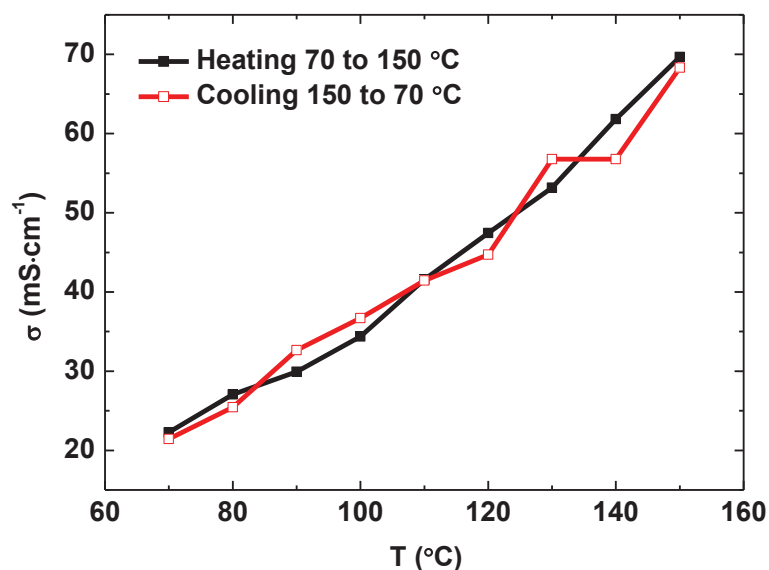


**Figure 4.13.** The replica conductivity measurements for P-25μ-0%CL membrane as a function of temperature

A preliminary assessment on endurance was performed by keeping the PIL-HPBI membranes at 150°C for up to 50 hours (Figure 4.14).

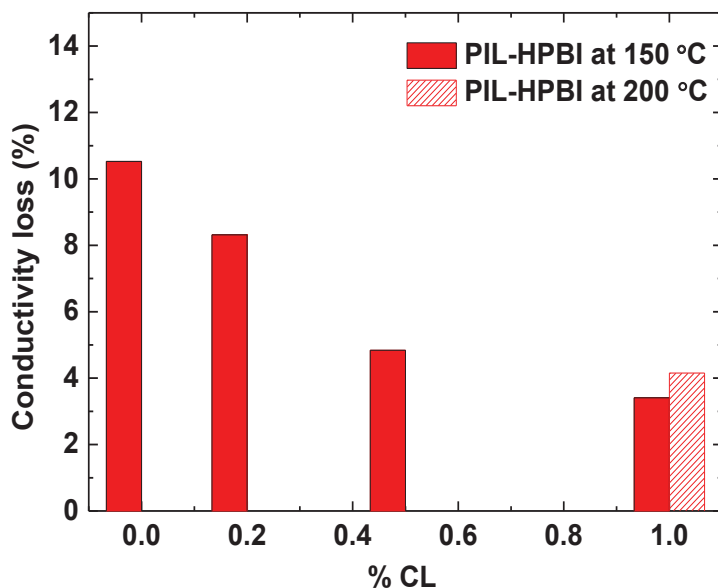


**Figure 4.14.** Proton conductivity decay of PEMs based on P-25μm microsieve after 50 h exposure at 150 °C and 200 °C.

In general, all the composite membranes showed performance decay with time on stream; however the effect was more pronounced over non cross-linked samples. The maximum decline in conductivities, ~10.5%, was registered for P-25μm-0%CL; whereas, for P-25μm-1%CL the decrease

was only 3.4%. Similar tendency was observed at 200°C, i.e. 4.1% decay for P-25µm-1%CL. The authors hypothesized that such conductivity decrease is related to the rearrangement of the pure PIL skin layer at higher temperatures. Nevertheless, the PIL-HPBI membrane surface revealed unaffected after the durability tests as no cracks or defects were detected visually (see Figure 4.15).

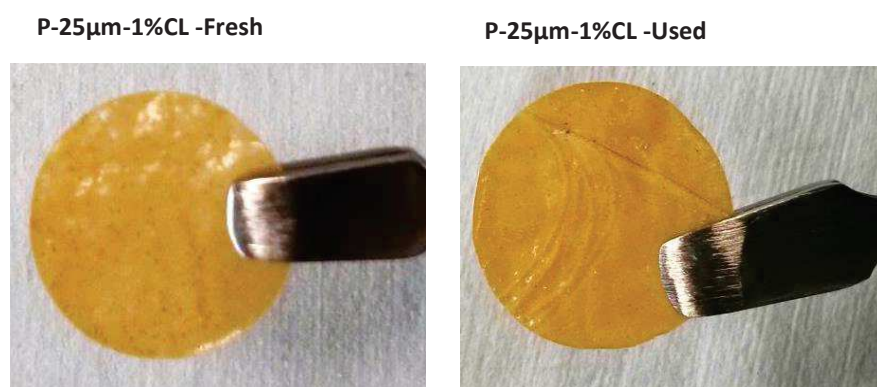


**Figure 4.15.** Appearance of P-25µm-1%CL PEM before and after conductivity tests

### **3.4.2 Influence of skin layer thickness**

For a better insight on the proton transport controlling step through PIL immobilized on asymmetric HPBI microsieves, the proton conductivities of PIL-HPBI obtained from P-15µm microsieves, with 11 µm thick skin layer, were also evaluated (see Figure 4.16). As evidenced, proton conductivity increases with temperature and is also higher for membranes prepared without any CL. The same trend was observed for thicker P-25 µm based membranes.

As shown in Figure 4.16.A, the conductivity values of PIL-HPBI membranes, for a given CL content, decrease when the skin layer thickness increases. At 150 °C, the proton conductivity of the P-15µm-0%CL membrane ( $73.5 \text{ mS}\cdot\text{cm}^{-1}$ ) is about  $4 \text{ mS}\cdot\text{cm}^{-1}$  higher than the value measured for the P-25µm-0%CL membranes with 21 µm thick skin layer. These experimental results could be correlated to the PIL content in the electrolyte membranes: 67.4% for P-15µm-0%CL vs. 63.3% P-25µm-0%CL. However, it is well known that the overall performance of composite electrolytes is strongly affected not only by the content but also by the distribution of the proton conducting phase within the membrane. Thus, for a better understanding, the activation energy for proton transport was also compared (see Figure 4.16.B and Table 4.6). Whatever the skin layer thickness of the HPBI microsieve support, the obtained  $E_a$  values are rather similar. In the case of P-15µm based membranes, the  $E_a$  values are 16.8 and 20.6 kJ/mol for P-15µm-0%CL and P-15µm-1%CL respectively; thus rather similar to those measured for P-25µm derived membranes (17.1kJ/mol for P-25µm-0%CL and 21.8 kJ/mol for P-25µm-1%CL).

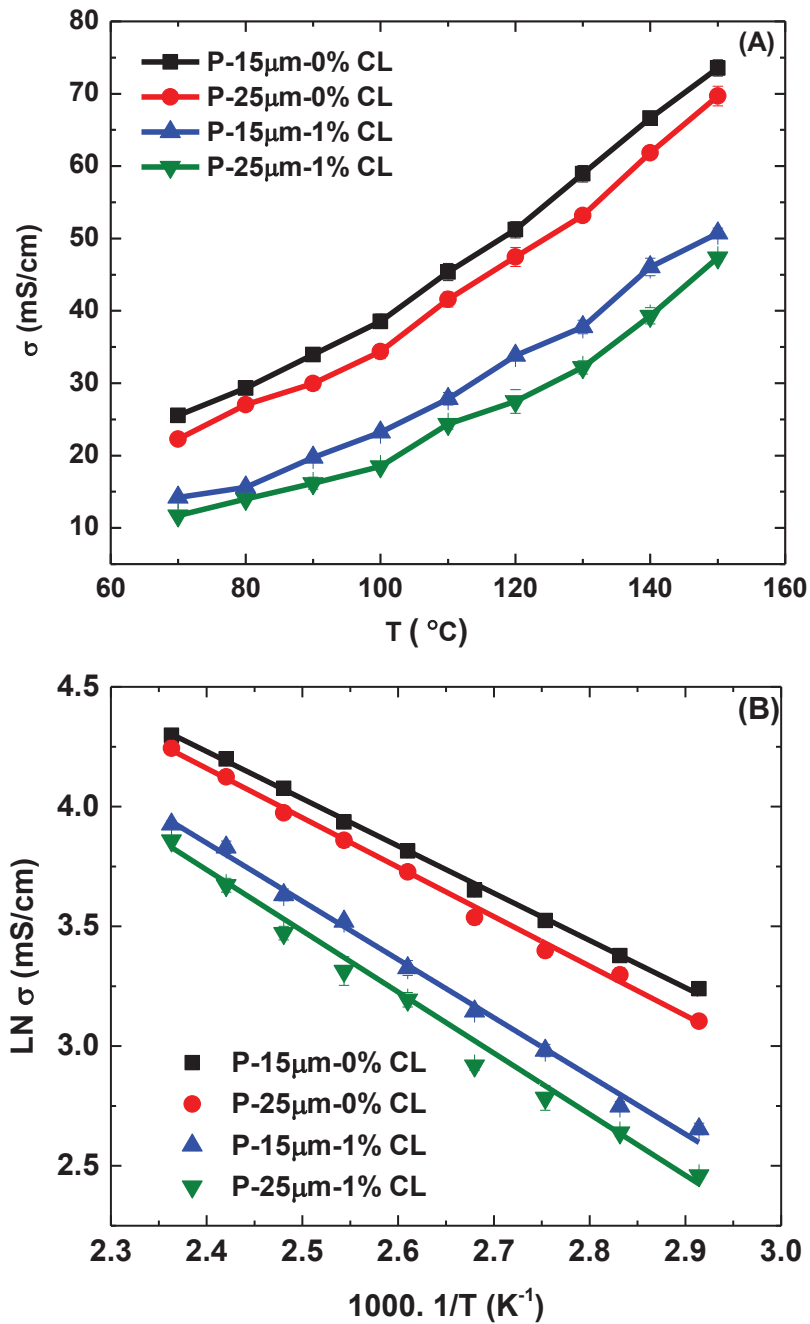


**Figure 4.16.** Effect of skin layer thickness on the proton conduction performance of PIL-HPBI membranes with 0% and 1% CL content: A) conductivity values; B) Arrhenius type plot

Based on the above  $E_a$  analysis and considering the membranes asymmetry (see Figure 4.5 and Figure 4.6), the hypothesis that the transport of protons through the skin layer is the controlling step seems plausible. This assumption is also supported by the identical intrinsic porosity of all the HPBI microsieves listed in Table 4.3 (see SEM cross-section views in Figures 4.6.D and 6.E). Thus, the PEM membranes derived from P-25 $\mu\text{m}$  microsieves, with 21  $\mu\text{m}$  thick skin layer, lead to slightly lower

conductivity values at the expense of improved mechanical properties. According to the above results, the optimal PIL-HPBI formulation as trade-off between proton transport and mechanical resistance corresponds to P-25 $\mu\text{m}$ -1%CL.

### **3.5 Effect of the membrane architecture: comparison between randomly and straight porous PBI supports**

Different approaches have been attempted by our group<sup>7, 27</sup> to fabricate PIL-based electrolyte membranes, able to transport H<sup>+</sup> ions under anhydrous conditions and in absence of mineral acids without sacrificing the mechanical behaviour. Our rationale is mainly focused on the selection of the PBI container with adequate pore architecture to improve both the proton transport and the dimensional stability at elevated temperatures. In this chapter, the influence of PBI architecture on proton conductivity has been comprehensively examined for the poly[1-(3H-imidazolium)ethylene]bis(trifluoromethanesulfonyl)imide based electrolytes with 1% CL content. The Nyquist plots of all the samples exhibited a compressed arc in the high-frequency region and an inclined straight line indicating that an ion diffusion process at the electrode–electrolyte interface plays an important role (see Figure 4.17).

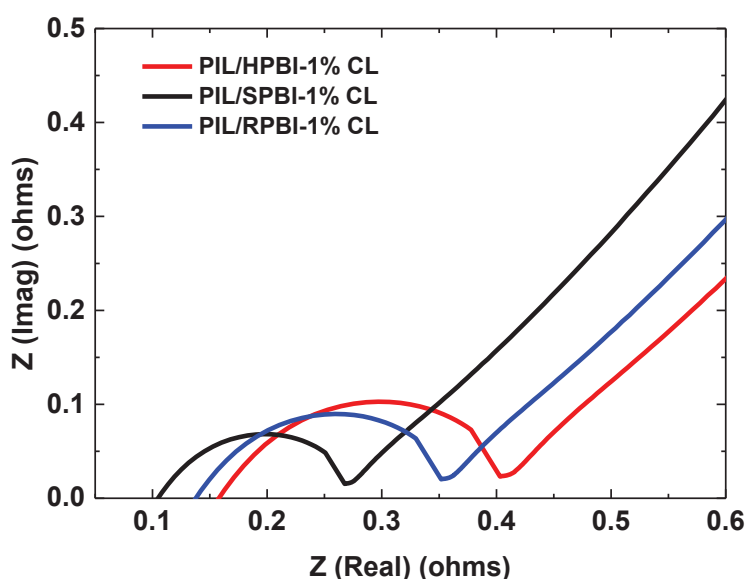


**Figure 4.17.** Nyquist plot of PIL-SPBI (based on dense PBI microsieve 36% in porosity), PIL-HPBI (based on P-25 $\mu\text{m}$  microsieve), and PIL-RPBI (based on randomly porous PBI support 68% in porosity, sponge-like structure, pore size diameters within the range of 50-300 nm on the air side and 35-50 nm on the glass side)

The conduction properties as a function of temperature in the range 70 to 200 °C, are shown in Figure 4.18.A for three different PBI supports under anhydrous conditions. These supports are the followings: the hierarchical P-25 $\mu$ m microsieve (HPBI) studied in this chapter, a dense PBI microsieve<sup>27</sup> (SPBI) having straight pores connecting both sides (17  $\mu$ m in diameter, 24  $\mu$ m thick and 36% porosity) presented in detail in chapter 3, and a randomly porous PBI support (RPBI) having pores in the sub-micrometric range (120  $\mu$ m thick and 68% in porosity). The derived electrolyte membranes are denoted as PIL/HPBI-1%CL, PIL/SPBI-1%CL and PIL/RPBI-1%CL respectively.

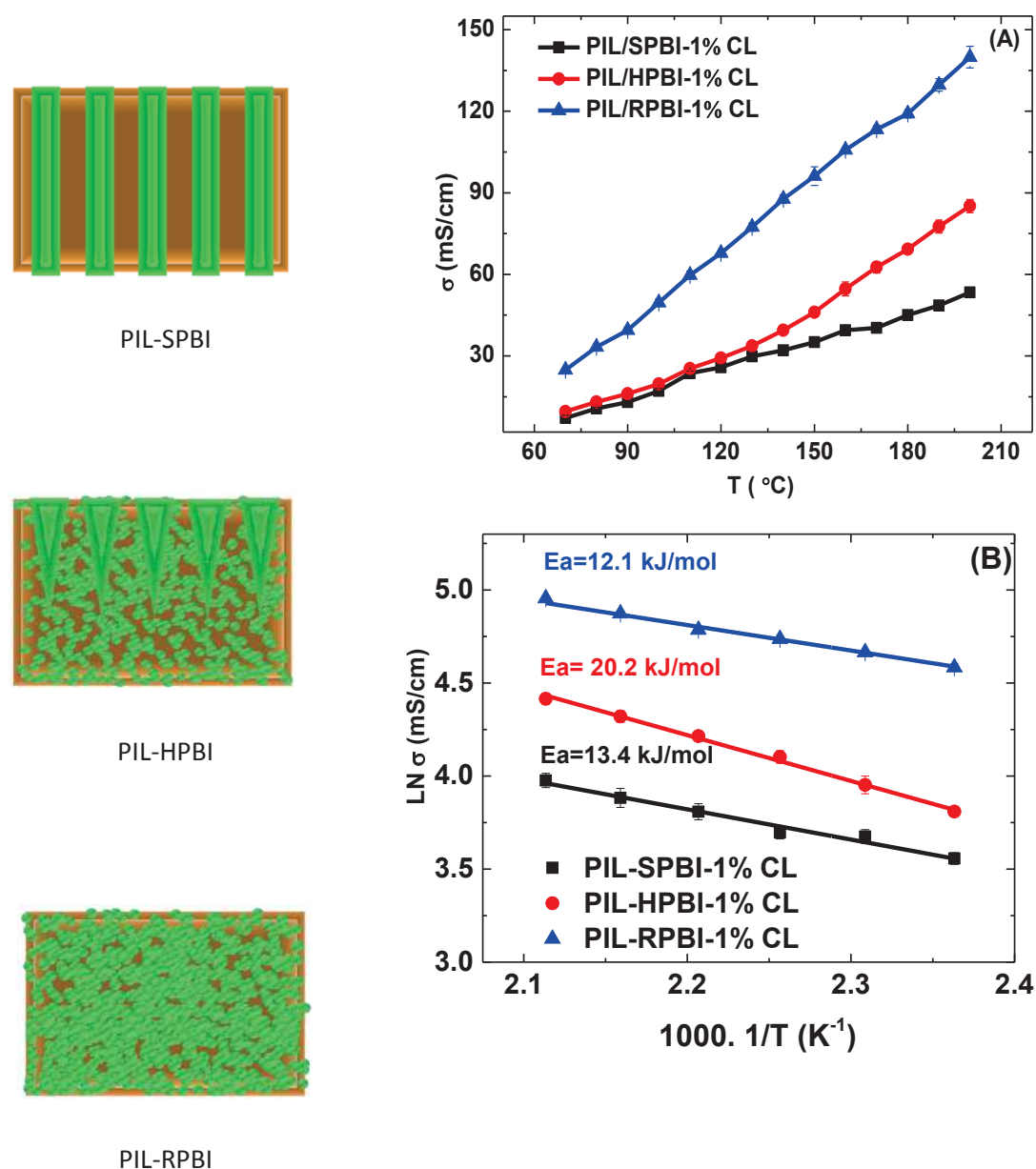


**Figure 4.18.** Evolution with temperature of the conduction performance of membranes PIL/PBI based membranes prepared with 1% cross-linker. Influence of the microsieve support architecture.

Among the tested samples, the PIL/RPBI-1%CL electrolyte membrane is the most attractive with a conductivity value as high as  $140 \text{ mS}\cdot\text{cm}^{-1}$ . This outperforming behaviour is not only attributed to the high pore volume of the support, providing PIL uptake values up to 86.5 wt % but also to the relevant connectivity of its channels formed during the phase inversion process. Unfortunately this architecture does not provide enough mechanical strength for practical operation.

On the other hand, the conductivity values for PIL/HPBI-1%CL (early referred as P-25 $\mu\text{m}$ -1%CL) increased from 47 to  $85 \text{ mS}\cdot\text{cm}^{-1}$  as the temperature increased from 150 to 200 °C. Compared to perforated dense microsieves, i.e. PIL/SPBI-1%CL with  $53 \text{ mS}\cdot\text{cm}^{-1}$  at 200 °C, the proton transport is faster for hierarchical microsieves in spite of lower PIL amount. This result is attributed both to the higher surface area provided by hierarchical microsieves and to the porous network connectivity at the macropore/intrinsic bulk porosity interface (see Figure 4.19).

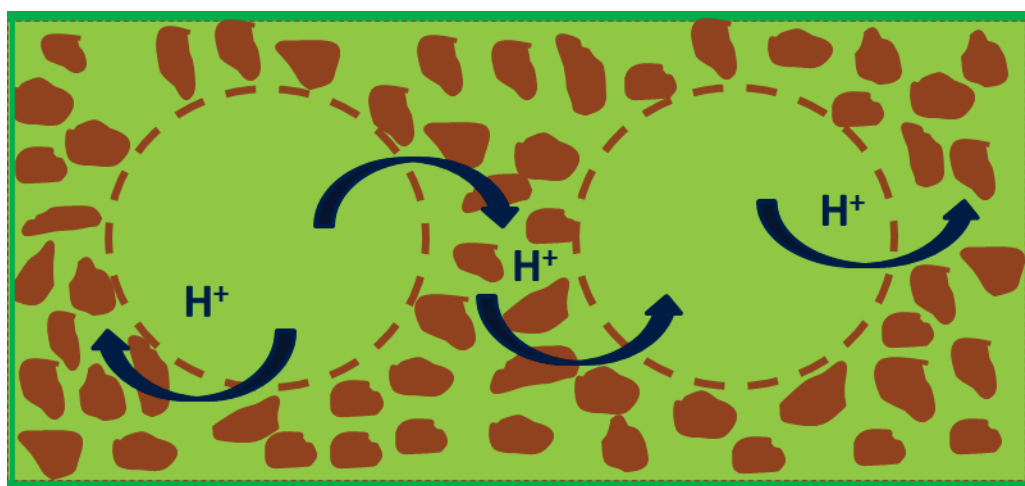


**Figure 4.19.** Postulated proton transport mechanism on PIL-HPBI membranes

Although, the HPBI- architecture leads to intermediate performance in terms of proton conduction performance; but its mechanical properties are greatly superior than those of the other tested architectures. Overall, such PIL-HPBI electrolyte membranes retain the advantageous features of both as higher and well-connected PIL loadings are achievable without sacrificing the mechanical strength.

The detailed analysis of the apparent Arrhenius-type activation energies for the three different PBI supports is presented in Figure 4.18.B. The  $E_a$  for proton transport via PIL moieties embedded in HPBI support is the highest 20.2 kJ/mol, followed by SPBI and RPBI matrix with 13.4 kJ/mol and 12.1 kJ/mol respectively. This finding corroborates our hypothesis suggesting that proton transport through the intrinsic porosity of the skin layer is the rate controlling step for conduction (see section 3.4.2).



In order to get a further insight on pore morphology, the surface topology of HPBI supports was examined. AFM 2D topography of both HPBI and RPBI (used as reference) supports are compared in Figure 4.20 (see also Figure 4.21 for 3D AFM surface images ).

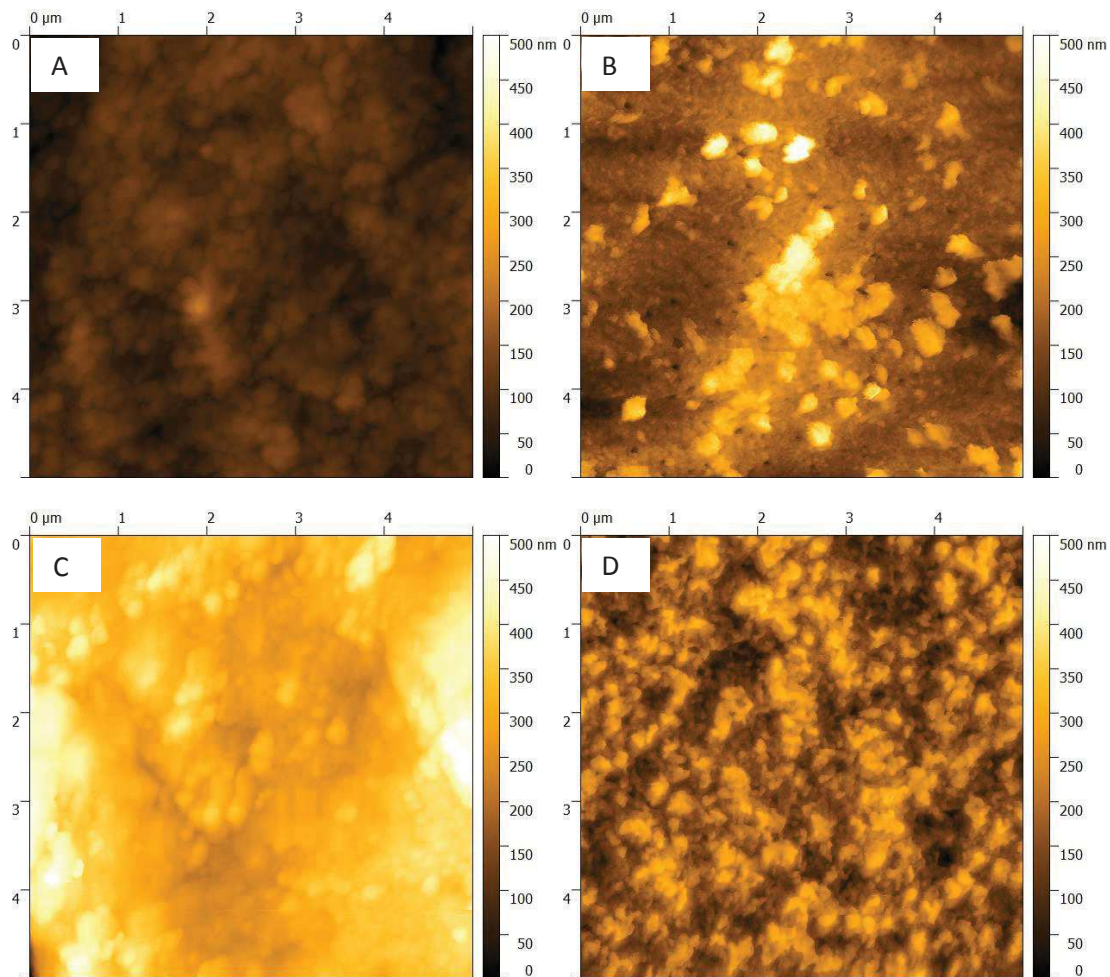


**Figure 4.20.** 2 D AFM surface images from pristine PBI supports: A) HPBI air side; B) HPBI mold side; C) RPBI air side; D) RPBI glass side

The evaluated roughness values, in the range of a few tens of nanometers, are summarized in Table 4.7. From these results, it can be concluded that HPBI and RPBI supports exhibit similar surface topology on their both sides.

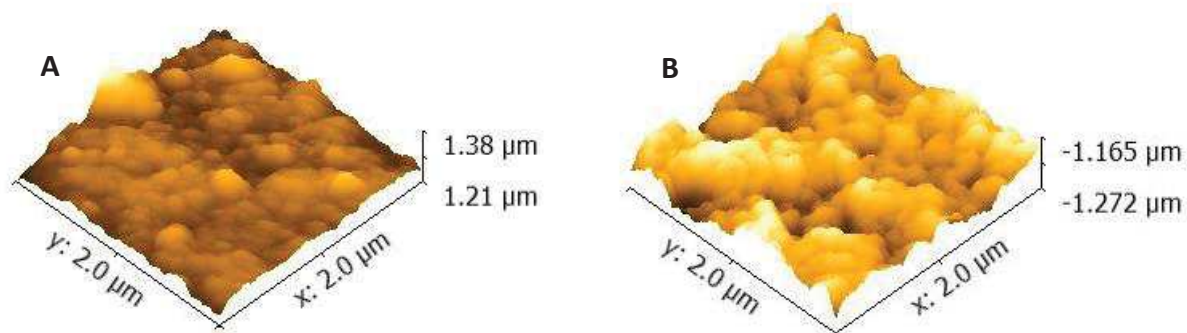


**Figure 4.21.** 3D AFM surface images of HPBI-air side (A) and RPBI air side (B).

**Table 4.7.** Surface topology characteristics of HPBI and RPBI supports measured by AFM.

Microsieve support	Average roughness (Ra) (nm)	Square mean roughness (RMS) (nm)
HPBI-Top (Air side)	20.3	25.7
HPBI-Bottom (Mold side)	50.5	67.4
RPBI-Top (Air side)	45.3	55.6
RPBI-Bottom (Glass side)	45.8	56.5

The microstructure of HPBI and RPBI supports were also analysed by TEM for a proper assessment on their pore connectivity through the membrane. The resulting images of the cross-section structure are shown in Figure 4.22 and Figure 4.23 respectively. As observed, liquid induced phase separation created small pores both at the air side and mold side surfaces, the sizes of these pores are within the roughness values estimated by AFM, i.e. below 50 nm.

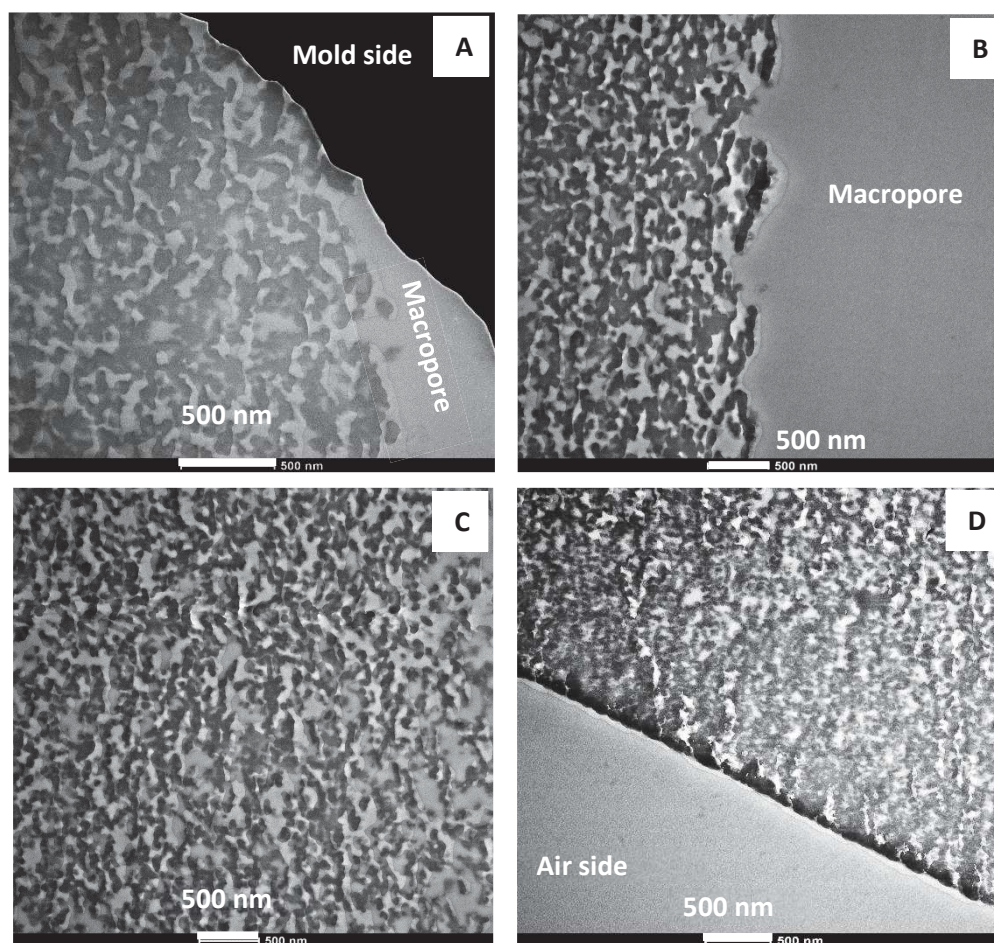


**Figure 4.22.** TEM images of the cross -section of HPBI support: (A) mold-side (bottom), (B) macropore interface between ordered channels wall and intrinsic porosity, (C) intrinsic porosity of the skin layer, (D) air side (top).

TEM observations reveal that the intrinsic pores of both HPBI and RPBI polymeric matrix are completely different in size and morphology, supporting the measured  $E_a$  values previously discussed (see Figure 4.18.B). A highly porous structure with closed-cell intrinsic pores with sizes between  $0.2\ \mu\text{m}$  and  $2.0\ \mu\text{m}$  (preferentially located near the air side, see Figure 4.23. C-D) is formed during phase inversion of RPBI<sup>7</sup>. The conduction pattern on PIL channels for RPBI/PIL-1%CL is almost unaffected by the substrate wall–PIL interactions. In fact, the registered  $E_a$  value resembles those previously reported for unsupported PIL-1%CL, i.e.  $12.3\ \text{kJ/mol}$ <sup>27</sup>.

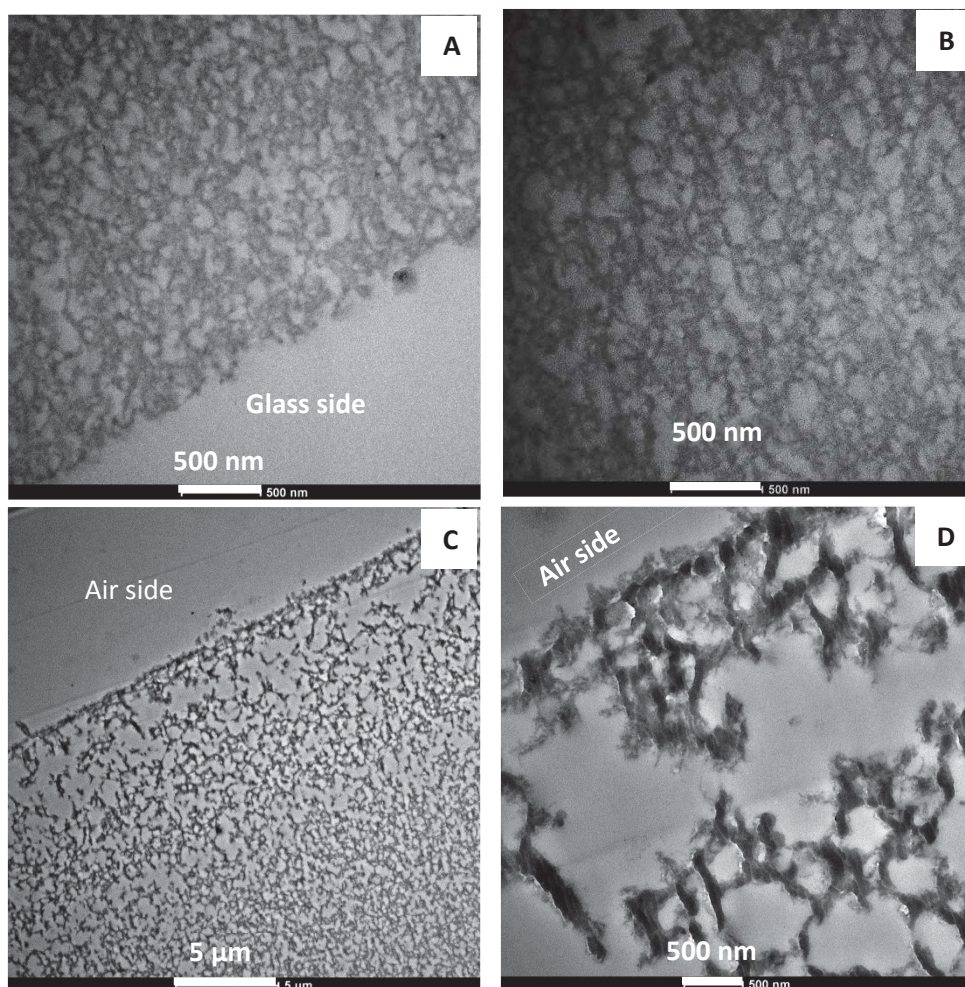


**Figure 4.23.** TEM images of the cross- section of RPBI support: (A) glass side (bottom), (B) Middle part, (C) air side (top), (D) air side at higher magnification.

Particularly remarkable is the porous structure of the macropore wall surface in the HPBI support (see Figure 4.22. A-B). Over this area, well-connected pores at the macropore/intrinsic porosity interface are clearly distinguished. In addition, worm-shape pores below  $0.2 \mu\text{m}$  in size are predominant along the whole thickness (see Figure 4.22. A-D). Unlike previously, the interactions of PIL molecules with the walls of the confining intrinsic PBI pores are not negligible. These pore-wall-fluid interactions anticipated by FTIR analyses (see section 3.2) slow down the proton transport dynamics and subsequently provokes an increase of  $E_a$ .

#### 4. Conclusions

Liquid induced phase separation micromolding (LIPS $\mu$ M) has been successfully used for manufacturing hierarchical porous polybenzimidazole (HPBI) microsieves (42-46% porosity, 30-40  $\mu$ m thick) with specific pore architecture (perforated macropores  $\sim$  9  $\mu$ m in size dispersed in nanoporous matrix with 50-100 nm as pore size). From those, proton exchange membranes were fabricated by infiltration of 1-H-3-Vinyl imidazolium bis(trifluoromethanesulfonyl)imide liquid and divinylbenzene (as cross-linker) followed by *in-situ* UV polymerization. The influence of the porous support architecture on proton transport performance and mechanical strength has been specifically investigated by means of comparison with straight macro-porous (36% porosity) and randomly nano-porous (68% porosity) PBI counterparts. The most outstanding results are shown by poly[1-(3H-imidazolium)ethylene]bis(trifluoromethanesulfonyl)imide polymeric ionic liquid (PIL) cross-linked with 1 % divinylbenzene supported on HPBI membranes with 21  $\mu$ m thick skin layer, achieving conductivity values of 85 mS $\cdot$ cm $^{-1}$  at 200 °C under anhydrous conditions and in the absence of mineral acids. These low-cost membranes are outperforming PEMs for prolonged operation at temperatures up to 200 °C. This chapter presents a feasible strategy to construct hierarchical PIL channels into a PBI matrix. These promising results pave the way for the future development of high temperature flexible electrolytes for electrochemical devices.

#### 5. References

1. Lemus, J.; Eguizábal, A.; Pina, M. P., Endurance strategies for the preparation of high temperature polymer electrolyte membranes by UV polymerization of 1-H-3-vinylimidazolium bis(trifluoromethanesulfonyl)imide for fuel cell applications. *International Journal of Hydrogen Energy* **2016**, *41* (6), 3981-3993.
2. van de Ven, E.; Chairuna, A.; Merle, G.; Benito, S. P.; Borneman, Z.; Nijmeijer, K., Ionic liquid doped polybenzimidazole membranes for high temperature Proton Exchange Membrane fuel cell applications. *Journal of Power Sources* **2013**, *222*, 202-209.
3. Jheng, L.-C.; Hsu, S. L.-C.; Tsai, T.-Y.; Chang, W. J.-Y., A novel asymmetric polybenzimidazole membrane for high temperature proton exchange membrane fuel cells. *Journal of Materials Chemistry A* **2014**, *2* (12), 4225.
4. Hopkinson, D.; Zeh, M.; Luebke, D., The bubble point of supported ionic liquid membranes using flat sheet supports. *Journal of Membrane Science* **2014**, *468*, 155-162.
5. Li, M.; Yang, L.; Fang, S.; Dong, S., Novel polymeric ionic liquid membranes as solid polymer electrolytes with high ionic conductivity at moderate temperature. *Journal of Membrane Science* **2011**, *366* (1-2), 245-250.
6. Mecerreyes, D., Polymeric ionic liquids: Broadening the properties and applications of polyelectrolytes. *Progress in Polymer Science* **2011**, *36* (12), 1629-1648.

7. Lemus, J.; Eguizábal, A.; Pina, M. P., UV polymerization of room temperature ionic liquids for high temperature PEMs: Study of ionic moieties and crosslinking effects. *International Journal of Hydrogen Energy* **2015**, *40* (15), 5416-5424.
8. Díaz, M.; Ortiz, A.; Vilas, M.; Tojo, E.; Ortiz, I., Performance of PEMFC with new polyvinyl-ionic liquids based membranes as electrolytes. *International Journal of Hydrogen Energy* **2014**, *39* (8), 3970-3977.
9. Iojoiu, C.; Martinez, M.; Hanna, M.; Molmeret, Y.; Cointeaux, L.; Leprêtre, J.-C.; Kissi, N. E.; Guindet, J.; Judeinstein, P.; Sanchez, J.-Y., PILs-based Nafion membranes: a route to high-temperature PEMFCs dedicated to electric and hybrid vehicles. *Polymers for Advanced Technologies* **2008**, *19* (10), 1406-1414.
10. Pont, A.-L.; Marcilla, R.; De Meazza, I.; Grande, H.; Mecerreyes, D., Pyrrolidinium-based polymeric ionic liquids as mechanically and electrochemically stable polymer electrolytes. *Journal of Power Sources* **2009**, *188* (2), 558-563.
11. Liang, B.; Jiang, Q.; Tang, S.; Li, S.; Chen, X., Porous polymer electrolytes with high ionic conductivity and good mechanical property for rechargeable batteries. *Journal of Power Sources* **2016**, *307*, 320-328.
12. Eguizábal, A.; Lemus, J.; Urbiztondo, M.; Garrido, O.; Soler, J.; Blazquez, J. A.; Pina, M. P., Novel hybrid membranes based on polybenzimidazole and ETS-10 titanosilicate type material for high temperature proton exchange membrane fuel cells: A comprehensive study on dense and porous systems. *Journal of Power Sources* **2011**, *196* (21), 8994-9007.
13. Kuiper, S.; van Rijn, C. J. M.; Nijdam, W.; Elwenspoek, M. C., Development and applications of very high flux microfiltration membranes. *Journal of Membrane Science* **1998**, *150* (1), 1-8.
14. Gielens, F. C.; Tong, H. D.; van Rijn, C. J. M.; Vorstman, M. A. G.; Keurentjes, J. T. F., Microsystem technology for high-flux hydrogen separation membranes. *Journal of Membrane Science* **2004**, *243* (1-2), 203-213.
15. H. D. Tong, F. C. G., J. G. E. Gardeniers, H. V. Jansen, C. J. M. van Rijn,; M. C. Elwenspoek, a. W. N., Microfabricated Palladium-Silver Alloy Membranes and Their. **2004**, *43* (15), 4182-4187.
16. Kniazeva, T.; Hsiao, J. C.; Charest, J. L.; Borenstein, J. T., A microfluidic respiratory assist device with high gas permeance for artificial lung applications. *Biomed Microdevices* **2011**, *13* (2), 315-23.
17. Bikel, M.; Çulfaz, P. Z.; Bolhuis-Versteeg, L. A. M.; Pérez, J. G.; Lammertink, R. G. H.; Wessling, M., Polymeric microsieves via phase separation microfabrication: Process and design optimization. *Journal of Membrane Science* **2010**, *347* (1-2), 93-100.
18. Carstensen, F.; Kasperidus, T.; Wessling, M., Overcoming the drawbacks of microsieves with micromeshes for in situ product recovery. *Journal of Membrane Science* **2013**, *436*, 16-27.
19. Vogelaar, L.; Lammertink, R. G.; Barsema, J. N.; Nijdam, W.; Bolhuis-Versteeg, L. A.; van Rijn, C. J.; Wessling, M., Phase separation micromolding: a new generic approach for microstructuring various materials. *Small* **2005**, *1* (6), 645-55.
20. Yan, F.; Ding, A.; Girones, M.; Lammertink, R. G.; Wessling, M.; Borger, L.; Vilsmeier, K.; Goedel, W. A., Hierarchically structured assembly of polymer microsieves, made by a combination of phase separation micromolding and float-casting. *Adv Mater* **2012**, *24* (12), 1551-7.
21. Gironès, M.; Akbarsyah, I. J.; Nijdam, W.; van Rijn, C. J. M.; Jansen, H. V.; Lammertink, R. G. H.; Wessling, M., Polymeric microsieves produced by phase separation micromolding. *Journal of Membrane Science* **2006**, *283* (1-2), 411-424.
22. Vogelaar, L.; Barsema, J. N.; van Rijn, C. J. M.; Nijdam, W.; Wessling, M., Phase Separation Micromolding—PS $\mu$ M. *Advanced Materials* **2003**, *15* (16), 1385-1389.
23. Vriezেকolk, E. J.; Kemperman, A. J. B.; Gironès, M.; de Vos, W. M.; Nijmeijer, K., A solvent-shrinkage method for producing polymeric microsieves with sub-micron size pores. *Journal of Membrane Science* **2013**, *446*, 10-18.
24. Wu, C.-G.; Lu, M.-I.; Chuang, H.-J., PVdF-HFP/P123 hybrid with mesopores: a new matrix for high-conducting, low-leakage porous polymer electrolyte. *Polymer* **2005**, *46* (16), 5929-5938.

25. Eguizábal, A.; J.Lemus; Roda, V.; Urbiztondo, M.; Barreras, F.; Pina, M. P., Nanostructured electrolyte membranes based on zeotypes, protic ionic liquids and porous PBI membranes: Preparation, characterization and MEA testing. *International Journal of Hydrogen Energy* **2012**, *37* (8), 7221-7234.
26. Eguizábal, A.; Lemus, J.; Pina, M. P., On the incorporation of protic ionic liquids imbibed in large pore zeolites to polybenzimidazole membranes for high temperature proton exchange membrane fuel cells. *Journal of Power Sources* **2013**, *222*, 483-492.
27. Kallem, P. E., A.; Mallada, R.; and Pina, M. P, Constructing straight Poly-ionic liquid microchannels for fast anhydrous proton transport straight *ACS applied materials & interfaces* **2016**, *8* (51), 35377-89.
28. Howlett, P. C.; Brack, N.; Hollenkamp, A. F.; Forsyth, M.; MacFarlane, D. R., Characterization of the Lithium Surface in N-Methyl-N-alkylpyrrolidinium Bis(trifluoromethanesulfonyl)amide Room-Temperature Ionic Liquid Electrolytes. *Journal of The Electrochemical Society* **2006**, *153* (3), A595.
29. Wang, J. T.-W.; Hsu, S. L.-C., Enhanced high-temperature polymer electrolyte membrane for fuel cells based on polybenzimidazole and ionic liquids. *Electrochimica Acta* **2011**, *56* (7), 2842-2846.
30. Rewar, A. S.; Chaudhari, H. D.; Illathalappil, R.; Sreekumar, K.; Kharul, U. K., New approach of blending polymeric ionic liquid with polybenzimidazole (PBI) for enhancing physical and electrochemical properties. *Journal of Materials Chemistry A* **2014**, *2* (35), 14449-14458.
31. Bauer, F.; Denneler, S.; Willert-Porada, M., Influence of temperature and humidity on the mechanical properties of Nafion® 117 polymer electrolyte membrane. *Journal of Polymer Science Part B: Polymer Physics* **2005**, *43* (7), 786-795.
32. Rodgers, M. P.; Berring, J.; Holdcroft, S.; Shi, Z., The effect of spatial confinement of Nafion® in porous membranes on macroscopic properties of the membrane. *Journal of Membrane Science* **2008**, *321* (1), 100-113.
33. Fang, J.; Lyu, M.; Wang, X.; Wu, Y.; Zhao, J., Synthesis and performance of novel anion exchange membranes based on imidazolium ionic liquids for alkaline fuel cell applications. *Journal of Power Sources* **2015**, *284*, 517-523.
34. Li, Q.; He, R.; Jensen, J. O.; Bjerrum, N. J., PBI-Based Polymer Membranes for High Temperature Fuel Cells – Preparation, Characterization and Fuel Cell Demonstration. *Fuel Cells* **2004**, *4* (3), 147-159.
35. Li, Q.; He, R.; Berg, R. W.; Hjuler, H. A.; Bjerrum, N. J., Water uptake and acid doping of polybenzimidazoles as electrolyte membranes for fuel cells. *Solid State Ionics* **2004**, *168* (1-2), 177-185.
36. Ma, Y. L.; Wainright, J. S.; Litt, M. H.; Savinell, R. F., Conductivity of PBI Membranes for High-Temperature Polymer Electrolyte Fuel Cells. *Journal of The Electrochemical Society* **2004**, *151* (1), A8.
37. Lobato, J.; Cañizares, P.; Rodrigo, M. A.; Linares, J. J.; Aguilar, J. A., Improved polybenzimidazole films for H<sub>3</sub>PO<sub>4</sub>-doped PBI-based high temperature PEMFC. *Journal of Membrane Science* **2007**, *306* (1-2), 47-55.
38. Vengatesan, S.; Santhi, S.; Sozhan, G.; Ravichandran, S.; Davidson, D. J.; Vasudevan, S., Novel cross-linked anion exchange membrane based on hexaminium functionalized poly(vinylbenzyl chloride). *RSC Advances* **2015**, *5* (35), 27365-27371.
39. Li, H.-Y.; Liu, Y.-L., Polyelectrolyte composite membranes of polybenzimidazole and crosslinked polybenzimidazole-polybenzoxazine electrospun nanofibers for proton exchange membrane fuel cells. *J. Mater. Chem. A* **2013**, *1* (4), 1171-1178.
40. Mamlouk, M.; Ocon, P.; Scott, K., Preparation and characterization of polybenzimidazole/diethylamine hydrogen sulphate for medium temperature proton exchange membrane fuel cells. *Journal of Power Sources* **2014**, *245*, 915-926.
41. Chopade, S. A.; So, S.; Hillmyer, M. A.; Lodge, T. P., Anhydrous Proton Conducting Polymer Electrolyte Membranes via Polymerization-Induced Microphase Separation. *ACS applied materials & interfaces* **2016**, *8* (9), 6200-10.

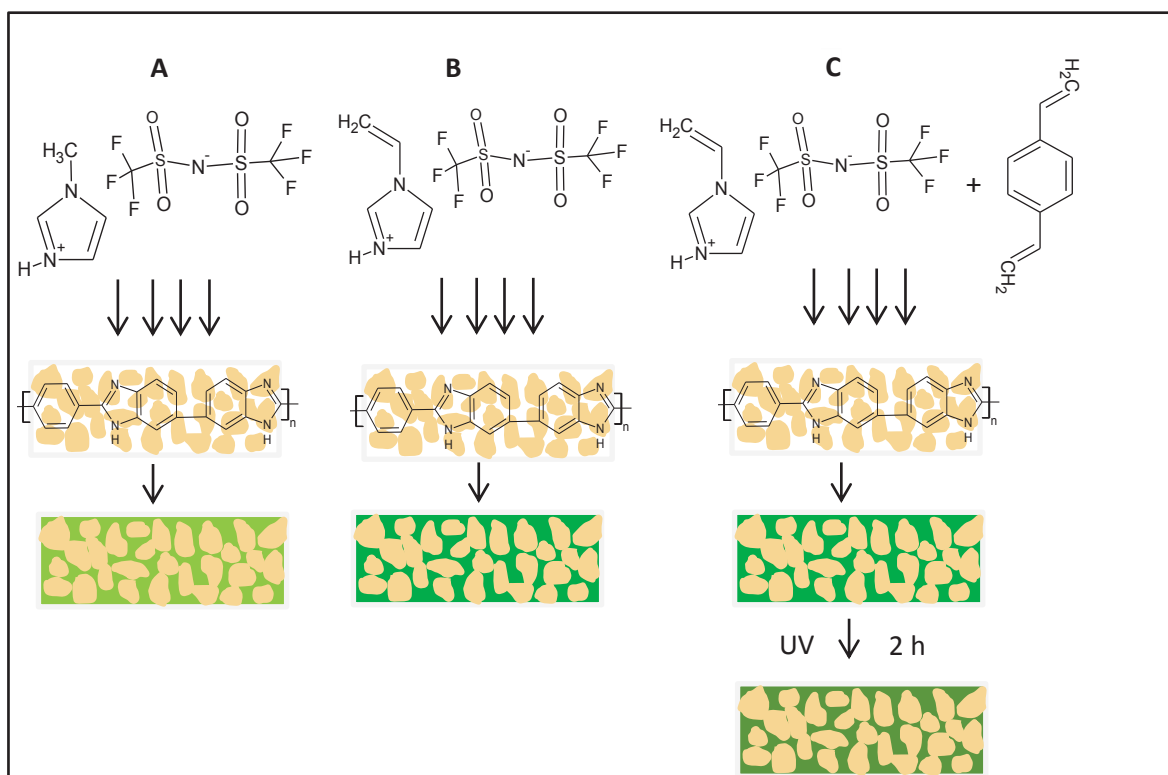






## Chapter -5

### Supported Ionic liquid membranes (SILMs) based on PBI and protic Ionic liquids for methane upgrading.





## 1. Introduction

The request for natural gas (methane, CH<sub>4</sub>) is growing worldwide and there is a rising need to develop methods for upgrading subquality gas reserves, which exist in relatively low quantities in remote zones. The global utilization of methane is above 3.1 trillion cubic meters (110 trillion standard cubic feet) each year, and is certainly one of the most challenging industrial application for gas separation membranes. Nitrogen (N<sub>2</sub>) and carbon dioxide (CO<sub>2</sub>), two common components in natural gas producing basins, are non-combustible contaminants that typically must be eliminated before gas can be marketed. Fourteen percent of U.S. natural gas comprises additional N<sub>2</sub>, and cannot be shipped to the national pipeline without treatment. Removal of this N<sub>2</sub> could allow access to an estimated 10 trillion scf (standard cubic feet per day) additional natural gas in the USA alone<sup>1-3</sup>.

Membrane-based nitrogen separation has a promising market in smaller natural gas operations, where cryo-genic distillation is uneconomical. In general glassy polymers are N<sub>2</sub>- permeable, while rubbery polymers are CH<sub>4</sub>- permeable<sup>2</sup>. For a gas mixture containing 10% N<sub>2</sub> in CH<sub>4</sub>, a membrane with a N<sub>2</sub>/CH<sub>4</sub> selectivity of 17 is required to achieve attractive separation in a single stage, but the best N<sub>2</sub>-selective membrane currently known has a selectivity of 12.5 (but very low permeability value, i.e. 0.8 Barrer according to Ohs et.al<sup>4</sup>), which is far below the value required; this is why CH<sub>4</sub>-permeable membranes are used for this separation. For a gas mixture containing 10% N<sub>2</sub> in CH<sub>4</sub>, Baker<sup>3</sup> has shown that a membrane with a CH<sub>4</sub> /N<sub>2</sub> selectivity of ~ 6, however there are no membranes that can achieve such performance<sup>1-2</sup>. The best CH<sub>4</sub>-selective membrane (Polyamide-polyether copolymer- PEBAX 2533) currently known has a CH<sub>4</sub> /N<sub>2</sub> selectivity of 4.2 with 20 barrer permeability of CH<sub>4</sub>. A process involving CH<sub>4</sub>-permeable rubbery membranes process remains the most feasible, though it requires considerable recompression of the permeate gas for delivery to the pipeline<sup>2</sup>. Baker<sup>1</sup> stated that recompression cost is not high enough to significantly impact on the process economics.

Membrane-based CO<sub>2</sub> separation has been pursued with particular focus on ionic liquid membranes, which differ from polymers in that they separate gases by differences in sorption rates rather than by diffusion rates<sup>2</sup>, however there are no studies focused on CH<sub>4</sub> upgrade/separation using ionic liquid membranes.

Ionic liquids (ILs) are salts that are liquid at, or near, room temperature. They have received significant attention in recent years due to several unique and favorable properties, such as their negligible vapor pressures and high solubility for organic and inorganic species. Knowledge on the solubilities and diffusivities of gases in ionic liquids (ILs) is important for the design of absorption

processes, such as the gas sweetening process. The solubilities of carbon dioxide (CO<sub>2</sub>), methane (CH<sub>4</sub>), ethane (C<sub>2</sub>H<sub>6</sub>), nitrogen (N<sub>2</sub>) and oxygen (O<sub>2</sub>) in several ILs have been studied intensively<sup>5-6</sup>. From these solubility studies, it was found that methane is 10 times more soluble than nitrogen<sup>7</sup>. Hence, instead of focusing on gas separation through polymeric membranes, we take an advantage of the ionic liquid's common 'concept of solubility' in the membrane.

Supported ionic liquid membranes (SILMs) strongly decrease the possible displacement of the liquid phase from the membrane pores through solvent evaporation, but also correspond to more stable membranes due to both high ILs viscosity and strong capillary forces between the IL and the supporting membrane<sup>6, 8</sup>. The most commonly used ILs are those with cations composed of imidazolium (IMIM) or pyridinium (Py) rings attached with one or more alkyl groups, because of their low melting points and stability under a wide range of conditions. Commonly used anions includes halide ions, tetrafluoroborate ([BF<sub>4</sub>]), hexafluorophosphate([PF<sub>6</sub>], and bis(trifluoromethylsulfonyl)imide anion ([TFSI])<sup>9</sup>. In this work, ILs with a cation based on the IMIM ring and anion based TFSI were chosen to fabricate SILMs, due to their good chemical and thermal stabilities and their extensive characterization in the literature<sup>10-11</sup>. These ionic liquids have also been used extensively in SILMs and CO<sub>2</sub> gas separation applications with promising results<sup>12-14</sup> and are considered as suitable candidates for SILMs development.

The incorporation of poly(ionic liquids) (PILs) in porous membranes was proposed as a solution to overcome the shortcomings of SILMs, in particular their stability affected by the IL leaching from the pores either at high temperatures or increasing pressure gradient across the membrane, which inhibit their practical use in gas separation processes. Researchers have prolonged the IL field to PILs to address the concerns about SILM operating stability and long-term performance<sup>15</sup>. PILs are ILs that contain a polymerizable functional group, such as a double bond. Polymerization of this functional group can result in the stringing together of long polymer chain structures, resulting in a dense polymer membrane that is linked chemically with an IL. In addition, the polymerization phase transition from liquid to solid state effectively improves the stability of the IL membranes<sup>8, 15-16</sup>.

Polybenzimidazoles (PBIs) are well known for their outstanding thermal stability, often exhibiting glass transition temperatures greater than 400°C in addition to flame retardance and chemical stability. Owing to these characteristics, they are promising materials for gas separation membranes that can be used at high temperatures<sup>17</sup>. PBI shows high selectivity for H<sub>2</sub> among the gases typically found in a reforming gas mixture (e.g., CO<sub>2</sub> and CH<sub>4</sub>), and in other high-temperature gas separations. However, PBI has very low gas permeability (often leads to low membrane flux) because of the

carbon chain rigidity and strong intermolecular hydrogen bonding, which produce a dense packing structure<sup>18-19</sup>.

Among large diversity of ILs, those based on the TFSI anion with imidazolium cation typically present a higher permeability of CH<sub>4</sub><sup>20-21</sup>. So far, all the reported SILMs (based on IMIM cation and TFSI anion) were prepared with the aprotic ILs<sup>14, 22-24</sup>. Unlike previously, our approach relies on the use of protic ILs i.e. IMIM cation without alkyl group at position 1 (R-N) but with acidic 'H' (H-N).

Herein, we report for the first time, usage of SILMs based on randomly porous PBI and protic ILs for gas permeation experiments. The objective of this work to develop and evaluate three classes of supported ionic liquid membranes (SILMs), based on PBI+ 1-H-3-methylimidazolium bis(trifluoromethane sulfonyl)imide (H-MIM TFSI), PBI+ 1-Vinyl-3-H-imidazolium bis(trifluoromethane sulfonyl)imide (V-MIM TFSI) and PBI+ poly[1-(3H-imidazolium)ethylene]bis(trifluoromethanesulfonyl)imide, to take advantage of the durability and thermal stability of the PBI in combination with the enhanced CH<sub>4</sub> gas permeability performance of protic ionic liquids with imidazolium cation and TFSI anion groups. The permeabilities of several single gases including CO<sub>2</sub>, N<sub>2</sub>, and CH<sub>4</sub> will be measured and then we will show how permeabilities change when the methyl group on imidazolium cation (at position 3) is replaced with vinyl group, as well as the influence of changing the temperature.

## 2. Experimental Section

### 2.1 Materials

All chemical reagents and solvents listed in the following were used as received: Poly[2,2-(m-phenylene)-5,5bibenzimidazole] (PBI Fumion APH Ionomer, Mw 59,000-62,000, Fumatech), LiCl(99 wt%, Sigma-Aldrich), Poly(vinylpyrrolidone) K30 (Mw=40000, Fluka), Poly(vinylpyrrolidone) K90 (Mw=360000, Fluka), 1-H-3-methylimidazolium bis(trifluoromethane sulfonyl)imide (98 wt%, Solvionic), 1-H-3-vinylimidazolium bis(trifluoromethane sulfonyl)imide (98 wt%, Solvionic), Divinylbenzene (80.0 wt %, Sigma-Aldrich), 2-hydroxy-2-methylpropiophenone (97.0 wt% Sigma-Aldrich), N-methyl-2Pyrrolidone (NMP anhydrous, 99.5 wt%, Sigma-Aldrich).

### 2.2 Polymer solution preparation

PBI was used as polymer for the membrane fabrication. Polymer solutions were prepared based on previous recipe developed in our group<sup>11</sup>. 11.5g of PBI powder, 1.5g of LiCl, 1.5g of PVP K30, 1.5g of PVP 90K and 84 g NMP were mixed at 175 °C for 24h to obtain 16% wt. of solids in polymer solution. The Polymer solution was then allowed to degas for two hours to ensure that all air bubbles were

removed from the solution. Addition of PVP and LiCl, controls macrovoids formation upon phase separation process and stabilizes the polymer solution respectively.

### **2.3 Randomly porous PBI membranes: by phase inversion method**

A schematic overview of the phase inversion process is depicted in Figure 5.1. Polymer solution consisting of PBI, PVP, LiCl and NMP was poured onto clean glass plate (Figure.5.1A) and casted using a casting knife with a thickness of 0.25 mm. After casting, the glass plate with polymer solution was immersed in coagulation bath (Figure. 1B) containing NMP/water (50/50) for 30 min at room temperature (RT). Then the plate was transferred into non solvent bath (pure water) at RT to wash out the traces of NMP (Figure. 1C), the exchange of solvent by water was completed during the 30 min at RT.

The membranes were peeled off from the plate. Subsequently solidified PBI supports were immersed in ethanol for 30 min, followed by hexane for 30 min, to make sure entire removal of water. Finally to remove all volatiles, membranes were sandwiched between two glass plates at 150 °C in an oven.

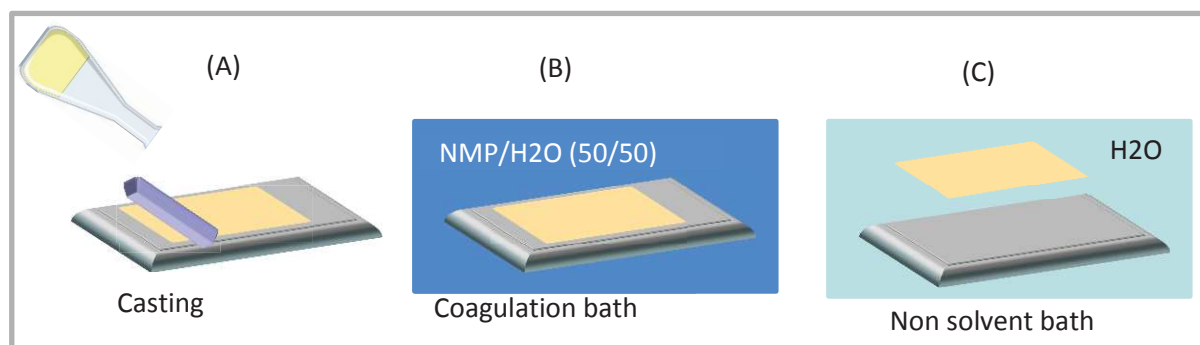


**Figure 5.1:** Schematic overview of phase inversion: (A) polymer solution casting on clean glass plate; (B) System immersed into mixture of 50:50% of NMP: water; (C) Glass plate with formed PBI supports into pure water (C).

### **2.4 Fabrication of supported ionic liquid membranes (SILMs)**

Randomly porous PBI (RPBI) membranes were infiltrated with ionic liquids based on earlier efforts in our group<sup>11</sup>. Three types of SILMs have been fabricated. The schematic illustration of the infiltration protocol is shown in Figure 5.2.

A) RPBI/IL: First of all, the protic ionic liquid (IL) 1-H-3-methylimidazolium bis(trifluoromethane sulfonyl)imide (H-MIM TFSI) was heated up to >55 °C to melt the salt, and then RPBI membrane was dried for both water and organics removal at 120 °C and under 100 mbar of vacuum.

Subsequently membrane was placed under vacuum for 1h to remove air bubbles and guarantee the monomer filtration through RPBI membrane. The infiltration process was conducted by pouring the IL on the PBI support surface at 170 °C and under vacuum of 160 mbar. After that, the membranes were removed out from the filter holder and the excess of IL on the membrane surface was wiped off with a tissue.

B) RPBI/MIL: the monomeric ionic liquid (MIL) 1-Vinyl-3H-imidazolium bis(trifluoromethane sulfonyl)imide (H-VIM TFSI) was heated up to 50 °C to melt the salt, and the above infiltration procedure was followed.

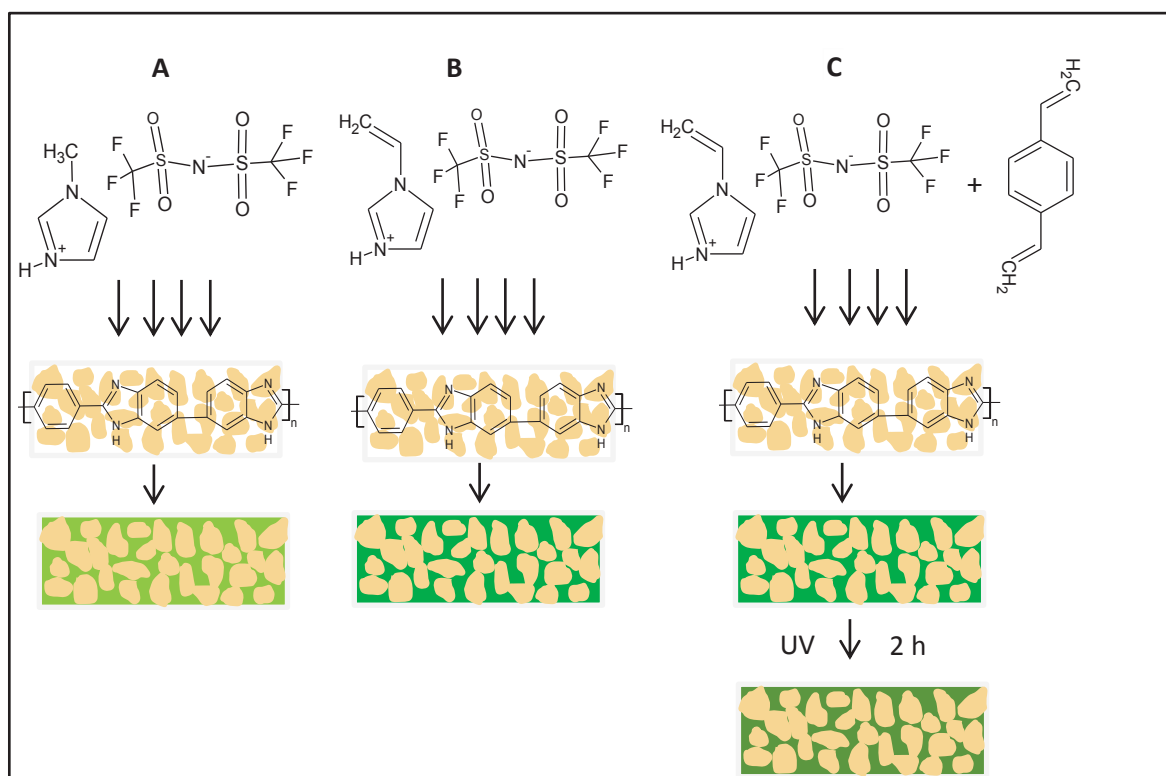


**Figure 5.2** : Schematic illustration of membrane pore filling and chemical structures of the used ionic liquids A) Infiltration of 1-H-3-methylimidazolium bis(trifluoromethane sulfonyl)imide (H-MIM TFSI); B) Infiltration of 1-Vinyl-3H-imidazolium bis(trifluoromethane sulfonyl)imide (H-VIM TFSI); C) Infiltration of H-VIM TFSI with divinylbenzene.

C) RPBI/PIL: the monomeric ionic liquid (MIL) 1-Vinyl-3H-imidazolium bis(trifluoromethane sulfonyl)imide was heated up to 50 °C to melt the salt, afterwards 1 mol% (referred to the MIL) of divinylbenzene (crosslinker-CL) was added and the mixture was thoroughly mixed. Subsequently, the above infiltration process was conducted. After that the membranes were removed out from the filter holder and excess of MIL on the membrane surface was wiped off with a tissue. A photo



initiator (2-hydroxy-2-methylpropiophenone) was added on the membrane top surface to initiate the photopolymerization process. In order to obtain the composite crosslinked RPBI/PIL membranes, each side of the membrane surface was exposed for 2h under a 365 nm UV lamp (Vilber Lourmat, with an intensity of 2.4 mW cm<sup>-2</sup>). After polymerization, the membrane was gently wiped from any residuals with lab paper.

## **2.5 Characterization methods**

### **2.5.1 Porosity**

The porosity of the as prepared RPBI membranes was determined by a helium displacement pycnometer (MicroMetrics AccuPyc 1330) equipped with 1 cm<sup>3</sup> sample module. The herein reported porosity values were evaluated for PBI microsieves above 50 cm<sup>2</sup> in surface area. Porosity was calculated using following equation.

$$Porosity (\emptyset) = \frac{V_{bulk} - V_{skeleton}}{V_{bulk}} \times 100$$

For all the samples, the reproducibility of the measurements was typically within  $\pm 0.01\%$  of the nominal porosity value.

### **2.5.2 SEM characterization**

Morphology, thickness, and pore size, of the as prepared RPBI membranes were studied by scanning electron microscopy SEM (FEI INSPECT 50).

### **2.5.3 Transmission Electron Microscopy (TEM)**

The membranes were embedded in epoxy resin, and ultrathin slices (about 50nm thickness) were cut with an ultramicrotome (Leica EM UC7) at room temperature. These slices were placed on TEM copper grids with carbon film, and analyzed by Transmission Electron Microscopy in a Tecnai T20 (FEI Company), at a working voltage of 200KV. TEM Bright Field Images were acquired with a side-mounted Veleta CCD Camera.

### **2.5.4 Atomic Force Microscopy (AFM)**

AFM measurements have been carried out by tapping mode using NSG30 ND-MDT tip (Multimode 8 system, Veeco/Bruker) with force constant around 22-100 N/m. Roughness average (Ra) and Root Mean Square (RMS) are both representations of surface roughness, but each is calculated differently. Ra is calculated as the Roughness Average of a surface, measured from microscopic

peaks and valleys. RMS is calculated as the Root Mean Square of a surface, measured from microscopic peaks and valleys. Ra and RMS were calculated using following equations.

$$Ra = \frac{1}{N} \sum_{i=1}^n |y_i|$$

$$RMS = \sqrt{\frac{1}{N} \sum_{i=1}^n y_i^2}$$

The roughness profile contains N ordered, equally spaced points along the trace, and  $y_i$  is the vertical distance from the mean line to the  $i^{th}$  data point.

### **2.5.5 Infrared Spectra Measurements**

ATR-FTIR analyses (Bruker VERTEX 70 equipped with Golden Gate ATR from 4000 to 600  $\text{cm}^{-1}$ , 256 scans and resolution of 4  $\text{cm}^{-1}$ ) were performed at room temperature to assess about the photopolymerization evolution in RPBI/PIL SILMs, and to investigate any possible interactions between the benzimidazole from the RPBI and the poly[1-(3H-imidazolium)ethylene] bis(trifluoromethane sulfonyl)imide.

### **2.5.6 Thermal studies**

Thermogravimetric analysis (TGA) was carried out using a Q500 IR TA instrument to evaluate the composition and thermal behavior of the as prepared SILMs. Studies were conducted using 4-5 mg samples, in the temperature range from room temperature to 900 °C at a controlled heating rate of 2°C /min under an inert atmosphere ( $\text{N}_2$ ).

### **2.6 Gas solubility and diffusion coefficient experimental measurements**

The  $\text{CO}_2$  and  $\text{CH}_4$  gas solubility, characterized by the Henry's law constant, and diffusion coefficient in the H-VIM TFSI were estimated according to a classical protocol published in the literature<sup>25</sup>. The schematic representation of the experimental set-up is shown in Figure 5.3. Firstly, the gas compartment (GC) was purged with the selected gas. Afterward, a mass of solvent of about 0.5 g, was placed in the absorption compartment (AC) with valve 3 closed. Then, GC was pressurized until a constant value of pressure of the pure gas, and afterward valve 1 and 2 were closed. After opening valve 3, the gas was expanded to the AC, and the pressure decay was followed in the system using a pressure transducer (Druck, PDCR 910 model, England). The pressure decay was related with the absorption of the gas by the solvent.

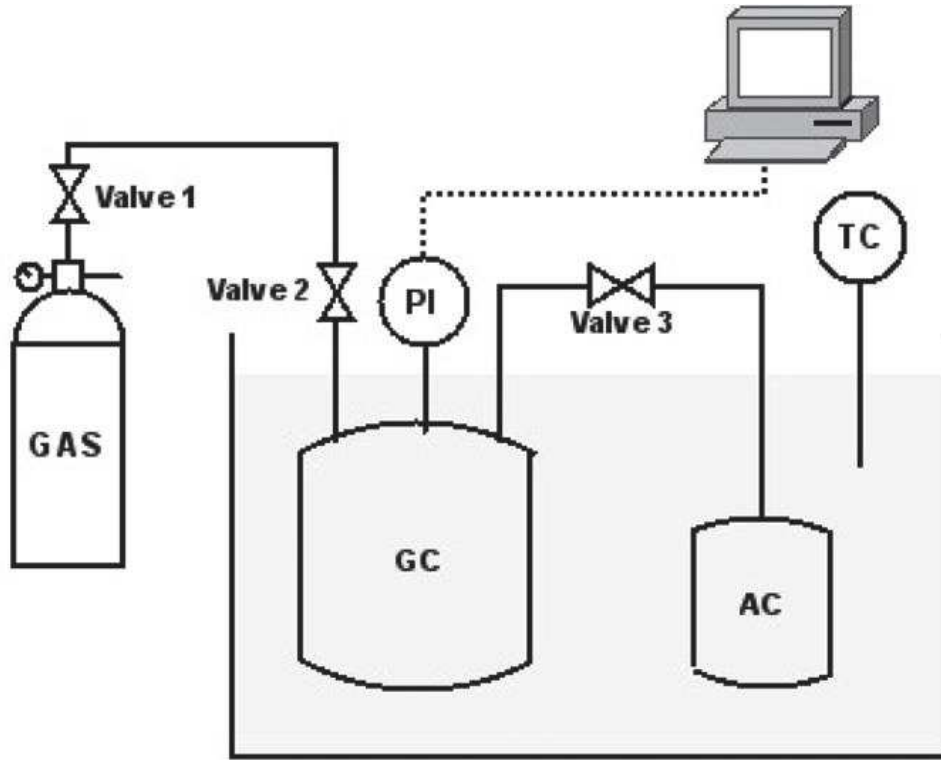


**Figure 5.3.** Gas absorption experimental set-up. GC, gas compartment; AC, absorption compartment; TC, temperature controller; PI, pressure transducer ( adopted from Ref<sup>25</sup>).

The experiments were estimated by fitting the pressure decay over time to a one-dimensional diffusion model using a non-linear least-squares method. Several assumptions were considered: (i) only diffusive transport occurs in the system; (ii) equilibrium is established at the gas/liquid interface; (iii) gas concentration in the liquid phase boundary is described by Henry's Law and (iv) gas diffusion coefficients are independent of their concentration for the partial pressures tested. It was also considered that the IL properties such as viscosity and density are constant at given temperature (60 °C). The partial pressure tested was 0.7 bar.

Combining the Fick's second law for the diffusion over IL thin-liquid film, with a mass balance on the gas phase above the liquid, the pressure decay is related to the system parameters and gas properties according to the following equation.

$$\ln \frac{P}{P_0} = \frac{k}{H_{gas}} \sum_{n=0}^{\infty} \frac{1}{(2n+1)^2} \left\{ \exp \left[ -\frac{(2n+1)^2 \pi^2 D_{gas} t}{4L^2} \right] - 1 \right\}$$

With

$$k = \frac{8RTV_{IL}\rho_{IL}}{\pi^2 V_{gas} MW_{IL}}$$

where  $H_{gas}$  (bar) is the Henry's constant for the gas in the ionic liquid,  $D_{gas}$  ( $\text{cm}^2 \cdot \text{s}^{-1}$ ) the gas diffusion coefficient,  $L$  (cm) is the IL film thickness,  $V_{IL}$  ( $\text{cm}^3$ ) and  $V_{gas}$  ( $\text{cm}^3$ ) are the volumes of the IL and pure gas in the absorption compartment and in the gas compartment, respectively,  $MW_{IL}$  ( $\text{g} \cdot \text{mol}^{-1}$ ) and  $\rho_{IL}$  ( $\text{g} \cdot \text{cm}^{-3}$ ) are the molecular weight and density of the IL, respectively.

## **2.7 Gas permeation experiments**

Single gas permeation measurements through the membranes were carried out by using the constant-volume and variable-pressure technique at controlled temperature, as described in the standard ASTM D 1434-82 (procedure V). The schematic representation of the experimental set-up (home-made system) is depicted in Figure 5.4. The apparatus consists essentially of a two compartments permeation cell separated by the tested membrane. The permeability is obtained by measuring the pressure increase in the downstream compartment (with a constant volume of  $5.25 \cdot 10^{-5} \text{ m}^3$ ) and using different MKS Baratron pressure transducers (range from 0.0 to  $1 \times 10^5$  Pa). The membranes and downstream cell walls were outgassed *in situ* during 15 h at high vacuum level using a turbomolecular pump (Leybold, Turbovac 50, 50). The permeability measurements were performed in the temperature range from 40 °C to 90 °C, using  $1.0 \times 10^5$  Pa of upstream pressure and by recording the pressure increase in the downstream compartment during 4 h. For each temperature change, the whole set-up was allowed to stabilize during at least 12 h.

It has to be noticed that the order of gas permeance measurements was the following:  $\text{N}_2$ ,  $\text{CO}_2$ ,  $\text{CH}_4$ . Between each measurement, membranes and cell were outgassed *in situ* during 12 h under high vacuum.

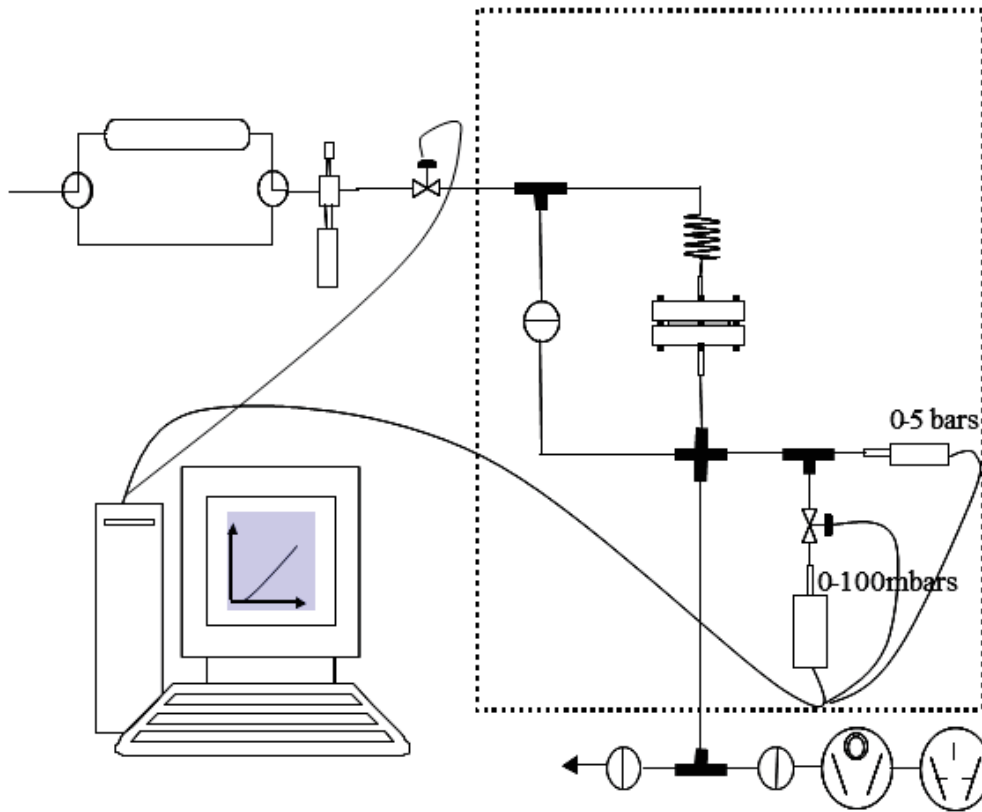


**Figure 5.4:** Schematic of the experimental set-up used for single gas permeation measurements.

The purity of the single gases ( $N_2$ ,  $CO_2$  and  $CH_4$  provided by Linde Gas) was of 99.95%, they were used without any further purification. A complete description of the apparatus and methodology used was already published<sup>26</sup>. A typical permeability curves present successively the transient and steady-states. During the latter, the mass transfer coefficient  $Q$ , according to the Fick's second law in the permeation conditions, can be simplified at infinite time:

$$Q_{t \rightarrow \infty} = \frac{DC_1}{l} \left( t - \frac{l^2}{6D} \right)$$

When a penetrant diffuses through a polymer film in which it is soluble, there is a transient state from the time the penetrant first enters the film until the steady state of flow is established. The intercept on the time axis of the extrapolated linear steady state portion of the curve is called the time lag,  $\theta$ . The time lag is used to determine the diffusivity  $D$  using the following equation:

$$D = \frac{l^2}{6\theta}$$

Where  $l$  is the film thickness and  $\theta$  is the time lag determined from the plot.

For permeability calculations, the mathematical treatment for thin films based on Fick's second law and reported by Crank<sup>27</sup> was used. The permeability coefficient was calculated using following equation.

$$P = \frac{VL}{AV_m T P_1} \left( \frac{dP_2}{dt} \right)$$

Where  $P$  ( $\text{mol}\cdot\text{m}^{-1}\cdot\text{s}^{-1}\cdot\text{Pa}^{-1}$ ) is the permeability coefficient,  $V$  ( $\text{m}^3$ ) is the apparatus volume of the apparatus;  $L$  (m) is the membrane thickness,  $A$  ( $\text{m}^2$ ) is the membrane surface area,  $V_m$  ( $\text{m}^3\cdot\text{mol}^{-1}$ ) is the gas molar volume at STP, and  $P_1$  (Pa) is the applied pressure.

All the permeability values are reported in Barrer. This unit is defined as follows:

$$1 \text{ Barrer} = 10^{-10} \frac{\text{cm}^3(\text{STP})\text{cm}}{\text{cm}^2 \text{ s cm}_{\text{Hg}}}$$

### 3. Results and discussion

#### 3.1 Preparation of random porous PBI supports

The random porous PBI supports (RPBI) were prepared successfully by phase separation method. The porosity measured by pycnometer was  $63.7\% \pm 2.7$ . SEM pictures of the prepared RPBI supports are shown in Figure 5.5, where the analysis of airside, glass side and cross-section are displayed. Pore sizes diameters within the range of 50-250 nm on air side and 30-50 nm on the glass side were observed respectively. The cross-section view reveals a sponge-like structure.

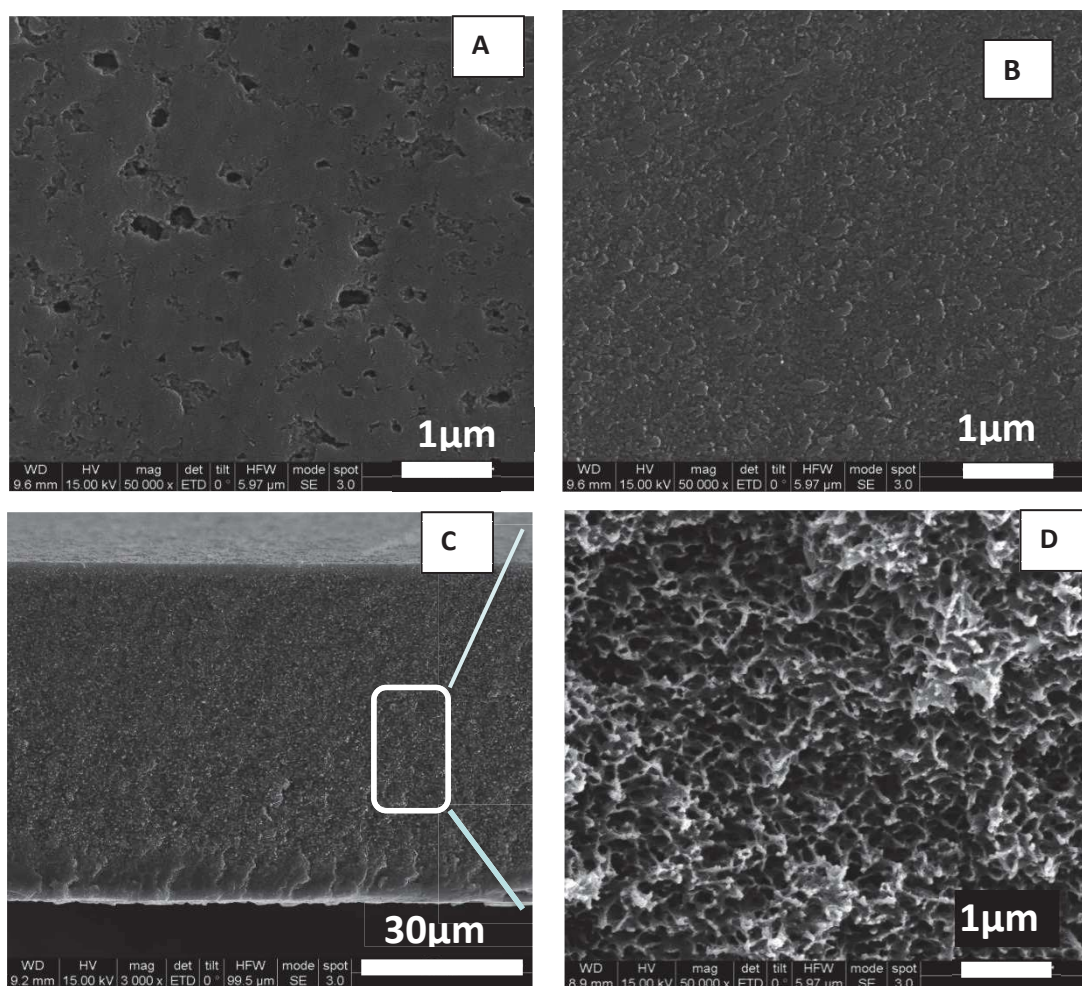


**Figure 5.5:** SEM analysis of random porous PBI membrane prepared by phase separation method from 16% wt of solids in polymer solution: A) Air (top) side; B) glass (bottom) side; C) cross-section; (d) detail of cross-section area.

To better understand the pore connectivity, the microstructure of RPBI support was studied by TEM and the resulting image is shown in Figure 5.6A. The white regions represent the pores and there can be observed interconnections between random pores over the whole membrane. In order to examine the surface roughness of the RPBI membrane in detail, the AFM surface images of glass side (bottom side) and air side (top side) analysis were analyzed (Figure 5.6B-C). It can be seen that the minor change in roughness parameters from top to bottom is attributed to the change in the sizes of interconnected open pores at both sides.

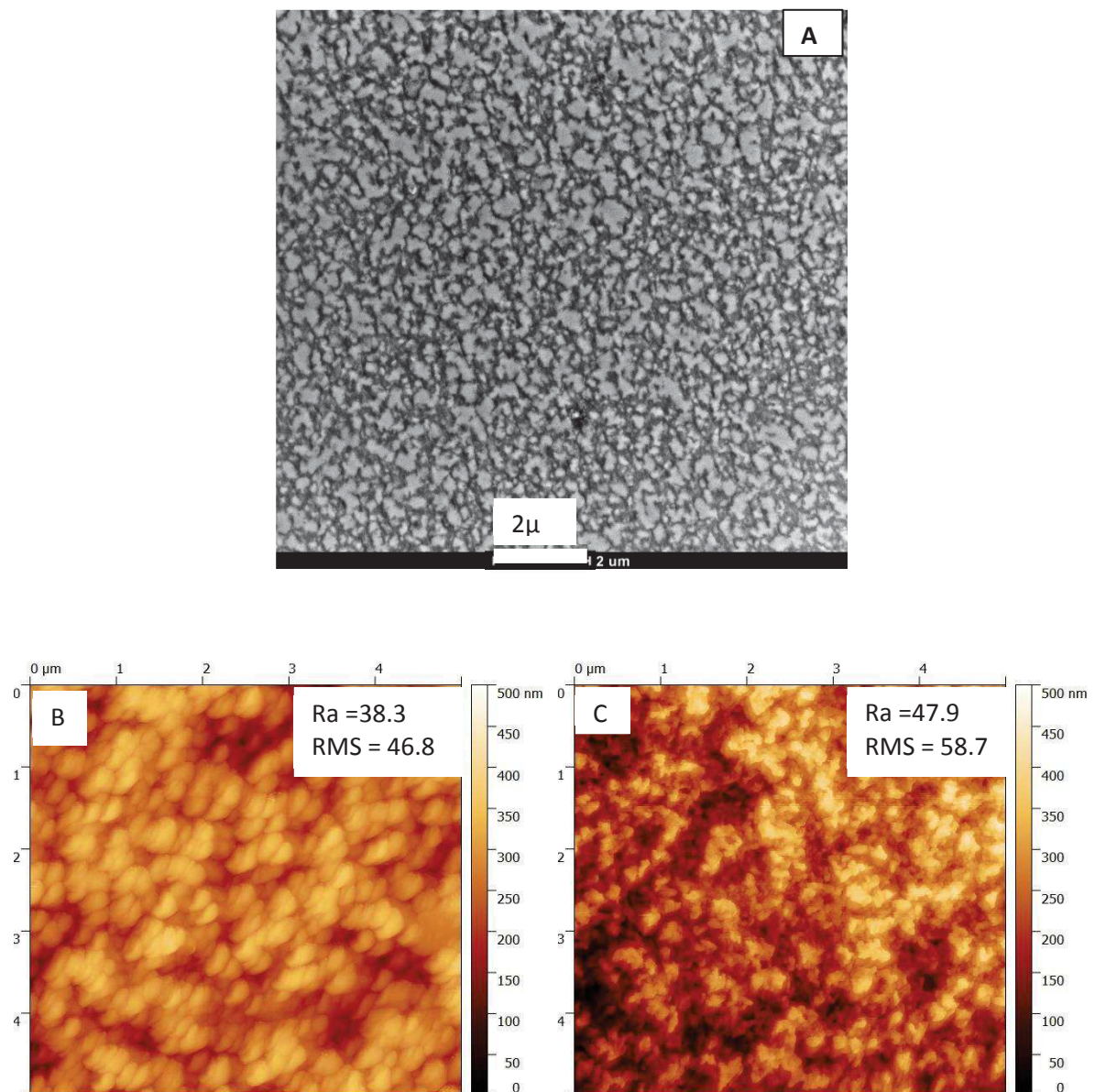


**Figure 5.6:** (A) TEM observation of RPBI membrane; three dimensional AFM surface images of (B) RPBI-glass (bottom) side and RPBI-air (top) side (C).



### **3.2 Fabrication of SILMs**

Due to the viscosity of H-MIM TFSI (i.e. 80 cP at 25 °C)<sup>28</sup> and V-MIM TFSI (14.3 cP at 50 °C), the use of both vacuum and high temperature was required to ensure efficient IL embedding within the RPBI membrane pores.

Table 5.1 summarizes the characteristics of the prepared SILMs. The experimental IL/MIL/PIL loadings calculated from simple weight measurements reasonably matches with those evaluated from TGA, but higher than theoretical values, due to the difficulty in wiping the excess of IL/MIL/PIL content.

**Table 5.1:** Main characteristics of SILMs prepared for this work.

Sample ref.	SILM	Loading (wt%)		
		Theoretical <sup>1</sup>	Experimental <sup>2</sup>	TGA
1	RPBI-IL	73.5	82.4	70.4
2	RPBI-MIL	77	86	83.1
3	RPBI-PIL	82.5	86.5	78.6

<sup>1</sup>Theoretical wt.% gain based on density of IL/MIL/PIL and porosity of the membrane; <sup>2</sup>based on weight measurement.

Figure 5.7 shows pictures of the prepared SILMs, as free- standing films. The resulting SILM based on IL (RPBI-IL) was extremely brittle to handle, due to the crystallinity of the IL at room temperature (melting point= 55 °C) whereas the RPBI-MIL was slightly brittle to handle (melting point ~ 40-45 °C). The SILMs based on PIL i.e. RPBI-PIL (Figure 5.7C) were handled without any difficulty.

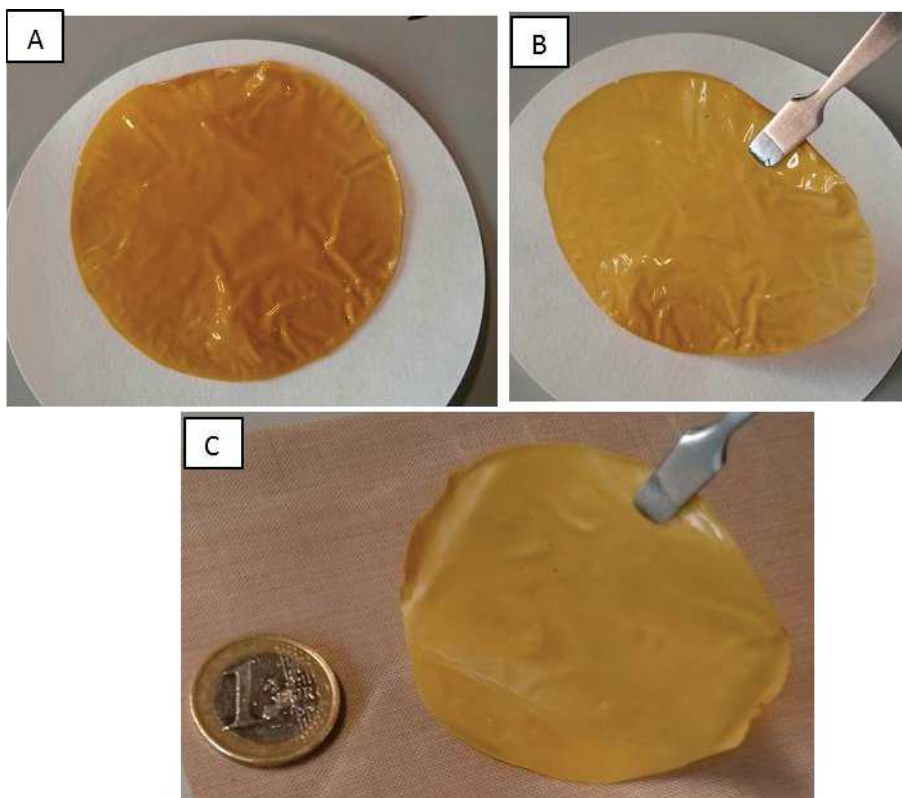


**Figure 5.7:** Photos of the prepared SILMs. A) IL based SILM (RPBI-IL); B) MIL based SILM (RPBI-MIL); C) PIL based SILM (RPBI-PIL).

### **3.3 Characterization**

The FTIR spectra were used to evidence the successful polymerization of vinyl-polymerizable groups from the IL. Accordingly, ATR-FTIR spectra of the composite membranes before (RPBI-MIL), and after UV radiation exposure for 2 h (RPBI-PIL) are presented in Figure 5.8.

The conversion degree of MIL to PIL was above 97% upon 2 h UV exposure as already confirmed in our previous studies (3<sup>rd</sup> chapter). As expected, the intense absorption bands in the range 1400-1000  $\text{cm}^{-1}$ , observed in both RPBI-MIL and RPBI-PIL membranes, are characteristic of the SO<sub>2</sub> and SNS vibrational modes of the bis(trifluoromethanesulfonyl)imide [TFSI] anion<sup>29</sup>. Two characteristic infrared absorbance bands in RPBI-MIL were selected to examine the disappearance of the vinyl-monomer: 1665-1630  $\text{cm}^{-1}$  (stretching vibration in  $-\text{CH}=\text{CH}_2$ ) and 995-920  $\text{cm}^{-1}$  (out of plane bending of  $-\text{CH}=\text{CH}_2$  groups). The disappearance of these characteristic peaks of the vinyl monomer in RPBI-PIL confirmed the successful polymerization.

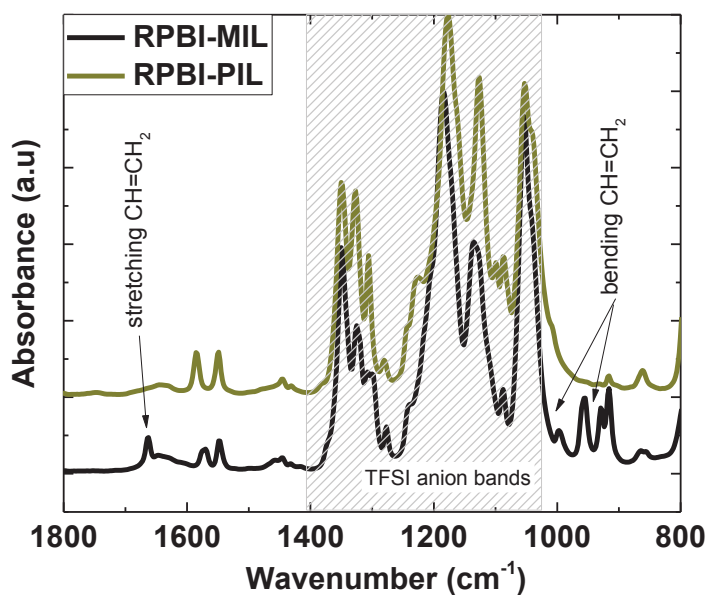


**Figure 5.8:** ATR-FTIR spectra of a composite SILM membrane before and after UV exposure.

The objective of this work was obtain SILMs for application at 25 °C (298.15K) and above. Figure 5.9 shows the TGA thermograms and derived DTG curves of all the prepared SILMs.

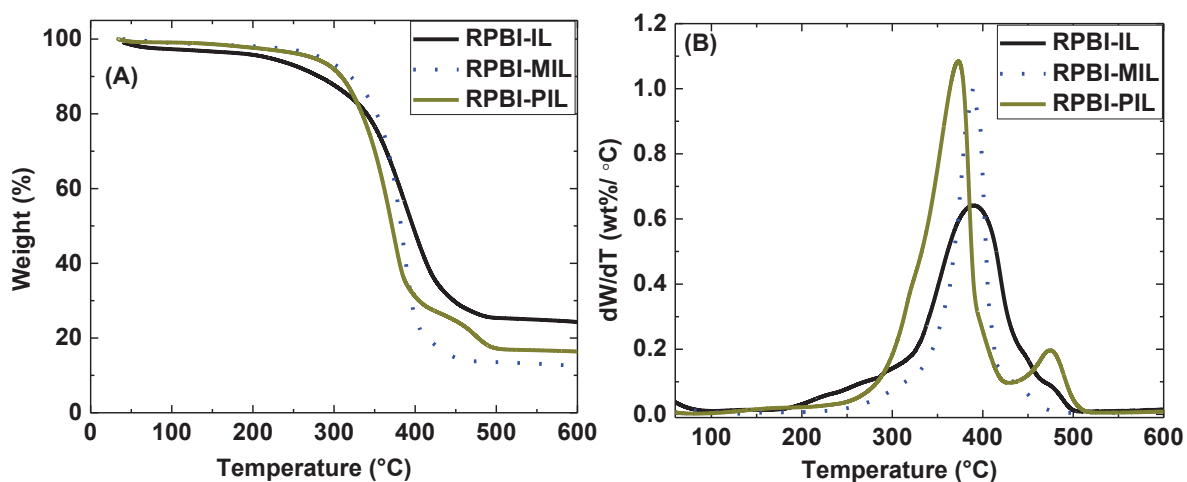


**Figure 5.9:** A) TGA thermograms and B) derived DTG curves of prepared supported ionic liquid membranes

A one stage thermal decomposition process (390 °C) was observed for RPBI-IL and RPBI-MIL due to the decomposition of IL and MIL respectively. Whereas in the case of RPBI-PIL membrane a two-stages decomposition was observed, the 1<sup>st</sup> weight loss corresponds to the PIL decomposition and the shoulder at around 480 °C is attributed to the interactions between PIL and RPBI support<sup>11</sup>.

Specially, very low weight losses, (0.7-1.5%) were measured for all of the SILMs within the 150°-200°C temperature range. It can be concluded that they are thermally stable up to 310 °C under N<sub>2</sub> atmosphere which suggests that all of these SILMs have good thermal stability.

The experimental Young's modulus and tensile strength values of RPBI-PIL were 0.2 GPa and 1.3 MPa respectively. The RPBI-IL and RPBI-MIL samples have not been considered for mechanical stability experiments due to handling constraints at room temperature.

### **3.4 Gas permeability of SILMs**

The single gas permeability results obtained in the present work are based on the following assumption: gas transport takes place entirely in the IL or PIL since the reported<sup>30</sup> permeabilities of dense PBI support are very low i.e. 0.3, 0.009 and 5 barrers for CO<sub>2</sub>, CH<sub>4</sub> and H<sub>2</sub> respectively. The experimental permeabilities of SILMs in this work are between 1.7 to 217 barrer for CO<sub>2</sub>, 6 to 535 barrer for H<sub>2</sub>, and 12.2 to 724 barrer for CH<sub>4</sub>. These values validate the assumption that the IL or PIL is the main contributor to gas permeability when comparing with the permeability of the support alone.

The influence of temperature on both gas permeability and ideal selectivity was studied in the range of temperatures from 40 to 90 °C.

#### ***3.4.1 Effect of the vinyl group (increase in the carbon number)***

The permeability of the SILMs prepared with the RPBI support and 2 different ILs was measured for the different gases. The studied ILs studied were protic H-MIM TFSI (IL) and the monomeric ionic liquid (MIL) H-VIM TFSI. These ILs were selected because they have the same anion (TFSI) but a different functional group on imidazolium cation. The permeabilities CO<sub>2</sub>, CH<sub>4</sub> and N<sub>2</sub> through the prepared composite RPBI/IL and RPBI/MIL membranes were measured and evaluated by using the method described in the experimental section. Results are presented in Figure 5.10.

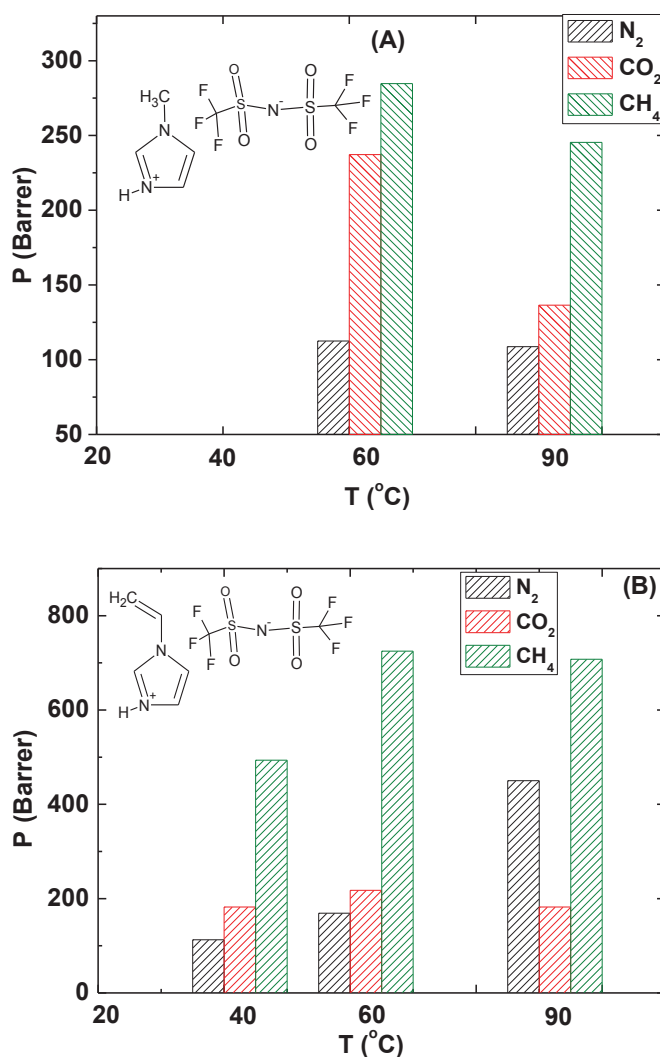


**Figure 5.10:** Influence of temperature on single gas permeability values for: (A) RPBI-IL and (B) RPBI-MIL membranes.

Since H-MIM TFSI is a crystalline solid at room temperature and its melting point is  $\sim 55$  °C (in agreement with Moschovi et al<sup>31</sup>), the experiments with RPBI-IL could not be carry out at 40 °C. The low gas permeabilities measured at 40 °C for RPBI-MIL are due to the physical state of the monomeric IL at room temperature (melting point of liquid H-VIM TFSI is  $\sim 40$ -45 °C). As observed in Figure 5.10, the gas permeability values at 60 °C increase in the order:  $\text{CH}_4 > \text{CO}_2 > \text{N}_2$  for both RPBI-IL and RPBI-MIL membranes.

It is shown that the effect of vinyl substitution on imidazolium group increases the  $\text{CH}_4$  permeability. The  $\text{CH}_4$  permeability values are in the order of 284-245 barrer and 724-707 barrer for RPBI-IL and RPBI-MIL membranes respectively, at 60-90 °C. The  $\text{CO}_2$  permeability values are in the order of 237-136 barrer and 217-182 barrer for RPBI-IL and RPBI-MIL membranes respectively, at 60-90 °C. Both

RPBI-IL and RPBI-MIL SILMs show a decrease in CH<sub>4</sub> permeability at 90 °C, which is attributed to a decrease in solubility when temperature increases. The high N<sub>2</sub> permeability may be attributed to the increase in diffusivity with increasing temperature.

The ratio of single gas permeability values measured for RPBI-MIL and RPBI-IL membranes are shown in table 5.2. In the tested temperature range, i.e. from 60 to 90 °C, the CH<sub>4</sub> permeability of RPBI-MIL membranes is always 2.5 to 3 times higher than that of RPBI-IL membranes.

**Table 5.2:** Ratio for the single gas permeability values through RPBI-MIL and RPBI-IL membranes.

Temp ( °C)	MIL-P <sub>N2</sub> /IL-P <sub>N2</sub>	MIL-P <sub>CH4</sub> /IL-P <sub>CH4</sub>
60	1.5	2.5
90	4.1	2.9

Anderson et.al.<sup>7</sup> presented the experimental results for CO<sub>2</sub> and CH<sub>4</sub> solubilities in different aprotic ILs, i.e. 1-hexyl-3-methylpyridinium bis(trifluoromethylsulfonyl)imide ([C<sub>6</sub>MPy TFSI]); 1-hexyl-3-methylimidazolium bis(trifluoromethylsulfonyl)imide([C<sub>6</sub>MIM TFSI]) and 1-butyl-3-methylimidazolium bis(trifluoromethylsulfonyl)imide([BMIM TFSI]). These ILs are similar to those used in this work (imidazolium- based cation and the same TFSI anion). The solubility results are reported in Table 5.3 as Henry's law constants (K<sub>H</sub>) for CH<sub>4</sub> and CO<sub>2</sub> at various temperatures. All Henry's law constants are calculated on a mole fraction basis. Large K<sub>H</sub> values corresponds to low gas solubility, while small K<sub>H</sub> values indicate high gas solubility.

**Table 5.3:** Values of Henry's law constant for CO<sub>2</sub> and CH<sub>4</sub> in different ILs

Published work	Gas	Henry's Law constants (H) (bar)					
		~10 °C	~25 °C	~40 °C	~50 °C	~60 °C	~90 °C
[C <sub>6</sub> MPy TFSI] <sup>7</sup>	CO <sub>2</sub>	25.4	32.8	-	46.2	-	-
	CH <sub>4</sub>	-	300	442	-	371	-
[BMIM TFSI] <sup>32</sup>	CO <sub>2</sub>	25.3	33	-	48.7	-	-
[C <sub>6</sub> MIM TFSI] <sup>33</sup>	CO <sub>2</sub>	24.2	31.6	-	45.6	-	-
	CH <sub>4</sub>	-	329	380	-	359	-
<b>Present work</b>							
[H-VIM TFSI]*	CO <sub>2</sub>	-	-	148		94	-
	CH <sub>4</sub>			31		26	-
poly[HVIM TFSI]*	CO <sub>2</sub>	-	-	3894		-	3143
	CH <sub>4</sub>	-	-	227		-	572

\*estimated from the permeability measurements herein performed

It is noticed that the CO<sub>2</sub> solubility values for [C<sub>6</sub>MPy TFSI] and [C<sub>6</sub>MIM TFSI] are virtually identical, suggesting that CO<sub>2</sub> solubility in these particular ILs is controlled primarily by interacting with TFSI anion, in agreement with the previous investigations<sup>7</sup>. From the table 5.3, it is clear that both CO<sub>2</sub> and CH<sub>4</sub> solubilities decrease when temperature is increased.

To study the influence of cation alkyl chain length, one can compare the solubility of CO<sub>2</sub> in [BMIM TFSI] and [C<sub>6</sub>MIM TFSI] (Table 5.3). The solubility increases slightly with increasing the chain length; this trend is also observed for ILs containing [BF<sub>4</sub>]<sup>-</sup> and [PF<sub>6</sub>]<sup>-</sup> anions<sup>34</sup>. The solubility of CH<sub>4</sub> is much less temperature dependent, as revealed by CH<sub>4</sub> permeability measurements through both RPBI/IL (284 -245 barrer at 60-90 °C) and RPBI/MIL (724 -707 barrer at 60-90 °C) SILMs.

In conclusion, the differences in gas permeability through the SILMs prepared with different carbon chain length on the imidazolium cation, for the same anion (TFSI), is discussed. The CH<sub>4</sub> permeability increases with the carbon chain length on the IL cation, at all the tested temperatures in the range 60-90°C. The increase in permeability with the carbon chain length is likely due to higher free volume in the IL. Overall, the alkyl chain length has a major effect on CH<sub>4</sub> permeability through the SILMs.

As far as we know, the ability of protic ILs to selectively transport CH<sub>4</sub> is surprising. In order to check the validity of these results, the solubility of CH<sub>4</sub> and CO<sub>2</sub> in [H-VIM TFSI] has been measured at 60 °C and it was found that the Henry constant value was very low i.e. 0.4 bar for CH<sub>4</sub> (high solubility). In the case of CO<sub>2</sub>, no pressure decay was observed over time, revealing a negligible CO<sub>2</sub> solubility in [H-VIM TFSI]. The vinyl group on imidazolium cation seems thus to be responsible for the high CH<sub>4</sub> solubility and associated CH<sub>4</sub> permeability through the corresponding SILMs. Furthermore, Henry constant (H) values for RPBI-MIL (HVIM TFSI) and RPBI-PIL (poly [HVIM TFSI]) were estimated from permeability measurements (Table 5.3). The 'H' values for RPBI-PIL are out from the classical range which could be attributed to defective membranes and for the RPBI-MIL, the tendency is acceptable. However, these values support the ability of protic ILs to selectively transport CH<sub>4</sub>.

Our hypothesis for explaining this original result is based on the difference between the structures of protic ILs (used in this work) and classical aprotic ILs (Table 5.3). Indeed, the protonated nitrogen in imidazolium cation is weakly acidic. It can form Brønsted acid-base interactions with TFSI anion, thus decreasing the affinity between CO<sub>2</sub> and the TFSI anion. Such interaction does not exist in aprotic ILs and the TFSI anion can attract CO<sub>2</sub> freely through Lewis acid-base interaction. Further work should be required with the assistance of theoretical calculations to demonstrate this hypothesis and investigate the absorption behavior of CH<sub>4</sub> and CO<sub>2</sub> in protic ILs.

### **3.4.2 PIL based SILMs**

The figure 5.10 shows the influence of temperature on the evolution of N<sub>2</sub>, CO<sub>2</sub> and CH<sub>4</sub> permeabilities through the PIL-based SILMs. An increase in single gas permeability is observed when the temperature increases from 40 to 90 °C.

According to the Figure 5.11A, increasing the temperature from 40-90° C causes the permeability of CH<sub>4</sub> to increase by a factor of ~3 (113 to 420 Barrer) due to higher solubility and stronger interactions with the SILM when the temperature increases. The high permeability values for N<sub>2</sub> (177 Barrer) and CO<sub>2</sub> (146 Barrer) at 90 °C are attributed to the high diffusivity of these gases when the temperature increases. These PIL based SILMs exhibit low gas permeabilities (for all the tested gases in the range 40-90°C) compared with RPBI-MIL membranes (monomeric IL- based SILM). The order of gas permeability values for the RPBI/PIL SILMs was: CH<sub>4</sub> > N<sub>2</sub> > CO<sub>2</sub>.

The logarithm of the N<sub>2</sub>, CO<sub>2</sub> and CH<sub>4</sub> permeability follows a linear relationship with the reverse of the temperature as shown in Figure 5.11.B. Therefore, the influence of temperature on gas permeability (P) can be described by an Arrhenius type relationship:  $P = P_0 \cdot \exp(-E_a/RT)$ . Where P<sub>0</sub> is the pre-exponential factor and E<sub>a</sub> is the activation energy for gas permeation.



The activation energies ( $E_a$ ) for permeation of  $\text{CO}_2$  and  $\text{CH}_4$  are reported in Table 5.4. These results are compared with literature data. The measured value of  $E_a$  (24.6 kJ/mol) for  $\text{CH}_4$  permeability is lower (16%) than values reported in the literature for membranes prepared with different commercial supports (Alumina support,  $E_a = 29.3 \text{ kJ/mol}$ )<sup>35</sup>. The polymerization of the monomer (MIL) within the support pores results in a decrease of chain mobility and leads to solid PIL structure with low permeability, as observed for  $\text{CH}_4$  and even more for  $\text{CO}_2$  and  $\text{N}_2$  (Figure 5.11 A). However, the increase in RPBI-PIL permeability when the temperature is increased from 60 to 90°C is more significant for  $\text{CH}_4$ .

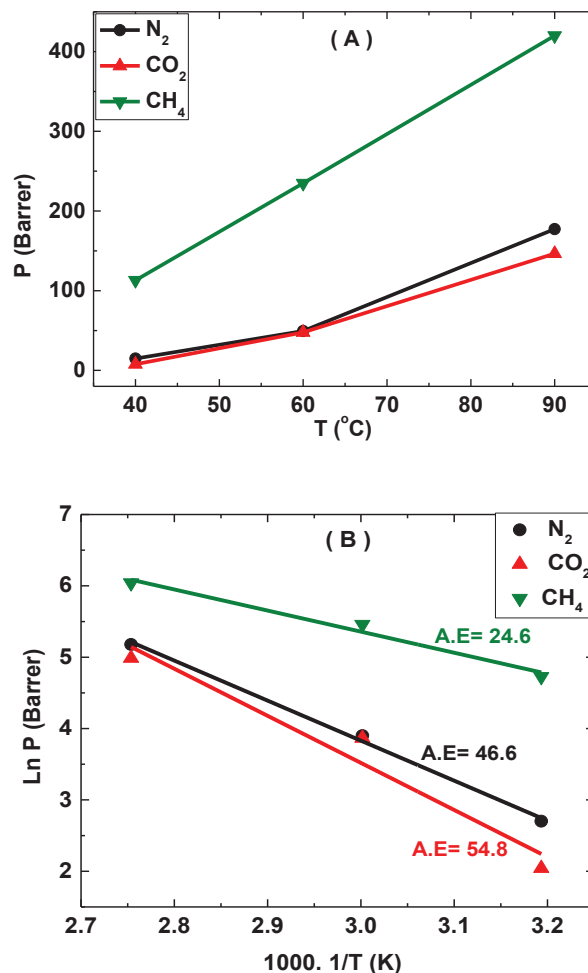


**Figure 5.11:** Influence of temperature on the evolution of single gas permeability values for RPBI-PIL membrane.

Moreover, the solid state (high viscosity) of PIL strongly impacts the membrane permeability, even though the PIL contains similar anion with strong interaction towards soluble gases. Indeed, CH<sub>4</sub> permeability values through RPBI-PIL membranes are lower than those measured for RPBI-MIL membranes. Furthermore, PIL has a higher density (MIL=1.6 g/mL, PIL=2.7 g/cm<sup>3</sup>) and therefore less free volume in its structure to dissolve gases. This explains why the gas permeability values through RPBI-PIL membranes are lower than those measured or reported for the other SILMs<sup>36</sup>.

**Table 5.4:** Comparison of experimental and literature data for the activation energies (E<sub>a</sub>) corresponding to single gas permeation through different types of SILMs.

Support	Gas	IL	E <sub>a</sub> (kJ/mol)
Polysulfone (PSF) <sup>37</sup>	CO <sub>2</sub>	HMIM TFSI	17.3
Alumina <sup>35</sup>	CO <sub>2</sub>	EMIM TFSI	8.03
Alumina <sup>35</sup>	CH <sub>4</sub>	EMIM TFSI	29.3
RPBI (this work)	CO <sub>2</sub>	H-VIM TFSI based -PIL	54.8
RPBI (this work)	CH <sub>4</sub>	H-VIM TFSI based -PIL	24.6

### 3.4.3 Ideal selectivity

The ideal selectivity was calculated taking into account the ratio of single gas permeabilities. The key difference between IL-based and polymer-based membranes is the impact of gas diffusivity on membrane selectivity. In IL membranes gas diffusivity selectivity is constant for a given gas pair, whereas the solubility selectivity controls the membrane selectivity<sup>21</sup>. In most polymeric membranes, the opposite behavior is observed: solubility selectivities are usually constant for gas pairs and diffusivity selectivity determines the membrane selectivity<sup>21, 38</sup>.

Membrane-based N<sub>2</sub> separation has a potential market in small natural gas operations. For such separations, membranes can either be N<sub>2</sub> permeable or CH<sub>4</sub> permeable. It was observed that the SILMs developed in this work can display relatively high CH<sub>4</sub>/N<sub>2</sub> ideal selectivity. The CH<sub>4</sub>/N<sub>2</sub> ideal selectivity for all the SILMs is plotted in Figure 5.12 as a function of CH<sub>4</sub> permeability. It is clear that the performance of the SILMs developed in this work are very promising in comparison with literature data for polymeric membranes (adapted from Lokhandwala et al.<sup>1</sup> and Scholes et al.<sup>2</sup>) and for other SILMs (based on imidazolium cation and TFSI anion with different supports)<sup>14, 20-24, 39-40</sup>. The

CH<sub>4</sub>/N<sub>2</sub> ideal selectivity of RPBI-MIL membranes is relatively constant in the temperature range 40-60 °C and higher than the values measured for RPBI-IL membranes at both 40 and 60 °C. Among all the prepared SILMs, RPBI-PIL displays the highest CH<sub>4</sub>/N<sub>2</sub> ideal selectivity, i.e. 7.6 with CH<sub>4</sub> permeability of 113 Barrer at 40 °C. Providing these results can be confirmed with membrane series, with gas mixtures and for long term experiments, the RPBI-PIL membranes appear as the most promising candidates for CH<sub>4</sub> upgrading applications.

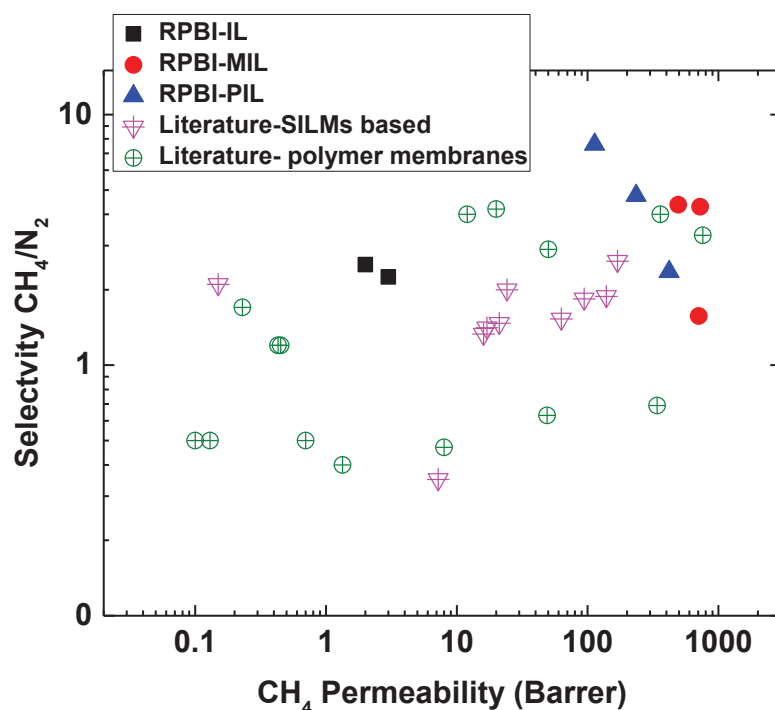


**Figure 5.12:** Comparison of ideal selectivity vs. permeability values for the membranes prepared in this work and for series of SILMs and polymer membranes reported in the literature.

#### 4. Conclusions

Three types of supported ionic liquid membranes have been prepared with 2 types of protic ionic liquids (ILs) based on the H-3-methylimidazolium TFSI and Vinyl-3-methylimidazolium TFSI. It has been shown that the SILMs based on the imidazolium cation are stable with temperature, especially those based on the PIL, possibly due to a better chemical affinity between the PIL and the RPBI support.

The effect of changing the functional group and carbon chain length on the imidazolium cation on the membrane single gas permeability was studied. An increase in CH<sub>4</sub> permeability with the carbon chain length of the IL cation was observed. The results obtained may be explained by solubility effects that become more relevant as the alkyl chain length of the IL cation increases. The single gas permeation results have also shown that the SILMs used in this work are permselective to CH<sub>4</sub> when compared with N<sub>2</sub>. For example, the RPBI-PIL membranes exhibit both high CH<sub>4</sub> permeability of 113 Barrer and high CH<sub>4</sub>/N<sub>2</sub> selectivity of 14.7 at 40 °C. The SILMs developed in this work thus have promising CH<sub>4</sub>/N<sub>2</sub> selectivities, higher than those reported in the literature for most polymeric membranes and for other SILMs membranes. Although their performance have still to be reproduced and tested for real gas mixture separations, the developed SILMs seems to be promising CH<sub>4</sub> upgrading applications.

## 5. References

1. Lokhandwala, K. A.; Pinnau, I.; He, Z.; Amo, K. D.; DaCosta, A. R.; Wijmans, J. G.; Baker, R. W., Membrane separation of nitrogen from natural gas: A case study from membrane synthesis to commercial deployment. *Journal of Membrane Science* **2010**, *346* (2), 270-279.
2. Scholes, C. A.; Stevens, G. W.; Kentish, S. E., Membrane gas separation applications in natural gas processing. *Fuel* **2012**, *96*, 15-28.
3. Baker, R. W.; Lokhandwala, K., Natural Gas Processing with Membranes: An Overview. *Industrial & Engineering Chemistry Research* **2008**, *47* (7), 2109-2121.
4. Ohs, B.; Lohaus, J.; Wessling, M., Optimization of membrane based nitrogen removal from natural gas. *Journal of Membrane Science* **2016**, *498*, 291-301.
5. Althuluth, M.; Overbeek, J. P.; van Wees, H. J.; Zubeir, L. F.; Haije, W. G.; Berrouk, A.; Peters, C. J.; Kroon, M. C., Natural gas purification using supported ionic liquid membrane. *Journal of Membrane Science* **2015**, *484*, 80-86.
6. Dai, Z.; Noble, R. D.; Gin, D. L.; Zhang, X.; Deng, L., Combination of ionic liquids with membrane technology: A new approach for CO<sub>2</sub> separation. *Journal of Membrane Science* **2016**, *497*, 1-20.
7. Anderson, J. L.; Dixon, J. K.; Brennecke, J. F., Solubility of CO<sub>2</sub>, CH<sub>4</sub>, C<sub>2</sub>H<sub>6</sub>, C<sub>2</sub>H<sub>4</sub>, O<sub>2</sub>, and N<sub>2</sub> in 1-Hexyl-3-methylpyridinium Bis(trifluoromethylsulfonyl)imide: Comparison to Other Ionic Liquids. *Accounts of Chemical Research* **2007**, *40* (11), 1208-1216.
8. Tome, L. C.; Marrucho, I. M., Ionic liquid-based materials: a platform to design engineered CO<sub>2</sub> separation membranes. *Chemical Society reviews* **2016**, *45* (10), 2785-2824.
9. Liang, L.; Gan, Q.; Nancarrow, P., Composite ionic liquid and polymer membranes for gas separation at elevated temperatures. *Journal of Membrane Science* **2014**, *450*, 407-417.
10. Lemus, J.; Eguizábal, A.; Pina, M. P., UV polymerization of room temperature ionic liquids for high temperature PEMs: Study of ionic moieties and crosslinking effects. *International Journal of Hydrogen Energy* **2015**, *40* (15), 5416-5424.
11. Lemus, J.; Eguizábal, A.; Pina, M. P., Endurance strategies for the preparation of high temperature polymer electrolyte membranes by UV polymerization of 1-H-3-vinylimidazolium bis(trifluoromethanesulfonyl)imide for fuel cell applications. *International Journal of Hydrogen Energy* **2016**, *41* (6), 3981-3993.

12. Shimoyama, Y.; Komuro, S.; Jindratsamee, P., Permeability of CO<sub>2</sub> through ionic liquid membranes with water vapour at feed and permeate streams. *The Journal of Chemical Thermodynamics* **2014**, *69*, 179-185.
13. Close, J. J.; Farmer, K.; Moganty, S. S.; Baltus, R. E., CO<sub>2</sub>/N<sub>2</sub> separations using nanoporous alumina-supported ionic liquid membranes: Effect of the support on separation performance. *Journal of Membrane Science* **2012**, *390–391*, 201-210.
14. Bara, J. E.; Gabriel, C. J.; Carlisle, T. K.; Camper, D. E.; Finotello, A.; Gin, D. L.; Noble, R. D., Gas separations in fluoroalkyl-functionalized room-temperature ionic liquids using supported liquid membranes. *Chemical Engineering Journal* **2009**, *147* (1), 43-50.
15. Sun, X.; Zhang, M.; Guo, R.; Luo, J.; Li, J., CO<sub>2</sub>-facilitated transport performance of poly(ionic liquids) in supported liquid membranes. *Journal of Materials Science* **2014**, *50* (1), 104-111.
16. Hu, X. D.; Tang, J. B.; Blasig, A.; Shen, Y. Q.; Radosz, M., CO<sub>2</sub> permeability, diffusivity and solubility in polyethylene glycol-grafted polyionic membranes and their CO<sub>2</sub> selectivity relative to methane and nitrogen. *Journal of Membrane Science* **2006**, *281* (1-2), 130-138.
17. Borjigin, H.; Stevens, K. A.; Liu, R.; Moon, J. D.; Shaver, A. T.; Swinnea, S.; Freeman, B. D.; Riffle, J. S.; McGrath, J. E., Synthesis and characterization of polybenzimidazoles derived from tetraaminodiphenylsulfone for high temperature gas separation membranes. *Polymer* **2015**, *71*, 135-142.
18. Han, S. H.; Lee, J. E.; Lee, K.-J.; Park, H. B.; Lee, Y. M., Highly gas permeable and microporous polybenzimidazole membrane by thermal rearrangement. *Journal of Membrane Science* **2010**, *357* (1-2), 143-151.
19. Pesiri, D. R.; Jorgensen, B.; Dye, R. C., Thermal optimization of polybenzimidazole meniscus membranes for the separation of hydrogen, methane, and carbon dioxide. *Journal of Membrane Science* **2003**, *218* (1-2), 11-18.
20. Ferguson, L.; Scovazzo, P., Solubility, Diffusivity, and Permeability of Gases in Phosphonium-Based Room Temperature Ionic Liquids: Data and Correlations. *Industrial & Engineering Chemistry Research* **2007**, *46* (4), 1369-1374.
21. Scovazzo, P.; Havard, D.; McShea, M.; Mixon, S.; Morgan, D., Long-term, continuous mixed-gas dry fed CO<sub>2</sub>/CH<sub>4</sub> and CO<sub>2</sub>/N<sub>2</sub> separation performance and selectivities for room temperature ionic liquid membranes. *Journal of Membrane Science* **2009**, *327* (1-2), 41-48.
22. Neves, L. A.; Crespo, J. G.; Coelho, I. M., Gas permeation studies in supported ionic liquid membranes. *Journal of Membrane Science* **2010**, *357* (1-2), 160-170.
23. Cserjési, P.; Nemestóthy, N.; Bélafi-Bakó, K., Gas separation properties of supported liquid membranes prepared with unconventional ionic liquids. *Journal of Membrane Science* **2010**, *349* (1–2), 6-11.
24. Tomé, L. C.; Mecerreyes, D.; Freire, C. S. R.; Rebelo, L. P. N.; Marrucho, I. M., Pyrrolidinium-based polymeric ionic liquid materials: New perspectives for CO<sub>2</sub> separation membranes. *Journal of Membrane Science* **2013**, *428*, 260-266.
25. Martins, C. F.; Neves, L. A.; Estevão, M.; Rosatella, A.; Alves, V. D.; Afonso, C. A. M.; Crespo, J. G.; Coelho, I. M., Effect of water activity on carbon dioxide transport in cholinium-based ionic liquids with carbonic anhydrase. *Separation and Purification Technology* **2016**, *168*, 74-82.
26. Joly, C.; Goizet, S.; Schrotter, J. C.; Sanchez, J.; Escoubes, M., Sol-gel polyimide-silica composite membrane: gas transport properties. *Journal of Membrane Science* **1997**, *130* (1), 63-74.
27. Crank, J., *The mathematics of diffusion*. Oxford university press: **1979**.
28. Eguizabal, A.; J.Lemus; Roda, V.; Urbiztondo, M.; Barreras, F.; Pina, M. P., Nanostructured electrolyte membranes based on zeotypes, protic ionic liquids and porous PBI membranes: Preparation, characterization and MEA testing. *International Journal of Hydrogen Energy* **2012**, *37* (8), 7221-7234.
29. Howlett, P. C.; Brack, N.; Hollenkamp, A. F.; Forsyth, M.; MacFarlane, D. R., Characterization of the Lithium Surface in N-Methyl-N-alkylpyrrolidinium Bis(trifluoromethanesulfonyl)amide Room-Temperature Ionic Liquid Electrolytes. *Journal of The Electrochemical Society* **2006**, *153* (3), A595.

30. Young, J. S.; Long, G. S.; Espinoza, B. F., Cross-linked polybenzimidazole membrane for gas separation. Google Patents: **2006**.
31. Moschovi, A. M.; Ntais, S.; Dracopoulos, V.; Nikolakis, V., Vibrational spectroscopic study of the protic ionic liquid 1-H-3-methylimidazolium bis(trifluoromethanesulfonyl)imide. *Vibrational Spectroscopy* **2012**, *63*, 350-359.
32. Jennifer L. Anthony; Jessica L. Anderson, E. J. M. a. J. F. B., Anion Effects on Gas Solubility in Ionic Liquids. *Journal of physical chemistry B* **2005**, *109* (13), 6366-6374.
33. Muldoon, M. J.; Aki, S. N. V. K.; Anderson, J. L.; Dixon, J. K.; Brennecke, J. F., Improving Carbon Dioxide Solubility in Ionic Liquids. *The Journal of Physical Chemistry B* **2007**, *111* (30), 9001-9009.
34. Blanchard, L. A.; Brennecke, J. F., Recovery of Organic Products from Ionic Liquids Using Supercritical Carbon Dioxide. *Industrial & Engineering Chemistry Research* **2001**, *40* (1), 287-292.
35. Adibi, M.; Barghi, S. H.; Rashtchian, D., Predictive models for permeability and diffusivity of CH<sub>4</sub> through imidazolium-based supported ionic liquid membranes. *Journal of Membrane Science* **2011**, *371* (1-2), 127-133.
36. Shahkaramipour, N.; Adibi, M.; Seifkordi, A. A.; Fazli, Y., Separation of CO<sub>2</sub>/CH<sub>4</sub> through alumina-supported geminal ionic liquid membranes. *Journal of Membrane Science* **2014**, *455*, 229-235.
37. Ilconich, J.; Myers, C.; Pennline, H.; Luebke, D., Experimental investigation of the permeability and selectivity of supported ionic liquid membranes for CO<sub>2</sub>/He separation at temperatures up to 125 °C. *Journal of Membrane Science* **2007**, *298* (1-2), 41-47.
38. Camper, D.; Bara, J.; Koval, C.; Noble, R., Bulk-Fluid Solubility and Membrane Feasibility of Rmim-Based Room-Temperature Ionic Liquids. *Industrial & Engineering Chemistry Research* **2006**, *45* (18), 6279-6283.
39. Condemarin, R.; Scovazzo, P., Gas permeabilities, solubilities, diffusivities, and diffusivity correlations for ammonium-based room temperature ionic liquids with comparison to imidazolium and phosphonium RTIL data. *Chemical Engineering Journal* **2009**, *147* (1), 51-57.
40. Scovazzo, P.; Kieft, J.; Finan, D.; Koval, C.; Dubois, D.; Noble, R., Gas separations using non-hexafluorophosphate [PF<sub>6</sub>]<sup>-</sup> anion supported ionic liquid membranes. *Journal of Membrane Science* **2004**, *238* (1-2), 57-63.









## **Chapter 6**

### **Summary, Conclusions and Future Work**



## 6.1 Development of Polybenzimidazole and Ionic Liquid based Membranes for High temperature PEMs

### 6.1.1 Summary

The success of the High temperature proton exchange membrane fuel cell (HT-PEMFC) direction is very much dependent on the development of the membrane material. With facilitated proton transport chemistries, great progresses in designing and fabricating facilitated PEMs have been accomplished.

The objective of this first part of the PhD was to fabricate highly conductive electrolyte membranes capable to operate above 120 °C under anhydrous conditions and in the absence of mineral acids, without sacrificing the mechanical behavior. The followed rationale is based on the combination of polybenzimidazole (PBI) microsieves as structural supports and poly-imidazolium based ionic liquid moieties as conducting phase.

Two types of PBI microsieves have been prepared following two different microfabrication processes (see Figure 6.1): straight porous PBI microsieves, denoted as SPBI; and hierarchically structured PBI microsieves, denoted as HPBI, respectively.

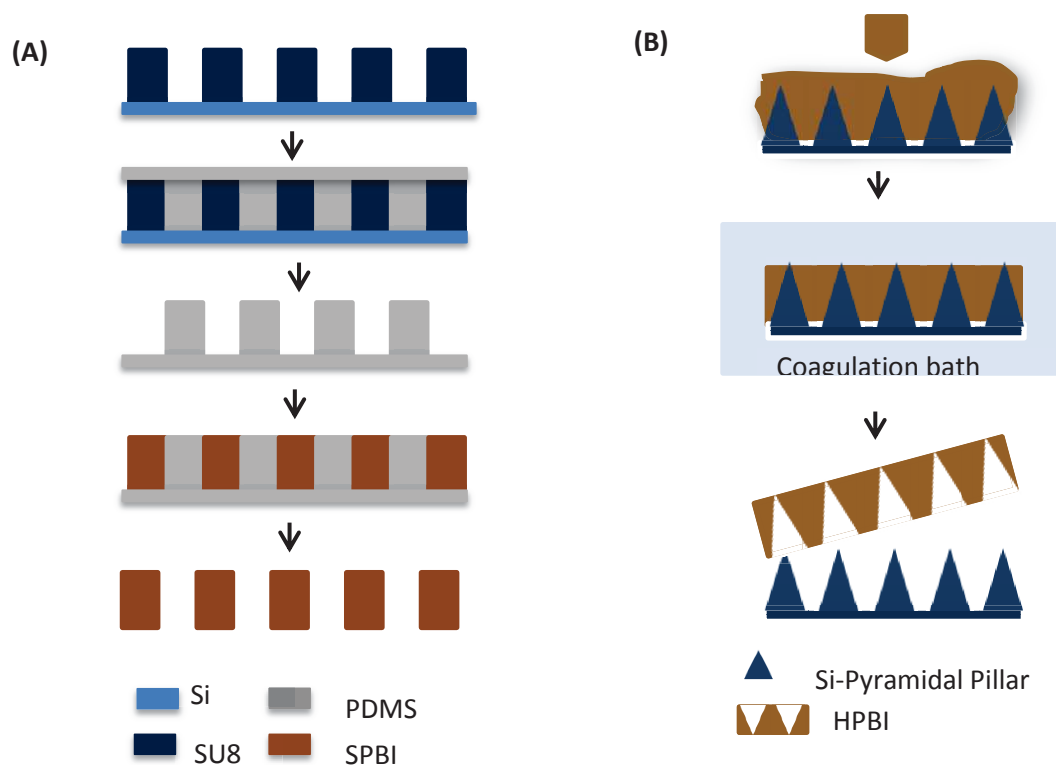


**Figure 6.1:** Schematic illustration of the fabrication processes: A) micro transfer moulding technique and B) Phase Separation MicroFabrication for SPBI and HPBI microsieves respectively.

Polymeric ionic liquids (PILs) have triggered great interest as all solid-state flexible electrolytes because of safety and superior thermal, chemical, and electrochemical stability. In this PhD thesis, the protic 1-H-3-vinylimidazolium bis(trifluoromethanesulfonyl)imide monomeric ionic liquid (MIL) has been mainly selected due to its high proton conductivity, low water uptake values as well as thermal stability.

The consecution of a polymeric container with optimized pore architecture is extremely essential since the performance of PEM based on immersing a porous support into ionic liquids (ILs), mainly depends on the porous structure. Therefore, our research efforts have been directed to improve both, the ion conductivity and the dimensional stability of the polymeric ionic liquid (PIL) supported membranes by a proper design of the porous architecture. Herein, the diminished dimensional and mechanical stability of poly[1-(3H-imidazolium)ethylene]bis(trifluoromethanesulfonyl)imide has been improved thanks to its infiltration on a polybenzimidazole (PBI) support with specific pore architecture (see Figure 6.2).

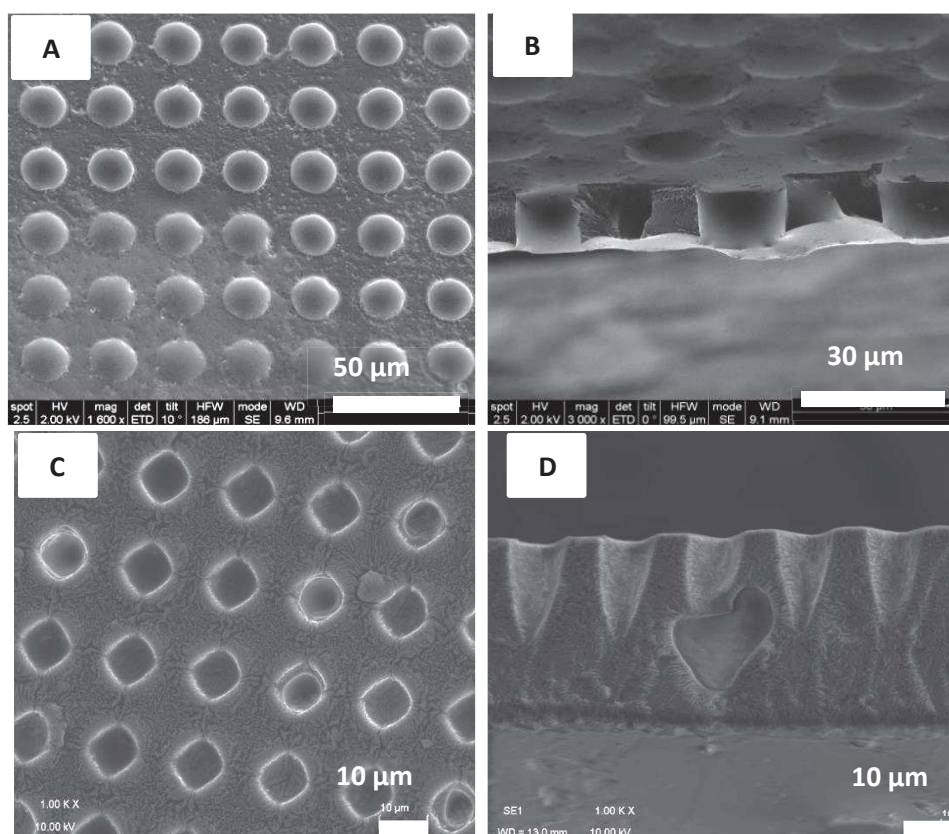


**Figure 6.2:** SEM images of the PIL-PBI membranes developed in this work for high temperature applications: A) PIL-SPBI surface; B) PIL-SPBI cross section; C) PIL-HPBI surface; D) PIL-HPBI cross section.

The infiltration configuration, cross-linker addition and “in situ” UV polymerization conditions were taken as optimization parameters for both PBI type microsieves. The important findings in this topic are included in the conclusions section below.

### **6.1.2 Conclusions**

In this study, we describe for the first time the fast anhydrous proton transport via polyionic liquid microchannels imprinted on PBI films. The results are quite encouraging and suggest that these PEMs might be incorporated in Fuel cells as substituent of conventional and expensive proton exchange membranes such as Nafion or Ultrex for high temperature applications. The main conclusions derived from the experimental results are:

1. For the consecution of SPBI containers by microtransfer molding technique, less than 25  $\mu\text{m}$  in thickness, 17  $\mu\text{m}$  in pore size and 36% in porosity, the PBI concentration in the final polymer casting solution (0.88% wt in DMAc) was the key factor controlling the PDMS mold wetting at 60 °C, and the replication process.
2. For the consecution of HPBI containers by liquid phase separation micromolding method, less than 40  $\mu\text{m}$  thickness, 9  $\mu\text{m}$  in macropore size and 42% in porosity, the casting distance between the casting Knife and the Si mold was the key factor controlling the replication process and the thickness of the PBI skin layer.
3. Flexible electrolyte membranes have been successfully prepared by the infiltration of 1-H-3-vinylimidazolium bis(trifluoromethane sulfonyl)imide solution into SPBI or HPBI microsieves followed by in situ 2 hours UV polymerization (365 nm-2.4 mW/cm<sup>2</sup>) of the ionic moieties. It has been observed the complete and uniform filling of PBI macropores with PIL in absence of cracks and defects, resulting in free standing films easy to handle without any difficulty.
4. All the composite PIL-PBI membranes are stable up to 300 °C, which is far above the operating temperature for HT PEMFCs. Hydrogen bonding interactions between the ionic liquid moieties and the confining PBI support at the pore-wall surface have been identified from the ATR-FTIR analysis and confirmed by TGA results and calculations of Arrhenius-type activation energies for proton transport.
5. A moderate enhancement in the thermal and mechanical stability of PIL-PBI membranes is attained by the cross-linking of the polycationic network by divinylbenzene (from 0.2 mol % up to 1 mol % referred to the MIL). The Young Modulus of PIL-PBI membrane is approximately 1 order of magnitude higher than the exhibited by the pure PIL counterpart and clearly superior to the characteristic value for acid-doped dense PBI

membranes. As expected, the  $E_a$  for proton transport slightly increases with the % of cross-linker agent due to the loss in long-range segmental motion, among the tested, the PIL-PBI samples containing 1 mol % of divinylbenzene as CL outstands as the optimal trade-off between proton transport and mechanical properties for proper handling and assembly.

6. The PBI microsieve architecture plays the key role on PEM's proton conductivity. The registered conductivity values for PIL-PBI microsieves are not only explained by the relative amount of proton conducting phase. When compared with PIL supported on randomly porous PBI (RPBI) support (120  $\mu\text{m}$  in thickness, less than 1  $\mu\text{m}$  in pore size and 68 %), the importance of PIL channels connectivity formed during the phase inversion process is clearly outlined. The proton transport is faster for PEMs prepared from HPBI in spite of lower PIL amount. This result is attributed both to the higher surface area provided by HPBI and to the porous network connectivity at the perforated macropore/intrinsic bulk porosity interface. Well-connected pores at the straight macropore/intrinsic porosity interface are clearly distinguished on the straight macropore wall surface. In addition, worm-shape pores below 200 nm in size are predominant along the whole thickness. The interactions of PIL molecules with the walls of the confining intrinsic PBI pores slow down the proton transport dynamics and subsequently provokes a notably increase of  $E_a$ .
7. The HPBI microsieve architecture leads to an intermediate behaviour in terms of conduction performance, when compared to RPBI and SPBI counterparts; but it is greatly superior in terms of mechanical properties. The HPBI microsieves retain the advantageous features of both as higher and well connected PIL loadings are achievable, without sacrificing the mechanical strength.

Overall, our results are of fundamental importance for the development of outperforming, low-cost PEMs as a good alternative to acid doped PBI for HTPEMs under anhydrous conditions. Table 6.1 collects all the reported conductivity data based on PBI and IL as a function of temperature for a proper comparison to the membrane conductivity values achieved in this PhD thesis. Except for the PIL-PBI based on randomly porous supports, the conduction performance of HTPEMs developed in this thesis is clearly outstanding when compared to the exhibited by PEMs without phosphoric acid doping.

**Table 6.1:** Comparison of our results with current progress concerning PBI-IL based HT-PEMs

System	PBI support type	IL/PIL name	T (°C)	$\sigma$ (mS.cm <sup>-1</sup> )	Reference
<b>Acid doped</b>					
PBI+H <sub>3</sub> PO <sub>4</sub> +IL <sup>1</sup>	Blend	1-methyl-3-propylmethylimidazolium Dihydrogenphosphate [PMImH <sub>2</sub> ][PO <sub>4</sub> ]	150	2	1
PBI+ H <sub>3</sub> PO <sub>4</sub> + IL-NaY zeolite <sup>2</sup>	Dense	1-H-3-methylimidazolium bis(trifluoromethanesulphonyl)imide ([HMI][TFSI])	200	54	2
PBI+HCL+IL a <sup>3</sup>	Dense	Diethylmethylammonium trifluoro methanesulfonate [DEMA][TfO]	160	21	3
ABPBI + H <sub>3</sub> PO <sub>4</sub> +IL <sup>4</sup>	Dense	1-butyl-3-ethylbenzimidazolium dihydrogen phosphate (BEBzIm- H <sub>2</sub> PO <sub>4</sub> )	150	0.1	4
PBI + H <sub>3</sub> PO <sub>4</sub> +IL <sup>5</sup>	Blend	1,3-di(3-methylimidazolium)propanebis (trifluoromethylsulfonyl)imide(PDC <sub>3</sub> )	180	81	5
PBI + H <sub>3</sub> PO <sub>4</sub> + IL <sup>6</sup>	Blend	1,6-di(3-methylimidazolium) hexane bis (hexafluorophosphate) (PDC <sub>6</sub> )	180	78	6
PBI+IL+ H <sub>3</sub> PO <sub>4</sub> <sup>7</sup>	Porous	1-ethyl-3-methylimidazolium bis(trifluoromethanesulfonyl)imide	160	60	7
PBI+ IL-graphite-oxide <sup>8</sup>	Blend	1-(3-aminopropyl)-3-methylimidazolium bromide	175	35	8
<b>Acid free</b>					
PBI+ IL <sup>9</sup>	Blend	1-hexyl-3-methylimidazolium trifluoromethanesulfonate (HMI-Tf)	250	16	9
PBI + IL <sup>10</sup>	Hybrid	Diethylamine bisulphate/sulphate ionic liquid	200	40	10
PBI+PIL <sup>11</sup>	Blend	poly(diallyl dimethyl ammonium trifluoride methane sulphonate	150	70	11
PBI+IL <sup>12</sup>	Randomly Porous	1-H-3methylimidazoliumbis (trifluoromethanesulfonyl)imide [HMIm] [TFSI]	150	1.5	12
PBI +PIL <sup>13</sup>	Randomly Porous	1-H-3-vinylimidazolium bis(trifluoromethanesulfonyl)imide	200	300	13
SPBI + Crosslinked PIL	Straight Porous	1-H-3-vinylimidazolium bis(trifluoromethanesulfonyl)imide	200	53.3	Our results
HPBI + Crosslinked PIL	hierarchic al Porous	1-H-3-vinylimidazolium bis(trifluoromethanesulfonyl)imide	200	85	Our results



### 6.1.3 Future work

We have prepared innovative HTPEMs consisting of straight and hierarchically structured PIL channels embedded in PBI microsieves. However, such ion conducting membranes should be integrated in a Membrane Electrode Assembly (MEA) that includes a gas diffusion layer and the electrocatalyst.

In general, membrane–electrode assemblies (MEA) are fabricated by hot pressing of the as-prepared electrodes onto the electrolyte membrane. The primary challenge in preparing MEAs is to achieve good contact between the membrane, catalyst layer and gas diffusion layer (GDL) in order to maximize catalyst utilization during cell operation. An integrated MEA structure is also essential to obtain long-term operation. As future work, the use of PBI fiber-mat structures is proposed as diffusional barriers to prevent the conductor leakage/dragging with time on stream from the PIL-PBI PEMs and at the same time, to reduce fuel cross-over. Some preliminary attempts on the preparation of PBI gas diffusion layers have been already performed by using electrospinning techniques (see Figure 6.3). From the point of view of large scale manufacturing, the PBI GDLs could be deployed on the both sides of the PIL-PBI membranes

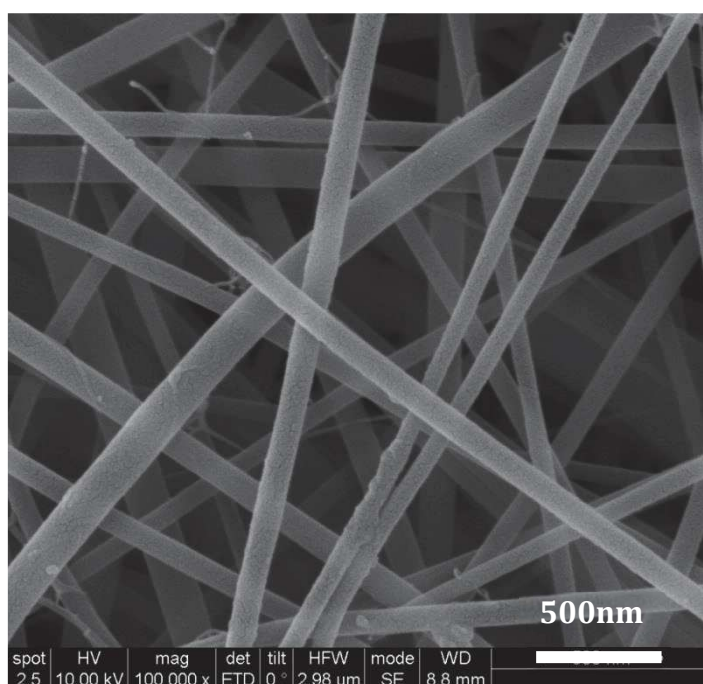


**Figure 6.3:** SEM images of pure PBI fibers prepared by electrospinning (Casting solution: 20 % PBI and 4 % LiCl in DMAc. Conditions: Positive voltage is 25.06kV and the rate is 0.25mL /h at 25 °C)

Another open research topic is the catalytic activation of the as prepared PIL-PBI membranes. A straightforward strategy could rely on the stabilization of catalytic nanoparticles in the ionic liquid

solution (definition of the optimal ionic liquid phase formulation) previous to UV polymerization step, or in a more controlled way after the bulky MIL embedding. In such way, the preparation of three-layer integrated membrane electrode assemblies MEAs would be notably simplified.

Although high conductivity and mechanical stability values were found in this work by using HPBI microsieves; there is a potential approach capable to eventually enhance the performance by foil stacking. The PBI micromonolith-type stack was prepared in our lab by the assembly of five PBI circular microsieves 20 mm in diameter for catalytic applications<sup>14</sup>. According to the procedure described in Figure 6.4, the desired numbers of PBI membranes are located in a stack; at the same time, two dense PBI O-rings are placed in the same stack but one on the top and the other at the bottom. A 5% wt. PBI solution in DMAc is deposited only on the round-corner of this stack and it is submitted at 90 °C during at least 4 hours. Using these PBI stack, proton exchange membranes were fabricated (Figure 6.5) by infiltration of 1-H-3-vinyl imidazolium bis(trifluoromethanesulfonyl)imide liquid followed by in-situ UV polymerization. Only 3 membranes are needed for that, and the surface available for PIL not only is limited to a cylinder, but also, the surface between layers is going to contribute to total surface.

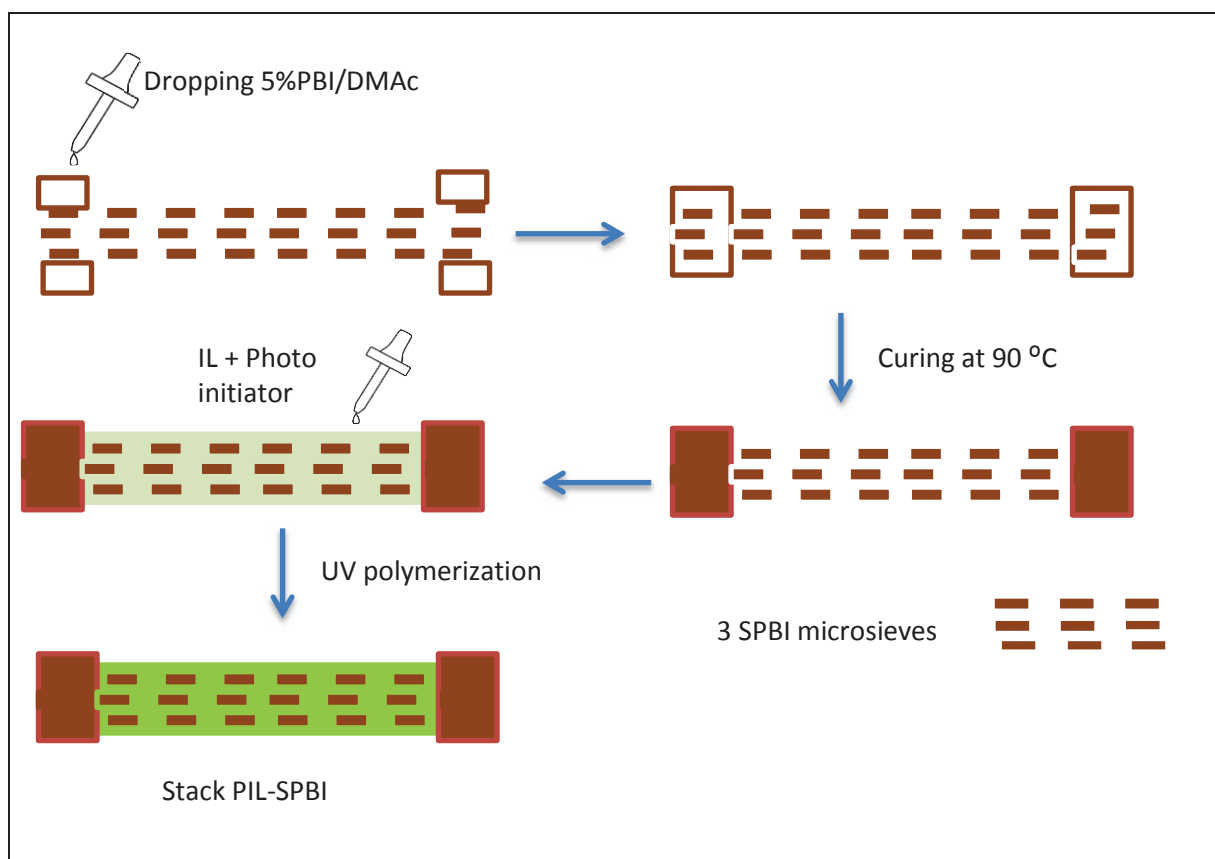


**Figure 6.4:** Schematic overview of PIL-PBI PEM based on PBI stack

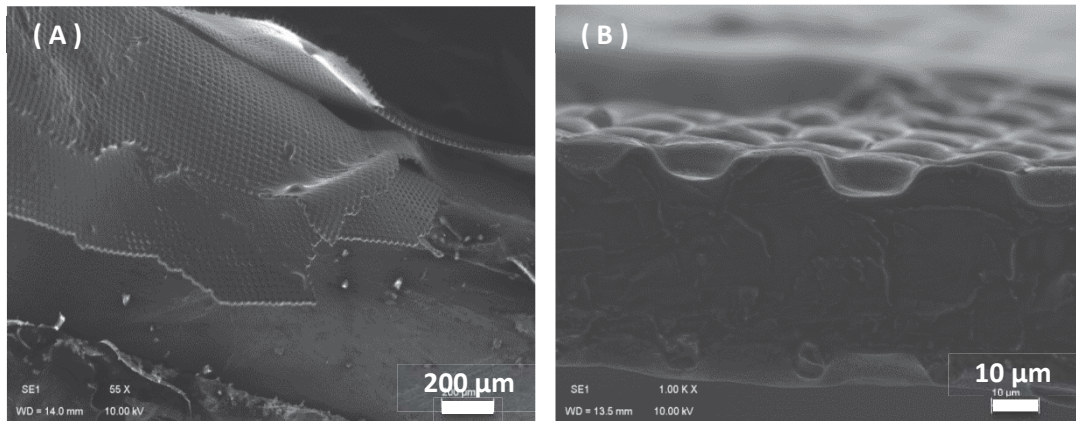


**Figure 6.5:** SEM images of stack PIL- stack PBI membranes: A) surface; B) Cross section images.

## **6.2 Supported Ionic liquid membranes (SILMs) based on PBI and protic Ionic liquids for methane upgrading.**

### **6.2.1 Summary**

The natural gas upgrading, i.e. removal of CO<sub>2</sub> and N<sub>2</sub>, is undoubtedly a major industrial gas separation application where membranes arise as promising alternative at small scale.

The objective of this second part of the work was to develop CH<sub>4</sub> selective Supported Ionic Liquid Membranes (SILMs). Once again, the rationale followed is based on the combination of polybenzimidazole (PBI) microsieves as structural supports, to take advantage of both endurance and thermal properties, and protic ionic liquids with imidazolium and trifluoromethane sulfonyl)imide ions due to their CH<sub>4</sub> solubility properties. Although the negligible protic ionic liquid vapor pressure alleviates one of the problems associated with traditional SILMs, namely liquid volatility; expulsion of the liquid from the membrane pores is a major concern. A proper design of the support, with sub-micron pores, combined with an ionic liquid having high surface tension could lead to SLIM with adequate physical stability for applications involving moderate to high trans-membrane pressures. Therefore, random porous PBI (RPBI) supports, obtained by phase separation method, have been extensively used. In addition, polymerization of RTILs could provide additional advantages in terms of safety, stability and mechanical properties.

In this study, three classes of SILMs, based on PBI with the protic 1-H-3-methylimidazolium bis(trifluoromethane sulfonyl)imide (IL), the monomeric 1-H-3-vinylimidazolium bis(trifluoromethane sulfonyl)imide (MIL) and the polymeric poly[1-(3H-imidazolium)ethylene]bis(trifluoromethanesulfonyl)imide(PIL) have been successfully fabricated and characterized by single gas permeation measurements. Results revealed that the prepared membranes were highly permselective to CH<sub>4</sub> and thus potentially very promising for CH<sub>4</sub>/N<sub>2</sub> gas mixture separation. The major outcomes of this topic are summarized in the conclusions section below.

### **6.2.2 Conclusions**

Herein, porous PBI supports is combined for the first time with commercially available ionic liquids based on the protic 1-H-3-methylimidazolium bis(trifluoromethane sulfonyl)imide to prepare CH<sub>4</sub>/N<sub>2</sub> selective SILMs. The single gas permeation results reveal that the SILMs studied in this work perform

better than previously reported polymeric membranes. The main conclusions obtained from the experimental results are:

1. For the successful preparation of RPBI supports (with pore sizes of 50-250 nm on air side and 30-50 nm on the bottom side and with a porosity of  $63.7\% \pm 2.7$ ) by phase separation method, the polymer casting solution with 16% wt. of solids was chosen.
2. All the developed SILMs are thermally stable up to 310 °C under N<sub>2</sub> atmosphere which indicated that all of these SILMs had good thermal stabilities. Among the developed SILMs, PIL based membrane was handled without any difficulty while others (i.e. IL and MIL based SILMs) were brittle to handle due to the crystalline state of IL and MIL at room temperature.
3. The vinyl group on imidazolium cation (i.e. MIL based SILMs) leads to an increase in CH<sub>4</sub> permeability, when compared to IL based SILMs. This result is attributed to the solubility factor, an effect that becomes more relevant as the alkyl chain length of the imidazolium cation increases (from methyl in the IL to vinyl in the MIL). It is observed for both IL and MIL based SILMs, that the single gas permeability values at 60 °C increases in the order : CH<sub>4</sub> > CO<sub>2</sub> > N<sub>2</sub>.
4. The polymerization of the monomer (MIL) into the PBI supports plays a significant role. The PIL based SILMs exhibited low gas permeability values compared with MIL based SILM for all the gases at all the applied temperatures. The polymerization of the MIL into the membranes results in higher viscosity and chain mobility inhibition leading to solid PIL structure and lower permeability. Nevertheless, these membranes are greatly superior in terms of handling and mechanical properties compared to IL based and MIL based SILMs. For the tested PIL based SILMs, the tendency for permeability values at all the tested temperatures is: CH<sub>4</sub> > N<sub>2</sub> > CO<sub>2</sub>. It is also observed that gas permeability values always increase with temperature within the 40-90°C window. Among the tested SILMs, PIL based SILMs have shown the highest CH<sub>4</sub>/N<sub>2</sub> ideal selectivity, i.e 7.6 ; i.e. superior to values reported in the literature for most polymeric membranes, which makes these membranes promising for CH<sub>4</sub> upgrading.

On the whole, taking into account the state of the art for CH<sub>4</sub> upgrading with membranes, it can be concluded that the use of SILMs appears as an emerging field with enormous potential, although membrane performance for real gas mixture separations has still to be demonstrated. The additional benefits derived from the use of ionic liquids (negligible volatility, chemical and structural platform to design endless tasks specific materials) and membrane modules (low energy consumption,

reduced environmental impact, large S/V ratio, easy incorporation to existing conventional unit operations) would also have to take into account on the feasibility studies.

### **6.2.3 Future work**

The superior CH<sub>4</sub>/N<sub>2</sub> performance of the herein developed SILMs can be appreciated through the analysis of values reported in the literature for conventional polymeric membranes. It is interesting to observe how the effect of the vinyl group chemistry can be used to make difference in permeability. Nevertheless, more efforts devoted to a comprehensive study of ionic liquid formulations selective to CH<sub>4</sub> are still required for further CH<sub>4</sub> selectivity promotion, including in the presence of gas mixtures.

In addition, an important concern that should be also considered for future research is the mechanical stability of the SILMs. The development of PIL-based membranes targeting the critical combination of high CH<sub>4</sub>/N<sub>2</sub> and high chemical and mechanical stability is required to place these membranes at the doorway of industrially relevant membrane-based gas separation processes.

Furthermore, the lack of experimental data under real industrial conditions requires additional investigation efforts. The evaluation of the behavior of SILMs under different humidity conditions and upon exposure to different chemical environments is essential for their application in gas separation processes. Particular focus on operating conditions may be recommended: testing the efficiency of SILMs at high pressures; testing different binary gas mixtures compositions, ranging from pure CH<sub>4</sub> to either pure CO<sub>2</sub> or N<sub>2</sub>, depending on the separation envisaged; testing gases with different humidity contents and performing long-term experiments.



## Résumé de la thèse

### 1. Membranes échangeuses de protons à haute température (HT-PEM) pour application dans les piles à combustible

Le succès des piles à combustible à base de HT-PEM dépend fortement du matériau membranaire. D'importants progrès ont été accomplis dans la conception de PEMs à transport facilité de protons. L'objectif de la première partie de ce travail de thèse était de fabriquer des membranes électrolytes à haute conductivité, capables de fonctionner au-dessus de 120°C dans des conditions anhydres, sans acides minéraux, et sans sacrifier la résistance mécanique. La stratégie suivie combine l'utilisation de micro-filtres (support) à base de polybenzimidazole (PBI) présentant un réseau de pores ordonnés, et de liquides ioniques (ILs) à base de polyimidazolium comme phase conductrice. Deux types de micro-filtres de PBI ont été préparés: avec un réseau de pores droits (SPBI), ou avec une structure poreuse hiérarchique (HPBI). Les ILs polymérisés (PIL) suscitent un grand intérêt comme tous les électrolytes flexibles à l'état solide en raison de leur sécurité d'utilisation et de leur bonne stabilité thermique, chimique et électrochimique. Dans ce travail, un IL monomérique protique 1-H-3-vinylimidazolium bis(trifluorométhanesulfonyl)imide a été choisi pour sa conductivité protonique élevée, sa faible rétention d'eau et sa bonne stabilité thermique. Puisque les performances d'une PEM formée par immersion d'un support poreux dans un IL dépendent surtout de la structure poreuse du support, il est essentiel d'optimiser l'architecture des pores réservoirs. Ainsi, nos travaux visent à améliorer à la fois la conductivité ionique et la stabilité dimensionnelle des PEMs à base de PIL par une conception appropriée de l'architecture poreuse. En effet, la faible stabilité dimensionnelle et mécanique du poly [1-(3H-imidazolium)éthylène] bis(trifluorométhanesulfonyl) imide est améliorée grâce à son infiltration dans un support PBI architecturé. La configuration d'infiltration, l'addition d'agent réticulant et les conditions de polymérisation UV "*in situ*" ont été considérées comme paramètres d'optimisation pour les deux types de micro-tamis en PBI.

### 2. Membranes à base de liquide ionique supporté (SILM) pour la valorisation du méthane

La valorisation du gaz naturel, intégrant l'élimination de CO<sub>2</sub> et N<sub>2</sub>, est l'une des applications de séparation des gaz industriels où les membranes sont une alternative prometteuse à petite échelle. L'objectif de nos travaux était de développer des membranes de type SILM, sélectives au CH<sub>4</sub>. Notre stratégie combine des micro-tamis à base polybenzimidazole (PBI) comme supports présentant une bonne endurance et de bonnes propriétés thermiques, et des liquides ioniques (ILs) protiques avec des ions imidazolium et trifluorométhane sulfonylimide pour la solubilité du CH<sub>4</sub>. Bien que la faible pression de vapeur du IL protique atténue sa volatilité dans les SILMs traditionnels, son expulsion hors des pores reste une préoccupation majeure. Un design approprié du support, avec des pores



submicroniques, combiné à un IL de tension superficielle élevée, devrait générer des SILMs plus stables, adaptées aux applications à pression transmembranaire modérée ou élevée. Ainsi, des supports PBI à porosité aléatoire (RPBI), obtenus par séparation de phase, ont été largement utilisés. En outre, la polymérisation des RTILs peut fournir d'autres avantages en termes de sécurité, de stabilité et de propriétés mécaniques. Dans cette étude, trois classes de SILMs à base de PBI, avec le IL protique 1-H-3-méthylimidazolium bis(trifluorométhane sulfonyl)imide (IL), le monomérique 1-H-3-vinylimidazolium bis(trifluorométhane sulfonyl)imide (MIL) et le polymérique poly[1-(3H-imidazolium)éthylène] bis(trifluorométhanesulfonyl)imide (PIL) ont été fabriqués avec succès et caractérisés en perméation de gaz purs. Des membranes perméatives au méthane ont été obtenues, qui sont très prometteuses pour la séparation de mélanges de gaz tels que CH<sub>4</sub>/N<sub>2</sub>.

### 6.3 References

1. Ye, H.; Huang, J.; Xu, J. J.; Kodiweera, N. K. A. C.; Jayakody, J. R. P.; Greenbaum, S. G., New membranes based on ionic liquids for PEM fuel cells at elevated temperatures. *Journal of Power Sources* **2008**, *178* (2), 651-660.
2. Eguizábal, A.; Lemus, J.; Pina, M. P., On the incorporation of protic ionic liquids imbibed in large pore zeolites to polybenzimidazole membranes for high temperature proton exchange membrane fuel cells. *Journal of Power Sources* **2013**, *222*, 483-492.
3. Liu, S.; Zhou, L.; Wang, P.; Zhang, F.; Yu, S.; Shao, Z.; Yi, B., Ionic-liquid-based proton conducting membranes for anhydrous H<sub>2</sub>/Cl<sub>2</sub> fuel-cell applications. *ACS applied materials & interfaces* **2014**, *6* (5), 3195-200.
4. Hernández Carrillo, R.; Suarez-Guevara, J.; Torres-González, L. C.; Gómez-Romero, P.; Sánchez, E. M., Incorporation of benzimidazolium ionic liquid in proton exchange membranes ABPBI-H<sub>3</sub>PO<sub>4</sub>. *Journal of Molecular Liquids* **2013**, *181*, 115-120.
5. Hooshyari, K.; Javanbakht, M.; Adibi, M., Novel composite membranes based on PBI and dicationic ionic liquids for high temperature polymer electrolyte membrane fuel cells. *Electrochimica Acta* **2016**, *205*, 142-152.
6. Hooshyari, K.; Javanbakht, M.; Adibi, M., Novel composite membranes based on dicationic ionic liquid and polybenzimidazole mixtures as strategy for enhancing thermal and electrochemical properties of proton exchange membrane fuel cells applications at high temperature. *International Journal of Hydrogen Energy* **2016**, *41* (25), 10870-10883.
7. Jheng, L.-C.; Hsu, S. L.-C.; Tsai, T.-Y.; Chang, W. J.-Y., A novel asymmetric polybenzimidazole membrane for high temperature proton exchange membrane fuel cells. *Journal of Materials Chemistry A* **2014**, *2* (12), 4225.
8. Xu, C.; Liu, X.; Cheng, J.; Scott, K., A polybenzimidazole/ionic-liquid-graphite-oxide composite membrane for high temperature polymer electrolyte membrane fuel cells. *Journal of Power Sources* **2015**, *274*, 922-927.
9. Wang, J. T.-W.; Hsu, S. L.-C., Enhanced high-temperature polymer electrolyte membrane for fuel cells based on polybenzimidazole and ionic liquids. *Electrochimica Acta* **2011**, *56* (7), 2842-2846.
10. Mamlouk, M.; Ocon, P.; Scott, K., Preparation and characterization of polybenzimidazole/diethylamine hydrogen sulphate for medium temperature proton exchange membrane fuel cells. *Journal of Power Sources* **2014**, *245*, 915-926.
11. Rewar, A. S.; Chaudhari, H. D.; Illathvalappil, R.; Sreekumar, K.; Kharul, U. K., New approach of blending polymeric ionic liquid with polybenzimidazole (PBI) for enhancing physical and electrochemical properties. *Journal of Materials Chemistry A* **2014**, *2* (35), 14449-14458.
12. van de Ven, E.; Chairuna, A.; Merle, G.; Benito, S. P.; Borneman, Z.; Nijmeijer, K., Ionic liquid doped polybenzimidazole membranes for high temperature Proton Exchange Membrane fuel cell applications. *Journal of Power Sources* **2013**, *222*, 202-209.
13. Lemus, J.; Eguizábal, A.; Pina, M. P., Endurance strategies for the preparation of high temperature polymer electrolyte membranes by UV polymerization of 1-H-3-vinylimidazolium bis(trifluoromethanesulfonyl)imide for fuel cell applications. *International Journal of Hydrogen Energy* **2016**, *41* (6), 3981-3993.
14. Eguizábal, A.; Urbiztondo, M. A.; Pina, M. P., Pt based catalytic coatings on poly(benzimidazole) micromonoliths for indoor quality control. *Catalysis Today* **2015**, *241*, 114-124.
15. Dai, Z.; Noble, R. D.; Gin, D. L.; Zhang, X.; Deng, L., Combination of ionic liquids with membrane technology: A new approach for CO<sub>2</sub> separation. *Journal of Membrane Science* **2016**, *497*, 1-20.



## Curriculum Vitae-PARASHURAM KALLEM

**Address:**

Chemical and Environmental Engineering Department. Nanoscience Institute of Aragon (INA). Edif. I+D+i, Campus Rio Ebro, c/Mariano Esquillor s/n.  
University of Zaragoza.  
50018 Zaragoza, Spain  
E-mail: [parshukallem@gmail.com](mailto:parshukallem@gmail.com)



**Permanant address:** Nandanam Village,  
Bhongir Mandal, 508285 .Telangana, India

<b>EDUCATION &amp; Research Experience</b>	
03-2013 to 03-2017	<p>PhD- EUDIME fellowship (Erasmus Mundus Doctorate in Membrane Engineering-II).</p> <p><i>Title: Development of Polybenzimidazole and Ionic Liquid based Membranes for High temperature Proton Exchange Membranes (PEMs) and Gas Separation Applications</i></p> <p><b>University of Zaragoza (Home University):</b> Chemical and Environmental Engineering Department. Nanoscience Institute of Aragon (INA), Zaragoza, Spain.</p> <p><b>University of Twente (Host university 1):</b> Membrane Science and Technology, AE, Enschede, The Netherlands.</p> <p><b>University of Montpellier -2 Host University 2:</b> Institut Européen des Membranes 34095, MONTPELLIER cedex 5- France</p>
3-2011to 2-2012	<p>Researcher Myonji University, Yongin. &amp; Incheon University, Incheon. South Korea,</p>
12-2008 to 02-2011	<p>Project Researcher. <b>CSMCRI</b> (Central Salt and Marine Chemicals Research Institute) Reverse Osmosis (Membrane) Division, Bhavnagar, Gujrat, India</p>
6-2006 to 5-2008	<p>M.Sc. Chemistry (Analytical) <b>Banaras Hindu University (BHU),</b> Varanasi, UP, INDIA</p>
6-2003 to 5-2006	<p>B.Sc. (Botany, Zoology &amp; Chemistry) <b>Osmania University,</b> Hyderabad, Telangana, India</p>

---

## PUBLICATIONS

---

10. **Parashuram Kallem**, Martin Drobek, Anne Julbe, Maria Pilar Pina, Reyes Mallada. 2016. Supported Ionic liquid membranes (SILMs) based on PBI and protic Ionic liquids for methane upgrading. RSC Advances. Ready to submit. (IF 3.2)
9. **Parashuram Kallem**, Martin Drobek, Anne Julbe, Erik J. Vriezolk, Reyes Mallada and Maria Pilar Pina. 2016. Hierarchical porous Polybenzimidazole microsieves: An efficient architecture for anhydrous proton transport via Poly-ionic Liquids. ACS Applied Materials & Interfaces. 2017, 9 (17), 14844–14857. (IF 7.14).
8. **Parashuram Kallem**, Adela Eguizabal, Reyes Mallada and Maria Pilar Pina. 2016. Constructing straight Poly-ionic liquid microchannels for fast anhydrous proton transport. ACS Applied Materials & Interfaces. 2016, 8 (51), 35377–35389. (IF 7.14).
7. **K. Parashuram**, S.K. Maurya, H.H. Rana, P.S. Singh, P. A.V.R. Reddy. 2013. Tailoring the molecular weight cut off values of polyacrylonitrile based hollow fibre ultrafiltration membranes with improved fouling resistance by chemical modification. Journal of Membrane Science, 425-426: 251-261. (IF 5.7)
6. P.S. Singh, P. Ray, J.J. Trivedi, A. Prakash Rao, **K. Parashuram** & A.V.R. Reddy. 2013. RO membrane treatment of domestic grey-water containing different detergent types. Desalination and Water Treatment. 52:22-24. (IF 1.209)
5. S.K. Maurya, **K. Parashuram**, P.S. Singh, P. Ray, A.V.R. Reddy. 2012. Preparation of polysulfone–polyamide thin film composite hollow fiber nanofiltration membranes and their performance in the treatment of aqueous dye solutions. Desalination. 304:11-19. (IF 4.8)
4. P S SINGH, **K PARASHURAM**, S MAURYA, P RAY, A V R REDDY. 2012. Structure-performance-fouling studies of polysulfone microfiltration hollow fibre membranes. Bulletin of Materials Science. 35: 817-822. (IF 0.9)
3. P.Ray, P.Singh, **P.Kallem**, S. Maurya, G.S. Trivedi. 2012. Structure and performance of nanofiltration membrane prepared in a large-scale at CSIR-CSMCRI using indigenous coating unit. Desalination. 288: 8-15. (IF 4.8)
2. Zongli Xie, Manh Hoang, Tuan Duong, Derrick Ng, Puyam S. Singh, Paramita Ray, A.V.R.Reddy, **K. Parashuram** and S. Maurya. 2011. Effect of Membrane Properties on Performance of Membrane Distillation for Ammonia Removal. Journal of Materials Science Research. 1-1: 37-44. (IF 0.4)
1. P.Ray, P.Singh, **K. Parashuram**, S. Maurya, J. J. Trivedi, A.V.R.Reddy. 2010. Preparation and surface modification of hollow fibre membranes for drinking water disinfection and water reclamation. International Journal of Nuclear Desalination. 4-2:149-161. ((IF 0.4; Journal ranking; Q3)

---

## PATENTS

---

4. AVR Reddy, Paramita Ray, Puyam Singh, **Parashuram Kallem**, Sandip Maurya, Jitendra Trivedi, High flux hollow fiber ultrafiltration membranes and process for the preparation thereof, *US patent, US 20130213875*.
3. AVR Reddy, Paramita Ray, Puyam Singh, **Parashuram Kallem**, Sandip Maurya, Jitendra Trivedi, High flux hollow fiber ultrafiltration membranes and process for the preparation thereof, *EP patent, EP 2616168*.
2. AVR Reddy, Paramita Ray, Puyam Singh, **Parashuram Kallem**, Sandip Maurya, Jitendra Trivedi, High flux hollow fiber ultrafiltration membranes and process for the preparation thereof, *WO patent, WO 2012035402*.
1. P.K. Ghosh, A.V.R. Reddy, S.L.Daga, A. Patel, P.Ray, P.S. Singh, **K. Parashuram**, A.P. Rao, J.J. Trivedi, P. Patel, R.B. Mandavia and C.V. Devmurari, Membrane based portable water purifier with squeezable hand operated rubber bulb for pressure generation, *Indian patent filed, 2009*.

---

## CONFERENCES

---

12. **Parashuram Kallem**, Maria Pilar Pina,(mapina@unizar.es), Martin Drobek, Kitty Nijmeijer, Jacques Roziere, Deborah Jones, Reyes Mallada, Anne Julbe, *"EUROMEMBRANE CONFERENCE- 2015"*, September 6-10, 2015, Aachen, Germany- **(Oral talk presenter)**
11. **Parashuram Kallem**, Adela Eguizabal, Kitty Nijmeijer, Maria Pilar Pina, Reyes Mallada  
*"XXXI EMS Summer School 2014 on Innovative Membrane Systems"* September 28 – October 3, 2014. ITM-CNR, Rende (CS) – Italy. **(Poster presenter)**.
10. **Parashuram Kallem**, Adela Eguizabal, Kitty Nijmeijer, Maria Pilar Pina, Reyes Mallada. *" 2014 Membrane Symposium and 14th Poster Day"*, September 8th 2014. Aachen, Germany. **(Poster presenter)**.
9. **Parashuram Kallem**, Adela Eguizabal, Maria Pilar Pina, Reyes Mallada, *"IX IBERO-AMERICAN CONGRESS ON MEMBRANE SCIENCE AND TECHNOLOGY"* Santander, Spain, May 25 to May 28, 2014. **(Flash& poster presenter)**.
8. Santosh Choudhari, **Parashuram Kallem**, Wook-Jin Chung, *" International Congress on Membranes and Membrane Processes (ICOM 2011)"* July 23-29, 2011, Amsterdam, The Netherlands. **(Poster presenter -ICOM1624)**.
7. Hercules Cascon, Arnel Beltran, **Parashuram Kallem**, Rey Eliseo C. Torrejos, Wook-jin Chung, *"International Congress on Membranes and Membrane Processes (ICOM 2011)"* July 23-29, 2011, Amsterdam, The Netherlands. **(Attendee-ICOM1299)**

6. P.Ray, P.S.Singh, A.V.R.Reddy, **P.Kallem**, J.J.Trivedi, G.S. Trivedi and A.P.Rao, “*APA International conference on Polymer science and Technology: vision and scenario*” New Delhi, India. 17-20th December, 2009. (**Poster presenter**).

5. Z. Xie, M. Hoang, T. Duong, D. Ng, P. S. Singh, P. Ray, A.V.R.Reddy, **K. Parashuram** and S. Maurya, Study of asymmetric hollow fibre membranes in membrane distillation for volatile removal from “*industrial wastewaters International Membrane Science and Technology Conference*” Sydney 2010, Australia.

4. P. Ray, P. S. Singh, **K. Parashuram**, J.J. Trivedi, C.V. Devmurari, N. N. Rao, S. Waghmare, A.V.R. Reddy, “*Proceedings of InDA-APDA Conference on Desalination and Water Purification*”, Chennai, India (2010) 485-466.

3. P. S. Singh, P. Ray, J. J.Trivedi, **K. Parashuram**, S.Sharma, A. Prakash Rao, A.V.R. Reddy, Membrane technologies for water recovery from industrial waste waters, “*InDA-APDA Conference on Desalination and Water Purification*” Mar. 10-12, 2010, Chennai, India.

2. P. Ray, P. S. Singh, **K. Parashuram**, J.J. Trivedi, C.V. Devmurari, N. N. Rao, S. Waghmare, A.V.R. Reddy, Preparation and surface modification of hollow fiber membranes for drinking water disinfection and water reclamation, “*InDA-APDA Conference on Desalination and Water Purification*”, Mar. 10-12, 2010 Chennai, India.

1. **.Parashuram Kallem**, Sandip Maurya, Puyam Singh\*, Paramita Ray, AVR Reddy, “*National Conference on Recent trends in Exotic materials(NCRTEM-2010)*”, Sharda University, Greater Noida, India (Feb-2010) – (**Oral talk presenter**).

---

#### AWARDS & HONOURS

---

1. Erasmus Mundus Joint Doctorate (EMJD) fellowship by EACEA .

2. Best poster award at *IX IBERO-AMERICAN CONGRESS ON MEMBRANE SCIENCE AND TECHNOLOGY* Santander, Spain, May 25 to May 28, 2014.

---

#### PROJECTS

---

**Researcher**, with the “Network Projects in Council of Scientific and Industrial Research (CSIR) Project number: NWP-47

*Title:* Hollow Fiber Technology for Waste Water Reclamation, Water Desalination and Various Industrial Applications.

*Role:* Development and surface modification of hollow fibre ultra-filtration membranes and their applications for water purification and other separations”.

---